

2

REPORT NO. NADC-88020-60

DTIC  
ELECTE  
MAY 17 1991  
S c D

AD-A235 994



# FUNDAMENTALS AND METHODS OF HIGH ANGLE-OF-ATTACK FLYING QUALITIES RESEARCH

Robert M. Seltzer and Glenn R. Rhodeside  
Air Vehicle and Crew Systems Technology Department (Code 6053)  
NAVAL AIR DEVELOPMENT CENTER  
Warminster, PA 18974-5000



JANUARY 1988

FINAL REPORT  
Period Covering January 1987 to January 1988  
Task No. 4.5  
Work Unit No. ZX170  
Program Element No. 62122N  
Project No. RR-22-A41

|               |                                     |
|---------------|-------------------------------------|
| Accession For |                                     |
| NTIS GRA&I    | <input checked="" type="checkbox"/> |
| DTIC TAB      | <input type="checkbox"/>            |
| Unannounced   | <input type="checkbox"/>            |
| Justification |                                     |
| By            |                                     |
| District      |                                     |
| Approval      |                                     |
| Dist          | Special                             |
| A-1           |                                     |

Approved for Public Release; Distribution is Unlimited

Prepared for  
OFFICE OF NAVAL TECHNOLOGY  
800 North Quincy St.  
Arlington, VA 22219-5000

DTIC FILE COPY

91-00037



91 5 16 002

## NOTICES

**REPORT NUMBERING SYSTEM** - The numbering of technical project reports issued by the Naval Air Development Center is arranged for specific identification purposes. Each number consists of the Center acronym, the calendar year in which the number was assigned, the sequence number of the report within the specific calendar year, and the official 2-digit correspondence code of the Command Officer or the Functional Department responsible for the report. For example: Report No. NADC 88020-60 indicates the twentieth Center report for the year 1988 and prepared by the Air Vehicle and Crew Systems Technology Department. The numerical codes are as follows:

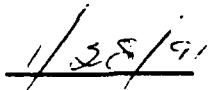
| CODE | OFFICE OR DEPARTMENT                             |
|------|--|
| 00   | Commander, Naval Air Development Center          |
| 01   | Technical Director, Naval Air Development Center |
| 05   | Computer Department                              |
| 10   | AntiSubmarine Warfare Systems Department         |
| 20   | Tactical Air Systems Department                  |
| 30   | Warfare Systems Analysis Department              |
| 40   | Communication Navigation Technology Department   |
| 50   | Mission Avionics Technology Department           |
| 60   | Air Vehicle & Crew Systems Technology Department |
| 70   | Systems & Software Technology Department         |
| 80   | Engineering Support Group                        |
| 90   | Test & Evaluation Group                          |

**PRODUCT ENDORSEMENT** - The discussion or instructions concerning commercial products herein do not constitute an endorsement by the Government nor do they convey or imply the license or right to use such products.

APPROVED BY:



DATE:



| REPORT DOCUMENTATION PAGE  |             |  |   | Form Approved<br>OMB No. 0704-0188                     |                                 |
|--|-------------|--|---|--|---------------------------------|
| 1a. REPORT SECURITY CLASSIFICATION<br>Unclassified   |             |  | 1b. RESTRICTIVE MARKINGS  |  |                                 |
| 2a. SECURITY CLASSIFICATION AUTHORITY  |             |  | 3. DISTRIBUTION / AVAILABILITY OF REPORT<br><br>Approved for Public Release;<br>Distribution is Unlimited |  |                                 |
| 2b. DECLASSIFICATION / DOWNGRADING SCHEDULE  |             |  |   |  |                                 |
| 4. PERFORMING ORGANIZATION REPORT NUMBER(S)<br>NADC-88020-60   |             |  | 5. MONITORING ORGANIZATION REPORT NUMBER(S)   |  |                                 |
| 6a. NAME OF PERFORMING ORGANIZATION<br>Air Vehicle and Crew Systems<br>Technology Department   |             | 6b. OFFICE SYMBOL<br>(If applicable)<br>6053 | 7a. NAME OF MONITORING ORGANIZATION   |  |                                 |
| 6c. ADDRESS (City, State, and ZIP Code)<br>NAVAL AIR DEVELOPMENT CENTER<br>Warminster, PA 18974-5000   |             |  | 7b. ADDRESS (City, State, and ZIP Code)   |  |                                 |
| 8a. NAME OF FUNDING / SPONSORING<br>ORGANIZATION<br>OFFICE OF NAVAL TECHNOLOGY   |             | 8b. OFFICE SYMBOL<br>(If applicable)<br>ONT  | 9. PROCUREMENT INSTRUMENT IDENTIFICATION NUMBER   |  |                                 |
| 8c. ADDRESS (City, State, and ZIP Code)<br>800 North Quincy Street<br>Arlington, VA 22219-5000   |             |  | 10. SOURCE OF FUNDING NUMBERS   |  |                                 |
| PROGRAM<br>ELEMENT NO.<br>62122N   |             | PROJECT<br>NO.<br>RR-22-A41                  | TASK<br>NO.<br>4.5  | WORK UNIT<br>ACCESSION NO.<br>ZX170                    |                                 |
| 11. TITLE (Include Security Classification)<br>Fundamentals and Methods of High Angle-of-Attack Flying Qualities Research  |             |  |   |  |                                 |
| 12. PERSONAL AUTHOR(S)<br>Robert M. Seltzer and Glenn R. Rhodeside   |             |  |   |  |                                 |
| 13a. TYPE OF REPORT<br>Final   |             | 13b. TIME COVERED<br>FROM 1/87 TO 1/88       |   | 14. DATE OF REPORT (Year, Month, Day)<br>1988, January |                                 |
| 15. PAGE COUNT<br>198  |             |  |   |  |                                 |
| 16. SUPPLEMENTARY NOTATION   |             |  |   |  |                                 |
| 17. COSATI CODES   |             |  | 18. SUBJECT TERMS (Continue on reverse if necessary and identify by block number)                         |  |                                 |
| FIELD<br>01  | GROUP<br>03 | SUB-GROUP<br>03                              | Flying Qualities, High Angle-of-Attack, Aerodynamics,<br>Stall, Spin, Aircraft Departure Criteria         |  |                                 |
| 19. ABSTRACT (Continue on reverse if necessary and identify by block number)   |             |  |   |  |                                 |
| <p>This report is intended for use as a collection and analysis of diverse data gathering, empirical, and analytical approaches to the high angle-of-attack aircraft stability and control problem; as a compendium of several methods of defining aircraft departure and spin susceptibility; as a reference for spin definition and spin recovery enhancement; as a review of specifications, regulations, and design guides as they pertain to high angle-of-attack flight; and as a medium for expounding where tomorrow's high angle-of-attack investigative attention should focus. The design of safe, effective fighter aircraft in the high angle-of-attack combat environment is reaching a critical point. Accepted flying qualities design guidelines (necessary to establish stability and control requirements) must be established to address</p> <p style="text-align: right;">(Continued)</p> |             |  |   |  |                                 |
| 20. DISTRIBUTION / AVAILABILITY OF ABSTRACT<br><input checked="" type="checkbox"/> UNCLASSIFIED / UNLIMITED <input type="checkbox"/> SAME AS RPT. <input type="checkbox"/> DTIC USERS  |             |  | 21. ABSTRACT SECURITY CLASSIFICATION<br>N/A   |  |                                 |
| 22a. NAME OF RESPONSIBLE INDIVIDUAL<br>Robert M. Seltzer   |             |  | 22b. TELEPHONE (Include Area Code)<br>(215) 441-1356  |  | 22c. OFFICE SYMBOL<br>Code 6053 |

UNCLASSIFIED

SECURITY CLASSIFICATION OF THIS PAGE

BLOCK 19 Continued

flight operations in the high angle-of-attack flight regime. Most of the research to date has focused on aircraft departure. Parameters/criteria to define desired high angle-of-attack flying qualities in the post-stall region (outside the realm of departure) are still unanswered.

TABLE OF CONTENTS (CONTINUED)

|  | <u>Page</u> |
|--|-------------|
| 2.2.4 Aerodynamic Characteristics Near Stall .....               | 48          |
| 2.2.4.1 Pitch-up .....   | 48          |
| 2.2.4.2 Deep Stall .....   | 52          |
| 2.2.5 Methods of Stall Control .....                             | 56          |
| 2.3 The Spin .....   | 68          |
| 2.3.1 General/Definition .....                                   | 68          |
| 2.3.2 Causes of Aircraft Spin .....                              | 73          |
| 2.3.3 Dynamics of the Spin .....                                 | 77          |
| 2.3.4 Inverted Spins .....                                       | 83          |
| 2.3.5 Spin Recovery .....  | 85          |
| 2.3.5.1 Conventional (Rudder, Stabilizer, Aileron) .....         | 85          |
| 2.3.5.2 Other Means of Spin Recovery .....                       | 93          |
| 3.0 METHOD OF DEPARTURE RESEARCH AND ANALYSIS .....              | 95          |
| 3.1 Wind Tunnel/Analytical Departure Prediction Techniques ..... | 95          |
| 3.1.1. Use of Wind Tunnel Data .....                             | 95          |

TABLE OF CONTENTS

|   | <u>Page</u> |
|---|-------------|
| LIST OF FIGURES .....   | v           |
| LIST OF TABLES .....  | xiv         |
| LIST OF SYMBOLS .....   | xv          |
| 1.0 INTRODUCTION .....  | 1           |
| 1.1 Background .....  | 1           |
| 1.2 Purpose .....   | 2           |
| 1.3 Approach .....  | 2           |
| 2.0 HIGH ANGLE-OF-ATTACK AERODYNAMICS AND STALL .....                               | 4           |
| 2.1 High Angle-of-Attack Terminology .....  | 4           |
| 2.2 The Stall .....   | 8           |
| 2.2.1 Definition .....  | 9           |
| 2.2.2 Fluid Dynamics of Flow Separation .....                                       | 11          |
| 2.2.3 Influence of Geometric Wing Parameters on Aircraft Stall Characteristics .... | 27          |

TABLE OF CONTENTS (CONTINUED)

|   | <u>Page</u> |
|---|-------------|
| 3.1.2 Rotary Balance Data .....   | 98          |
| 3.1.3 Some Observations Concerning High Angle-of-Attack Static Aerodynamics .....         | 107         |
| 3.2 Dynamic Model Flight Testing .....  | 112         |
| 3.3 Piloted Simulations .....   | 119         |
| 3.4 Full-Scale Aircraft Flight Testing .....  | 122         |
| 4.0 HIGH ANGLE-OF-ATTACK MILITARY SPECIFICATIONS AND FLYING QUALITIES<br>CRITERIA .....   | 128         |
| 4.1 Military Specifications .....   | 128         |
| 4.1.1 MIL-F-8785C, Flying Qualities of Piloted Airplanes .....                            | 128         |
| 4.1.2 High Angle-of-Attack Flight Test Demonstration Requirements<br>and Procedures ..... | 130         |
| 4.1.3 MIL-STD-1797, Military Standard Flying Qualities of Piloted Vehicles .....          | 131         |
| 4.2 Departure Susceptibility Prediction Criteria .....                                    | 135         |
| 4.2.1 Bihle Applied Research Departure and Roll Reversal Boundaries .....                 | 137         |
| 4.2.2 Weissman-STI Departure Susceptibility Criterion .....                               | 139         |

TABLE OF CONTENTS (CONTINUED)

|   | <u>Page</u> |
|---|-------------|
| 4.2.2.1 STI Departure Rating Scale .....  | 144         |
| 4.2.2.2 Investigation of the Bihle and Weissman/STI Criteria Using a Total<br>G-Simulator ..... | 152         |
| 4.2.3 Kalviste Departure Susceptibility Criterion .....   | 160         |
| 4.2.4 Other Departure Susceptibility Criterion .....  | 170         |
| 4.2.5 Summary of Departure Susceptibility Parameters/Criterion .....                            | 171         |
| 5.0 CONCLUSIONS .....   | 173         |
| 6.0 RECOMMENDATIONS .....   | 176         |
| 6.1 General .....   | 176         |
| 6.2 Aerodynamic Math Models At High Angles-of-Attack .....                                      | 177         |
| 6.2.1 Determination of Forced Oscillation Data .....  | 177         |
| 6.2.2 Determination of Aerodynamic Rotary Balance Data .....                                    | 178         |
| 6.3 Extension of High Angle-of-Attack Flying Qualities Criteria .....                           | 179         |
| 7.0 REFERENCES .....  | 182         |
| APPENDIX A — Glossary of Defined Terms .....  | 192         |

LIST OF FIGURES

| <u>Figure No.</u> | <u>Title</u>  | <u>Page</u> |
|-------------------|---|-------------|
| 1                 | Aerodynamic Stall of an Airfoil .....   | 10          |
| 2                 | Prandtl's Boundary Layer Flow Model Over an Airfoil .....   | 11          |
| 3                 | Effect of Pressure Gradient on Boundary Layer Profiles .....  | 12          |
| 4                 | Flow Around an Airfoil with Separation .....  | 13          |
| 5                 | (a) Lift Curve Slope for a Gradual Airfoil Stall .....  | 14          |
|                   | (b) Lift Curve Slope for an Abrupt Airfoil Stall .....  | 14          |
| 6                 | Comparison of Pressure Distribution of Separated and Attached<br>Flow Over an Airfoil .....                   | 15          |
| 7                 | Newtonian Shear Distribution in A Boundary-Layer Near a Wall .....  | 16          |
| 8                 | Comparison of Laminar and Turbulent Boundary Layers .....   | 17          |
| 9                 | Transition From Laminar to Turbulent Flow Over a Flat Plate .....   | 19          |
| 10                | Local Skin Friction in Incompressible Flow .....  | 20          |
| 11                | Mean Streamline Pattern in Laminar Separation Followed by Turbulent<br>Reattachment .....                     | 21          |
| 12                | Separation Positions for Various Reynolds Number Ranges .....   | 21          |
| 13                | Effect of Reynolds Number on Section Characteristics of the GA(W)-1<br>Airfoil Model Smooth, $M = 0.15$ ..... | 22          |

## LIST OF FIGURES (CONTINUED)

| <u>Figure No.</u> | <u>Title</u>   | <u>Page</u> |
|-------------------|--|-------------|
| 14                | $C_{L_{MAX}}$ — Overshoot Characteristics for Leading- and Trailing-Edge Stall .....                     | 24          |
| 15                | Complete Dynamic Loop Effects on Normal Force Coefficient as a Function of Frequency .....               | 24          |
| 16                | Events of Dynamic Stall on NACA 0012 Airfoil .....   | 26          |
| 17                | Examples of Post WWII Type Aircraft Configurations .....   | 27          |
| 18                | Airfoil Geometry Nomenclature .....  | 28          |
| 19                | Variation of $C_{l_{MAX}}$ with Thickness Ratio of NACA 24xx Airfoils for Various Reynolds Numbers ..... | 29          |
| 20                | Comparison of Various Airfoil Shapes .....   | 30          |
| 21                | Effect of Camber on Airfoil Pressure Distribution .....  | 30          |
| 22                | Maximum Lift at $Re = 6 \times 10^6$ as a Function of Thickness Ratio and Nose Radius .....              | 31          |
| 23                | Variation of Pressure Distribution on Airfoil with Increase in Angle-of-Attack .....                     | 32          |
| 24                | Types of Wing Section Stalls .....   | 33          |
| 25                | Classification of Airfoil Stall by Hazen (1967) .....  | 35          |
| 26                | Boundaries for Various Types of Airfoil Stall .....  | 36          |

## LIST OF FIGURES (CONTINUED)

| <u>Figure No.</u> | <u>Title</u>  | <u>Page</u> |
|-------------------|---|-------------|
| 27                | Initial Stall Characteristics of Plane Wings with Constant Symmetrical Sections .....             | 37          |
| 28                | Wing Planform Nomenclature .....  | 38          |
| 29                | Generation of Vortex System by Finite Aspect Ratio Wing .....                                     | 39          |
| 30                | Vortex Sheet Trailing Behind a Wing .....   | 40          |
| 31                | Prandtl Vortex System .....   | 40          |
| 32                | Effect of Finite Aspect Ratio on the Lift-Curve .....   | 41          |
| 33                | Downwash Distribution of a Finite Wing .....  | 42          |
| 34                | Effect of Downwash of a Finite Wing on Wing Lift Distribution .....                               | 42          |
| 35                | Vortex System of a Delta Wing .....   | 43          |
| 36                | Typical Influence of Sweepback on Lift-Curve slope .....  | 44          |
| 37                | Cross-Flow at the Surface of a 45° Swept Wing .....   | 44          |
| 38                | Lift Curve Slopes for Swept Tapered Wings .....   | 45          |
| 39                | Variations of $C_{L_{MAX}}$ with Sweepback for Wings Having Planforms Other than Triangular ..... | 46          |
| 40                | Spanwise Lift Coefficient Distribution for Various Wing Planform Taper Ratios .....               | 47          |

LIST OF FIGURES (CONTINUED)

| <u>Figure No.</u> | <u>Title</u>   | <u>Page</u> |
|-------------------|--|-------------|
| 41                | Typical Influence of Wing Taper on Stall Progression .....                           | 47          |
| 42                | Example of Longitudinal Pitch-up Instability .....                                   | 48          |
| 43                | Effect on Wing Aspect Ratio and Sweep on Stability Boundaries for the Wing Alone ... | 49          |
| 44                | Illustration of Stalled and Vortex Flows at High Angle-of-Attack .....               | 49          |
| 45                | Stalled Wing Wake Tail Immersion .....   | 50          |
| 46                | Typical Longitudinal Stability Component Build-up .....                              | 51          |
| 47                | Effect of Horizontal-Tail Location on Pitch-up Tendencies .....                      | 51          |
| 48                | Loss of Elevator Effectiveness for a Configuration with Deep Stall .....             | 52          |
| 49                | Typical Deep Stall Time Histories .....  | 53          |
| 50                | "Supernormal" Stabilator .....   | 54          |
| 51                | Free-body-diagram of Unstalled Supernormal Stabilator .....                          | 55          |
| 52                | Typical Stall Strip .....  | 57          |
| 53                | Exaggerated View of Wing Tip Washout .....   | 57          |
| 54                | Example of Aerodynamic Twist .....   | 58          |

## LIST OF FIGURES (CONTINUED)

| <u>Figure No.</u> | <u>Title</u>  | <u>Page</u> |
|-------------------|---|-------------|
| 55                | Wing Vortex Producing Devices: (a) Leading-edge and Rear Fences<br>(b) Snag (c) Leading-edge Notch (d) Leading-edge Fairing ..... | 59          |
| 56                | Wing Leading-Edge Type Devices .....  | 59          |
| 57                | Effect of Leading-edge Slat on NACA 64A010 Airfoil With and Without Flaps .....   | 60          |
| 58                | Effect of Leading-edge Flap on NACA 64A010 Airfoil With and Without Flaps .....   | 61          |
| 59                | Lift Data for Various Leading-edge Devices .....  | 62          |
| 60                | Trident Wing with Vortex Generators .....   | 62          |
| 61                | Types of Vortex Generators .....  | 63          |
| 62                | Suction Boundary Layer Control Concepts .....   | 64          |
| 63                | Experimental Lift Curves for a NACA 63A009 Airfoil with Porous Nose .....   | 65          |
| 64                | Blowing Boundary-layer Control Concepts .....   | 65          |
| 65                | Influence of Blowing on the Lift Curve-Slope and Pressure Distribution for Various<br>Blowing Methods .....                       | 66          |
| 66                | Effect of Blowing on Aerodynamic Characteristics .....  | 67          |
| 67                | Example of Flow at High Angle-of-Attack for a Blunt Body with a Spike .....   | 68          |
| 68                | Various Phases of the Spin .....  | 72          |

## LIST OF FIGURES (CONTINUED)

| <u>Figure No.</u> | <u>Title</u>   | <u>Page</u> |
|-------------------|--|-------------|
| 69                | Mechanics of Autorotation .....  | 74          |
| 70                | Changes in $C_L$ and $C_D$ with $\alpha < \alpha_s$ and $\alpha > \alpha_s$ .....                    | 75          |
| 71                | Difference in Resultant Aerodynamic Forces Resulting in an Autorotative Yaw Couple .....             | 75          |
| 72                | (a) Force Definition During a Steady Spinning Aircraft .....   | 77          |
|                   | (b) Attitude Definition of a Steady Spinning Aircraft .....  | 77          |
| 73                | Balance Between Inertial and Aerodynamic Pitching Moments in a Steady State Spin .....               | 80          |
| 74                | Angular Rates in a Spin .....  | 81          |
| 75                | Definition of an Inverted Spin .....   | 83          |
| 76                | Flows on the Vertical Tail for an Upright and Inverted Spin .....                                    | 84          |
| 77                | Roll and Yaw Rates of an Upright and Inverted Spin .....   | 85          |
| 78                | Spin Recovery Methods .....  | 86          |
| 79                | Spin Recovery Controls as Determined by Mass Distribution .....                                      | 88          |
| 80                | Aircraft Angular Rates in a Right Spin .....   | 91          |
| 81                | Pictorial Representation of Control Effectiveness for Spin Recovery of a Conventional Aircraft ..... | 92          |

LIST OF FIGURES (CONTINUED)

| <u>Figure No.</u> | <u>Title</u>   | <u>Page</u> |
|-------------------|--|-------------|
| 82                | Water Tunnel Flow Visualization Photograph of F-18 Model at $\alpha = 40^\circ$ .....  | 96          |
| 83                | (a) Sketch of Rotary Balance Apparatus .....   | 100         |
|                   | (b) Model Installed on Rotary Balance .....  | 100         |
| 84                | Analytical Determination of the Magnitude of the Steady State Rotational Vector ...  | 102         |
| 85                | Effect of Aircraft Component Buildup on Aircraft Yawing Moment Coefficient .....   | 106         |
| 86                | Variation of Yawing Moment Coefficient with Angle-of-Attack for Several Models of the Same Configuration ( $\beta = 0^\circ$ ; Controls Neutral) ..... | 107         |
| 87                | Contemporary Fighter Configuration with Long Pointed Nose .....  | 108         |
| 88                | Asymmetric Yawing Moment with Angle-of-Attack for Three Airplane Configurations ...  | 109         |
| 89                | Rotary Yawing Moment Coefficient at 60 degrees, Angle-of-Attack and zero Degrees Sideslip for Three Different Nose Shapes .....                        | 109         |
| 90                | Variation of Yawing Moment Coefficient with Angle-of-Attack for the Same Model and Configuration ( $\beta = 0^\circ$ ; Controls Neutral) .....         | 110         |
| 91                | Sketches of Separated Vortex Sheets on Fuselage Forebody .....   | 111         |
| 92                | Cross-section View of Vertical Spin Tunnel .....   | 113         |
|                   | (a) Schematic Diagram  |             |
|                   | (b) Test Section at NASA Langley   |             |

## LIST OF FIGURES (CONTINUED)

| <u>Figure No.</u> | <u>Title</u>   | <u>Page</u> |
|-------------------|--|-------------|
| 93                | Aircraft Tethered Model Wind Tunnel Testing .....                                  | 115         |
| 94                | Radio Controlled Model Mounted on Helicopter Launch Platform .....                 | 117         |
| 95                | Summary of High- $\alpha$ Scaled Dynamic Testing .....                             | 118         |
| 96                | MIL-STD-1797 Requirement: Post-Stall Gyration and Spins .....                      | 132         |
| 97                | MIL-STD-1797 Requirement: Recovery from Post-Stall Gyration and Spins .....        | 134         |
| 98                | Preliminary Causes of Aircraft Departure from Controlled Flight .....              | 136         |
| 99                | Bihle Applied Research Departure Susceptibility Design Guidelines .....            | 138         |
| 100               | Departure Susceptibility Rating vs. Lateral Closed-loop Divergence Parameter ..... | 141         |
| 101               | Expected Stall Behavior as a Function of $C_{n_{\beta DYN}}$ .....                 | 142         |
| 102               | Northrop Departure Criteria .....  | 142         |
| 103               | Weissman Departure and Spin Susceptibility Criterion .....                         | 143         |
| 104               | Northrop Modified Weissman Departure and Susceptibility Criterion .....            | 145         |
| 105               | STI Modified Weissman Departure and Susceptibility Criterion .....                 | 145         |
| 106               | STI Departure Rating Scale .....   | 147         |
| 107               | Qualitative Information Required to Qualify Pilot Departure Ratings .....          | 148         |

LIST OF FIGURES (CONTINUED)

| <u>Figure No.</u> | <u>Title</u>   | <u>Page</u> |
|-------------------|--|-------------|
| 108               | STI Loss of Control/Departure/Recovery Debriefing Guide .....  | 150         |
| 109               | Revised STI Departure Rating Scale .....   | 151         |
| 110               | Integrated Bihrie/Weissman-STI F-14A Departure Susceptibility Criterion Plane .....  | 154         |
| 111               | Departure Susceptibility Integration Criterion Boundary Correlation .....  | 156         |
| 112               | (a) NADC Proposed Departure Rating Scale .....   | 158         |
|                   | (b) NADC Proposed "Cooper-Harper like" Departure Rating Scale .....  | 159         |
| 113               | Development of the Kalviste Coupled Parameters/Criterion .....   | 161         |
| 114               | Summary of High-AOA Stability and Controllability Parameters/Criteria .....  | 172         |
| 115               | Forced Oscillation Wind Tunnel Test Rolling Moment Derivative Due To<br>Roll Rate Variation With Oscillation Amplitude ..... | 178         |
| 116               | Effects of Angles of Incidence on Aircraft Stability .....   | 180         |
| 117               | Yaw-Rate/Pitch-Rate Effects on Aircraft Stability .....  | 180         |
| 118               | Stability Boundaries for Sideslip/Roll-Rate Variations .....   | 181         |

LIST OF TABLES

| <u>Table No.</u> | <u>Title</u>  | <u>Page</u> |
|------------------|---|-------------|
| I                | Spin Mode Modifiers .....   | 6           |
| II               | Digest of Pilot Comments on Specific Aircraft High Angle-of-Attack Flight Characteristics ..... | 69          |
| III              | Simulator Comparison Survey .....   | 124         |
| A-I              | Dynamic Scaling Factors .....   | 196         |

## LIST OF SYMBOLS

| <u>Symbol</u>      | <u>Definition</u>  | <u>Units</u> |
|--------------------|--|--------------|
| AOA                | Angle-of-Attack  | deg          |
| AR                 | Aspect Ratio, $b^2/s$  | —            |
| b                  | Reference wing span  | ft           |
| $\bar{c}$          | Mean aerodynamic chord or chord  | ft           |
| $C_D$              | Drag Coefficient, $D/\bar{q}s$   | —            |
| $C_{D_{\alpha}}$   | Change in drag coefficient with angle-of-attack, $\partial C_D/\partial \alpha$  | —            |
| $c_l$              | Section Lift coefficient   | —            |
| $C_l$              | Rolling Moment coefficient, $\mathcal{L}/\bar{q}Sb$  | —            |
| $C_{l_p}$          | Change in rolling moment coefficient with rolling velocity, $\partial C_l/\partial (pb/2U_o)$                              | —            |
| $C_{l_r}$          | Change in yawing moment coefficient with yawing velocity, $\partial C_l/\partial (rb/2U_o)$                                | —            |
| $C_{l_{\delta_i}}$ | Change in rolling moment coefficient with deflection of control surfaces, ( $i = a, r$ ), $\partial C_l/\partial \delta_i$ | —            |
| $C_{l_{\beta}}$    | Change in rolling moment coefficient with sideslip angle, $\partial C_l/\partial \beta$                                    | —            |
| $C_L$              | Coefficient of lift, $L/\bar{q}s$  | —            |
| $C_{L_{\alpha}}$   | Change of lift coefficient with angle-of-attack, $\partial C_L/\partial \alpha$  | —            |

# NADC 88020-60

## LIST OF SYMBOLS (CONTINUED)

| <u>Symbol</u>              | <u>Definition</u>   | <u>Units</u> |
|----------------------------|---|--------------|
| $C_m$                      | Pitching moment coefficient, $M/\bar{q} S \bar{c}$  | —            |
| $C_{m_\alpha}$             | Change in pitching moment coefficient with angle-of-attack, $\partial C_m / \partial \alpha$                              | —            |
| $C_{m_\beta}$              | Change in pitching moment coefficient with sideslip angle, $\partial C_m / \partial \beta$                                | —            |
| $C_n$                      | Yawing moment coefficient, $N/\bar{q} S b$  | —            |
| $C_n$                      | Forebody yawing moment coefficient  | —            |
| $C_{n_p}$                  | Change in yawing moment coefficient with rolling velocity, $\partial C_n / \partial (pb/2U_o)$                            | —            |
| $C_{n_r}$                  | Change in yawing moment coefficient with yawing velocity, $\partial C_n / \partial (rb/2U_o)$                             | —            |
| $C_{n_{\delta_i}}$         | Change in yawing moment coefficient with deflection of control surface ( $i = a, r$ ), $\partial C_n / \partial \delta_i$ | —            |
| $C_{n_\alpha}$             | Change of yawing moment coefficient with angle-of-attack, $\partial C_n / \partial \alpha$                                | —            |
| $C_{n_\beta}$              | Change in yawing moment coefficient with sideslip angle, $\partial C_n / \partial \beta$                                  | —            |
| $C_{n_{\text{BAPPARENT}}}$ | Departure Criteria Parameter (McDonnell Douglas Aircraft)   | —            |
| $C_{n_{\text{BDYN}}}$      | Stability Axis Dynamic Directional Stability Parameter (Moul & Paulson, 1958)   | —            |
| $c_r$                      | Root Chord  | ft           |
| $c_t$                      | Tip Chord   | ft           |

LIST OF SYMBOLS (CONTINUED)

| <u>Symbol</u> | <u>Definition</u>  | <u>Units</u>         |
|---------------|--|----------------------|
| $C_Y$         | Side Force Coefficient, $Y/\bar{q}s$   | —                    |
| $C_{Y_p}$     | Change in Side force coefficient with rolling velocity, $\partial C_Y/\partial(\bar{q}b/2U_o)$ | —                    |
| $C_{Y_r}$     | Change in Side force coefficient with yawing velocity, $\partial C_Y/\partial(\bar{q}b/2U_o)$  | —                    |
| D             | Drag force   | lbs                  |
| g             | Acceleration of gravity (32.17)  | ft/sec <sup>2</sup>  |
| $G_z$         | Normal acceleration  | ft/sec <sup>2</sup>  |
| h             | Altitude of center-of-gravity  | ft                   |
| $I_x$         | Moment of Inertia about $x_B$ -axis, $\int (y^2 + z^2) dm$                                     | slug-ft <sup>2</sup> |
| $I_y$         | Moment of Inertia about $y_B$ -axis, $\int (x^2 + z^2) dm$                                     | slug-ft <sup>2</sup> |
| $I_z$         | Moment of Inertia about $z_B$ -axis, $\int (x^2 + y^2) dm$                                     | slug-ft <sup>2</sup> |
| $I_{xz}$      | Product of Inertia, $\int xz dm$   | slug-ft <sup>2</sup> |
| IYMP          | Inertia yaw moment parameter, $\frac{I_x - I_y}{mb^2}$   | —                    |
| $K_i$         | Radius of Gyration, $K_i = \sqrt{I_i/m}$ ; $i = xx, yy, zz$                                    | ft                   |
| $l$           | Length   | ft, in               |
| L             | Lift Force   | lb                   |

LIST OF SYMBOLS (CONTINUED)

| <u>Symbol</u> | <u>Definition</u>   | <u>Units</u>                          |
|---------------|---|---------------------------------------|
| $L$           | Aerodynamic moment about $x_B$ -axis (rolling moment)   | ft-lb                                 |
| LCDP          | Lateral Control Departure Parameter   | —                                     |
| $L_\alpha$    | Change in Rolling Moment with angle-of-attack, $1/I_x \cdot \partial C_l / \partial \alpha$   | $\frac{1}{\text{sec}^2 - \text{rad}}$ |
| $L_\beta$     | Change in Rolling Moment with sideslip angle, $1/I_x \cdot \partial C_l / \partial \beta$     | $\frac{1}{\text{sec}^2 - \text{rad}}$ |
| $m$           | Aircraft mass   | slugs                                 |
| $M$           | Aerodynamic moment about $y$ -axis (pitching moment)  | ft-lb                                 |
| $M$           | Mach number   | —                                     |
| $M_q$         | Change in pitching moment with pitching velocity, $1/I_y \cdot \partial \dot{M} / \partial q$ | $\frac{1}{\text{sec}^2 - \text{rad}}$ |
| $M_\alpha$    | Change in pitching moment with angle-of-attack, $1/I_y \cdot \partial M / \partial \alpha$    | $\frac{1}{\text{sec}^2 - \text{rad}}$ |
| $M_\beta$     | Change in pitching moment with sideslip angle, $1/I_y \cdot \partial M / \partial \beta$      | $\frac{1}{\text{sec}^2 - \text{rad}}$ |
| $N$           | Aerodynamic moment about $z_B$ -axis (yawing moment)  | ft-lb                                 |
| $N_\alpha$    | Change in pitching moment with angle-of-attack, $1/I_z \cdot \partial N / \partial \alpha$    | $\frac{1}{\text{sec}^2 - \text{rad}}$ |
| $N_\beta$     | Change in pitching moment with sideslip angle, $1/I_z \cdot \partial N / \partial \beta$      | $\frac{1}{\text{sec}^2 - \text{rad}}$ |

## LIST OF SYMBOLS (CONTINUED)

| <u>Symbol</u> | <u>Definition</u>                           | <u>Units</u>       |
|---------------|---|--------------------|
| p             | Rolling angular velocity                    | rad/sec            |
| P             | Pressure                                    | lbs                |
| PYMP          | Propelling yaw moment parameter             | —                  |
| q             | Pitching angular velocity                   | rad/sec            |
| $\bar{q}$     | Dynamic pressure, $\bar{q} = 1/2\rho V_T^2$ | lb/ft <sup>2</sup> |
| r             | Yawing angular velocity                     | rad/sec            |
| $R_s$         | Spin radius                                 | ft                 |
| Re            | Reynolds number                             | —                  |
| s             | Laplace operator                            | —                  |
| S             | Reference wing area                         | ft <sup>2</sup>    |
| t             | time  | sec                |
| t             | thickness                                   | ft                 |
| t/c           | thickness ratio                             | —                  |
| T             | Thrust                                      | lb                 |
| T             | Period                                      | sec                |

LIST OF SYMBOLS (CONTINUED)

| <u>Symbol</u>                | <u>Definition</u>   | <u>Units</u>           |
|------------------------------|---|------------------------|
| $T_{\theta_1}, T_{\theta_2}$ | Longitudinal transfer function roots  | rad/sec                |
| $T_{\phi_1}, T_{\phi_2}$     | Lateral transfer function numerator roots   | rad/sec                |
| $u, v, w$                    | Body Axis velocity (positive along the $x_B, y_B, z_B$ -axes respectively)                  | ft/sec                 |
| $U_0$                        | Forward Equilibrium Velocity  | ft/sec                 |
| $V$                          | Characteristic Velocity   | ft/sec                 |
| $V_T$                        | Total Velocity  | ft/sec                 |
| $W$                          | Weight  | lbs                    |
| $X$                          | Longitudinal body axis force  | lb                     |
| $x, y, z$                    | Body-axis coordinate system   | —                      |
| $X_U$                        | Change in x-axis Force with forward body-axis velocity, $1/m \cdot \partial X / \partial U$ | $\frac{1}{\text{sec}}$ |
| $X_W$                        | Change in x-axis Force with normal body-axis velocity, $1/m \cdot \partial X / \partial W$  | $\frac{1}{\text{sec}}$ |
| $Y$                          | Side Force  | lb                     |
| $Z$                          | Normal Force  | lb                     |
| $Z_U$                        | Change in z-axis Force with forward body-axis velocity, $1/m \cdot \partial Z / \partial U$ | $\frac{1}{\text{sec}}$ |
| $Z_W$                        | Change in z-axis Force with forward body-axis velocity, $1/m \cdot \partial Z / \partial W$ | $\frac{1}{\text{sec}}$ |

## LIST OF SYMBOLS (CONTINUED)

| <u>Symbol</u>                   | <u>Definition</u>  | <u>Units</u>          |
|---------------------------------|--|-----------------------|
| <u>Greek</u>                    |  |                       |
| $\alpha$                        | Angle-of-attack  | rad                   |
| $\alpha_s$                      | Stall angle-of-attack  | rad                   |
| $\alpha_{ND}$                   | Nondimensional angle-of-attack derivative with respect to time | —                     |
| $\alpha - \beta, \alpha_\delta$ | Departure prediction criteria axis system                      | —                     |
| $\beta$                         | Sideslip angle   | rad                   |
| $\gamma$                        | Flight path angle  | rad                   |
| $\gamma$                        | Spin helix angle   | rad                   |
| $\delta$                        | Control surface deflection                                     | —                     |
| $\delta$                        | Boundary layer thickness                                       | —                     |
| $\zeta_\phi$                    | Damping of second order lateral transfer function numerator    | —                     |
| $\Lambda_{c/4}$                 | Quarter-chord sweepback angle                                  | deg                   |
| $\theta$                        | Pitch angle  | deg                   |
| $\lambda$                       | Taper Ratio, $c_t/c_r$   | —                     |
| $\rho$                          | density  | slugs/ft <sup>3</sup> |

## LIST OF SYMBOLS (CONTINUED)

| <u>Symbol</u>         | <u>Definition</u>   | <u>Units</u>                         |
|-----------------------|---|--------------------------------------|
| $\mu$                 | Coefficient of Viscosity,   | $\frac{\text{lbs-sec}}{\text{ft}^2}$ |
| $\mu$                 | Nondimensional mass (or relative Density Factor), $\frac{m}{\rho S b}$                | —                                    |
| $\nu$                 | Kinematic Viscosity   | $\text{ft}^2/\text{sec}$             |
| $\sigma$              | Helix Angle — inclination of the Flight Path from the Vertical, $\tan^{-1} (R_s r/V)$ | rad                                  |
| $\tau$                | time constant   | sec                                  |
| $\tau$                | shear stress  | $\text{lb/ft}^2$                     |
| $\phi$                | roll angle  | rad                                  |
| $\chi$                | Yaw attitude  | rad                                  |
| $\omega_E$            | Engine RPM  | rev/sec                              |
| $\omega_\phi$         | Natural frequency of second order lateral transfer function numerator                 | rad/sec                              |
| $\Omega, \omega$      | Rotational Velocity, $\sqrt{P^2 + Q^2 + R^2}$   | rad/sec                              |
| $\frac{\Omega b}{2V}$ | Nondimensional rotation rate  | —                                    |
| $(\cdot)$             | Derivative with respect to time   | —                                    |
| $(\cdot)_0$           | Initial Condition   | —                                    |
| $(\cdot)'$            | Stability derivative with inertial coupling effects                                   | —                                    |

LIST OF SYMBOLS (CONTINUED)

| <u>Subscript Symbols</u> | <u>Definition</u>                        |
|--------------------------|--|
| a                        | Aileron                                  |
| A                        | Aerodynamic                              |
| aero                     | Aerodynamic                              |
| B                        | Body Axes                                |
| c/4                      | quarter-chord                            |
| cg                       | center-of-gravity                        |
| CR                       | critical                                 |
| e                        | elevator                                 |
| E                        | engine                                   |
| i                        | induced, inertial                        |
| l                        | lower, left, local                       |
| l, m, n                  | rolling, pitching, yawing moment         |
| max                      | Maximum                                  |
| n                        | normal direction to airfoil leading-edge |
| o                        | local angle-of-attack                    |
| osc                      | oscillation component of rotation        |
| r                        | rudder, right, root                      |
| u                        | upper                                    |
| s                        | Stability Axes                           |
| ss                       | steady state component of rotation       |
| t,T                      | Total, tip                               |
| w                        | Downwash Velocity                        |
| $\infty$                 | freestream                               |

LIST OF SYMBOLS (CONTINUED)

| <u>Acronyms and Abbreviation Symbols</u> | <u>Definition</u>                 |
|--|-----------------------------------|
| AOA                                      | Angle-of-Attack                   |
| DOF                                      | Degree-of-Freedom                 |
| IYMP                                     | Inertial Yawing Moment Parameter  |
| MAT                                      | Maximum Augmented Thrust          |
| PCAS                                     | Pitch Command Augmentation System |
| PSG                                      | Post Stall Gyration               |
| SAS                                      | Stability Augmentation System     |

## 1.0 INTRODUCTION

### 1.1 Background

Engineers have attempted to overcome the limitations imposed on the aircraft vehicle since the beginning of powered flight. Nowhere is this more true than with the flight dynamics of the high angle-of-attack realm. Research efforts into the causes of loss of stability and control during high angle-of-attack maneuvering have been administered to establish bases from which safe envelope expansion may be realized. A better understanding of the mechanics and aerodynamics of high angle-of-attack flight has led to improved recovery techniques and, more importantly, departure prevention methods.

The need for high angle-of-attack and departure research is supported by continuing losses of both lives and aircraft. It is hypothesized, based on available evidence, that many of the aircraft lost in the Vietnam Conflict for which no cause was ever determined were lost because of poor stalling and departure characteristics (Reference (1)). Since the Vietnam era, departure awareness has heightened, and accelerated high angle of attack research efforts have emerged. Considerable attention focuses on departure resistance for Class IV military aircraft, i.e., highly maneuverable fighter/attack vehicles. Yet, the departure problem is not uncommon in aircraft Classes I, II and III. Assuring adequate control power and departure warning cues is not limited to fighter aircraft.

With the advent of two phenomena, 1) new, highly sophisticated electronics, avionics, displays, and weapons and 2) the modern fighter/attack pilot's need for sustained high angle of attack maneuvering, many disciplines are now considered integral parts of the total solution for innocuous high angle of attack flight. The primary areas of research are flying qualities, flight controls, and aerodynamics. In addition, human factors engineering carries heightened importance. Specifically, the human pilot's ability to retain control of the aircraft during violent although non-departure maneuvers, to aid in preventing departure, and possibly to effect a successful departure or spin recovery while experiencing disorienting

accelerations and angular rates is manifest. An offshoot of human factors development, displays technology, is also very important.

A paramount goal of this report is to draw attention to departure research by describing work that has already been accomplished and by reviewing what knowledge already exists in the area. It is hoped that this report will stimulate enough understanding and interest that the motivation for further work will be clearly evident. One of the continual goals of studies in this area, aside from attempting to achieve the obvious maneuvering benefits, is to quantify new and usable (pertinent and up-to-date) flying qualities specifications. An eventual goal is to put forth a comprehensive high angle of attack specification, or at least a document for inclusion as the high angle of attack/departure section of some specification in the offing, such as MIL-STD-1797 (Reference (1)).

## 1.2 Purpose

This report is intended for use as a collection and analysis of diverse data gathering, empirical, and analytical approaches to the high angle of attack problem; as a compendium of several methods of defining aircraft departure and spin susceptibility; as a reference for spin definition and spin recovery enhancement; as a review of specifications, regulations, and design guides as they pertain to high angle of attack flight; and as a medium for expounding where tomorrow's high angle of attack investigative attention should focus.

## 1.3 Approach

Because a cognizance of the fundamentals of high angle of attack aerodynamics is necessary to understand the causes and mechanisms of departure, the first section of this report presents a comprehensive review of aerodynamic theory pertinent to high angle-of-attack aerodynamics and the stall. Where possible, throughout this section ("High Angle-of-Attack Aerodynamics and Stall"), and the

ones to follow, the principles discussed will be tied into their effect on high-angle-of-attack aircraft design applications.

This section will also address in detail the phenomena of aircraft spin. This section includes a discussion of the aerodynamic factors that cause spin, and the three phases associated with a spin; namely, the incipient phase, the fully developed phase and the spin recovery phase.

The next section expounds on the various experimental and analytical techniques used to predict the dynamic characteristics of aircraft at high angles-of-attack. The methods covered in this section include, conventional wind tunnel testing, rotary balance wind tunnel testing, dynamic model flight testing, piloted simulation and full-scale aircraft flight testing.

The final section of this report examines the current military specifications that address high angle-of-attack aircraft flight characteristics. A compilation of the major departure susceptibility criteria is also included. Each of the major criteria are discussed with a brief description of its derivation and application.

## 2.0 HIGH ANGLE-OF-ATTACK AERODYNAMICS AND STALL

The effects on an aircraft as it enters and negotiates high angle-of-attack flight are by nature nonlinear. It is an accepted fact for fighter aircraft that high angle of attack stability and control, stalling characteristics, and spin tendency are based on all aircraft components (wings, tail, forebody shape, engines) and the interactive effects they have on one another. To ignore the effects of any component or combinations of components may prove to be a gross assumption, especially for modern military aircraft with unconventional control surface combinations.

### 2.1 High Angle-of-Attack Terminology

The following definitions are taken from MIL-S-83691A, "Military Specification: Stall/Post-Stall/Spin Flight Test Documentation Requirements for Airplanes," (Reference (2)). Wording and interpretation of the definitions for these terms varies, but in general are accepted by the Flying Qualities Community.

Stall angle of attack: the angle-of-attack for maximum usable lift at a given flight condition ( $\alpha_s$ , defined in MIL-F-8785, see section 2.2.1).

Stall warning: the natural airplane behavior or artificial signal(s) that indicates to the pilot the approach of maximum usable lift. Normally, the onset and development of stall warning shall be described as a function of angle-of-attack or airspeed for a given airplane state.

Wing rock: uncommanded lateral-directional motion, viewed by the pilot primarily as roll oscillation.

Bucking: uncommanded pitching oscillation.

Nose slice: uncommanded lateral-directional motion viewed by the pilot primarily as a divergence in yaw.

Pitch-up: uncommanded, sudden increase in angle-of-attack.

Post-stall: the flight regime involving angles of attack greater than nominal stall angles of attack.

The airplane characteristics in the post-stall regime may consist of several more or less distinct types of airplane motion: departure, post-stall gyration, spin, and deep stall.

Loss-of-control-warning: the natural airplane behavior or artificial signal(s) that indicate to the pilot the approach of loss-of-control. As per stall warning, the onset and development of loss-of-control warning shall be described as a function of angle-of-attack or airspeed for a given airplane state.

**Note:** Natural stall warning and loss-of-control warning encompass successive angle-of-attack ranges. For some designs or flight conditions, departure may occur with only a slight increase in angle-of-attack beyond that for maximum usable lift. In such cases, stall warning and loss-of-control warning become practically synonymous and descriptions of flight characteristics should emphasize this fact when appropriate. However, in those cases when departure occurs at a significantly higher angle-of-attack than that for maximum usable lift, natural stall warning and loss-of-control warning should be independently discussed.

Departure: the event in the post-stall flight regime which precipitates entry into a post-stall gyration, spin, or deep stall condition. The departure may be characterized by divergent, large-amplitude, uncommanded aircraft motions, such as nose slice or pitch-up. Departure is synonymous with complete loss-of-control.

Post-Stall Gyration (PSG): uncontrolled motion about one or more airplane axes following departure. While this type of airplane motion involves angles of attack higher than the stall angle, lower angles may be encountered intermittently in the course of the motion. When the airplane motion is other than random about all axes, a further classification of the PSG may be used for descriptive purposes. Such terms as snap roll, rolling departure or tumble may be appropriate; however, they should all imply a PSG. The PSG is differentiated from a spin by the lack of a predominant, sustained yawing motion and by the potential for exhibiting sub-stall angles of attack,

Spin: a sustained yaw rotation at angles-of-attack above stall. The rotary motions of the spin may have oscillations in pitch, roll and yaw superimposed upon them. The incipient spin is the initial, transitory phase of the motion during which it is not possible to identify the spin mode. The developed spin is the phase of the spin during which it is possible to identify the spin mode. The fully developed spin is attained when the trajectory has become vertical and no significant change is noted in the spin characteristics from turn to turn.

Erect Spin: characterized by positive angle-of-attack and load factor.

Inverted Spin: characterized by a negative angle-of-attack and load factor.

Flat Spin: most serious type of spin in which the pitch attitude,  $\theta$ , is nearly zero and the angle-of-attack approaches 90 degrees.

**Note:** Spin modes may be identified by average values of angle-of-attack and body axis yaw rate and by the magnitude of the three-axis angular oscillations. One modifier from each group listing in Table I may be used to characterize the mode.

TABLE I SPIN MODE MODIFIERS (Reference (2)).

| SENSE    | ATTITUDE        | RATE            | OSCILLATIONS          |
|----------|-----------------|-----------------|-----------------------|
| Erect    | Extremely Steep | Slow            | Smooth                |
| Inverted | Steep           | Fast            | Mildly Oscillatory    |
|          | Flat            | Extremely rapid | Oscillatory           |
|          |                 |                 | Highly Oscillatory    |
|          |                 |                 | Violently Oscillatory |

Deep stall: an out-of control flight condition in which the airplane is sustained at an angle of attack well beyond the  $\alpha_s$  value while experiencing negligible rotational velocities. The deep stall may be distinguished from a PSG by the lack of significant motions other than a high rate of descent.

Extremely susceptible to departure: departure from controlled flight will generally occur with the normal application of pitch control alone or with small roll and yaw control inputs.

Susceptible to departure: departure from controlled flight will generally occur with the application or brief misapplication of pitch and roll and yaw controls that may be anticipated in operational use.

Resistance to departure: departure from controlled flight will only occur with a large and reasonably sustained misapplication of pitch and roll and yaw controls.

Extremely resistant to departure: departure from controlled flight can only occur after an abrupt and inordinately sustained misapplication of gross, abnormal, pro-departure controls.

Recovery: the transition from out-of-control conditions to controlled flight. This is normally considered to be that period between pilot initiation of recovery controls and that point when the angle-of-attack is at a value below stall and no significant, uncommanded angular motions remain.

**Note:** The out-of-control recovery procedure requirements specified in Section 3.4.2 of MIL-S-83691A are directed primarily toward departures at a positive angle-of-attack rather than at a negative angle-of-attack. Erect flight is emphasized because out-of-control occurrences in training and operational activities usually take place more often and with more susceptibility at a positive angle-of-attack. Also, recovery capabilities from erect out-of-control conditions (positive angle-of-attack) are usually less favorable than from inverted situations (negative angle-of-attack) and the recommended recovery procedures correspondingly more extensive. The out-of-control recovery procedure shall always apply to loss of control from erect flight, but it may serve for both erect and inverted flight if the recovery procedures are identical (neutral controls for example). Also, an airplane may experience a

departure at negative angle-of-attack that can be easily countered by a simple relaxation of pro-departure controls. In this instance, an inverted out-of-control recovery procedure may not be warranted since an adequate flight characteristics description in the Flight Manual would suffice. However, if the airplane exhibits a departure at negative angle-of-attack that requires an intricate recovery procedure, consideration should be given to specifying both an erect and inverted out-of-control recovery procedure. Roll and yaw control displacements are allowable steps in the recovery procedures for erect and inverted spins in the event the out-of-control recovery procedure does not satisfy spin recovery requirements.

A separate recovery procedure may be proposed for the deep stall since this out-of-control mode is of a unique nature and may require recovery techniques (prolonged nose down pitch control, control stick pumping, asymmetric thrust, configuration changes, for example) that are significantly more extensive than normal stall recovery techniques and totally distinct from the out-of-control and spin recovery requirements.

Dive pullout: the transition from the termination of recovery to level flight.

Total Recovery Altitude: the sum of the altitude losses during the recovery and dive pullout.

Recovery Rolls: uncommanded rolling motions near or below stall angle-of-attack that may occur during the recovery phase of the spin or PSG.

## 2.2 The Stall

"Good" stall behavior of a wing is of great importance in the design of an aircraft for both mission performance and stability and control reasons. Performance considerations drive the lift-coefficient of the wing to its highest value ( $C_{L_{MAX}}$ ) while stability and control considerations are concerned with the forces and moments acting on the aircraft near and at stall. In this section, the discussion of the wing-stall phenomenon is broken down into four sub-sections and expanded in more detail. First a

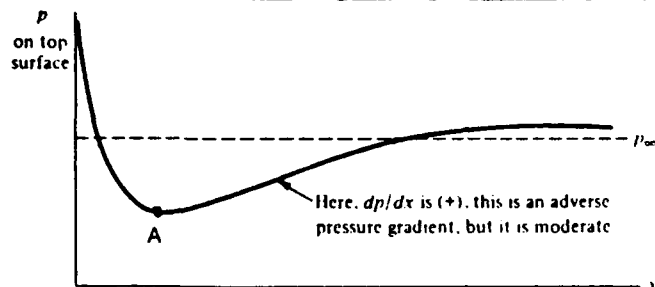
definition of stall will be presented. The next section will present background material explaining the fluid dynamics that causes flow separation and the final two sections will discuss the effects of wing planform geometry and stall control devices on aircraft stall characteristics.

#### 2.2.1. Definition

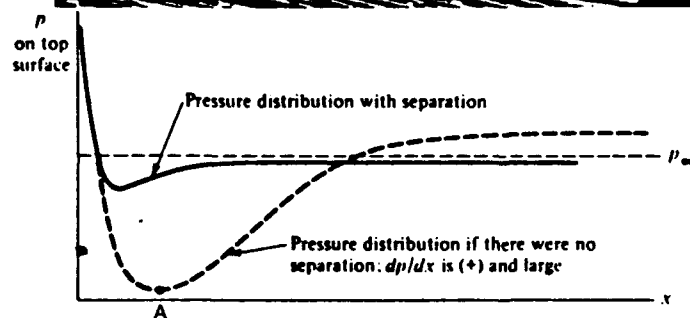
As defined previously, a lifting surface (wing, stabilizer, etc.) is said to be "stalled" when the lifting surface exceeds the angle-of-attack value associated with the maximum usable lift for a given test condition. Because a lifting surface stalls due to flow separation, (which is not totally predictable by either wind tunnel tests or analysis) the stall phenomena can be unpredictable (see Figure 1). For this reason, the definition of stall angle-of-attack as given above must be broadened to account for actual aircraft flight characteristics that might preclude the use of the above stall angle-of-attack definition. The flying qualities Military Specification (MIL-F-8785) does this by giving the following three definitions of stall angle-of-attack,

- Angle-of-attack for the highest load factor, normal to the flight path, that can be attained at a given speed or Mach number.
- Angle-of-attack for a given airspeed or Mach number at which uncommanded pitching, rolling or yawing occur.
- Angle-of-attack for a given airspeed or Mach number at which intolerable buffeting is encountered.

The lowest angle-of-attack based on these three definitions defines the stall angle.



a. Flow Past an Airfoil at Low Angle-of-Attack



b. Flow Past an Airfoil at a Large Angle-of-Attack  
(Note, the flow separation on the top surface)

Figure 1. Aerodynamic Stall of an Airfoil (Reference (3) and (4))

### 2.2.2. Fluid Dynamics of Flow Separation

In this sub-section three questions are addressed concerning the fluid dynamics of airfoil flow separation. They are: 1) Why does a flow separate from a surface? 2) What are the consequences of flow separating over an airfoil? 3) What fluid dynamic parameters influence flow separation? The answer to the first question is combined in the concepts of an adverse pressure gradient ( $dp/dx > 0$ ) and the velocity profile through the boundary layer. Prandtl showed that flow separation (like that in figure 1b) is caused by excessive momentum loss of the fluid near the wall in a boundary layer trying to move downstream against increasing pressure (i.e., adverse pressure gradient). The boundary layer fluid dynamic model introduced by Prandtl, considers the flow over a surface to consist of two layers. The first layer is a thin region close to the surface in which the viscosity effects are confined. Outside this layer the fluid is regarded to be inviscid for the most part. Both theory and experiment have supported Prandtl's boundary-layer flow model (Reference (4)). An illustration of this flow model over an airfoil is depicted in figure 2 below.

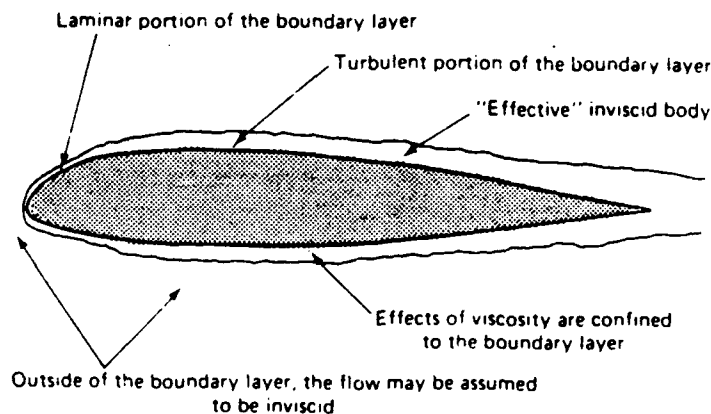


Figure 2. Prandtl's Boundary Layer Flow Model Over an Airfoil (Reference (5))

Figure 3 below shows a typical sequence of the boundary layer profiles as it progresses along the top of a lifting body.

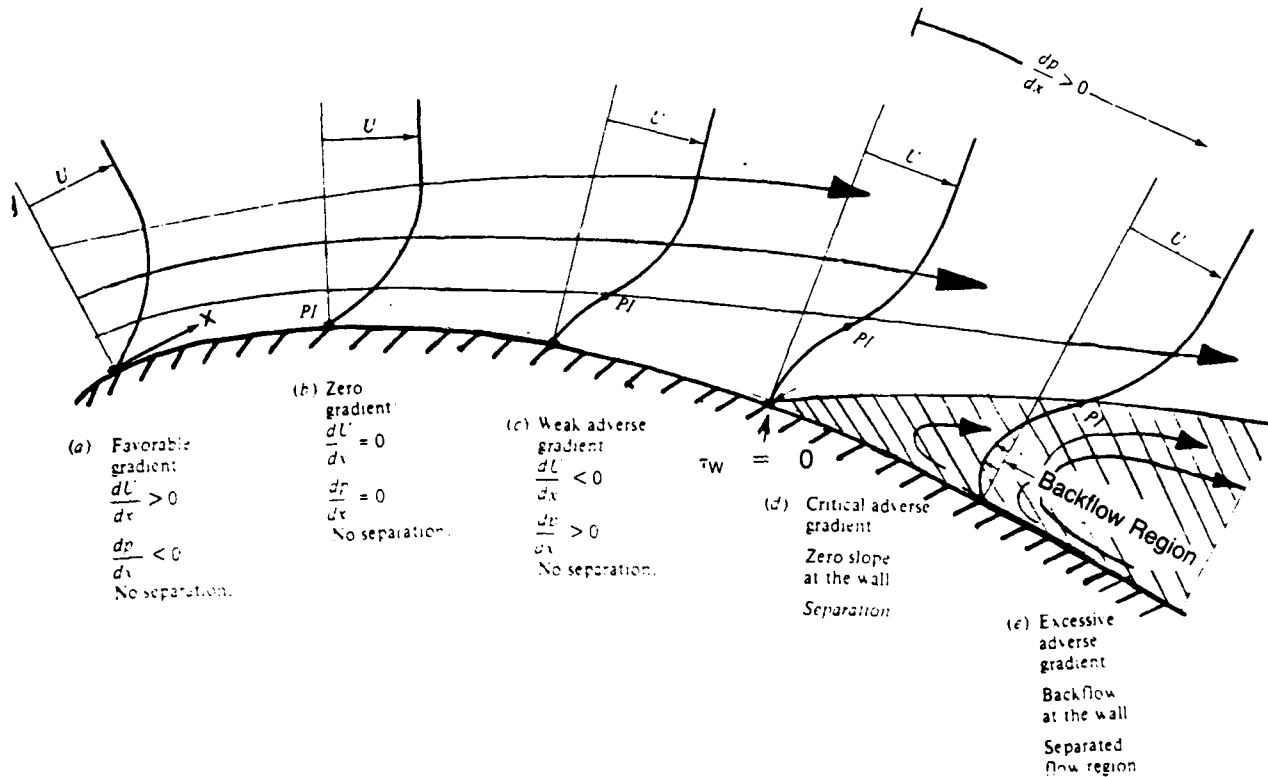


Figure 3. Effect of Pressure Gradient on Boundary Layer Profiles  
 (PI = Profile Point of Inflection) (Reference (6))

A favorable pressure gradient occurs on the front of the body (a), zero pressure gradient occurs just upstream (b), and an adverse gradient develops progressively as it moves to the rear of the body (c)-(e). The resulting loss of momentum of the fluid is especially strong near the surface where the fluid velocity within the boundary layer is low due to frictional forces. Hence, with the presence of an adverse pressure gradient (see plot of  $p$  vs  $x$  in figure 1b)  $\partial u / \partial y$  near  $y = 0$  becomes smaller and smaller the greater the distance over which the adverse gradient persists. At some distance downstream of the pressure minimum (point (a) in Figures 1 and 2) a point is reached where a moderate adverse gradient exists. Here the wall shear stress,  $\tau_w$ , is exactly zero,  $(\partial u / \partial y) |_{y=0} = 0$  (point D of Figure 3).

This is defined as the separation point because beyond this point (point (d)) any stronger gradient will cause the direction of flow to reverse near the surface, the boundary layer to thicken greatly and the main flow separates from the surface (see also Figure 1b).

The overall flow pattern, when separation occurs, depends greatly on the particular flow. The upstream flow behind the separation point is normally fed by recirculation of the separating fluid (see Figure 4). Rotational flow in this case is not confined to a thin layer next to the boundary plus a thin wake. Vorticity introduced in the boundary layer is carried by the separated flow into regions originally assumed to be irrotational to obtain the inviscid flow solution. Thus the presence of separation significantly modifies the original flow model and the inviscid flow can no longer be analyzed without taking into account the boundary layer effects.



Figure 4. Flow Around an Airfoil with Separation (Reference (7))

Trailing edge separation is progressive with angle-of-attack (corresponding to the associated increased upper-surface adverse pressure gradient strength) and is usually characterized by a gradual stall. For some airfoils however, the separation point leaps forward and stall occurs rapidly and dangerously (see Figure 5). More will be said concerning the effect of the airfoil shape on stall characteristics in a later section.

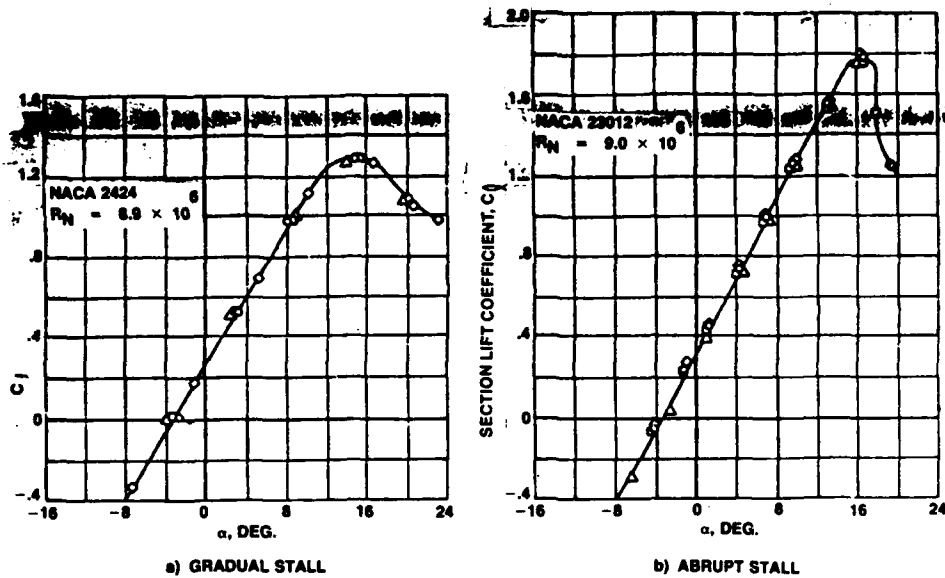


Figure 5. (a) Lift Curve Slope for A Gradual Airfoil Stall

(b) Lift Curve Slope for An Abrupt Airfoil Stall (Reference (8))

This concludes the discussion of the first posed question concerning the causes of flow separation from a surface and leads into the next question of, "What are the consequences of flow separating over an airfoil?" Two consequences of flow separation over an airfoil were illustrated in figure 1 which showed a comparison of the pressure distribution of a flow that has separated versus one that has not. The first consequence is the pressure distribution with separation, given by the solid line, does not dip to as low a pressure minimum and secondly the pressure near the trailing edge does not recover to a value above  $P_x$ . The consequences of these two facts is explained by the solid and dashed arrows of figure 6. The arrows qualitatively represent the pressure distributions about an airfoil for separated and attached flow respectively.

The first consequence of separation is a loss of lift. Separation does not affect the bottom surface (for this particular airfoil) but comparing the solid and dashed arrows of the figure on the top surface just downstream of the leading edge, shows that the solid arrows indicate a higher pressure. Because the

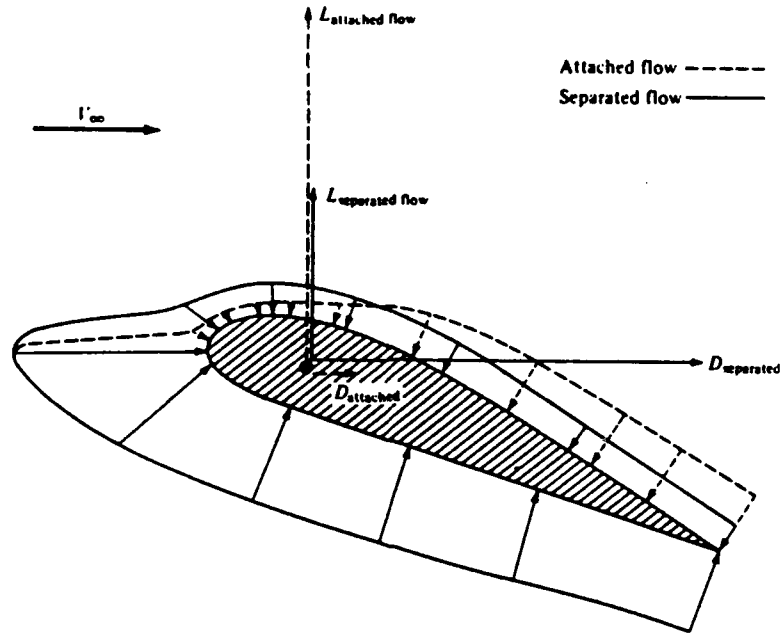


Figure 6. Comparison of Pressure Distribution of Separated and Attached Flow Over an Airfoil (Reference (3))

net lift force results from the pressure differential between the upper and lower surfaces (vertical component), the lift force is lower when the flow separates (i.e., the pressure differential is less). The second consequence of separation is a large increase in drag commonly referred to as, "pressure drag due to separation." The pressure drag is derived from the altered pressure distribution due to separation. The integration over the surface of the downstream horizontal components (in the drag direction) of the static pressure forces acting normal to the elements of the surface gives the pressure drag. Recall that pressure drag (also referred to as "form" drag) is quite different from the skin friction drag arising from frictional stresses acting tangentially on the body.

A qualitative result of the detached flow is that the resulting wake becomes turbulent and the vortical flows produced contribute unsteady effects. Common pilot observed aircraft characteristics associated with the stall such as, buffet (ranging from light to heavy), wing rock or loss of control about any axis such as uncontrollable pitch-up or pitch down, "wing drop" or directional "slicing," may define the actual stall. These characteristics are label descriptors that directly indicate the unpredictable

vortical flows and unsteady effects present in the stall regime of flight. Presently, boundary-layer theory can predict the separation point but cannot accurately estimate the usually low pressure distribution in the separated region. The study of turbulence and separated flow is a major effort in fluid dynamics today. For a more detailed discussion on the new techniques now being developed for analyzing the strong interaction effects caused by separated flows the reader is referred to references (9)-(11).

Finally the question of, "What fluid dynamic parameters influence flow separation?" will be discussed. Three primary fluid flow characteristics will be considered in the context of their effect on flow separation. They are: 1) laminar vs. turbulent boundary layer flow, 2) Reynolds number effects and 3) effects of lifting surface pitch rate ( $\dot{\alpha}$ ).

The boundary layer is defined as the layer adjacent to a body within which the major effects of viscosity are concentrated (i.e., the viscous forces are of the same order of magnitude as the inertial forces). Figure 7 illustrates the boundary layer profile near a solid surface.

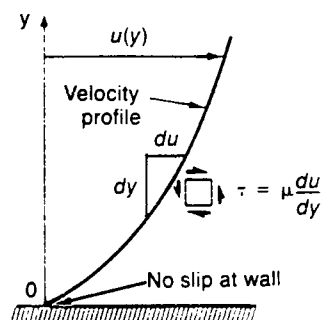


Figure 7. Newtonian Shear Distribution in a Boundary-Layer Near a Wall (Reference (3))

The shear stress ( $\tau$ ) is proportional to the slope of the velocity profile and is greatest at the surface. Also within this thin layer the velocity of the fluid increases from zero at the wall to its full value which corresponds to external frictionless flow. This can be seen because the velocity gradients become so small outside the boundary layer that the shear stresses acting on a fluid element are negligible. Thus the effect of viscous terms may be ignored for the flow external to the boundary layer (i.e., to a high degree it may be regarded as inviscid).

The boundary layer is characterized by two types of flow — laminar and turbulent. Laminar flow is characterized by smooth and regular streamlines and a fluid element moves smoothly along a streamline. On the other hand, turbulent flow is characterized by streamlines that break up and a fluid element moves in a random and irregular fashion (Reference (3)). Two important fluid characteristics that discern these two types of flow and have a significant impact on where flow separation will occur are: (1) the boundary-layer velocity profiles and, (2) the local shear stress,  $\tau_w$ . Turbulent boundary layers are characterized by higher velocities near the surface than the laminar profile and also exhibit greater shear stress than laminar flow. The mathematical formulation stating these facts has not been presented, instead the comparative differences between these two types of flow is illustrated in figure 8. For a more detailed treatment of the subject see reference (7). As noted in figure 8, at a given

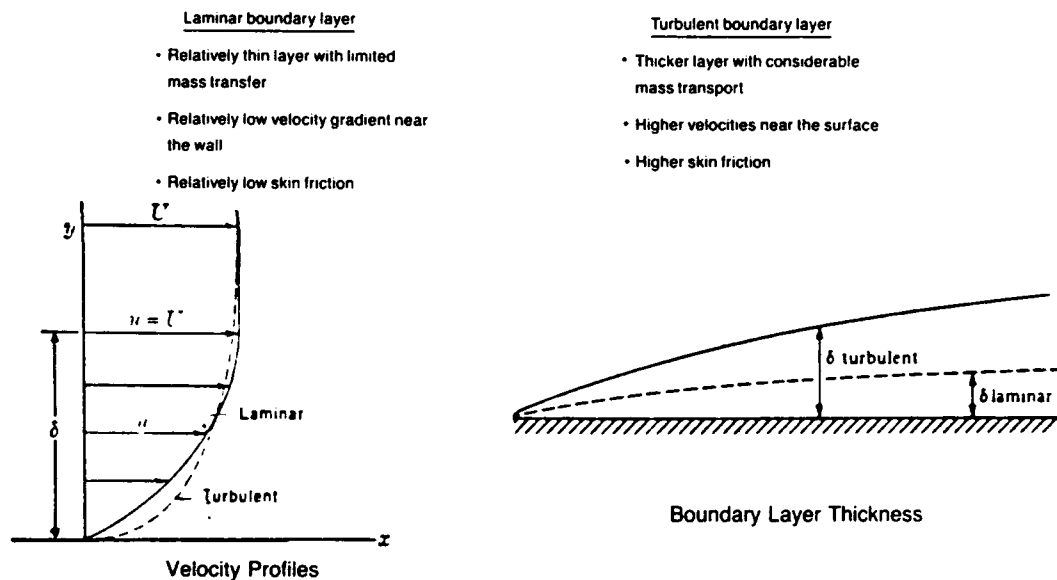


Figure 8. Comparison of Laminar and Turbulent Boundary Layers. (references (3) and (12))

distance from the surface, the velocity of a fluid element in a turbulent boundary layer is higher than in a laminar boundary layer. Hence there is more flow kinetic energy nearer the surface and therefore is less likely to separate than laminar boundary layers. This is a very important fact. While maintaining a laminar flow as long as possible is an advantage from a drag standpoint (less shear stress), it does not benefit stall characteristics, due to the higher probability of flow-separation. It is apparent that the longer

the flow remains intact, the further delayed the stall, the higher the angle-of-attack, and as a result the greater the corresponding value of  $C_{L_{max}}$  at stall. More will be said concerning boundary layer control for achieving higher  $C_{L_{max}}$  values and better stall characteristics in the section on stall control devices (section 2.2.5).

As mentioned earlier, the fluid-flow over the lifting surface of interest in most cases can be divided into two regions: (1) a viscous boundary layer adjacent to the surface and (2) an essentially inviscid flow outside the boundary layer. This model of the flow-field, and whether the flow is characterized by laminar or turbulent flow characteristics is very sensitive to the dimensionless similarity parameter termed Reynolds number. Reynolds number is the primary parameter correlating the viscous behavior of Newtonian<sup>1</sup> fluids. It is a measure of the ratio of the inertial forces to viscous forces acting on a fluid element and is defined by equation (1).

$$Re = \frac{\rho V \ell}{\mu} = \frac{V \ell}{\nu} \sim \frac{\text{Inertial Forces}}{\text{Viscous Forces}} \quad \text{EQ (1)}$$

In equation (1)  $V$  and  $\ell$  represent the characteristic velocity and length scales of the flow and  $\nu$ , the kinematic viscosity, is a property of the fluid medium defined by the ratio of the fluid density,  $\rho$ , to the coefficient of viscosity<sup>1</sup>,  $\mu$ .

For the purposes of this discussion, the effects of Reynolds number on flow separation will be confined to the range of Reynolds number that is realistic and of primary concern to the aircraft aerodynamicist. Flows characterized by Reynolds number on the order of  $10^4$  or greater will be considered. Furthermore it will be assumed that the body immersed in the fluid is streamlined (the

---

<sup>1</sup> See Appendix A — Glossary of Defined Terms

affect of airfoil shape on flow-separation will be addressed in the next section, "Influence of Geometric Wing Planform Parameters") and negligible compressibility effects are present (if compressibility affects exist, energy exchanges and temperature differences must be included (See reference (13)).

In discussing laminar and turbulent boundary layer formation over an airfoil the following formation is typical. The flow always starts out from the leading-edge as laminar. Then as reference (14) describes it, "there is some point downstream of the leading edge where the laminar boundary layer becomes unstable in the sense that a small disturbance may generate imbalances in the forces acting on the fluid elements, causing the disturbance to grow as it proceeds downstream in the flow. A wave motion occurs, the amplitude of which grows as it propagates downstream and unless some stabilizing influence intervenes transition to turbulent boundary layer flow follows."

The transition from laminar to turbulent flow in the boundary layer is pictorially shown in figure 9 for a flat plate.

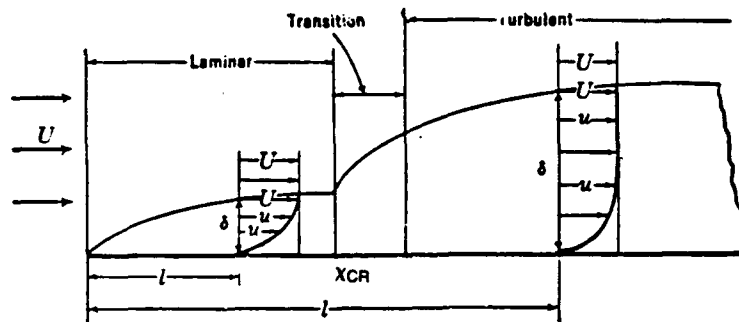


Figure 9. Transition From Laminar to Turbulent Flow (boundary layer thickness exaggerated for clarity) Over a Flat Plate (Reference (9))

The transition is most clearly discernible by a sudden and large increase in the boundary-layer thickness and in the shearing stress near the surface. The value of  $x$  where transition is said to take place is called the critical value,  $x_{CR}$ . In turn,  $x_{CR}$  allows the Critical Reynolds Number for transition to be defined as,

$$Re_{CR} = \frac{\rho_x V_x x_{CR}}{\mu_x}$$

In general any influence that decreases the critical Reynolds number also hastens transition. As can be seen in figure 10, at Reynolds numbers above approximately  $2 \times 10^5$  the boundary layer may be either laminar or turbulent. The reason for the overlap is the fact that at any Reynolds number greater than the critical value, disturbances generated for instance by surface roughness or turbulence can cause the transition from a laminar to turbulent boundary-layer.

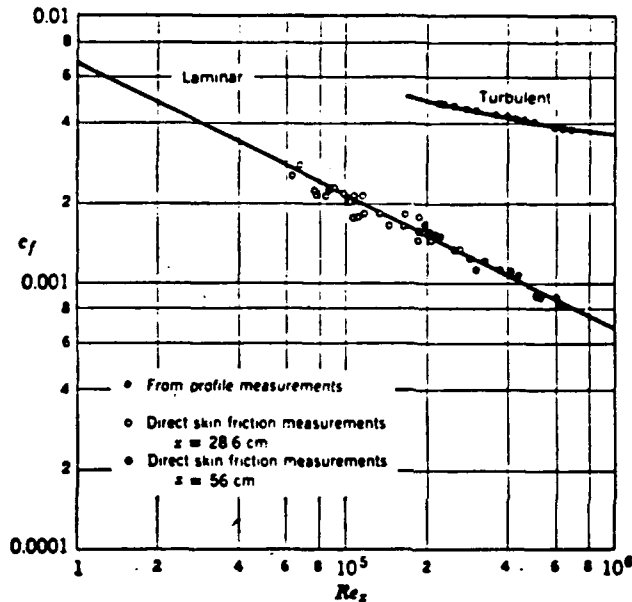


Figure 10. Local Skin Friction in Incompressible Flow. The lower curve refers to laminar flow; the upper to turbulent. (Dhawan, 1953, *Courtesy of NASA*) (Reference (14))

As indicated by the flow critical Reynolds number, the following three separation phenomena are possible.

At large Reynolds numbers (typically greater than  $1 \times 10^6$ ) the transition is spontaneous and flow-separation is delayed (if it occurs) to the trailing-edge region. At very low Reynolds number ( $Re < 0.5 \times 10^5$ ) the laminar layer may separate and stay separated. This phenomenon is referred to as laminar separation. A third possible transition scenario, primarily occurring at moderate values of

Reynolds number (approximately  $\sim 1 \times 10^6$ ), involves laminar separation followed by turbulent re-attachment. In this case there forms a so-called separation bubble (see figure 11) and as a result, the boundary-layer is much more unstable than the previous attached one at the less "energerized" lower Reynolds number flow.

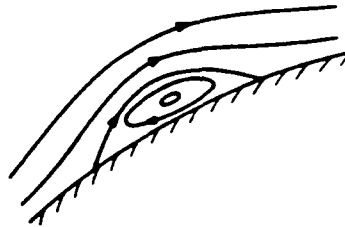


Figure 11. Mean Streamline Pattern in Laminar Separation Followed by Turbulent Reattachment (Reference (12))

Laminar separation is usually not permanent at flight values of the Reynolds number except when it occurs on some wing sections near the leading edge under conditions corresponding to maximum lift, (Reference (15)). Otherwise, the flow returns to the surface almost immediately as a turbulent layer. This turbulent boundary layer extends to the trailing edge and remains attached except at sufficiently high angle-of-attack. Figure 12 illustrates these three scenarios for the case of a circular Cylinder.

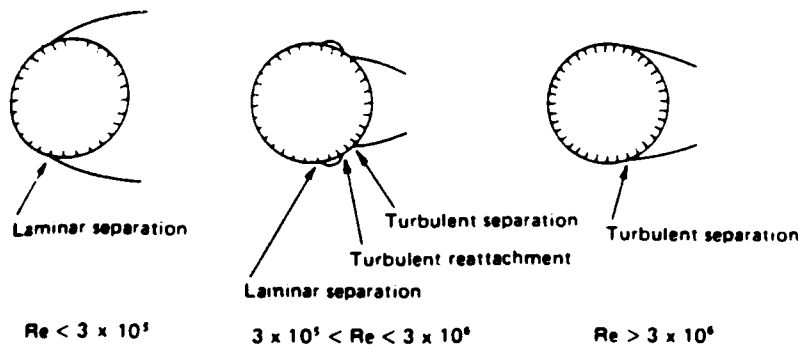


Figure 12. Separation Positions for Various Reynolds Number Ranges (Reference (12))

Figure 13 illustrates how the lift curve shape can be affected by Reynolds number for moderate and thick airfoils. For thin airfoils where laminar separation is common, it has been found that laminar separation occurs independently of Reynolds number. As expected, the higher Reynolds number cases

show an increase in  $C_{L_{MAX}}$  reflective of the "added" energy in the flows. The Reynolds number effects are seen to be very influential in defining the stall region of the lift curve. This fact becomes very important when interpreting wind tunnel test data obtained at different Reynolds numbers (than actual flight condition) using models that are geometrically similar but of different size.

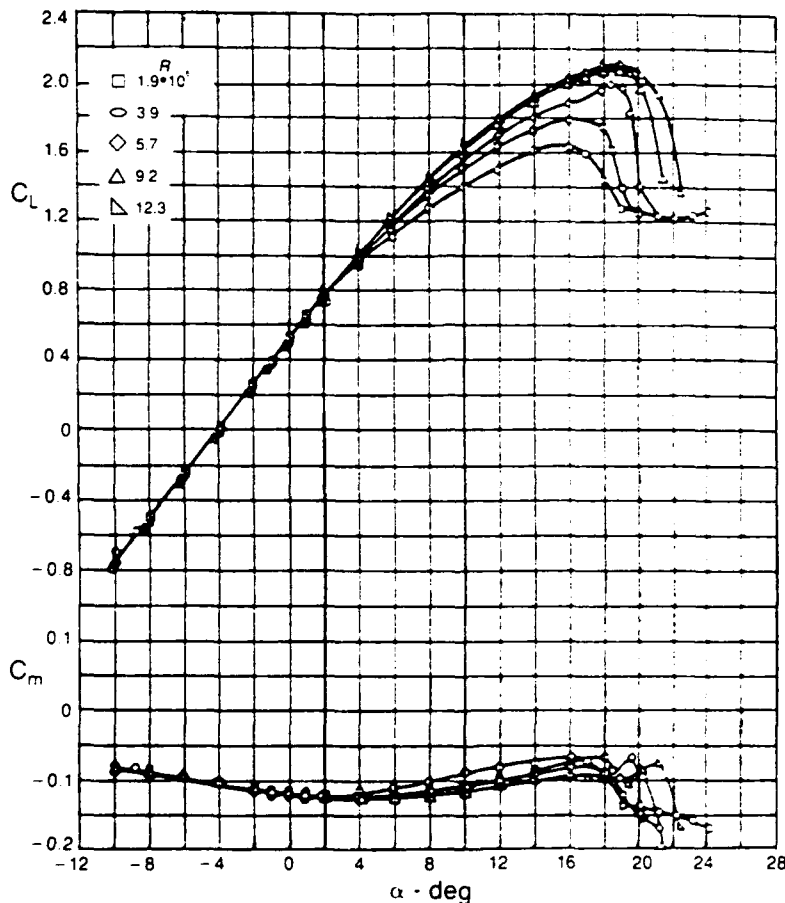


Figure 13. Effect of Reynolds Number on Section Characteristics of the GA(W)-1 Airfoil Model Smooth,  $M = 0.15$  (Reference (16))

Of course the phenomenon of flow separation is not limited to the three factors just discussed. Other factors influencing separation associated with the flow characteristics include, Mach number, turbulence and noise. Since transition is the result of amplification of disturbances, those factors that

influence the magnitude of the disturbances will also effect the separation phenomenon. Some of the factors known to effect the magnitude of the disturbances include, roughness of the surface, surface temperatures and surface shape.

Except for surface shape, these factors just mentioned will not be discussed. Instead the reader is referred to references (3) and (13) for a more thorough treatment on the subject of factors influencing transition and flow-separation.

The last factor influencing flow separation (i.e. stall) to be addressed is the effects of lifting surface pitch rate ( $\dot{\alpha}$ ). References (17) and (18) document several instances where substantial overshoot of the static maximum lift coefficient ( $C_{L_{max}}$ ) occur for aircraft penetrating the stall at non-zero angle-of-attack rates ( $\dot{\alpha} \neq 0$ ) (Reference (19)). As discussed previously, when and where separation occurs is determined by the boundary-layer profile shape and the adversity of the local pressure gradient. The overshoot of  $\alpha_s$  (and correspondingly  $C_{L_{max}}$ ) for a pitching airfoil at low Mach numbers is almost entirely caused by the pitch rate induced flow acceleration on the leeward side which causes a delay in the adverse pressure gradient formation and thus delay flow separation (Reference (19)). The decrease in the "adversity" of the pressure gradient is noted as being proportional to the dimensionless frequency induced plunging factor ( $\bar{c}\dot{\alpha}/U_\infty$ ).

A second oscillation induced effect that has been found to contribute to the overshoot of the static  $C_{L_{max}}$  value, is the effect of the induced change on the effective Reynolds number or turbulence level of the flow (Reference (19)). Oscillatory stall data for airfoils (Reference (20)) has shown that the oscillating airfoils seem to have a much higher turbulence level than the static airfoils (Reference (21)). This effect is also to a first approximation proportional to the dimensionless frequency-induced plunging factor, ( $\bar{c}\dot{\alpha}/U_\infty$ ). Figures 14a and 14b depict the angle-of-attack overshoot,  $\Delta\alpha_s$ , for leading and trailing edge type stalls respectively.

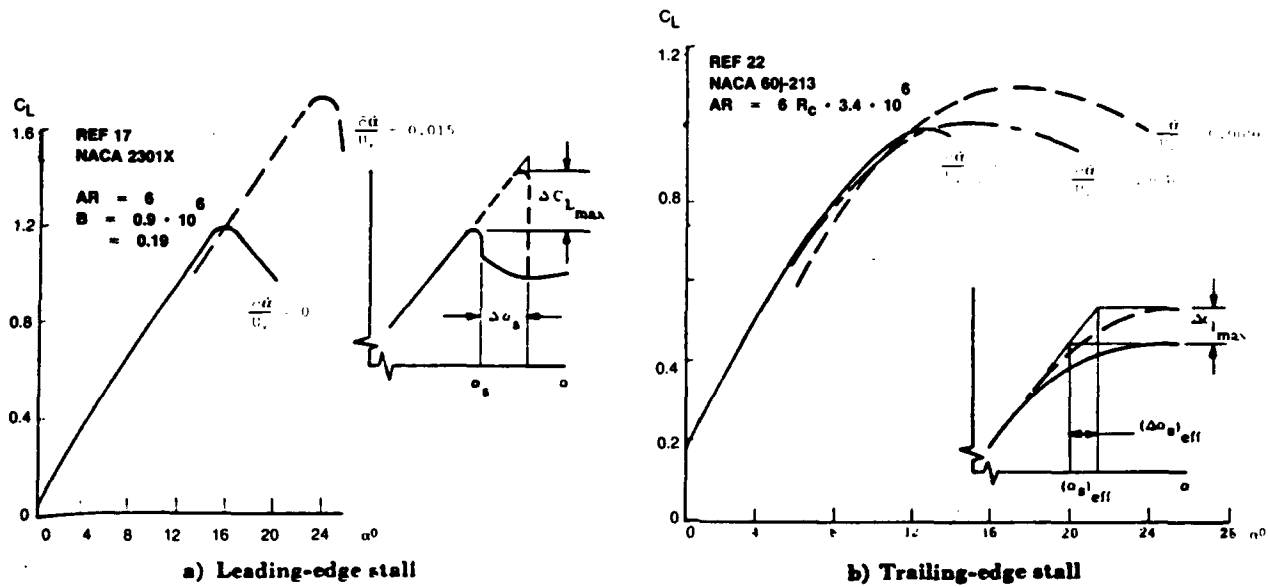


Figure 14.  $C_{L,MAX}$  — Overshoot Characteristics for Leading- and Trailing-Edge Stall (Reference (19))

These same two factors that cause large dynamic overshoot of static stall, are also responsible for the "undershoot" static reattachment phenomenon. Figure 15 illustrates the complete dynamic loop effects on normal force characteristics for trailing-edge separation.

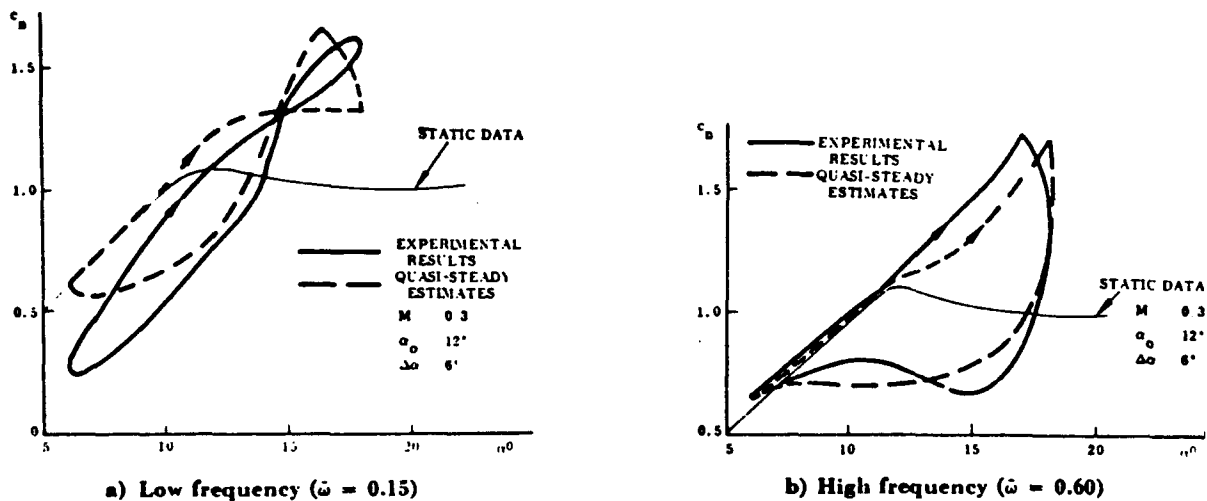


Figure 15 Complete Dynamic Loop Effects on Normal Force Coefficient as a Function of Frequency. (NACA 0012 Airfoil Section, Reference (23))

The dashed-line in these figures represent quasi-steady estimates to predict the unsteady airfoil characteristics versus instantaneous angle-of-attack. The quasi-steady method applied here utilizes the limiting value of  $Re \rightarrow \infty$  to obtain the "upstroke" unsteady estimates. Similarly the limiting characteristics for  $Re \rightarrow 0$  are used to predict the reattachment characteristics. A thorough discussion on this particular quasi-steady method for predicting dynamic characteristics for airfoils is given in references (19) and (24).

A more recent review of research in dynamic stall is presented in reference (25). In this treatment of the subject, Carr sites the work of Ham and Gorelick (1968) (Reference (26)) which showed that additional lift could be created by rapid pitching of airfoils and that this additional lift was associated with a vortex formed on the airfoil during the unsteady motion. Taken from reference (25) figure 16 depicts the development of  $C_N$  and  $C_M$  versus angle-of-attack and the corresponding boundary layer behavior for a dynamically stalling airfoil. The data shown is for a NACA 0012 airfoil oscillating in pitch, but the stall development is typical of virtually all airfoils experiencing fully developed dynamic stall (Reference (25)). As indicated by point (c) in figure 16, the vortex shedding process begins near the leading edge of the airfoil after the viscous flow no longer remains thin and attached. As the vortex enlarges and moves down the airfoil, strong pitching moment effects are induced (d, f) producing the phenomenon known as dynamic stall (Reference (25)). Reference (25) notes that most of the research concerning the events of dynamic stall has been performed on airfoils oscillating in pitch. Further efforts directed toward evaluating different types of motion more closely related to fighter aircraft maneuvering are required. Additionally, the measurement of the details of the viscous flow that includes the influence of Reynolds number, compressibility effects, and the effects of three dimensionality are recommended by reference (25) as necessary steps to increase the level of understanding associated with dynamic stall.

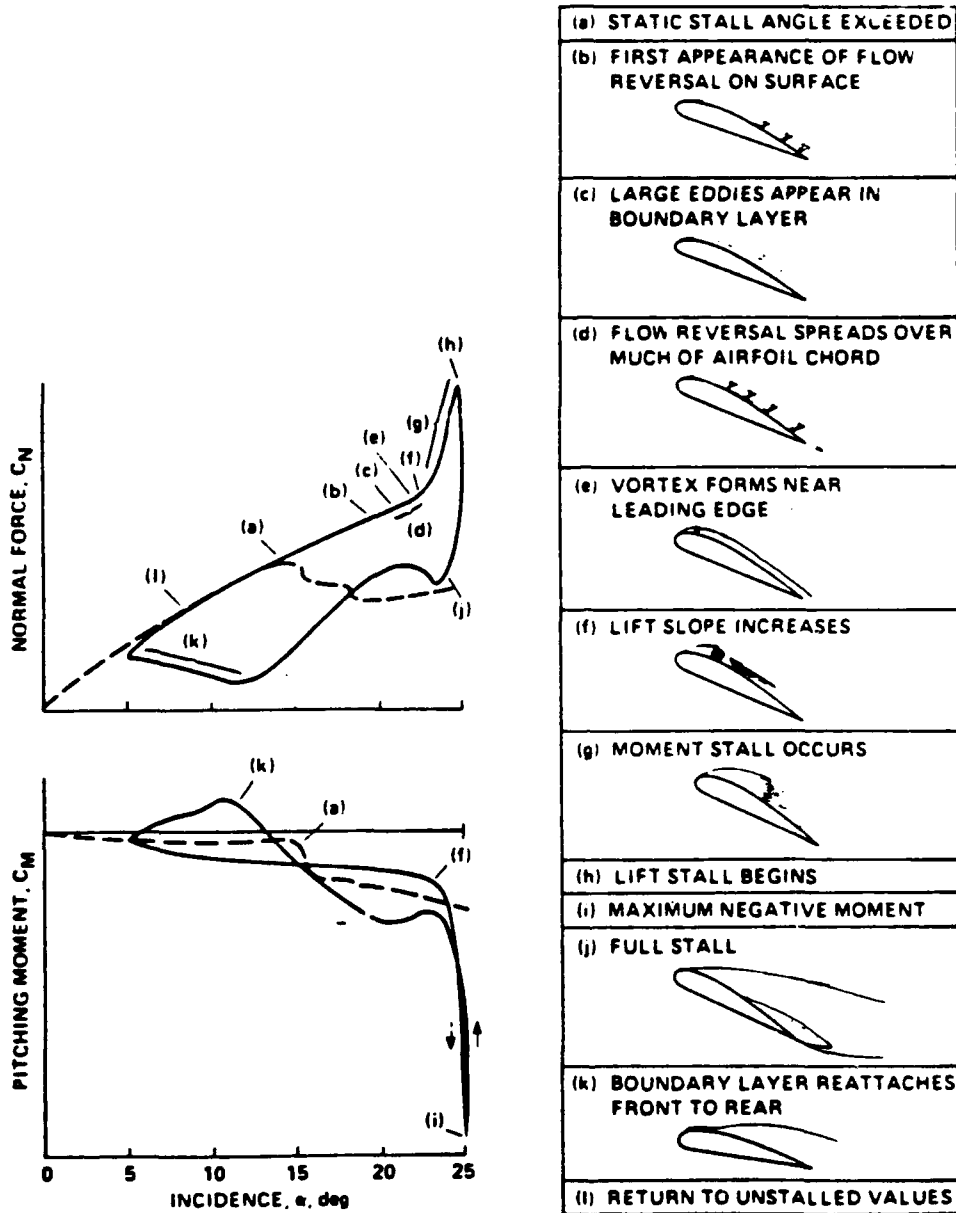
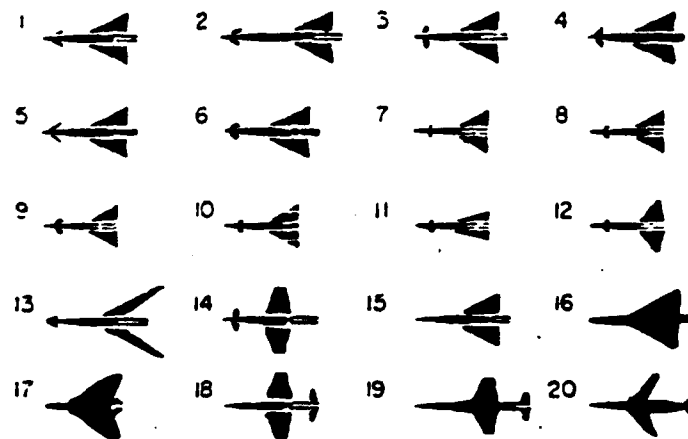


Figure 16. Events of Dynamic Stall on NACA 0012 Airfoil. (Reference (25))

### 2.2.3. Influence of Aircraft Wing Geometric Parameters on Aircraft Stall Characteristics.

Analytically the conditions associated with the "classical stall" are defined to occur at the angle-of-attack corresponding to the maximum lift coefficient. However, as previously discussed, many aircraft exhibit characteristics that vary widely at stall and often do not exhibit the "classical stall" characteristics. The major reason for this fact stems from the post World War II evolution of swept-wing designs with close-coupled tail surfaces resulting in many designs that exhibit extremely nonlinear aerodynamics at high angle-of-attack (Reference (27)) (See figure 17).



Coplanar Tail : 18  
High Tail : 19, 20

Figure 17. Examples of Post WWII Type Configurations. (Reference (27))

These designs, and even more so, today's current fighter design configurations, stall characteristics are no longer primarily a function of the wing design. The importance of wing design has not been diminished in the design of desired stall characteristics, the fact is, forebody-wing-empennage integrated design considerations have been found to be of equal design importance and not separate design entities. Where appropriate the subject of integrated forebody-wing-empennage design will be touched upon in this section. This section will concentrate on the geometric wing characteristics that affect the shape of the lift-curve and thus longitudinal stall characteristics.

The shape of the wing lift-curve is primarily a function of the wing-section (airfoil) characteristics and the three-dimensional geometric wing characteristics. The primary wing-section characteristics that affect the lift curves shape include, airfoil camber, thickness and leading-edge radius. While the primary three-dimensional wing characteristics include wing aspect ratio (AR), sweepback angle ( $\Lambda_{c4}$ ), and taper ratio ( $\lambda$ ).

Figure 18 illustrates the standard airfoil geometry nomenclature. In addition, Appendix A provides a review of some of the terms used (Note, the wing section characteristics to be discussed, i.e.,  $\alpha_0$ ,  $C_{l_{max}}$ ,  $dC_l/d\alpha$ , a.c., are dependent only on the profile shapes of the sections and are independent of the wing's planform characteristics).

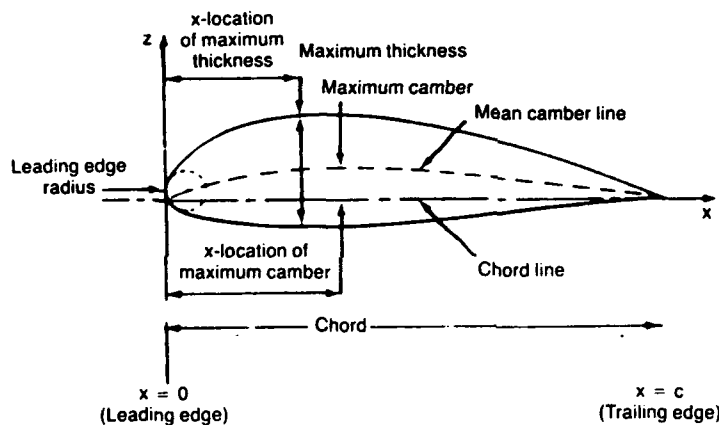


Figure 18. Airfoil Geometry Nomenclature (Reference (5) )

The maximum thickness and the thickness distribution strongly influence the airfoil section characteristics (lift-curve slope, maximum lift coefficient, aerodynamic center and center of pressure location). To some limit, the maximum lift coefficient for an airfoil increases as the maximum thickness of the airfoil increases. This can be explained in terms of the resulting pressure gradient produced by the flow. The maximum local velocity to which a fluid particle accelerates as it flows around an airfoil section increases as the maximum thickness increases. In turn the minimum pressure value is smallest for the thicker airfoil. Hence the airfoil which derives its lift from the pressure being higher on the lower surface of the airfoil than on the upper surface will attain a correspondingly higher  $C_{l_{max}}$  value. As discussed, this reasoning does not apply when the adverse pressure gradient becomes so large, that

the conditions necessary to induce flow separation become more likely. This explains the concave shape of the variation of  $C_{l_{max}}$  with thickness ratio of the NACA 24XX airfoils depicted in figure 19. This figure is taken from reference (16) and shows, at least for this camber function, that a thickness ratio of about 12 percent is optimum.

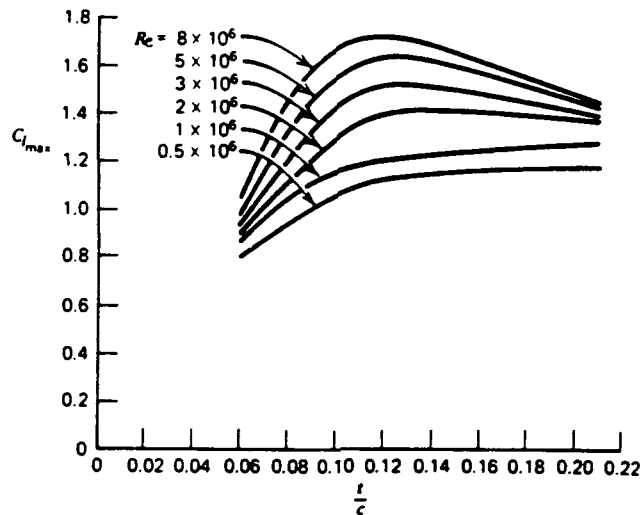


Figure 19. Variation of  $C_{l_{max}}$  with Thickness Ratio of NACA 24xx Airfoils for Various Reynolds Numbers (Reference (16))

Reference (15) points out that for the new low speed (LS) airfoils (see Figure 20, NASA GA(W)-1) the maximum lift occurs at around 15 percent thickness.

The thickness distribution for an airfoil likewise affects the pressure distribution and the characteristics of the boundary-layer. In general, as the location of the maximum thickness point moves aft, the pressure gradient in the mid-chord region decreases. The resultant more favorable pressure gradient in the mid-chord region promotes boundary layer stability, increases the probability that the flow remains laminar and may delay transition to turbulent flow. (Reference (5)).

The effect of camber on the pressure distribution about an airfoil section is shown in figure 21 as compared to a symmetric airfoil for two different angles-of-attack.

The basic concept illustrated in figure 21 is to show that camber primarily affects the zero-lift angle-of-attack,  $\alpha_0$  and the pitching moment,  $C_m$ .

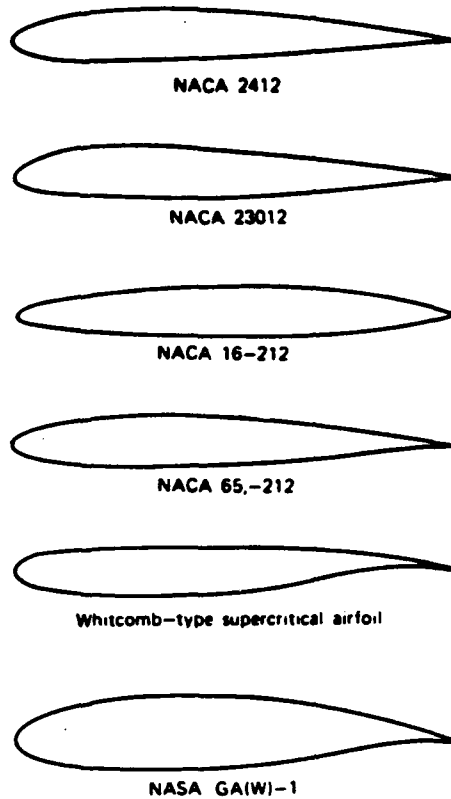


Figure 20. Comparison of Various Airfoil Shapes. (Reference (16))

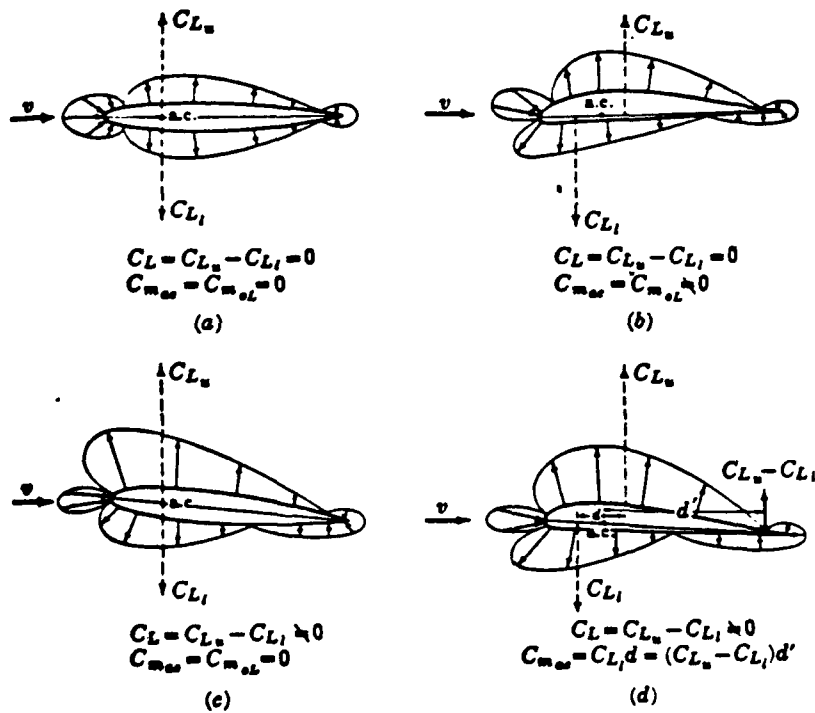


Figure 21. Effect of Camber on Airfoil Pressure Distribution (Reference (28))

Any increase in camber will make  $\alpha_0$  and  $C_m$  more negative. In terms of affecting the lift curve in the region of stall, camber's beneficial effects are a function of the airfoils leading edge radius and thickness. The increment to maximum lift due to camber is least for sections with relatively large radius leading edges; and is more effective on thin sections than on thicker ones. In addition a more forward position of maximum camber produces a higher value of  $C_{l_{max}}$ . (Reference (15)). Figure 22 of reference (9) shows how  $C_{l_{max}}$  increases with leading edge radius for a given airfoil thickness. The ratio,  $(z_{5.0})$ , a parameter indicative of leading-edge radius, is the ratio of section thickness at 5 percent to the maximum thickness.

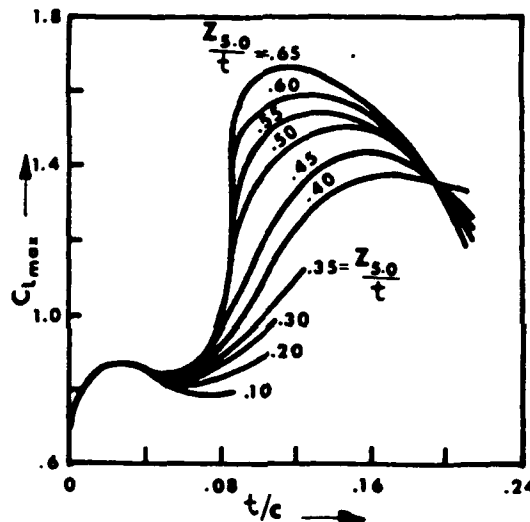


Figure 22. Maximum Lift at  $Re = 6 \times 10^6$  as a Function of Thickness Ratio  $t/c$  and Nose Radius  $z_{5.0}/t$  ( $z_{5.0}$  is  $z$  elevated at  $x/c = 0.05$ ; from Nonweiler, 1955, 1956). (Reference (9) )

From figure 22 it is seen that  $C_{l_{max}}$  is not affected by the nose radius of thin airfoils ( $t/c < .08$ ). A sharp leading-edge or a very small nose radius airfoil ( $z_{1.25}/c < 0.009$  at all Reynolds numbers) exhibit the special characteristics of thin-airfoil stall. Reference (8) describes thin airfoil stall as follows,

At small angles-of-attack, separation occurs at the nose followed by reattachment. The boundary-layer is neither typically laminar nor turbulent, but the turbulent characteristics

prevail as the trailing edge is approached. With an increase in angle-of-attack, the reattachment point moves downstream so that the separated region becomes larger and the lift decreases correspondingly. When the separated flow region is extended over the entire suction surface, then the value of  $C_l$  decreases with an increase in angle-of-attack.

For separation at large angles-of-attack (corresponding to maximum lift) the shape of the nose (i.e., radius, droop) is the most important geometrical parameter because its shape determines the pressure distribution in the neighborhood of the nose (see Figure 23).

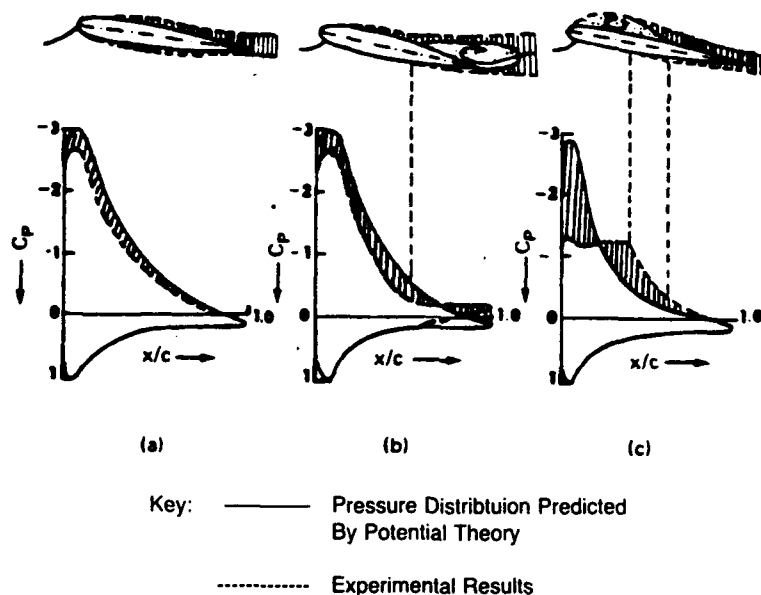


Figure 23. Variation of Pressure Distribution on Airfoil with Increase in Angle-of-Attack: (a) unseparated flow; (b) rear separation; (c) leading-edge separation and long bubble (qualitative distributions: first inviscid approximation and experiment; from Thwaites, 1960). (Reference (9))

Figure 24 of reference (29) illustrates well the influence that thickness, camber and leading-edge radius might have on the various types of stalls that can develop. Figure 24a illustrates a thin symmetrical airfoil ( $t/c < 0.08$ ) characterized by a small leading edge radius. In this case the large adverse pressure gradient produced at the leading edge induces leading edge flow separation. This is primarily due to the sudden failure of the boundary layer to reattach itself to the surface following separation of the laminar boundary layer near the leading-edge. Thicker airfoils ( $t/c > 0.12$ ),

representative of figure 24b, typically create large adverse pressure gradients near the upper-surface trailing-edge inducing trailing-edge flow separation at sufficiently high angles-of-attack. In this case the stall is a result of the progressive forward movement of turbulent separation. (Reference (16)). Finally, an airfoil of moderate thickness ( $0.8 < t/c < 0.12$ ) as shown in figure 24c may exhibit a tendency for separation to occur simultaneously at both leading and trailing edges.

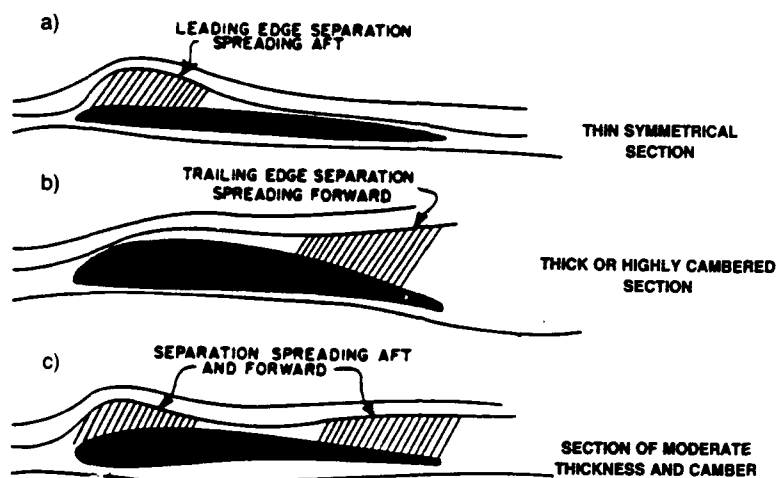


Figure 24. Types of Wing Section Stalls (Reference (29))

For good stall design, the associated loss in lift should be smooth with no abrupt or insidious losses past  $C_{l_{max}}$ . This describes the lift-curve characteristics associated with a gradual, well defined stall initiated by trailing edge separation (see figure 5a). An aircraft having this type of lift-curve slope would probably exhibit satisfactory aerodynamic stall warning (buffet). Figure 5b is an example of a lift curve with unfavorable stall characteristics. In this figure, the lift curve exhibits a well-defined peak followed by a very rapid decrease in lift coefficient for a small increase in angle-of-attack. This type of lift-curve can result from leading-edge flow separation as shown in figure 24a. An airplane with this type of lift-curve would exhibit little or no aerodynamic stall warning, and an abrupt loss in lift. This stall may be quite violent because the sharpness of the lift curve occurring after  $C_{l_{max}}$  indicates that one wing can easily stall prior to the other generating rolling motion at the stall. The asymmetric stall can be caused by

small differences in wing sections along the span or small differences in local flow direction due to vertical gusts or yawing motion. This asymmetric stalling phenomenon describes the initial conditions necessary for spin entry as discussed later in section 2.3.2.

As a result of additional work Hazen (1967) has accomplished concerning separation over an airfoil at high angle-of-attack, he classified the separation phenomenon into the following four categories (a) trailing-edge, (b) thick-section bubble<sup>1</sup>, (c) short bubble (laminar separation) and (d) long bubble (Reference (9)). These are shown in figure 25 and the description of these as taken from reference (9) has been included in Appendix A under "separated flow". Reference (9) points out that, "some doubt exists concerning the details of the fundamental processes of stall involved, and mixed flow types are not uncommon particularly in the range of Reynolds numbers  $2 \times 10^6$  to  $1 \times 10^7$ ."

Boundaries for the various types of airfoil separation phenomena mentioned were correlated with  $Re_c$  (Reynolds number based on the streamwise values of chord and velocity) and the quantity  $z_{1.25}/c$  ( $z_{1.25}$  is the upper surface ordinate of the airfoil at 1.25 percent chord). Figure 26 shows the resulting boundaries (Gault 1957). The data base for the study included aerodynamic characteristics of over 150 different airfoils, both symmetrical and cambered over a range of Reynolds number from  $0.7 \times 10^6$  to  $2.5 \times 10^6$ .

Boundaries for the various types of separation for the initial stall of wings is given in figure 27. In this case the boundaries are plotted as a function of  $(Re_{cl})_n$  (Reynolds number based on the velocity and chord at the wing tip and the subscript n indicates the normal direction to the leading edge) and  $(z_{1.25}/c)_n$ . Wings that exhibited leading-edge separation fell in regions 1 and 2, while those that exhibited initial trailing-edge separation fell in regions 2, 3 and 4. Reference (9) notes that, "the effect of boundary-layer outflow on highly swept wings might be expected to result in the shift of the boundaries indicated in figure 27. Lack of sufficient data (at the time) on three dimensional flow makes it impossible to prove this shift or to substantiate the correlation precisely for initial separation types."

<sup>1</sup>bubble — refers to the separation bubbles that are generated when the flow creates a circulatory motion near the airfoil surface (Reference (9))

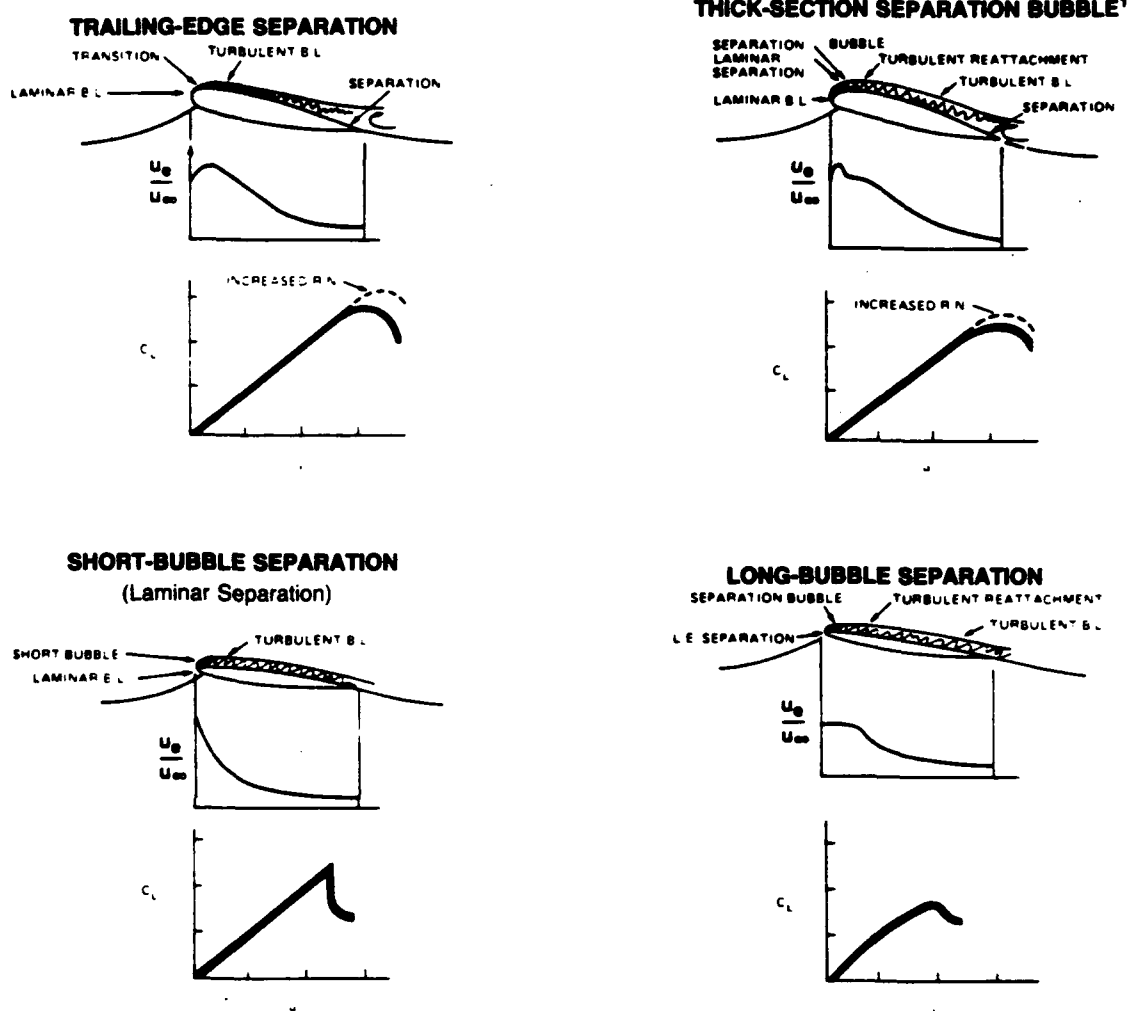


Figure 25. Classification of Airfoil Stall by Hazen (1967) (Reference (9))

<sup>1</sup>This separation process can also occur on thin airfoils ( $t/c < .09$ ) and is usually called, "Thin Airfoil Stall."

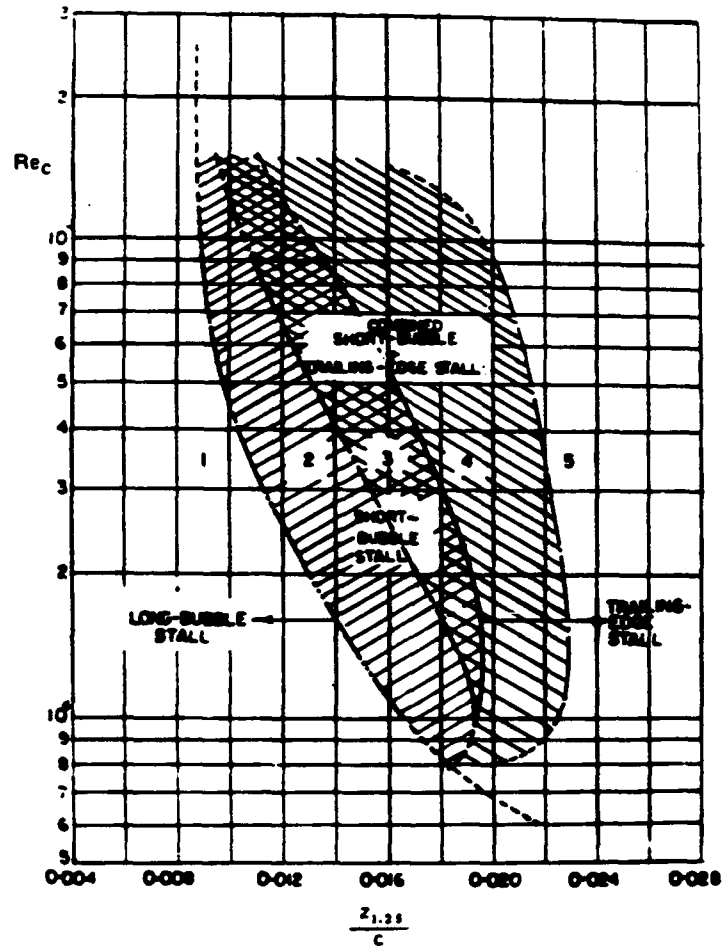


Figure 26. Boundaries for Various Types of Airfoil Stall (from Chappell, 1968). (Reference (9))

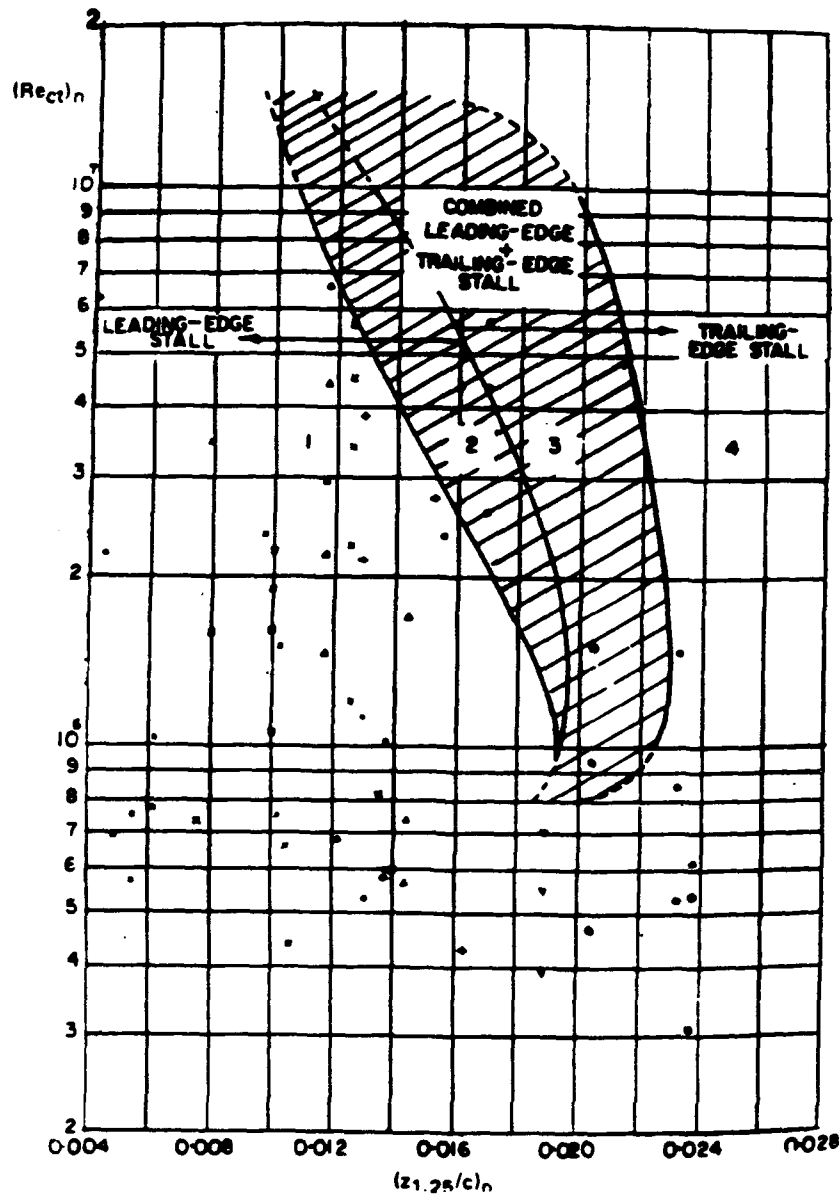


Figure 27. Initial Stall Characteristics of Plane Wings with Constant Symmetrical Sections (from Chappell, 1968). (Reference (9) )

Up to this point the discussion of stall behavior and the factors that affect it have mainly concentrated on the 2-dimensional airfoil. Note that basic airfoil stall behavior does not necessarily imply sudden overall wing stall behavior. In fact the effects of wing planform and thrust can significantly alter the stall characteristics of a wing as compared to the stall characteristics of its airfoil(s). Wing planform design influences the downwash pattern, the progression of the stall (i.e., portion of the wing

that stalls first) and the overall lift-curve shape. The most influential planform parameters are aspect-ratio (AR), sweep back angle ( $\Lambda_{c/4}$ ), taper ratio ( $\lambda$ ) and wing twist. Figure 28 illustrates the standard nomenclature used to describe a wing's geometry.

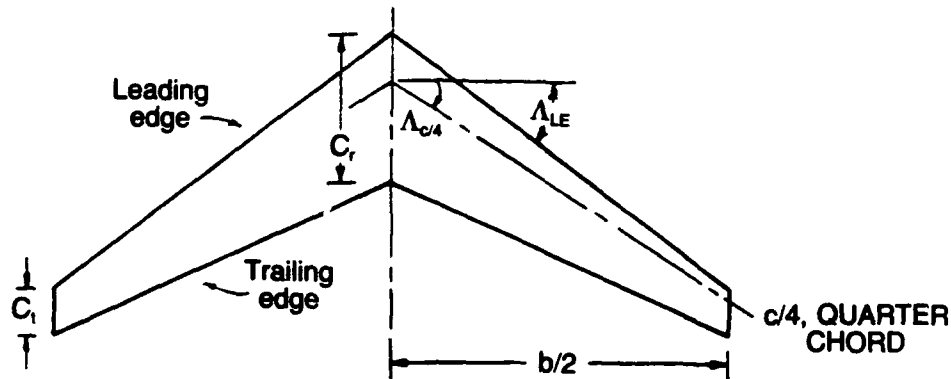


Figure 28. Wing Planform Nomenclature (Reference (8))

Fundamentally the basic difference between the stall characteristics of a wing and a two dimensional airfoil are attributed to the vortex system generated by a finite aspect ratio wing. Reference (16) describes the generation of this vortex system as follows,

The pressure difference between the upper and lower surfaces of the wing causes a spanwise flow outward toward the tips on the lower surface, around the tips and inward toward the

center of the wing. Combined with the freestream velocity, the spanwise flow produces a swirling motion of the air trailing downstream of the wing (illustrated in figure 29). Immediately behind the wing, the vortex system is shed in the form of a vortex sheet (see figure 30) which rolls up rapidly within a few chord lengths to form a pair of oppositely rotating line vortices called trailing vortices. The generated trailing vortices, not present with a two-dimensional airfoil, induces an additional velocity field (termed downwash,  $w$ ) at the wing that must be considered, in addition to the effects of spanwise flow, in calculating the aerodynamic characteristics of each of the wing sections.

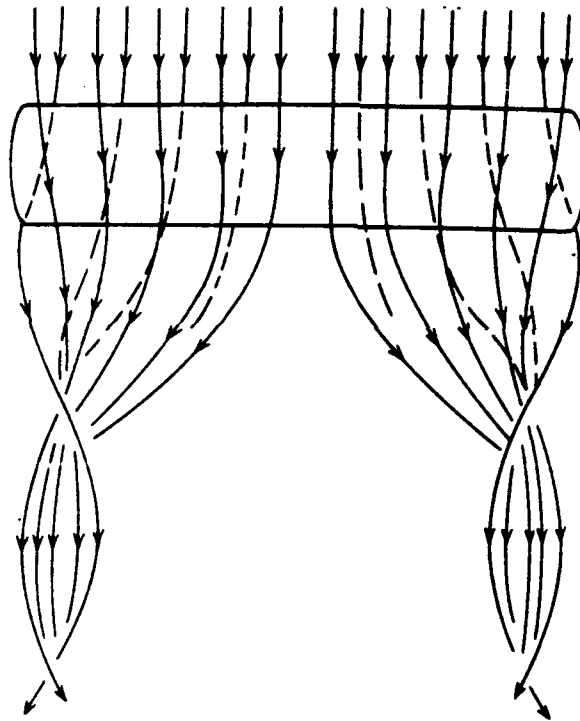


Figure 29. Generation of Vortex System by Finite Aspect Ratio Wing (Reference (16))

For wings of large aspect-ratio ( $AR > 6$ ) (i.e., for which  $c \ll b$  and excluding sections near the tips) this vortex model was most simply modelled by Prandtl and is well known as "Prandtl's Lifting Line Theory." Prandtl's model is based on the theory that the flow past a finite wing can be represented as the flow past a certain vortex sheet. Prandtl showed that lift per unit span is directly proportional to

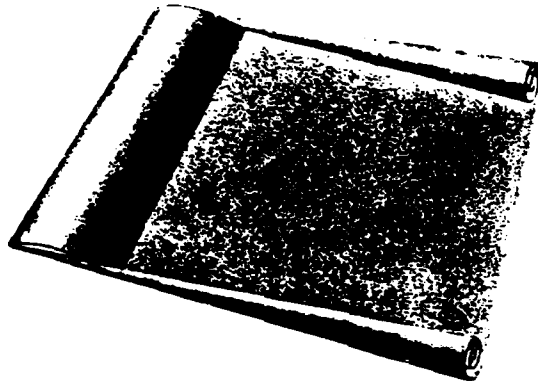


Figure 30. Vortex Sheet Trailing Behind a Wing (Reference (4))

circulation and that the wing can be mathematical modeled by a hypothetical bound and trailing vortex system (see Figure 31).

Prandtl then approximated the bound portion of the vortex sheet by a single bound vortex line (known as the lifting line) to represent the wing. (See Figure 31) The theoretical approach for wings of very low aspect ratio ( $AR < 3$ ) is entirely different from the theory just presented. In this case the concept of wing-section characteristics is not applicable. Instead Jones showed that, for wings with aspect ratios approaching zero, the lift depends on the angle of attack and on the positive rate of increase of span in the direction of the air flow. (Reference (15)). The reader is referred to references

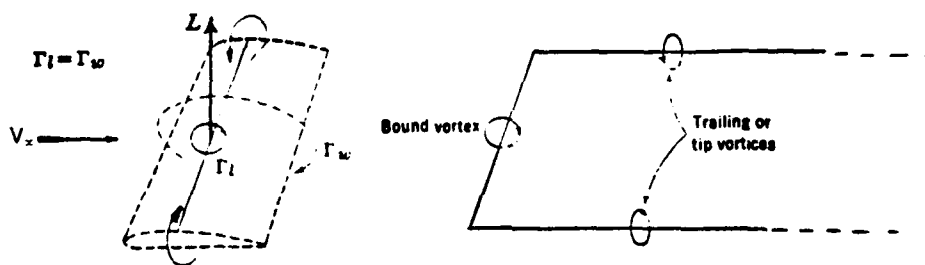


Figure 31. Prandtl Vortex System (Reference (28))

(15) and (30) for a description of Jones' Theory. For a more detailed description of Prandtl's lifting line theory and refinements thereof to include smaller aspect ratios and tip effects see references (6) and (14).

Utilizing the Prandtl Lifting Line Theory as a basis for understanding, the geometric effects on the stall characteristics can be explained by understanding the geometric effect on the wing's spanwise lift distribution resulting from the described vortex system downwash distribution. The influence of wing aspect ratio on wing lift characteristics will be the first parameter expanded on. The finite-span effects on the wing lift-curve slope are shown in figure 32. Figure 32 shows the effect of a finite wing is to reduce the lift-curve slope while the zero-lift angle remains the same. The theory of finite wing spans attributes this fact to the presence of a downwash velocity,  $w$ , induced along the span by the vortex system. At any position along the wing span, the vector addition of the downwash and freestream velocity results in a local velocity,  $V_\ell$ , and effective reduced angle-of-attack. (See Figures 33 and 34). Thus to maintain the same lifting force with a finite span the total angle-of-attack,  $\alpha$ , must be increased by an amount equal to the induced angle-of-attack ( $\alpha_i$ ).

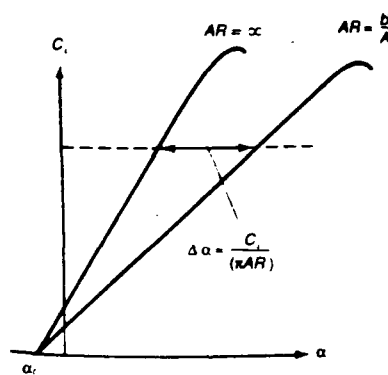


Figure 32. Effect of Finite Aspect Ratio on the Lift-Curve (Reference (6))

Note also that the effect of the induced downwash velocity by the trailing vortices is to rotate the lift vector downstream. This effectively contributes another component of drag known as induced drag. It should be apparent that the slope of the lift-curve effected by the wing aspect ratio, will influence the angle-of-attack and the pitch attitude at which aerodynamic stall occurs. If the slope of the lift curve is shallow the angle-of-attack for stall may be obtained at a very high angle-of-attack.

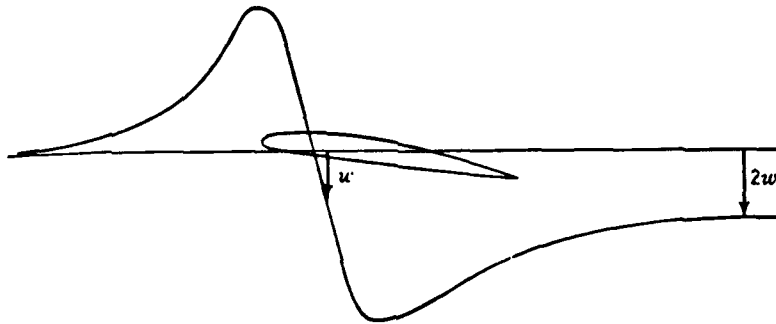


Figure 33. Downwash Distribution of a Finite Wing (Reference (28))

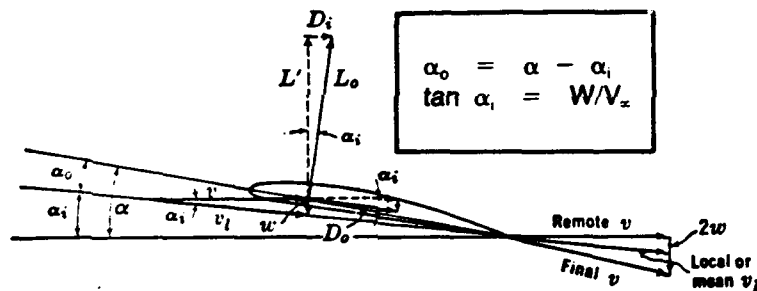


Figure 34. Effect of Downwash of a Finite Wing on Wing Lift Distribution (Reference (28))

Another geometric wing parameter that influences the lift curve slope is wing sweep. Recall the primary reason for using wing sweepback is to avoid/delay compressibility effects in the transonic flight regime. The advantage realized by employing wing sweep at high mach numbers however has its

disadvantages during low speed flight where the infinite wing and negligible viscous effect assumptions no longer hold as well. The following simple analysis (from Reference (15)) illustrates the effect of sweep on the lift curve slope for a non-delta wing.<sup>1</sup>

The lift on a unit area of the wing is given by EQ(2)

$$\begin{aligned} L &= 1/2\rho \cdot V_{\infty}^2 \cdot (C_{l_{\alpha}} \cdot \alpha) \text{ where } C_{l_{\alpha}} \equiv C_{l_{\alpha}} \cdot \alpha \\ &= 1/2\rho \cdot (V_{\infty} \cos \Lambda)^2 \cdot C_{l_{\alpha}} \cdot \alpha \end{aligned} \quad \text{EQ (2)}$$

where  $C_{l_{\alpha}}$  is the lift-curve slope for an unswept two-dimensional wing. The corresponding lift-curve slope for a swept wing with respect to the freestream velocity is then given by equation (3)

$$\begin{aligned} C_{l_{\alpha}} (\Lambda \neq 0) &= L / (1/2\rho V_{\infty}^2 \alpha \cos^2 \Lambda) \\ &= C_{l_{\alpha}} \cos \Lambda \end{aligned} \quad \text{EQ (3)}$$



Figure 35. Vortex System of a Delta Wing (Courtesy of the Office National D'Etudes Et De Recherches Aérospatiales.) (Reference (16))

<sup>1</sup>The aerodynamic analysis of a delta wing is complicated by the nonlinear affects associated with the highly swept leading edge. See figure 35 and refer to references (31) and (32) for a detailed discussion on this theory.

Figure 36 illustrates the effect of sweepback on the lift-curve slope. Qualitatively, sweeping a wing causes an outward crossflow of the boundary-layer air caused by a considerable pressure gradient towards the receding tips (Reference (7)). This is shown in figure 37. As a result of this crossflow there is a thickening of the boundary-layer at the tip. At the same time the wing sweep also causes the loading at the tip to increase. For these reasons the swept wing is much more likely to stall outboard in comparison to a similar unswept wing. The characteristics of tip stall common to swept wings is undesirable mainly for the following three reasons, 1) the loss of roll control effectiveness (assuming conventional outboard aileron-type effectors) associated with tip stall, 2) tip stall is a major cause of the very dangerous asymmetric, one-wing stall, and 3) the characteristics of tip stall are also a major attributing factor to the equally dangerous phenomenon of pitch-up (to be discussed later in section 2.2.4.1).

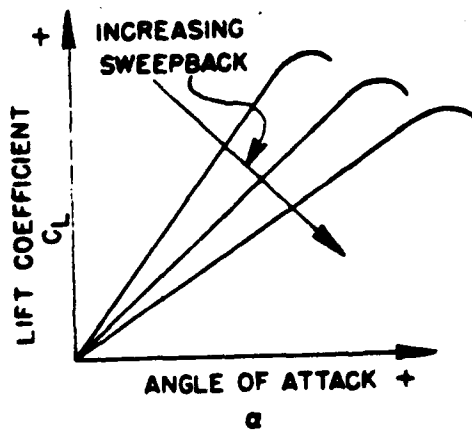


Figure 36. Typical Influence of Sweepback on Lift Curve Slope (Reference (29) )

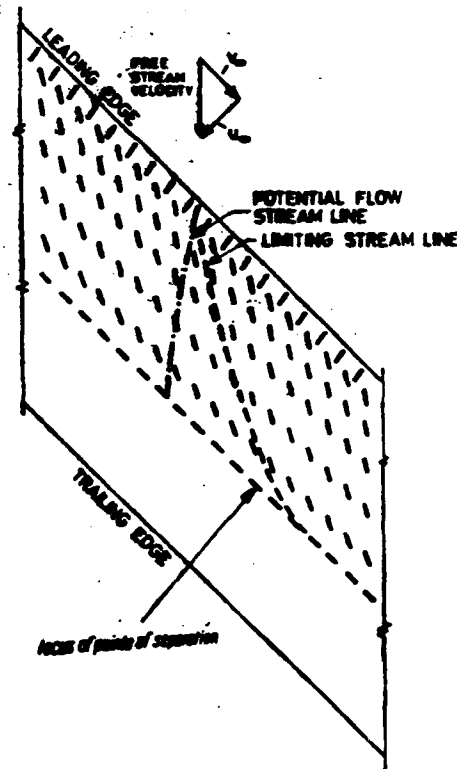


Figure 37. Cross Flow at the Surface of a 45° Swept Wing (Reference (13))

For wings with high angles of sweep forward, the inherent crossflow toward the wing root promotes a stall pattern from root to tip. This is a more desirable flow pattern for the purpose of maintaining roll control in the case of conventional aircraft with outboard lateral control surfaces. Another disadvantage characteristic of the tip stall is that in general little or no stall warning occurs. In contrast, wing root stall is usually preceded by buffeting of the fuselage and tail caused by turbulence shed from the root section (Reference (29)).

Figure 38 taken from reference (16) presents some experimental results showing the trend of the lift-curve slope ( $C_{L_\alpha}$ ) values as a function of sweepback for low mach numbers. It points out the trend of decreasing lift-curve slope values with increasing wing sweep.

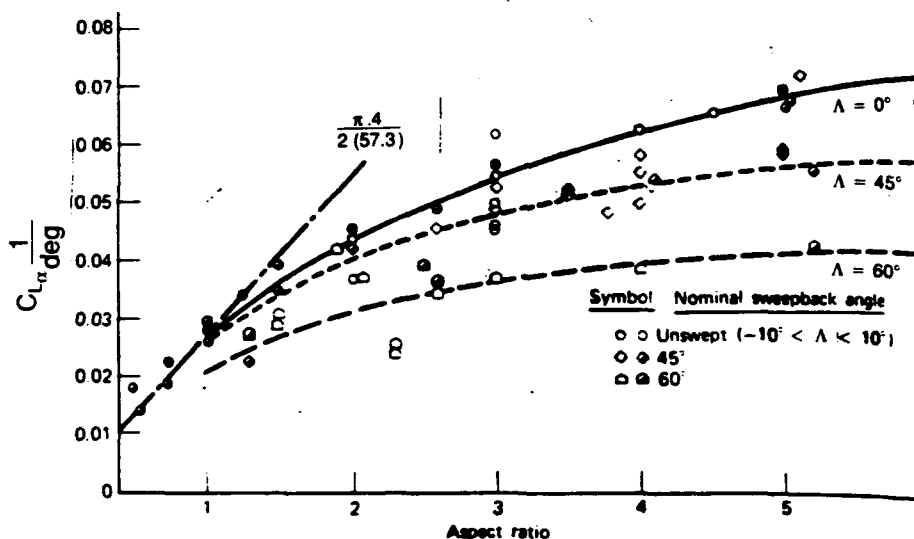


Figure 38. Lift Curve Slopes for Swept, Tapered Wings. (Reference (16) )

Figure 39, also taken from reference (16) demonstrates that the aerodynamic effects of wing sweep has little effect on  $C_{L_{\max}}$  and if anything indicates a tendency for  $C_{L_{\max}}$  to increase with wing sweep. This is contrary to what one might expect (i.e.,  $C_{L_{\max}}$  would decrease as  $\cos^2 \Lambda$ ). Interestingly, reference (8) points out that certain boundary-layer and separation phenomena are determined independently by the crosswise component of velocity. Furthermore the effect of sweepback is to increase the area of stable

laminar flow over the wing and to decrease the lift coefficient at which flow separation occurs.

Admittedly reference (16) states that figure 39 includes other factors affecting  $C_{L_{max}}$ . Apparently aspect ratio is one of these factors as previously discussed (the data of figure 39 includes wings with aspect ratios up to 6.6 only).

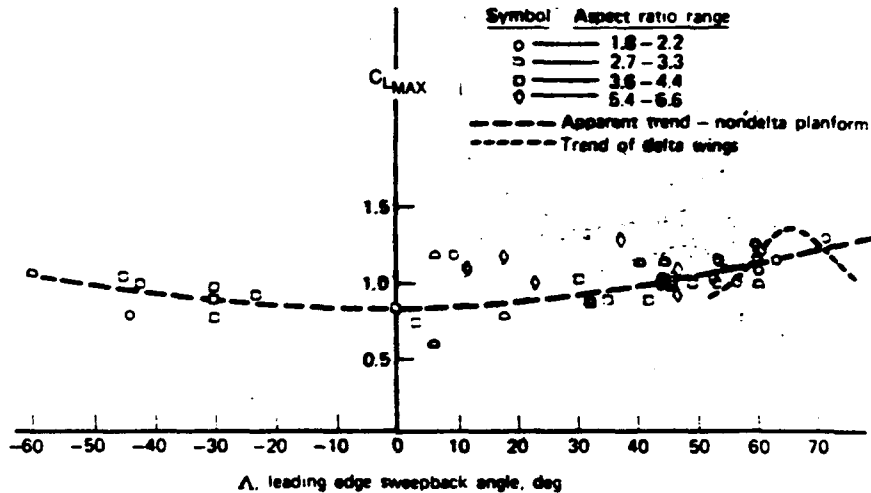


Figure 39. Variation of  $C_{L_{max}}$  with Sweepback for Wings Having Planforms Other Than Triangular. (Reference (16))

Another principal wing planform parameter that has a significant effect on aircraft stall characteristics is the wing's taper ratio<sup>1</sup>. In general high taper ratio wings promote tip stall. This is illustrated in figure 40. For the higher taper ratio, the spanwise variation in chord decreases faster than the lift does causing a local  $C_l$  near the tip to be much higher than one near the root. When this occurs the sections near the wing tip will stall first. As figure 40 highlights, the spanwise distribution of downwash (which dictates the wing-section angle-of-attack and hence section lift coefficient distribution along the span) is the determining factor which influences what part of the span first reaches a stalled condition. Figure 41 taken from reference (29) further illustrates the progression of a stalled wing as a function of wing planform taper ratio.

<sup>1</sup> See Appendix A — Glossary of Defined Terms

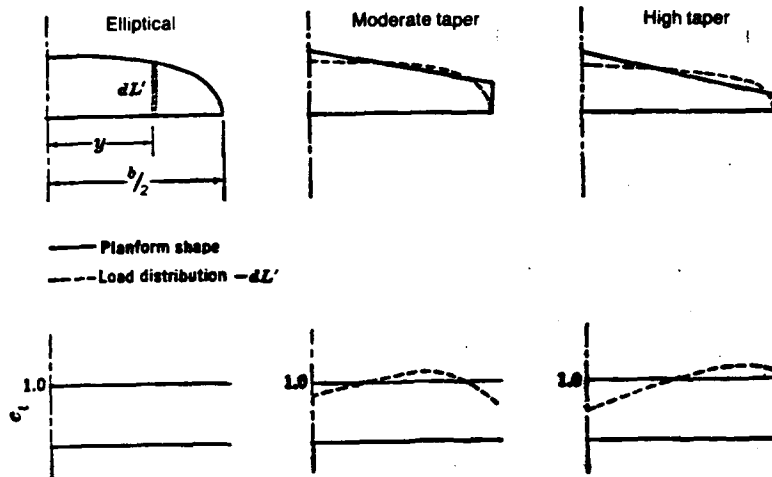


Figure 40. Spanwise Lift Coefficient Distribution for Various Wing Planform Taper Ratios. (Reference (28)).

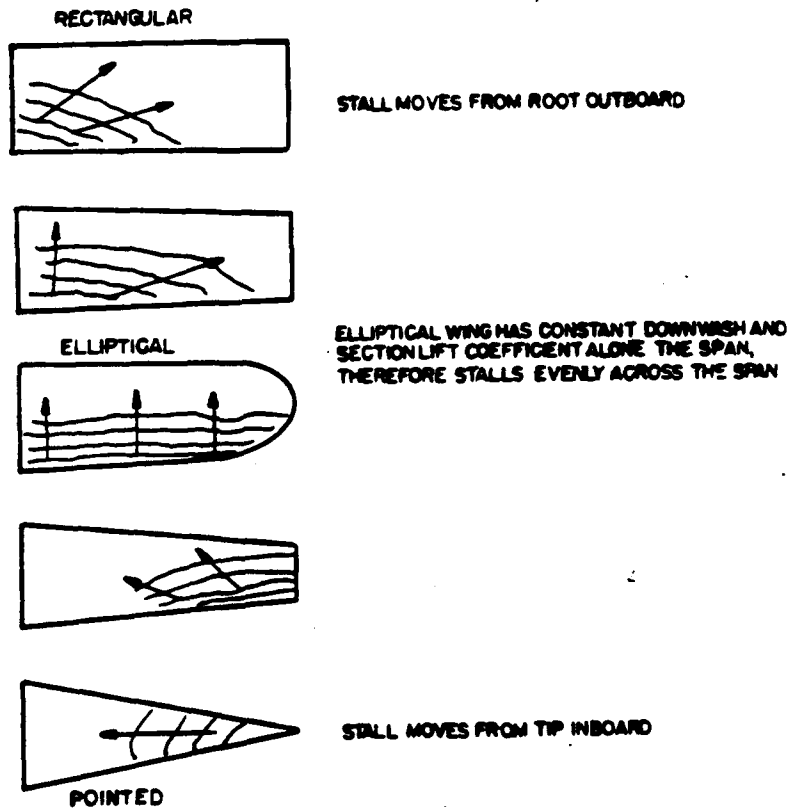


Figure 41. Typical Influence of Wing Taper on Stall Progression (Reference (29)).

## 2.2.4. Aerodynamic Characteristics Near Stall

## 2.2.4.1. Pitch-up

Pitch-up is a longitudinal instability phenomenon characterized by an increase in the aircraft nose-up pitching moment as a function of increasing lift/angle-of-attack (see Figure 42). Pitch-up is most notably the result of the distribution of lift along a swept wing and secondarily a result of fuselage lift. As discussed previously, the byproduct of a swept wing planform is for the stall to begin at the wing tips and progress inboard as the angle-of-attack increases. The loss of lift at the tips causes a concentration of the lift at the middle portion of the wing and likewise results in the center-of-pressure<sup>1</sup> moving forward. (Reference (33)). In addition, the increased concentration of lift inboard, increases the downwash behind the center portion of the wing affecting the stabilizer (thus increasing the stabilizer induced angle-of-attack). This factor likewise contributes to a further forward shift in the center-of-pressure with the net effect of producing a nose-up change in the pitching moment. (Reference (33)).

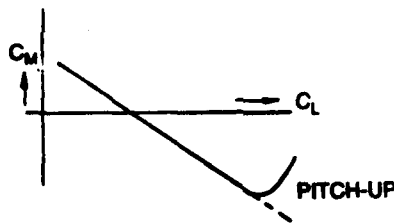


Figure 42. Example of Longitudinal Pitch-up Instability (Reference (33) )

Figure 43 illustrates the strong dependence of pitch-up on wing planform geometry. High values of both aspect ratio and wing sweep angle promote the occurrence of pitch-up due to their influence in causing the center-of-pressure to shift forward. (The stable region marked is only approximate and may be influenced by airfoil variation, wing twist, boundary layer fences, engine pylons and leading-edge high-lift devices). In the case of short-span straight wing aircraft, reference (33) takes exception from the data of figure 43. Reference (33) points out that pitch-up may be produced due to the effects of increased stabilizer downwash at high angles-of-attack caused by the short-span wing tip vortices.

The effect of fuselage and nacelle lift is generally small (relative to the wing), is difficult to predict,

<sup>1</sup> See Appendix A — Glossary of Defined Terms

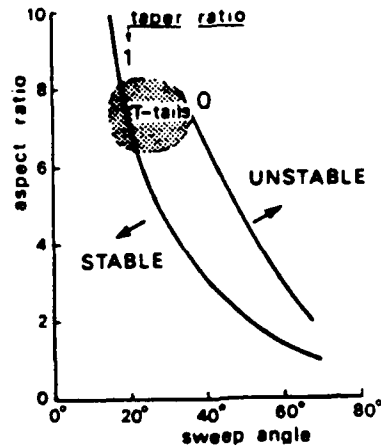


Figure 43. Effect of Wing Aspect Ratio and Sweep on Stability Boundaries for the Wing Alone (Reference (34))<sup>1</sup>

and often ignored in preliminary design. However the shift in the location of the center-of-pressure due to the nacelles and fuselage can be a substantial destabilizing factor at high angles-of-attack (See (Reference (34))). To design an aircraft with "good" high angle-of-attack flying qualities, the vertical location of the stabilizer relative to the wing must be carefully considered. Figures 44 and 45 show the vortical/streamline flows which impinge on tail surfaces as they leave the wing and the forebody of an aircraft.

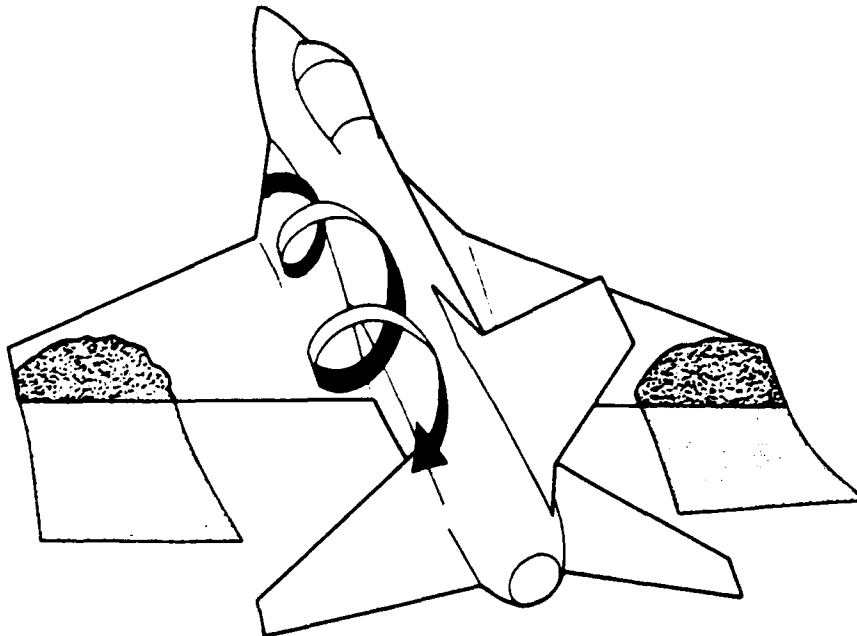


Figure 44. Illustration of Stalled and Vortex Flows at High Angle-of-attack (Reference (35))

<sup>1</sup>Originally taken from, Shortal, Joseph A., and Maggin Bernard, Effect of Sweepback and Aspect Ratio on Longitudinal Stability Characteristics of wings at low speeds. NACA TN 1093, 1946.

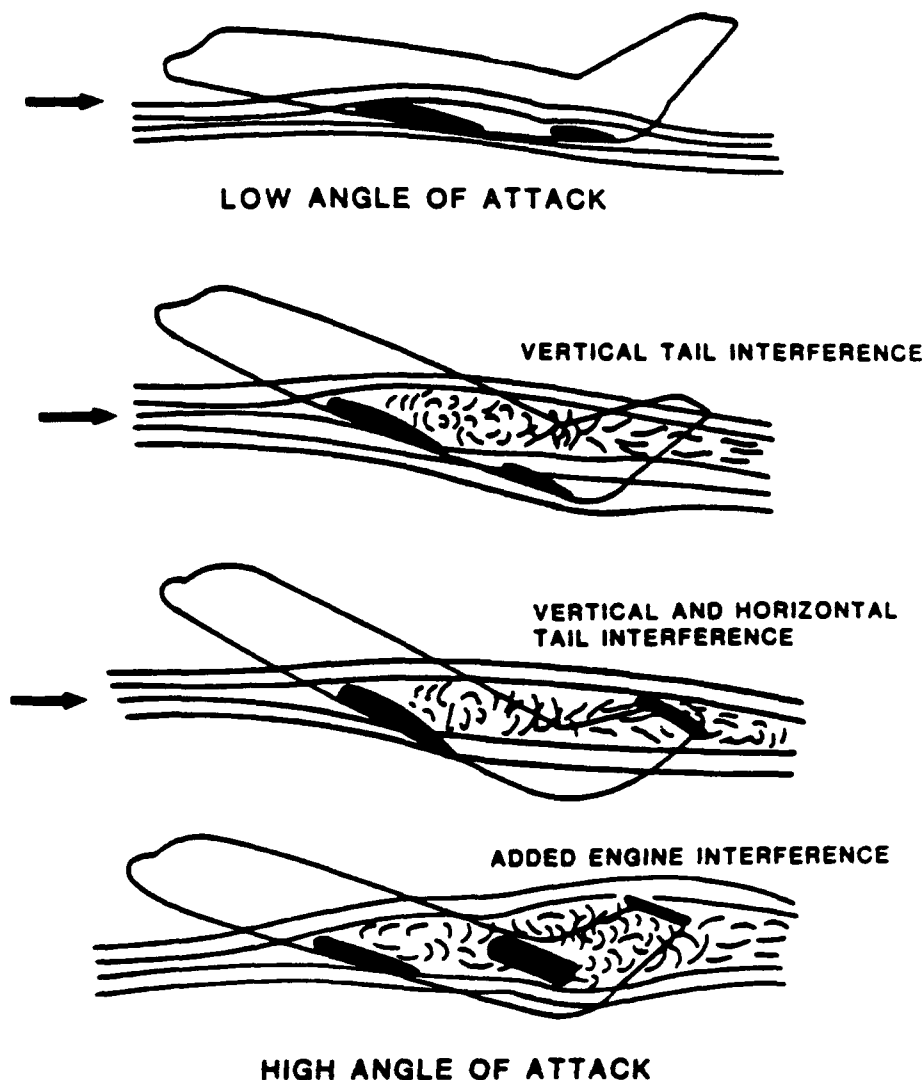


Figure 45. Stalled Wing Wake Tail Immersion (Reference (29) )

As an aircraft's angle-of-attack increases, the tail surfaces may enter and leave regions of vortical and unsteady flows even before stall. Loss and reattainment of lift and pitching moment increments from the tail (see Figure 46) may occur as it passes through these regions resulting in peculiar, nonlinear flying qualities.

It is desirable to position the horizontal stabilizer out of the wake of wing's downwash to help prevent pitch-up and loss of pitch and yaw control (See Figure 47). In general, the T-tail configuration is not successful in accomplishing this. In contrast, the lower tail positions are better from a post-stall stability perspective though the location of the wake when flaps are deflected must be considered.

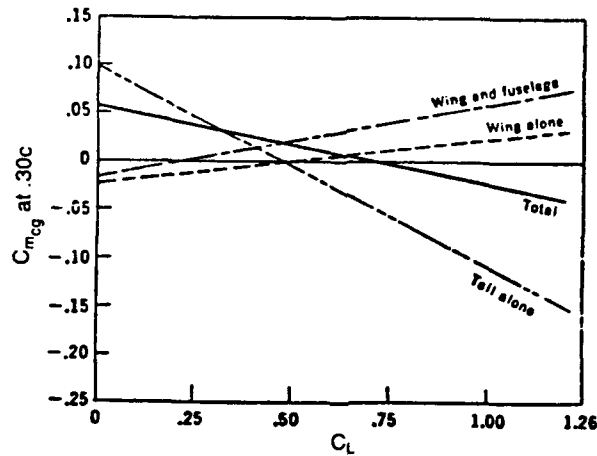


Figure 46. Typical Longitudinal Stability Component Build-up (Reference (28) )

The factors influencing the occurrence of pitch-up mentioned is by no means complete.

Sweepback, aspect ratio and stabilizer position can be considered the major influencing factors contributing to pitch-up. However other factors that include propulsive effects (propellor slipstream effects), and engine location (see Figure 45) can not be neglected on many configurations (i.e., their effect on aerodynamic center location, vortex system generation, etc.).

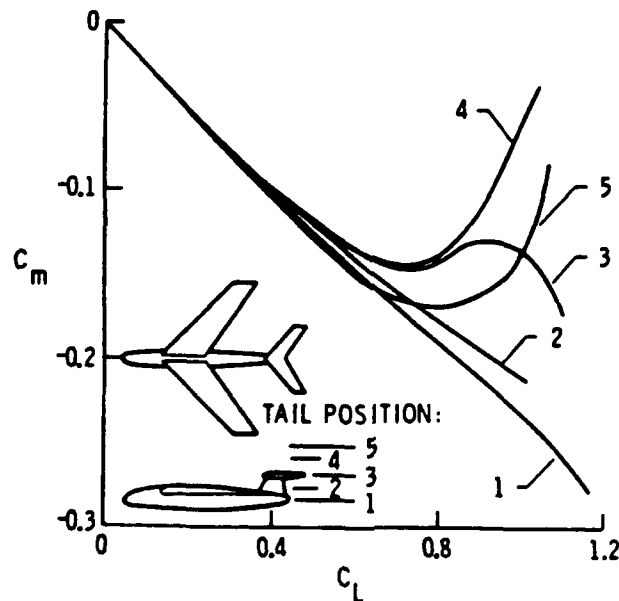


Figure 47. Effect of Horizontal-tail Location on Pitch-up Tendencies. (Reference (35))

## 2.2.4.2. Deep Stall

As a result of pitch-up and the vertical sink of the aircraft arising out of the loss of lift on the wings at stall, the angle-of-attack might be increased to a very large value well above the stalling angle. The aircraft might become stabilized in this condition making recovery difficult or even impossible due to loss of elevator effectiveness (Reference (33)). This condition is known as "deep stall." Aircraft configurations which have longitudinal control surfaces set high up on the vertical tail are the most prone to the deep stall phenomena. This is because the new trim points associated with the deep stall condition are caused by the effects of the horizontal stabilizer becoming saturated in the combined wakes of the fuselage, wing and possibly the engine nacelles. (See Figure 45). At the same time that the stabilizer is immersed in the wake, the wing flow has progressed to a well-developed separation. The net effect is to produce a nonlinear variation of pitching moment with angle-of-attack. This is illustrated in figure 48 for angles-of-attack approximately greater than twenty degrees.

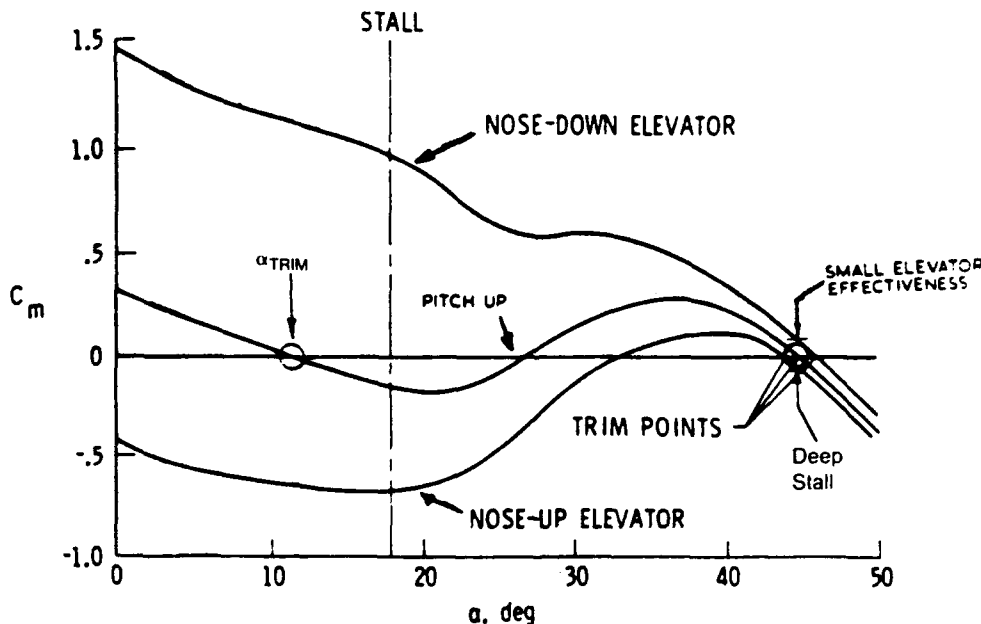


Figure 48. Loss of Elevator Effectiveness for a Configuration with Deep Stall (Reference (35))

The plot shows a substantial reduction in elevator effectiveness as a result of the impingement of the low energy wing wake on the elevator. As a result there exists insufficient nose-down control necessary to recover from the deep stall trim point (Reference (33)).

The effect of using a conventional stall recovery technique (reduce aircraft angle-of-attack by applying down elevator control) after a deep stall has been entered is shown in the time history plots of figure 49.

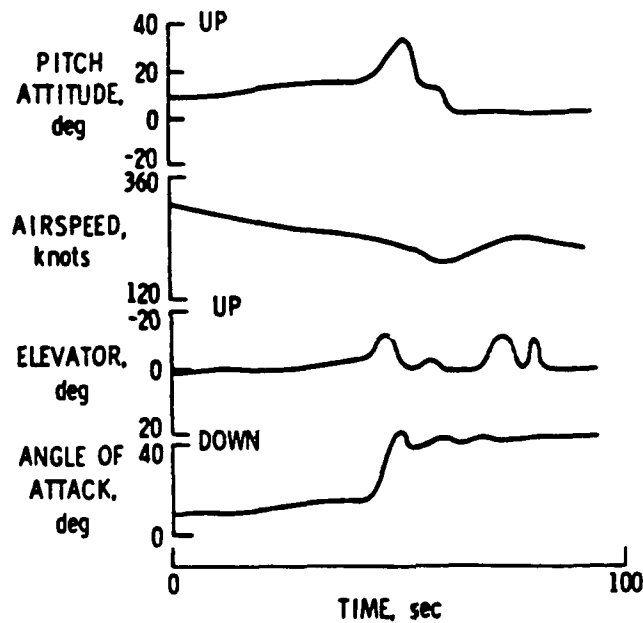


Figure 49. Typical Deep Stall Time Histories (Reference (35))

From figure 49 it is seen that a successful recovery from a deep stall condition can be misinterpreted by an untrained pilot. In this respect the deep stall can pose a significant danger to the pilot. Often however this can even be considered a moot point if insufficient altitude necessary for recovery is not available to the pilot. Figure 49 shows that the pilot recovery technique results in an increased airspeed and a nose-level attitude ( $\Theta = 0$  degrees). This can be incorrectly perceived by the pilot (with the exception of a steady sink rate the aircraft can look as if it is maintaining steady, level flight) as "successful" stall recovery when in fact recovery is not possible from the deep stall condition given here (Reference (35)).

Not overlooking the value and foresight of tailored configuration design and prudent use of wind tunnel testing, certain airframe design modifications have been found to help alleviate the problems

associated with deep stall. One of these methods includes slotting the stabilizer to increase its effectiveness at high angles-of-attack.

A more innovative approach to aid in deep-stall recovery has been studied by Dynamic Engineering Incorporated (DEI). Using scale-model aircraft and a specially designed Schweizer I-36 sailplane for in-flight testing, the company has been testing a flight control system concept that involves pivoting the entire stabilator (see figure 50). The purpose of pivoting the stabilator is to achieve controlled flight by

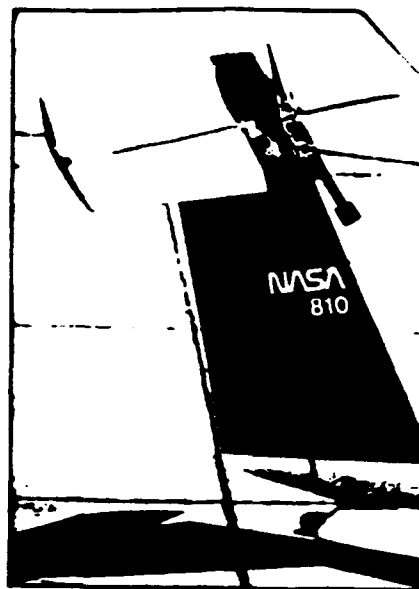


Figure 50. "Supernormal" Stabilator (Reference (36) )

aiming the stabilator into the relative wind that strikes the airplane from below. By doing this the tail surface becomes unstalled and is capable of providing pitch control. The lift force produced by the unstalled "supernormal" stabilator is directed such that a stabilizing pitching moment is produced. In addition the now-streamlined stabilator permits an increased flow of air over the vertical stabilizer and rudder allowing directional control which is ordinarily not present at deep-stall angles-of-attack (reference 36). This is illustrated in figure 51. As noted in reference (36), the supernormal elevator concept is not original to DEI. The concept closely resembles a passive system described by Carl Goldberg. The "Goldberg Dethermalizer" also used a pivoting stabilizer for the purpose of returning

model gliders from flyaway conditions. Goldberg described his invention in the September 1943 issue of "Model Airplane News" (Reference (37)). Reference (36) indicates that,

"Although the results of free-flight, wind tunnel, and limited analytical investigations have indicated attractive potential advantages for several aircraft classes when flown in Supernormal flight<sup>1</sup>, there are a number of concerns, and data is required to provide the necessary confidence prior to proceeding with full-scale application and demonstration."

For a more thorough discussion of the supernormal flight (SNF) concept see references (34.), (38) and (39).

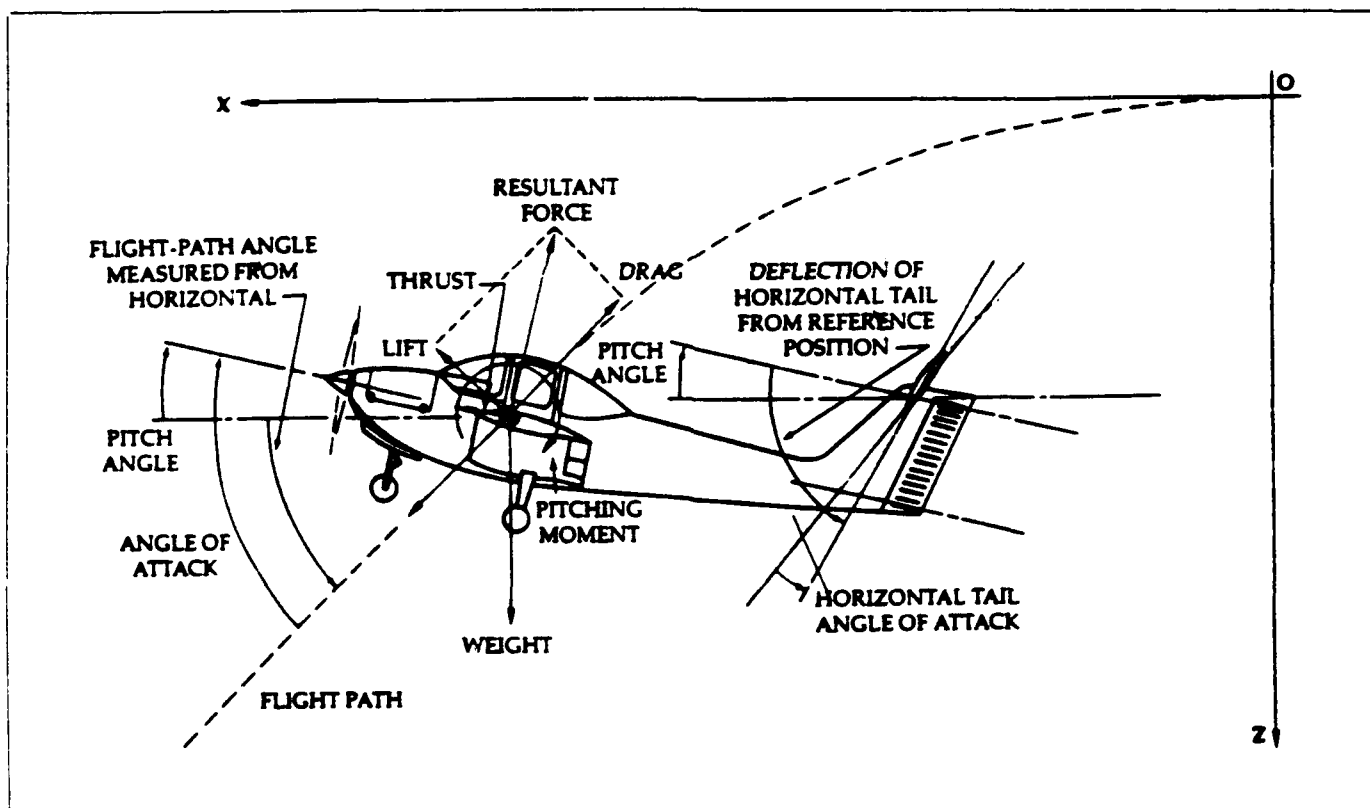


Figure 51. Free-body-diagram of Unstalled "Supernormal" Stabilator (Reference (36) )

A less desirable alternative used currently to prevent the occurrence of deep-stall is to use angle-of-attack limiting control systems such as stick pushers. Use of this method attempts to prevent pitch-up from occurring and thus avoid the possibility of entering the deep-stall flight regime entirely.

<sup>1</sup> See Appendix A — Glossary of Defined Terms

The interested reader is referred to references (40)-(42) for additional works that research the phenomenon of deep-stall.

#### 2.2.5. Methods of Stall Control

The problem of controlling flow separation and thus improving wing stall characteristics entails determining a way to secure a sufficiently high energy level for the fluid along the entire flow path in order to overcome the adverse pressure gradient and viscous friction in the neighborhood of the wing surface. The different methods used to control flow separation can be categorized into two groups depending upon whether they require the use of auxiliary power or not. The most widely used methods that do not utilize auxiliary power discussed in this section include: (1) stall strips, (2) geometric twist, (3) aerodynamic twist, (4) slots and slats, (5) stall fences and snags, and (6) vortex generators. Methods that utilize auxiliary power to prevent/delay separation do so by "energizing" the surface fluid, reducing viscosity or by properly regulating skin temperature. Two methods to be discussed in this section are 1) suction and 2) blowing.

In many cases the prevention of wing stall is not as important as the characteristics exhibited by the stall. In the wing design of conventional aircraft, good stall characteristics generally imply that the pilot has adequate aerodynamic stall warning cues. Furthermore when a stall is entered the dynamics are predictable and have no tendency to aggravate lift recovery such that the pilot is unable to regain level flight without excessive loss of altitude or buildup of speed.

This design philosophy is best illustrated by the first stall control device mentioned; namely the stall strip. The stall strip is usually a small angular strip attached to the root leading-edge of the wing as depicted in figure 52. By using a stall strip the flow is disturbed near the root such that root area stall is induced first. This method is not preferred because it limits rather than improves  $C_{L_{max}}$ . It turns out that the use of stall strips is usually a design "after-thought" to improve stall warning cue characteristics found to be unsatisfactory during flight testing.

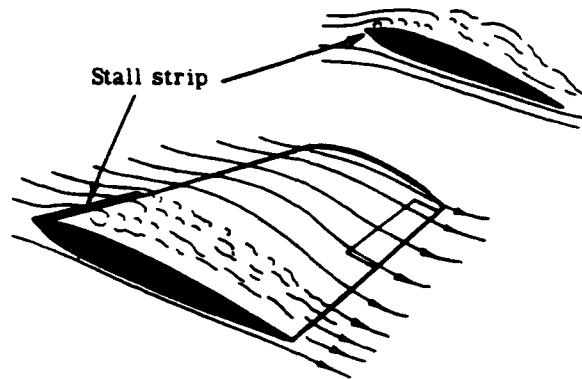


Figure 52. Typical Stall Strip (Reference (43) )

The next two stall control methods entail tailoring the wing's spanwise geometric properties. The first one, geometric washout, is used to describe a wing having built-in twist so the wing tip has a lower angle-of-incidence, and thus lower angle-of-attack than the root section (see Figure 53). The objective of wing tip washout is to have the root section stall first while maintaining lateral control throughout the stall. Typically the difference in incidence from root to tip is two to three degrees. Geometric tip washout is most effective for wings with moderate taper and is relatively ineffective for high values of taper ratio (reference (41)).

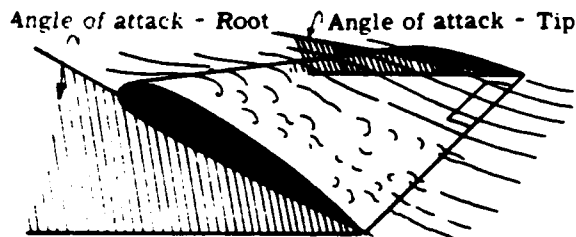


Figure 53. Exaggerated View of Wing Tip Washout (Reference (43))

Aerodynamic twist is the other method that employs tailoring the wing's spanwise geometric properties. More specifically it refers to changing the airfoil section from root to tip, effecting a spanwise variation of camber and position of maximum camber (reference (14)). (See figure 54). Aerodynamic twist aims to achieve the same design objectives as geometric washout, namely to induce root section

stall first to effect enhanced stall warning cues and provide improved lateral control through the stall. Aerodynamic twist achieves this by tailoring the spanwise variation of absolute angle-of-attack and center of pressure.

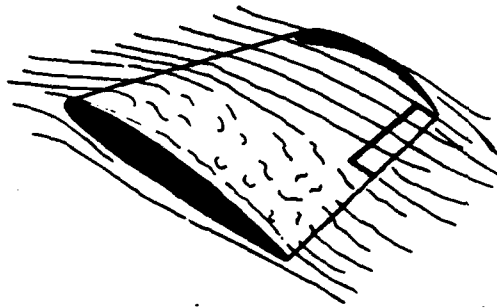


Figure 54. Example of Aerodynamic Twist (Reference (43))

Though geometric washout and aerodynamic twist are helpful in preventing wing tip stall, many times it is not enough to prevent tip stall characteristics from occurring on highly swept tapered wings typical of fighter aircraft. Another approach used to inhibit or eliminate tip stall is by the use of stall fences and snags. Both of these stall control methods attempt to prevent the boundary layer from moving outward toward the tips caused by the spanwise pressure gradient characteristic of a swept wing. The stall fence is a chordwise strip as shown in figure 55a and an example of a snag (leading-edge discontinuity) is shown in figure 55b. The snag attempts to inhibit the spanwise flow by generating a vortex just above the wing surface and as a result energize the flow perpendicular to the wing leading-edge. The stall fence, like the snag, is also based on the principle of generating vortex flow to energize the flow perpendicular to the wing. In many cases the stall fence has the additional effect of inhibiting spanwise flow by its physical presence. Other stall control devices (shown in figure 55) that also utilize the vortex generating principle include, (c) leading-edge notch, and (d) leading-edge fairing.

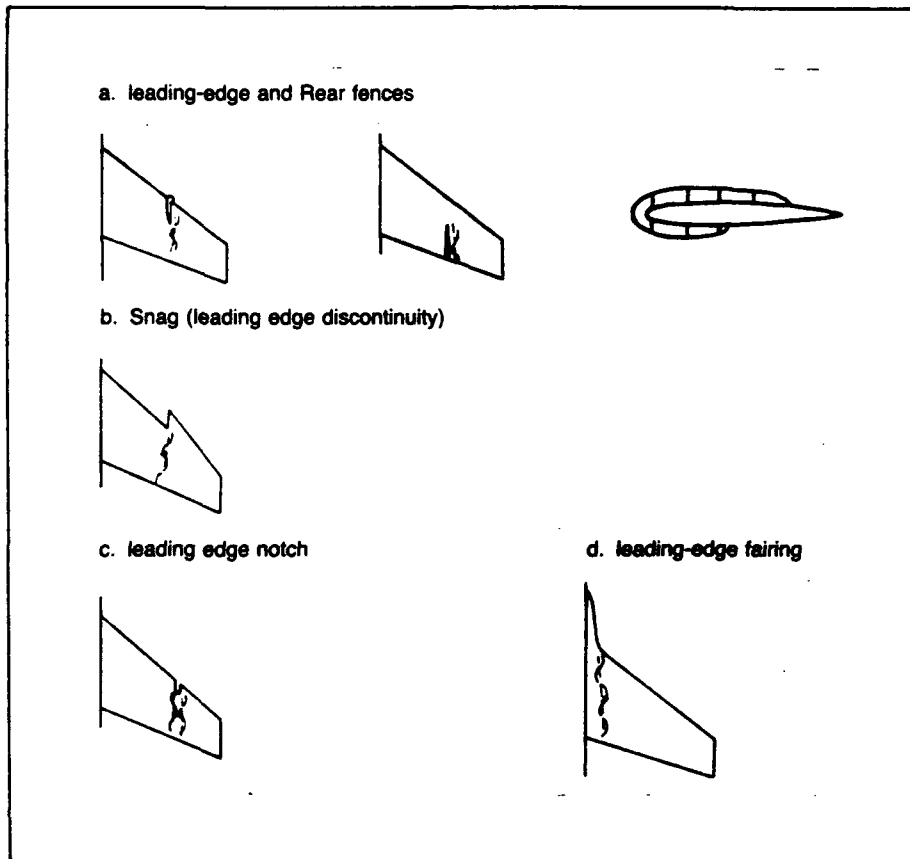


Figure 55. Wing Vortex Producing Devices (Reference (8) and (13))

The installation of leading-edge slot devices is another option available for use in designing for good stall characteristics. Various leading-edge devices are shown in figure 56 taken from reference (8).

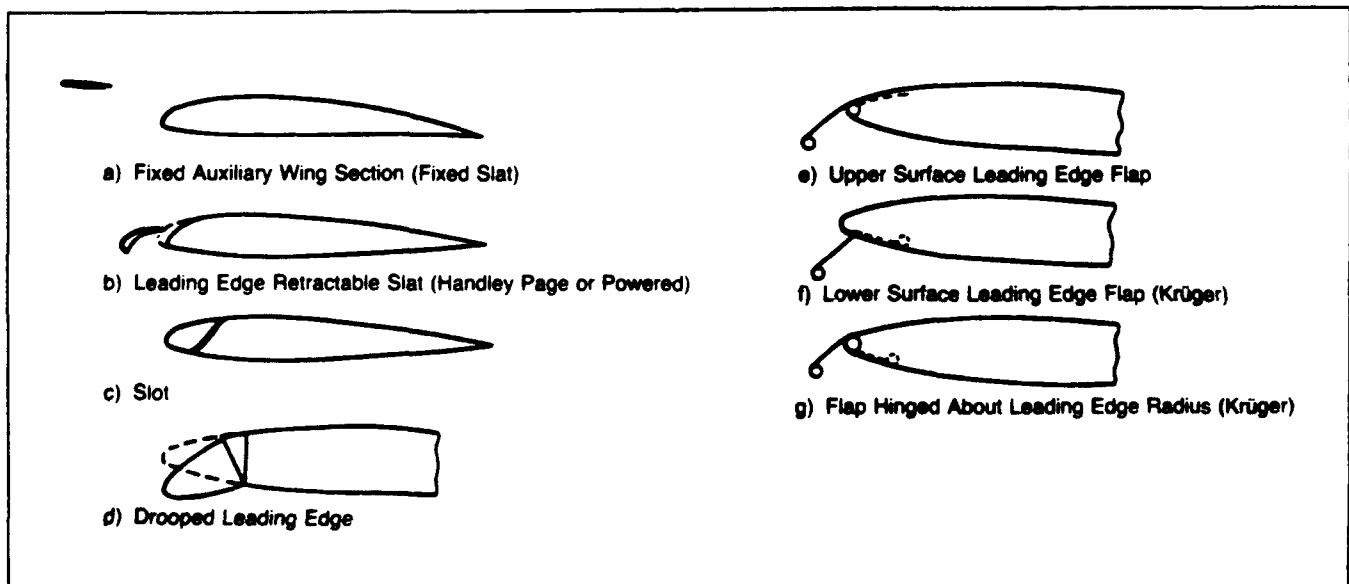


Figure 56. Wing Leading Edge Type Devices (Reference (8))

Figure 56a and b depict slats that may be either fixed in a position or retractable. Figure 56c depicts a slot modification, and figures 56d through g illustrate different types of leading-edge flaps. The purpose of each of these devices is to reduce the severity of the adverse pressure peak that causes leading-edge separation at high angles-of-attack. By mitigating the pressure peak, the effective result is to delay separation and thus stall. Figures 57 and 58 taken from reference (9) illustrate examples of the

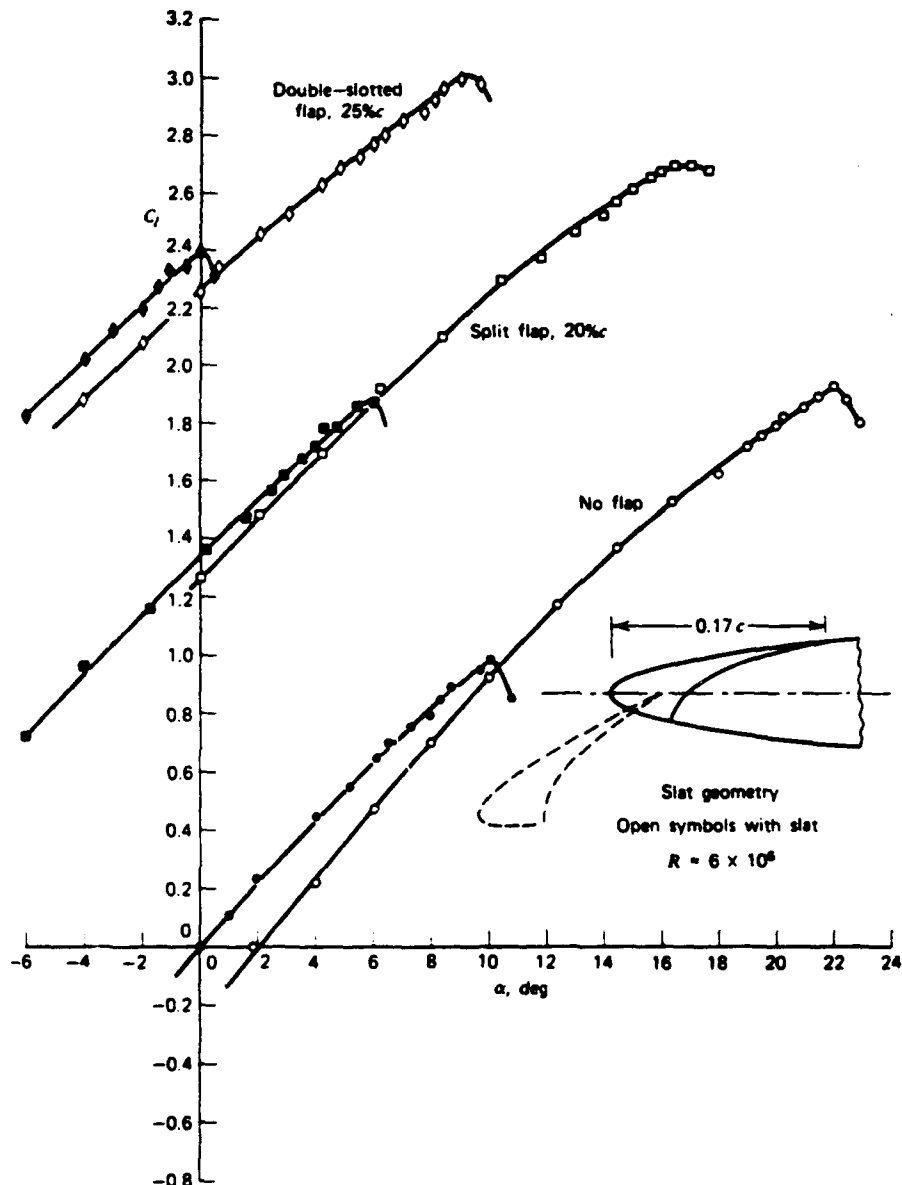


Figure 57. Effect of Leading Edge Slat on NACA 64A010 Airfoil With and Without Flaps. (Reference (9) )

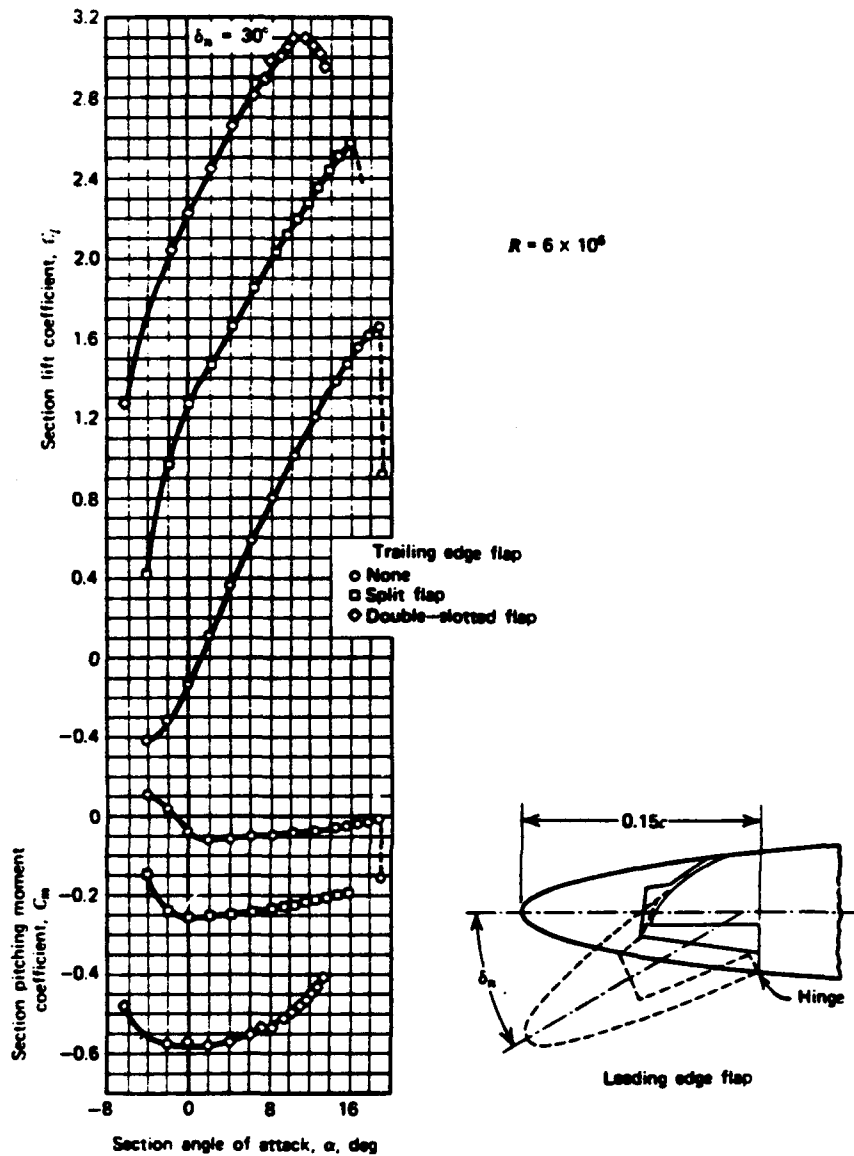


Figure 58. Effect of Leading Edge Flap on NACA 64A010 Airfoil With and Without Flaps. (Reference (9)).

effect slats and flaps might have on the lift curve respectively. Figure 59 illustrates the means by which the increase in  $C_{l_{max}}$  is achieved (i.e., chord extension, camber or boundary layer control) for the slat, Krueger flap, droop leading-edge and slot leading-edge devices. In many cases these devices have been used over part of the outboard portions of the wing span to prevent tip stall.

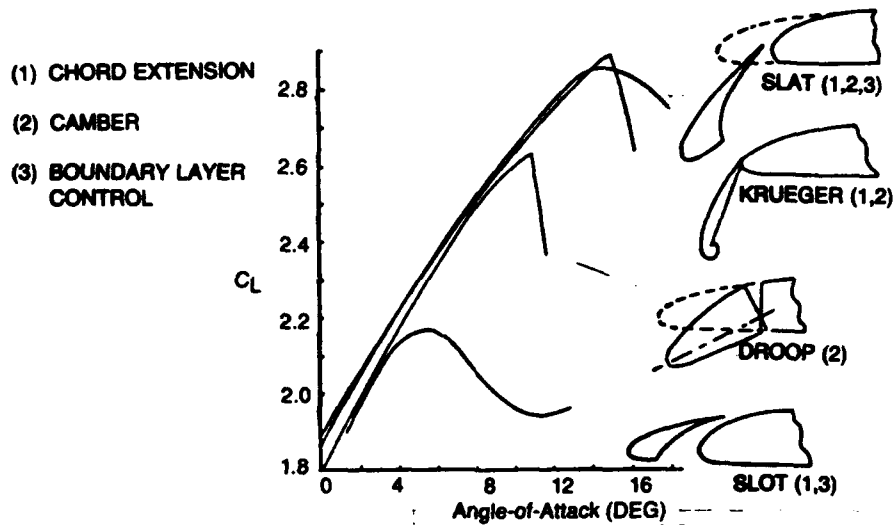


Figure 59. Lift Data for Various Leading-edge Devices (Reference 44)

The last device without auxiliary power to be discussed concerning stall control is vortex generators. Vortex generators are very small, low aspect ratio wings placed vertically at some angle-of-attack on the wing surface as shown in figure 60.



Figure 60. Trident Wing with Vortex Generators. Photo provided by Hawker-Siddeley Aviation Ltd. (Reference (12))

In general vortex generators are used to prevent or delay separation in a situation where the boundary-layer is turbulent but insufficient to prevent separation (Reference (12)). Each vortex generator produces a longitudinal vortex extending downstream. These vortices enhance the mixing across the boundary-layer bringing rapidly moving fluid from outside the boundary-layer in close to the wing surface. By supplementing the mixing due to turbulence, separation is delayed by effectively reducing the pressure gradient (Reference (44)). Many of the other type of devices that can be classified as vortex generators are given in figure 61.

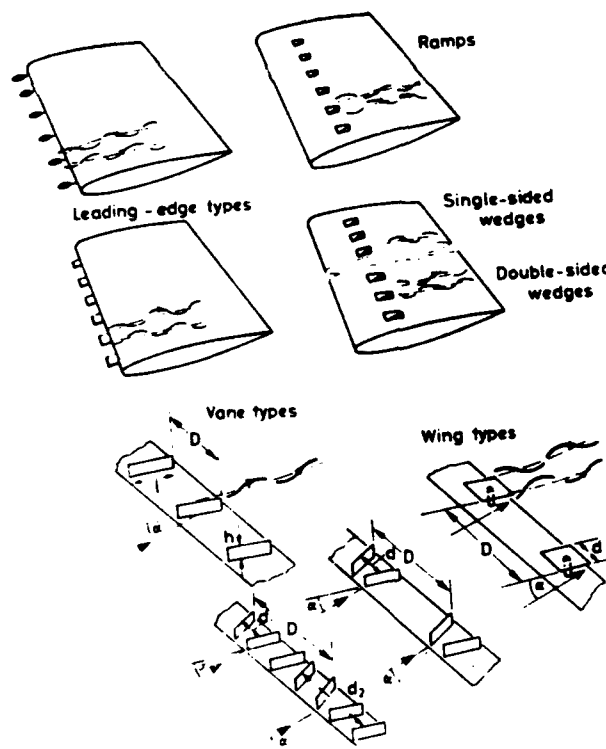


Figure 61. Types of Vortex Generators (Reference (13))

The boundary-layer control techniques that require auxiliary power include suction and blowing techniques. The principle underlying boundary-layer suction is to eliminate or decrease the effect of viscosity on separation. By the use of suction, the decelerated flow particles within the boundary-layer are removed before separation occurs in order that the newly formed boundary layer may overcome the

adverse pressure gradient (reference (44)). Figure 62 below shows some of the practical concepts being studied in order to apply the suction boundary-layer control method to wing leading and trailing edges. Successful application of boundary-layer suction has been documented (F-86F airplane, 1953) to not only increase lift but also reduce skin friction drag by delaying the transition to turbulent flow (reference (8)).

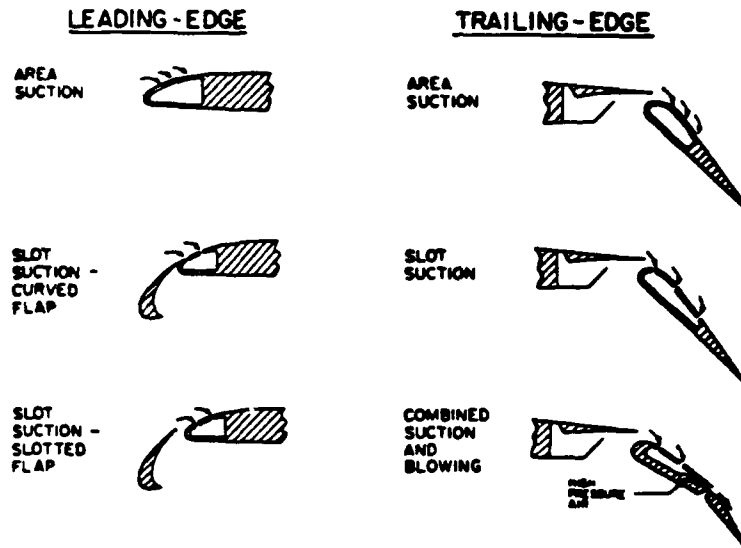


Figure 62. Suction Boundary-layer Control Concepts (Reference (44) )

Figure 63 illustrates the significant increase in maximum lift realized for a NACA 63A009 airfoil using porous nose suction. The term  $C_o$  defines the amount of energy used to provide the suction.

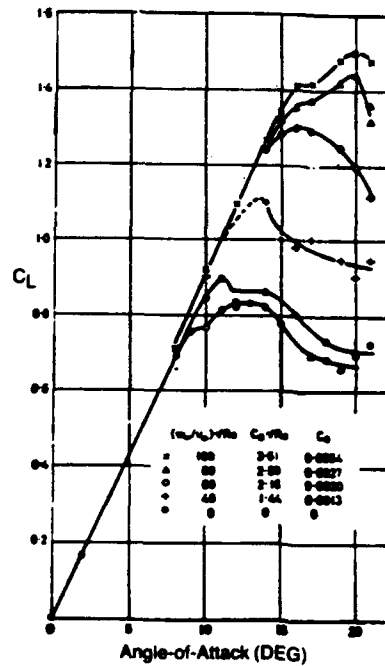


Figure 63. Experimental Lift Curves for an NACA 63A009 Airfoil With Porous Nose (Reference (13) )

Blowing is another method that utilizes auxiliary power to effect boundary-layer control. The principle behind blowing is to add energy to the surface fluid by injecting a foreign fluid in the neighborhood of the surface wall. Figure 64 below illustrates some of the current practical blowing leading and trailing edge boundary-layer control concepts.

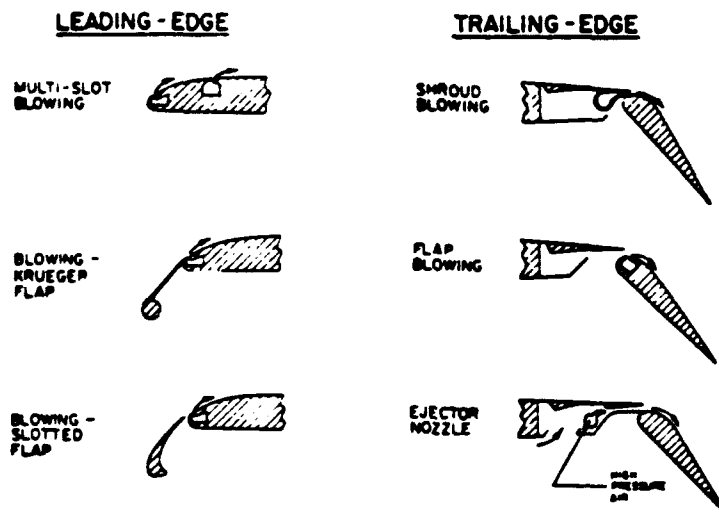


Figure 64. Blowing Boundary-layer Control Concepts (Reference (44))

Reference (9) distinguishes two types of blowing, tangential blowing and normal blowing. Tangential blowing, as it implies, describes injecting a fluid parallel to the surface to augment the momentum of the shear layer close to the surface, whereas normal blowing describes injecting the fluid normal to the wall to increase the mixing rate. The blowing technique termed "blown flap," has been a very important method used to improve low speed lift and stability characteristics during takeoff and landing phases of flight. For many STOL aircraft operating at high angles-of-attack and utilizing large flap angles, the boundary layer is unable to negotiate the large adverse pressure gradients on the upper surface of the wing leading-edge and flap knee. As a result flow separation takes place at either or both of these places. Taken from reference (9), figure 65 illustrates the effect of blowing on lift as a function of angle-of-attack and the pressure distributions over the upper wing surface for various positions of upper-surface blowing.

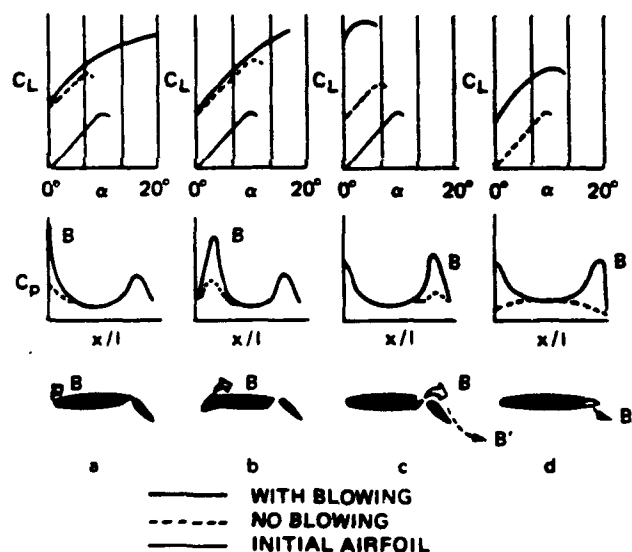


Figure 65. Influence of Blowing on the Lift-Curve-Slope and Pressure Distribution for Various Blowing Methods (Reference (9) )

Bamber (1931) showed that the optimum position of the blowing slot on the upper surface is beyond the midchord. The optimum for a 14.5 percent thick airfoil lies between one-half to two-thirds chord from the leading edge. An example of the blowing effects from this position are shown in figure 66 for a NACA 84-M wing section. The author of reference (7) points out that careful attention must be given to the shape of the slit in order to prevent the jet from dissolving into vortices at a short distance behind the exit section.

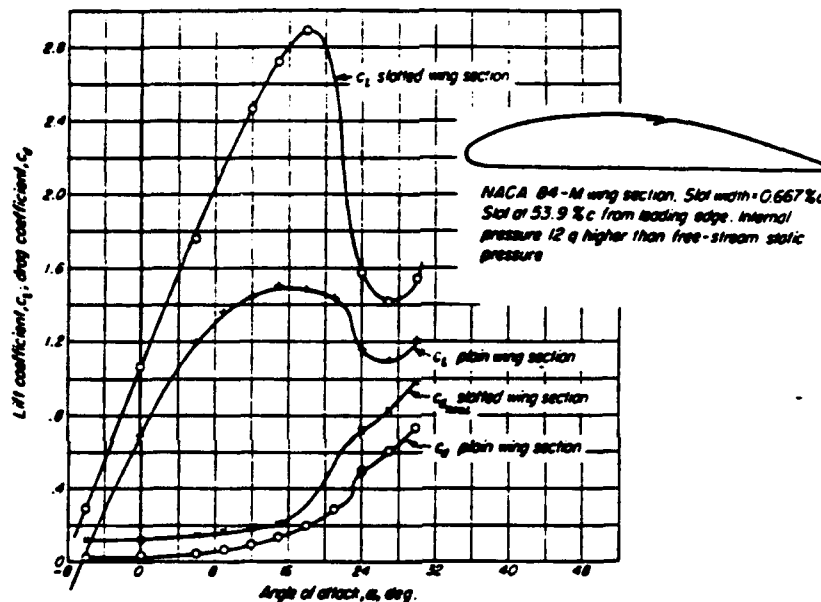


Figure 66. Effect of Blowing on Aerodynamic Characteristics. Slot at 53.9% c from Leading Edge (NACA TN 323) (Reference (8))

In addition to the suction and blowing techniques being employed separately for use in boundary-layer control, the availability of a high pressure source makes it possible to combine the two techniques (Reference (44)).

The additional design complexities that arise due to the power requirements of both suction and blowing boundary-layer control techniques has not been discussed in this section, but of course their important considerations for practical application should be realized. (See Reference (8) for a discussion of power requirements and considerations.)

Entire textbooks (References (8) and (10)) have been written on methods to change or control the character and development of the boundary layer; this section claims to only present those most widely used for application to flow over a wing-type surface. For the purpose of this section, only the boundary layer control methods whose primary objective is to prevent boundary layer separation were presented. However, it should be noted that it might be desirable in some instances to intentionally initiate boundary layer separation. An example of this is shown below in figure 67 where a probe is used on a blunt supersonic body to delay separation, reduce drag and increase lift at high angles-of-attack.

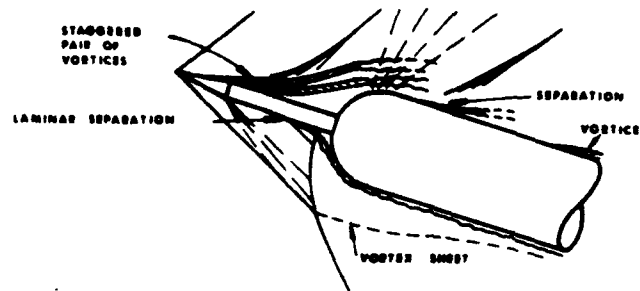


Figure 67. Example of Flow at High Angle-of-attack for a Blunt Body With a Spike (Reference (9))

## 2.3 The Spin

### 2.3.1 General/Definition

The spin, which can occur only after stall, has many interesting and singular properties. Any loss of control can be disastrous, but an unexpected spin during combat can be fatal. Table II provides a digest of comments from operational class IV squadron pilots expressing their views concerning specific

TABLE II DIGEST OF PILOT COMMENTS OF HIGH-AOA FLYING QUALITIES FOR CONTEMPORARY CLASS IV AIRCRAFT (Reference (47) )

| AIRCRAFT   | OVERALL HIGH AOA F.Q.   | DEPARTURE CHARACTERISTICS   | CUES   | OTHER  |
|------------|---|---|--|--|
| A-7        | Departure hazard inappropriate to ground attack mission   | Strong adverse yaw<br>Severe nose slice<br>Predictable-repeatable<br>Easily recovered                           | Buffet   | PCAS turned off at high $\alpha$<br>Wing stores increase stability                                 |
| A-10       | High AOA — usually defensive<br>No adverse flying characteristics<br>No worry about departure or spin<br>High pitch rate capability — can pull through stall warning too fast | Very resistant to departure<br>Very mild stall — little warning<br>Mild buffet<br>Some wing rock<br>Mild yaw    | $\alpha$ : Aural tone<br>Peak performance — steady<br>Stall-beep<br>V: Noise level<br>Stick position             | Ailerons remain effective in stall — like Cessna   |
| F-4C, D, E | Acceptable to good for fighter<br>Departure hazard for ground attack<br>Good control effectiveness<br>Must change control technique to rudder maneuvering                     | Strong adverse yaw<br>Abrupt noise slice/roll<br>Predictable-repeatable<br>Recoverable (if sufficient altitude) | $\alpha$ : Buffet (poor, early, heavy)<br>Stick position<br>V: Stick force<br>Dig-in<br>Opt. Turn: Aircraft buzz | Force harmony problems at low dynamic pressure<br>Can over-rotate or over-g<br>Roll SAS turned off |

TABLE II (Continued) DIGEST OF PILOT COMMENTS OF HIGH- $\alpha$  FLYING QUALITIES FOR CONTEMPORARY CLASS IV AIRCRAFT  
(Reference (47) )

| AIRCRAFT                    | OVERALL HIGH $\alpha$ F.Q.   | DEPARTURE CHARACTERISTICS  | CUES  | OTHER  |
|-----------------------------|--|--|---|--|
| F-4E<br>(Leading edge slat) | Excellent<br>Better separation between $C_{L_{max}}$ and departure $\alpha$<br>Less roll rate capability<br>Use aileron and rudder to roll | Reduced adverse yaw<br>Departure resistant<br>Roll departure<br>Somewhat unpredictable at very high $\alpha$<br>Recovers quickly | $\alpha$ : Buffet (good, steady, increase)<br>Aural tone<br>Stick position<br><br>V: Buffet increase<br>Stick force<br><br>Opt. Turn: Aircraft buzz | Roll SAS turned off  |
| F-5E                        | Excellent<br>Can point aircraft at very low speeds<br>Never worry about $\alpha$<br>Loose aileron roll power — must use rudder maneuvering | Departure resistant<br>Rudder induced high yaw rate<br>Difficult to recover  | $\alpha$ : Buffet; stick position<br><br>V: Flap horn<br><br>Opt. Turn: Buffet  | No roll rate CAS<br><br>Full aft stick — max $\alpha$<br><br>Centerline stores degrade stability significantly |
| F-14A                       | Good — "Honest"<br>High control power<br>Requires rudder maneuvering   | Adverse aileron yaw<br>Departure resistant<br>Yaw/roll departure<br>Severity is speed dependent                                  | Generally poor<br><br>Buffet<br><br>Stick position<br><br>Stick force   | Main problem with asymmetric thrust<br><br>PCAS turned off at high $\alpha$                                    |

(Reference (47) )

| AIRCRAFT | OVERALL HIGH AOA F.O.  | DEPARTURE CHARACTERISTICS  | CUES  | OTHER  |
|----------|--|--|---|--|
| F-15A    | Excellent<br>High longitudinal control power<br>Some worry about over-g<br>SRI makes airplane consistent and repeatable<br>Can override SRI  | Departure resistant<br>Nose slice<br>Recover hands off<br>Auto roll if inverted  | $\alpha$ : Mild wing rock decreasing roll power nose drop at stall<br>Opt. Turn: Light Buffet | Consistent Fs/g longitudinal CAS<br>PCAS turned off at high $\alpha$<br>SRI provides all stick maneuvering<br>$p\alpha + \delta$ , causes inverted auto roll |
| F-16A    | Excellent maneuvering<br>Maneuver with abandon: no worry about about g or departure<br>Tendency to excessive use of high $\alpha$ because of poor cues<br>Limiters "take over control", save poorly skilled pilot, restrict highly skilled pilot | Departure preventing system<br>Can be tricked into Lat/Dir departure g-overshoot super stall<br>Automatic anti-spin system<br>Recovery sometimes difficult | None<br>No stick cues<br>No buffet<br>No artificial cues                                      | Constant $F_z/n$ CAS<br>SRI provides all stick maneuvering<br>Maneuver limits on $n, \alpha, p$<br>Need limit changes with stores                            |
| F/EB-111 | No warning of impending stall/departure<br>Flying qualities excellent right up to departure<br>Suddenly fall off cliff   | Insidious<br>Departure susceptible<br>Nose slice/roll<br>Unpredictable<br>Non-recoverable at low altitude  | No natural cues (stick, force, buffet)<br>Artificial:<br>Shaker<br>Horn<br>Lights             | FCS provides uniform and cueless flying qualities<br>Autotrim can produce inadvertent stall<br>High $\alpha$ encounter often related to change in thrust     |

aircraft high angle-of-attack flying qualities. As compiled by the authors of reference 47 (Donald Johnston and Robert Heffley), the pilot comments revealed that their main concern involved departure/spin resistance flight cues and the role of the flight control system (Reference (47)). Section 2.3.2 will focus on understanding the dynamics that cause a spin as reflected by the comments of column II of Table II, "Departure Characteristics", as well as addressing the aerodynamic factors that cause a spin, and how spin recovery can be accomplished.

The spin is defined as a maneuver during which the aircraft descends rapidly in a helical movement, about a vertical axis, at an angle-of-attack greater than the aircraft stall angle-of-attack (Note,  $\alpha_s$  may be negative or positive). The spinning motion can be very complicated and involve simultaneous rolling, yawing and pitching while the aircraft is at high angles-of-attack and sideslip. The description and study of a spin is usually considered in three phases; (1) incipient (2) steady state (or developed) and (3) the recovery. These three phases are illustrated in figure 68.

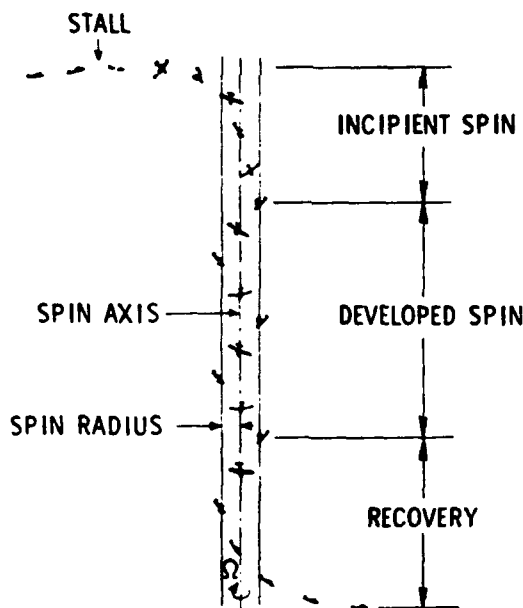


Figure 68. Various Phases of the Spin. (Reference (45)).

Reference (27) describes the incipient and developed spin phases as follows,

Incipient Phase - that portion of a spin occurring from the time the airplane stalls and rotation starts until the spin axis becomes vertical or nearly vertical. Typically this includes the first one, or two turns before the spin becomes fully developed.

Developed Spin - Characterized by the attitude, angles, and motions of the aircraft being somewhat repeatable from turn-to-turn and the flight path is approximately vertical. The spinning motion is made up of rotation about the airplane center-of-gravity plus translatory motion of the center-of-gravity; however, it is primarily a rotary motion and is affected mainly by the inertial and aerodynamic moments acting on it. In the purest sense all accelerations are zero along the body axes.

Recovery - is defined as the transitional event from out-of-control flight to controlled flight. The recovery period of time normally is counted from the time the pilot initiates recovery controls to the point at which the angle-of-attack is below  $\alpha_s$  and no significant uncommanded angular motions remain (Reference (46)).

For a given aircraft configuration there may exist a small finite number of steady state spin modes. This means it is possible to spin an aircraft only for a limited number of unique sets of angle-of-attack, angle-of-side slip, roll angle, spin rate and spin radius. There are also aircraft that never reach true steady state spins but attain only partially developed spins. As described by reference (33) the difference is that in the partially developed spin there exists force or moment imbalance about one of the axes.

### 2.3.2 Causes of Aircraft Spin

Fundamentally an aircraft will enter a spin after stall occurs if the post-stall dynamics are characterized by rolling and/or yawing disturbances such that a phenomenon known as autorotation results. The origin of these disturbances is most commonly due to an asymmetric stall progression that

causes the sudden drop of one wing. Two other examples of lateral-directional disturbances include: (1) coupling of pitch-up and lateral asymmetry and, (2) directional coupling or a yaw departure such as a nose slice.

Autorotation is the term used to describe the aerodynamic pro-spin rolling and yawing moment that can develop at and above stall with lateral controls in the neutral position. This aerodynamic moment is made up of two main parts, one arises from the rolling motion of the aircraft (i.e., the  $l_p$  contribution) and the other arises from the dihedral effect (i.e.,  $l_p$  contribution) (Reference (33)). Under normal flight conditions ( $\alpha < \alpha_s$ ), the rolling moment due to the roll rate dynamic derivative,  $l_p$ , is negative indicating that the rolling moment produced opposes or damps the roll rate disturbance. However at and beyond stall it is possible for the sign of the derivative to become positive and the rolling moment produced acts to reinforce the rolling motion of the aircraft perpetuated by the roll disturbance. Figures 69 through 71 are used to illustrate in more detail the mechanics of autorotation. Consider an aircraft subject to a right rolling motion caused by some yawing and/or rolling disturbance occurring after stall. The effect of the rolling disturbance is to decrease the z-component of the free-stream velocity vector on the left wing and increase it on the right wing. Similarly, due to the yawing disturbance, the x-component of the freestream velocity vector is increased on the left wing and decreased on the right wing. The result is an unequal angle-of-attack distribution between the wings of the aircraft. This is illustrated vectorially in figure 69 taken from reference (8).

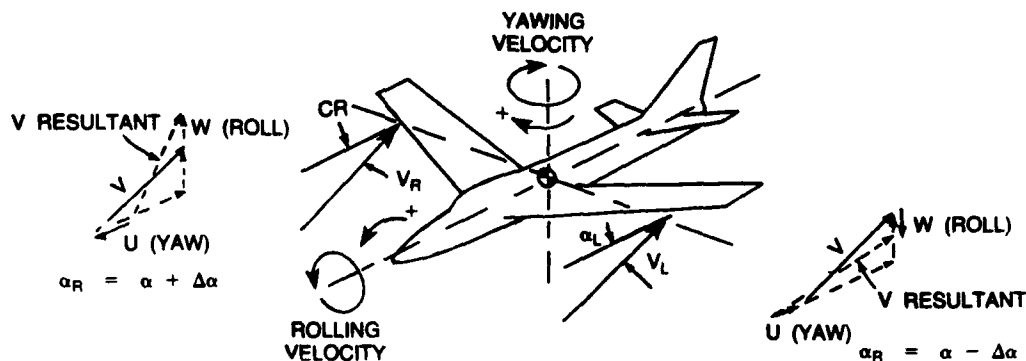


Figure 69. Mechanics of Autorotation (Reference (8))

Because the wing is operating at a point above the stall angle-of-attack (point B of figure 70) the downgoing right wing (experiencing the effective increased angle-of-attack; i.e., due to roll rate, yaw rate and dihedral effect) will experience a decrease in lift and an increase in drag as compared with the upgoing left wing.

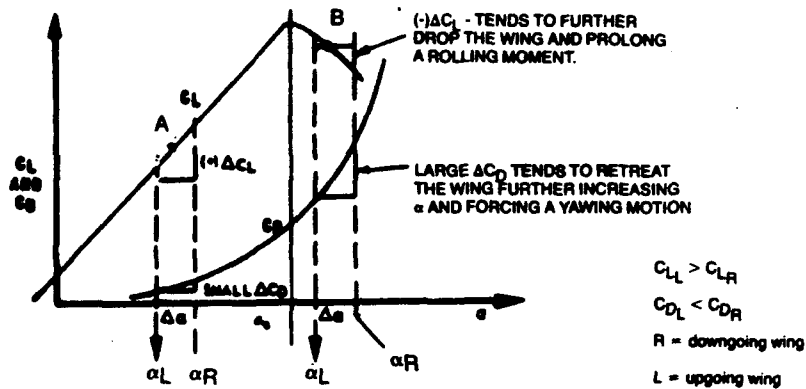


Figure 70. Changes in  $C_L$  and  $C_D$  With  $\alpha < \alpha_s$  and  $\alpha > \alpha_s$  (Reference (46))

The differential in aerodynamic forces that results (see figure 71) cause the autorotative couples which sustain the precipitating rolling and yawing motions.

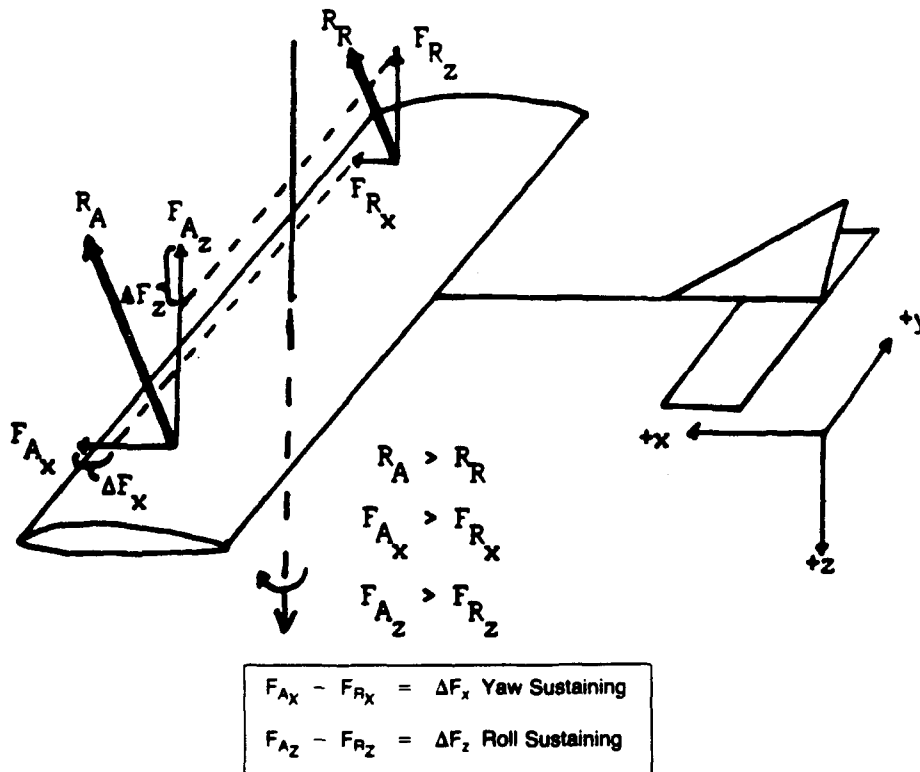


Figure 71. Difference in Resultant Aerodynamic Forces Resulting in Autorotative Yawing Couple (Reference (46))

Of course each component of the aircraft, and not just the wing contribute to the overall aircraft static ( $C_{l_p}$ ,  $C_{n_p}$ ) and dynamic stability ( $C_{l_p}$ ,  $C_{n_p}$ ,  $C_{n_r}$ ,  $C_{l_r}$ ). Factors such as the vertical tail and fuselage contributions are usually secondary in importance compared to the wing contribution when considering lateral stability, but nevertheless must be considered. Their importance is a function of the particular configuration (i.e., tail size, fuselage shape, etc.) and on the actual condition of flight (i.e, mach number, angle-of-attack, sideslip angle). Before leaving the topic of the causes of autorotation, it must be emphasized, as noted by Bernard Etkin (author of Reference (48)), "that the rolling and yawing motions are inextricably coupled, and conclusions concerning lateral-directional behavior of a particular aircraft must be made by dynamic analysis. It can be said that aircraft flight in the post-stall flight regime is affected by very different nonlinear aerodynamic forces than those acting upon the aircraft during unstalled flight". It is especially true that the stability derivatives that depend on the lift-curve slope of the wing ( $C_{l_p}$ ,  $C_{n_p}$  and  $C_{n_r}$ ) have the most significant behavior change in the post-stall flight regime (reference 33). In most cases it is correct to say that the stability derivative  $C_{l_p}$  becomes positive;  $C_{n_p}$  may become positive and  $C_{n_r}$  may also become greater in post-stalled flight (reference (33)). Each of these changes contributes to autorotation, the aerodynamic phenomenon which initiates and sustains a spin.

Aerodynamic considerations are by no means the only factors effecting the post-stall motions of an aircraft. The inertia characteristics of the aircraft are equally important as will be shown through the development of the equations of motions to be discussed next. As a brief example of this, in yaw, the fuselage moment of inertia is an anti-spinning moment while the wing moment of inertia is a pro-spinning one. Ordinarily the aerodynamic and inertial moments are the dominant ones but gyroscopic influences of rotating masses such as engine spools can also become a contributing factor.

### 2.3.3 Dynamics of the Spin

In a fully developed spin the motions in roll, yaw and pitch initiated by the autorotative phenomena are opposed by the inertia moments until eventually a equilibrium balance is achieved between them. If an equilibrium condition does not exist then the aircraft will not attain a steady state and the spin will be oscillatory instead. The condition of equilibrium in the spin is usually determined with respect to two different set of axes, (1) the spin axis and (2) a set of body axes  $Oxyz$  fixed relative to an aircraft reference line (see figure 72).

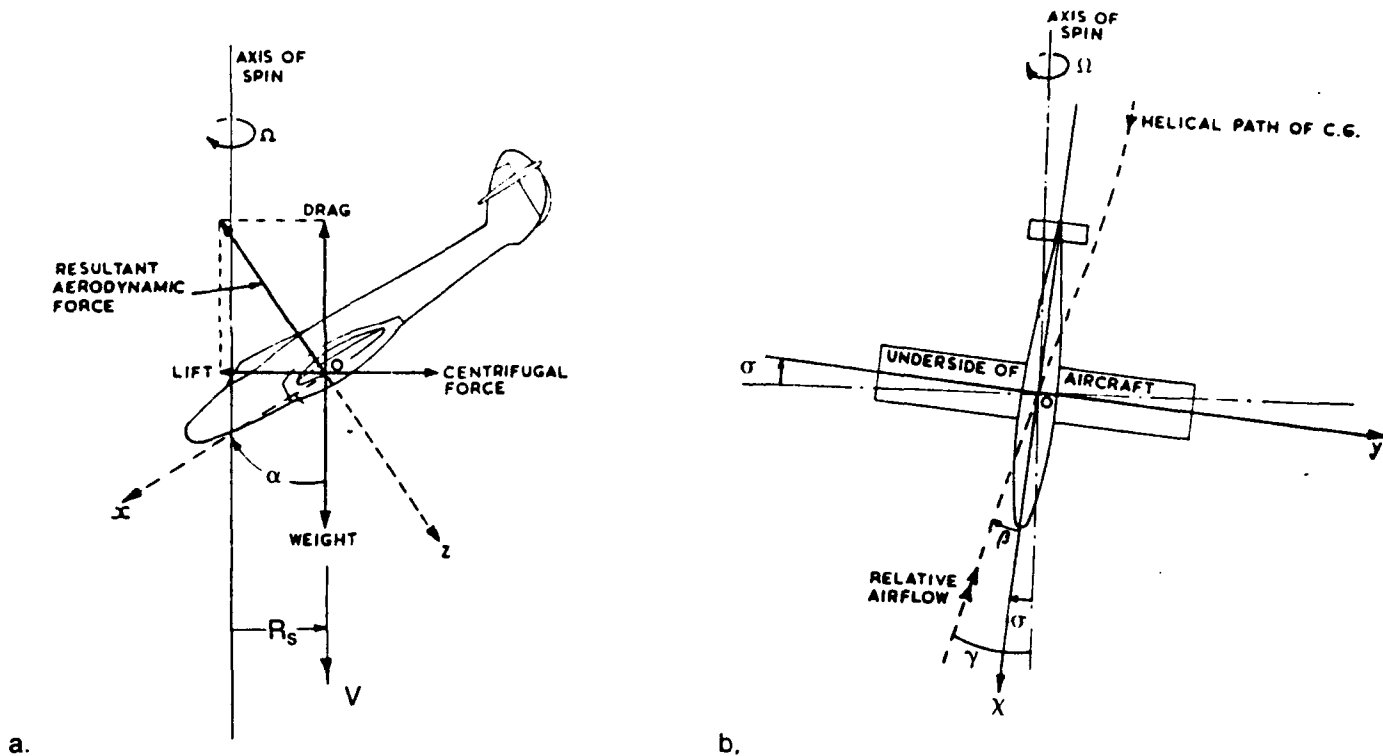


Figure 72. (a) Force Definition During a Steady Spinning Aircraft  
(b) Attitude Definition of a Steady Spinning Aircraft (Reference (31))

The balance of forces and moments determines the equilibrium values of the spin radius ( $R$ ), the sideslip angle ( $\beta$ ), rate of descent ( $\dot{h}$ ), angle-of-attack ( $\alpha$ ), etc. of the aircraft. Figure 72a illustrates the balance of forces in a spin. The three main forces acting on an aircraft in a spin are the resultant aerodynamic force, the centrifugal force, and the weight. Since the resultant relative airflow in a spin is approximately vertical (with respect to the earth), the vertical component of the resultant aerodynamic force is typically referred to as "drag" and the horizontal component as "lift" (see figure 72a). If a steady spin is assumed (no oscillations are present about the rotation axes), it follows that the force equations reduce to the following relationships: (1) side force is zero (2) drag equals weight and (3) lift is balanced by centrifugal force. These three relationships are given in equations (4) through (6).

$$F_y = 0 \quad \text{EQ (4)}$$

$$mg = \frac{1}{2} \rho V^2 SC_D \quad \text{EQ (5)}$$

$$m R_s \Omega^2 = \frac{1}{2} \rho V^2 SC_L \quad \text{EQ (6)}$$

Note that equation (6), indicating zero side force, implies that the aircraft bank angle ( $\phi$ ) is assumed equal to zero.

Reference (49) points out that the balance of the forces acting in the spin is a relatively unimportant factor in determining the final equilibrium conditions of sideslip angle, angle-of-attack, etc. Instead, it is the balance of moments that chiefly determines the equilibrium values. The three body axes moment equations are given by equations (7) through (9) for zero angular accelerations.

$$\begin{array}{c} \text{Aero} \qquad \text{Inertial} \qquad \text{Gyroscopic} \qquad \text{Misc.} \\ \qquad \qquad \text{Coupling} \qquad \text{Terms} \qquad \text{rockets, Spin} \\ \qquad \qquad \qquad \qquad \qquad \qquad \qquad \qquad \text{chutes, etc.} \end{array}$$

$$\dot{p} = \frac{L}{I_x} + \frac{I_y - I_z}{I_x} qr + \frac{L_{gyro}}{I_x'} + \frac{L_{other}}{I_x''} \quad \text{EQ (7)}$$

$$\dot{q} = \frac{M}{I_x} + \frac{I_z - I_x}{I_y} pr + \frac{M_{gyro}}{I_y'} + \frac{M_{other}}{I_y''} \quad \text{EQ (8)}$$

$$\dot{r} = \frac{N}{I_z} + \frac{I_x - I_y}{I_z} pq + \frac{N_{gyro}}{I_z'} + \frac{N_{other}}{I_z''} \quad \text{EQ (9)}$$

To understand the dynamics of the spin it is essential to have a good understanding of the balancing moment equations. The balancing of the pitching moments (aerodynamic and inertial) acting on the aircraft is illustrated in figure 73 and will be used as an example (a discussion on the yaw and roll balancing moments is similarly given in Reference (33)). An explanation of the inertial coupling terms of equation (8) can be given based on the principles of gyroscopic precession. Consider the aircraft of figure 73 with its axis of rotation in the Oz direction and rotating at a yaw rate, r, in the clockwise direction viewed from above. When the aircraft rolls to the right, it precesses in the nose-up direction. The nose-up pitching moment produced is equal to  $I_z pr$ . Similarly, if the aircraft rotates about the Ox direction at an angular roll rate p, clockwise from the rear, then when the aircraft yaws right (viewed from the rear) it precesses in the nose down direction. The pitching moment produced is equal to  $-I_x pr$ . Thus the inertial coupling always produces two moments which act in opposite directions. This highlights the fact that the magnitude of the inertial moment is dependent on the mass distribution of the aircraft. In the case of the pitching moment, since  $I_z$  is always greater than  $I_x$  the resulting moment always acts in the nose-up direction for an erect spin. Figure 73b illustrates the inertial nose-up pitching moment, as just described in terms of the centrifugal forces acting on imaginary concentrated masses due to the rotation of the aircraft about the spin axis. The inertial nose-up pitching moment tends to increase the angle-of-attack and "flatten" the spin, while the aerodynamic forces acting on the wing and horizontal tail produce a nose-down moment exactly equal and opposite to satisfy the necessary equilibrium spin state.

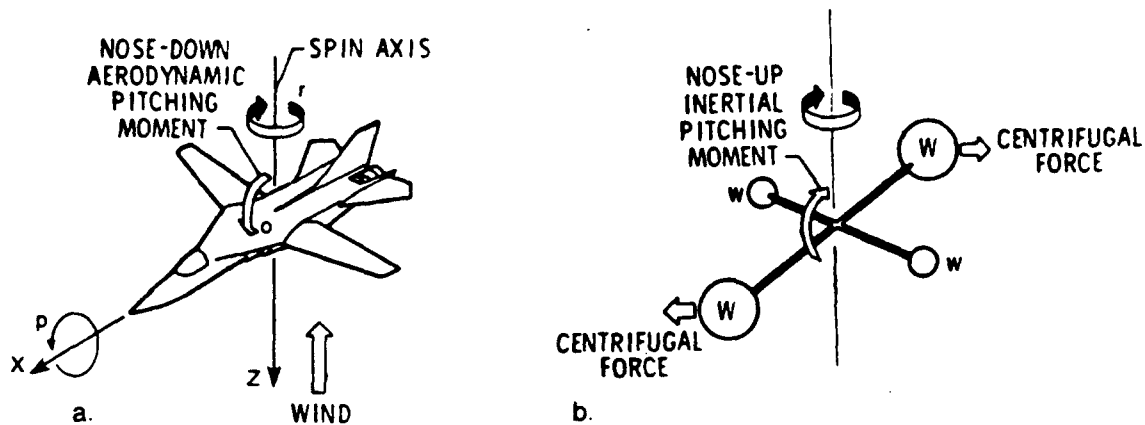


**Figure 73. Balance Between Inertial and Aerodynamic Pitching Moments in a Steady State Spin (Reference (27)).**

The rotary motion of the aircraft about the spin axis can be resolved into its component relative to the set of axes fixed to the body. From figures 72b and 74 these components are given by equations (10) through (12) where  $\sigma$  is the inclination of the flight path from the vertical as defined by equation (13).

$$\rho = r \cos \alpha \cos (\beta + \sigma) \quad \text{EQ (10)}$$

$$p = r \sin (\beta + \sigma) \quad \text{EQ (11)}$$

$$r = r \sin \alpha \cos (\beta + \Omega) \quad \text{EQ (12)}$$

$$\sigma = \arctan (R_s r/V) \quad \text{EQ (13)}$$

This angle,  $\sigma$  is referred to as the helix angle. According to reference (49) this is a convenient notation as adopted by Bamber, Zimmerman and House (references (50) and (51)) because the axes rotations are defined in terms of  $\alpha$  and  $\beta$  (see figure 72b). First the aircraft is considered to be yawed through an angle  $= -(\beta + \sigma)$ , then the aircraft is pitched from the vertical by the angle,  $\alpha$ . The necessary requirements that must be satisfied for equilibrium of the aerodynamic and inertial terms

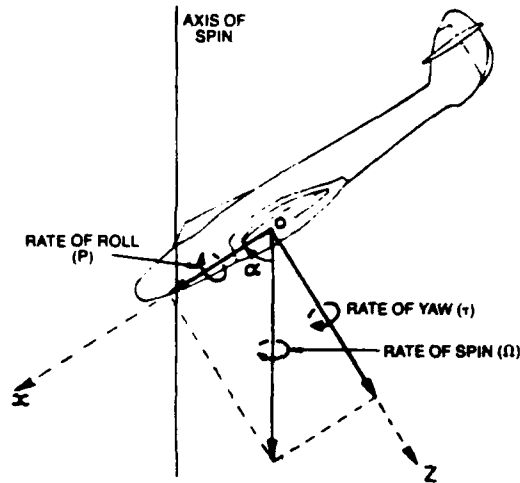


Figure 74. Angular Rates in a Spin (Reference (33) ).

(neglecting gyroscopic and other contributing moment terms for this development), and thus for a steady spin, is found by substituting equations (10-12) into equations (7-9) and solving for the aerodynamic coefficients. Doing this yields equation (14-16).

$$C_m = (4/\rho S \cdot c \cdot b^2) (\Omega b/2V)^2 (I_x - I_z) \sin 2\alpha \cos^2 (\sigma + \beta) \quad \text{EQ (14)}$$

$$C_l = (4/\rho S \cdot b^3) (\Omega b/2V)^2 (I_z - I_y) \sin \alpha \sin 2 (\sigma + \beta) \quad \text{EQ (15)}$$

$$C_n = (4/\rho S \cdot b^3) (\Omega b/2V)^2 (I_y - I_x) \cos \alpha \sin 2 (\sigma + \beta) \quad \text{EQ (16)}$$

Solving Equation (6) for the spin Radius,  $R_s$  and substituting into equation (13),  $\sigma$  can be redefined in terms of  $\Omega b/2V$  as given by equation (17).

$$\sigma = \tan^{-1} \left[ \frac{\rho \cdot S \cdot b \cdot C_l}{4m(\Omega b/2V)} \right] \quad \text{EQ (17)}$$

It can now be seen that both the aerodynamic and inertial terms (left and right sides of equations (14) through (16) respectively) are functions of  $\Omega b/2V$ ,  $\beta$ , and  $\alpha$ . Thus there are three equations to solve for three unknowns ( $\Omega b/2V$ ,  $\beta$ ,  $\alpha$ ) in order to determine the static spin equilibrium conditions. The analysis presented here concerning the determination of equilibrium spin conditions is taken from reference (49). Calculating the equilibrium values of  $\Omega b/2V$ ,  $\beta$ , and  $\alpha$ , solves equations (14) through (16), and thus satisfies the necessary condition that the spin mode be statically stable. The other requirement that must be satisfied for a fully developed spin to develop is that the static spin equilibrium conditions determined as described, satisfy

$$\frac{dC_l}{d\Omega} < 0 \text{ and } \frac{dC_n}{d\Omega} < 0$$

to ensure dynamic stability.

Indications of probability of recovering from a spin mode in flight are given from this spin prediction analysis of reference (49). If a spin mode is predicted for pro-spin control surface settings and not for neutral or anti-spin settings the mode is assumed recoverable. However, ease of recovery must be determined by examination of damping or autorotative tendencies through the recovery region.

An assumption made in Reference (49) declares  $C_{m_{\text{zero}}}$  is not a strong function of  $\beta$  for most aircraft. For fighter aircraft at high angles of attack, large values of the  $C_{m_{\beta}}$  and  $C_{n_{\alpha}}$  derivatives are not uncommon. The graphical method presented in Reference (49) for determining spin mode flight conditions is probably still valid but may require the addition of these terms for a more precise solution.

## 2.3.4. Inverted Spins

Although most research deals with erect spins, inverted spins occur frequently enough to warrant some discussion. The definition of an inverted spin is basically the same as an erect spin with one exception. The forces and moments must again be balanced, however an inverted spin occurs at a negative angle-of-attack by definition. This is illustrated in figure 75.

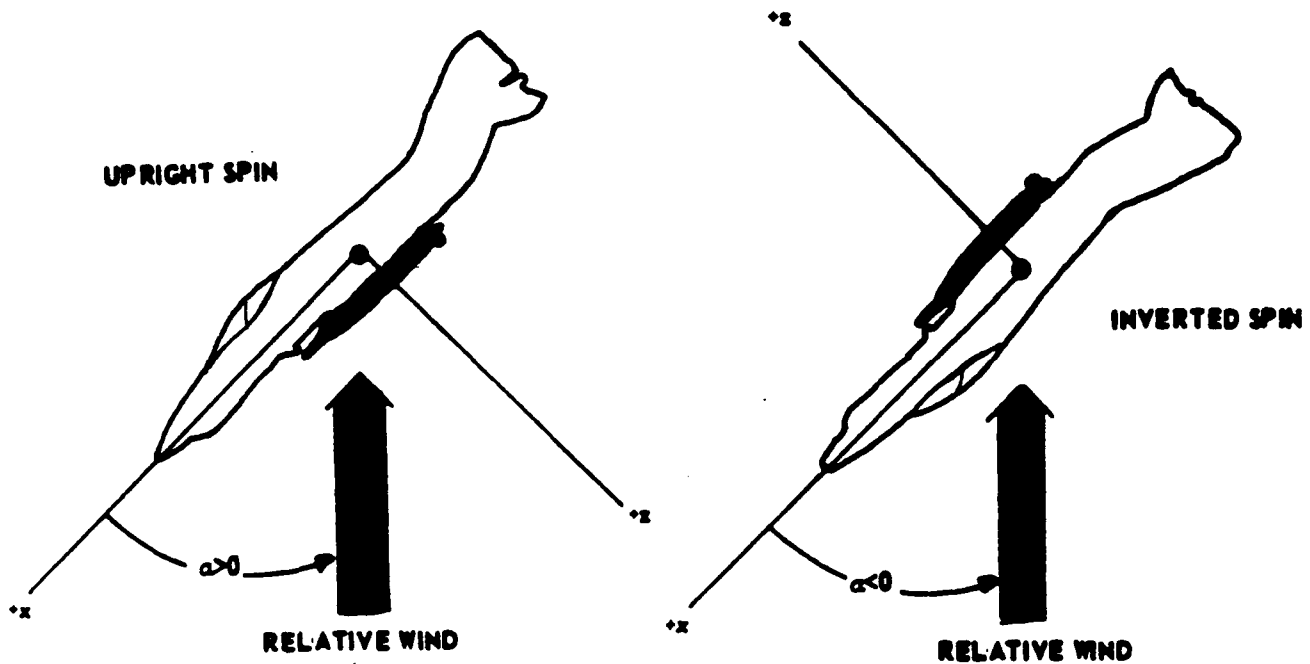


Figure 75. Definition of an Inverted Spin (Reference (46) )

Because the angle-of-attack is negative the dynamics of the inverted spin are different from the erect spin due to the relative change of flow impingement on the fuselage, vertical fin and horizontal stabilizer. In an inverted spin, an aircraft with a low set stabilizer will usually be characterized by less shielding of the fin and rudder by the wake of the wing, fuselage, and horizontal tail as compared to an

erect spin (See figure 76). As a consequence of this an improvement in directional control power is usually encountered. Under these conditions the inverted spin will be steeper and generally recovery will be easier from a controls standpoint (Reference (31)).

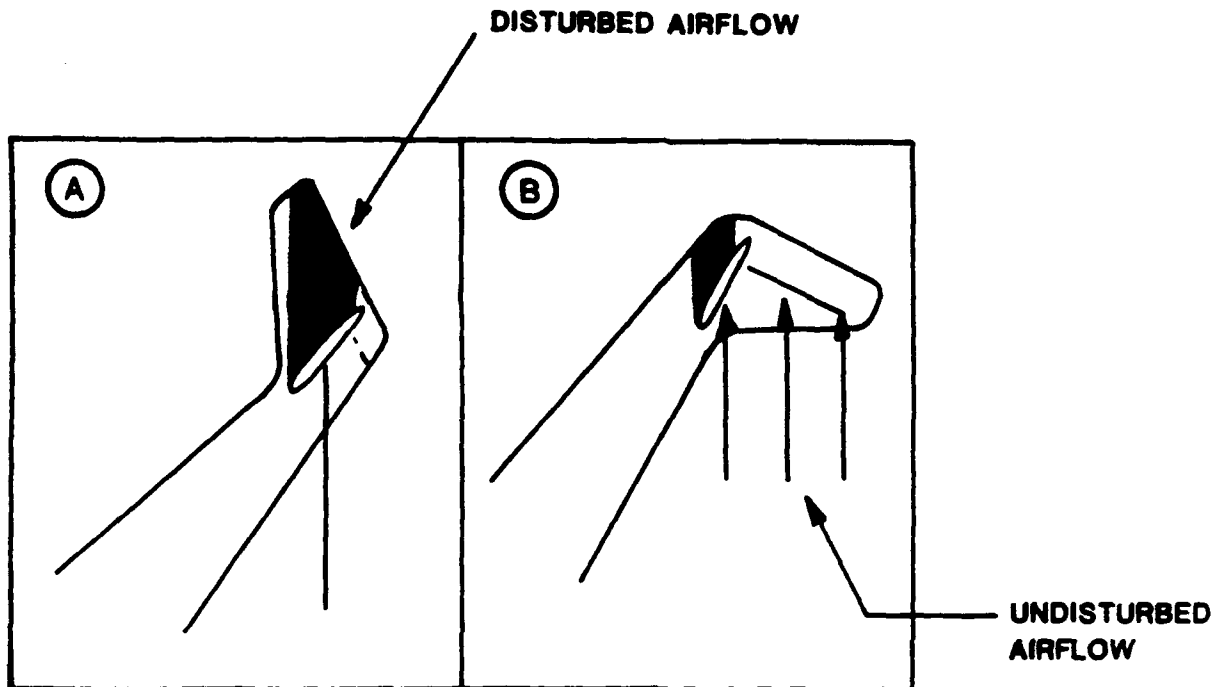


Figure 76. Flows on the Vertical Tail for an Upright (A) and Inverted Spin (B) (Reference (29) )

However it turns out that successful spin recovery is highly dependent upon human factors that can effect individual pilots to varying degrees. For this reason, the statement that inverted spins are generally easier to recover from must be qualified. For instance, the inverted spin is considered more disorienting than an upright spin for two main reasons. Firstly, inverted spins involve negative-g flight, and secondly, roll rate is always opposite to yaw rate in an inverted spin (note, that the spin direction in either an erect or inverted spin is determined by the sense of the yaw rate). As seen by the pilot, the aircraft will be rolling opposite to the direction of the spin (see Figure 77). This can be lethal for pilots who mistakenly judge spin direction by the direction of roll. As reference (29) points out, the chances of

making this error are considerably more likely during a PSG or the incipient phase of the spin when oscillations are extreme. Also adding to the confusion is the fact that in inverted spins ( $|\alpha|$  nearly equals  $|\alpha_s|$ ) the rolling motion is the largest rotation rate (Reference (46)).

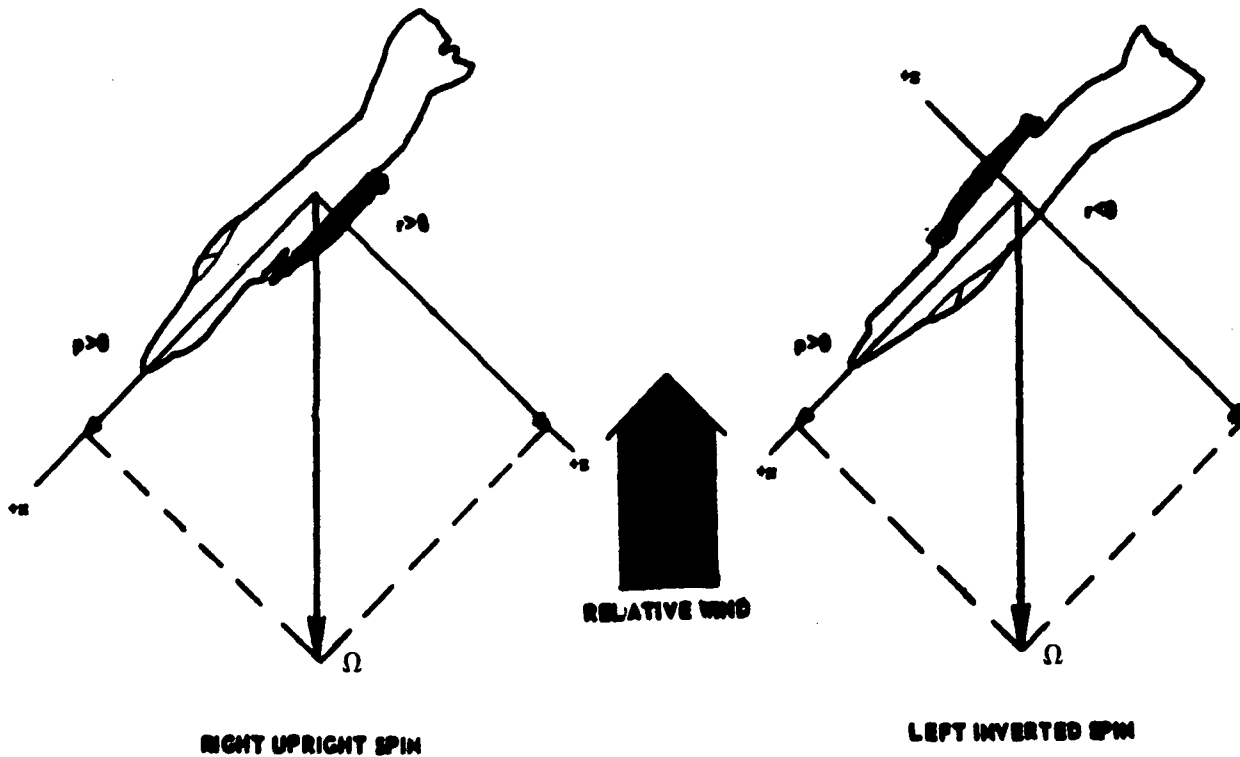


Figure 77. Roll and Yaw Rates of an Upright and Inverted Spin. (Reference (46))

### 2.3.5 Spin Recovery

#### 2.3.5.1 Conventional (Rudder, Stabilizer, Aileron)

Spin recovery, defined earlier as the transitional event from out-of-control conditions to controlled flight, is attained by effecting a change in the steady state moment balance between the aircraft aerodynamic and inertial moments (assuming gyroscopic moment terms and other miscellaneous external moment terms are negligible). To achieve recovery not only must the spin equilibrium be

disturbed, but prolonged angular accelerations in the proper opposing direction are required. The general methods available for generating anti-spin moments are presented in figure 78 with the applicable terms of the general equations they affect.

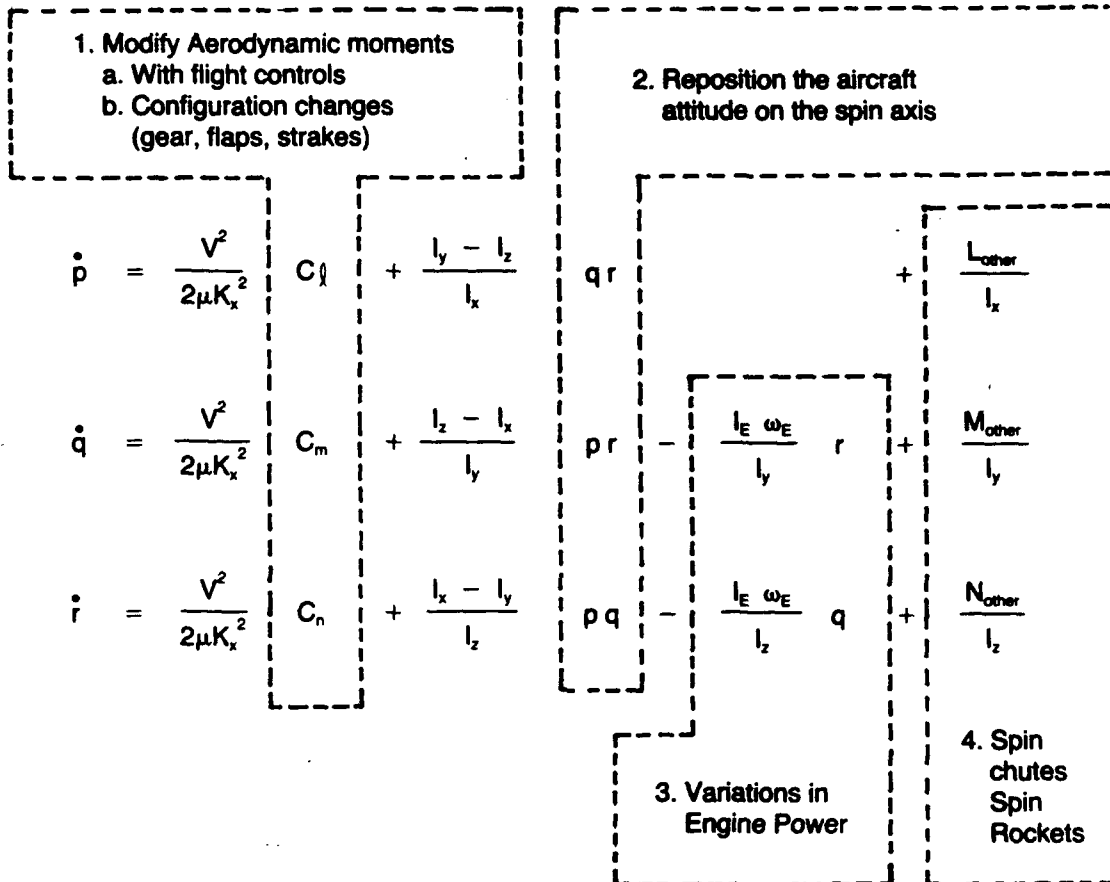


Figure 78 Spin Recovery Methods (Reference (46) )

Alteration of the aerodynamic moments ( $C_l$ ,  $C_m$ ,  $C_n$ ) through the use of flight controls is the conventional means of spin recovery (1.a. of figure 78); seldom are configuration changes (i.e., flap extension, landing gear, etc.) presently used to accomplish spin recovery. The spin recovery technique to be applied is a function of aircraft aerodynamics and mass distribution of the specific configuration being flown. The mass distribution between the wing and fuselage is the predominant factor that determines the way in which the aircraft, while spinning, responds to control deflections, especially to elevator and aileron control. The mass distribution of the aircraft is normally expressed in terms of the inertia yawing moment parameter, IYMP. The inertia yawing moment parameter is a nondimensional factor relating the rolling and pitching moments of inertia and is defined by equation (18).

$$\text{IYMP} = \frac{I_x - I_y}{mb^2} \quad \text{EQ (18)}$$

IYMP has been found to be a normalizing factor (reference (45)) and because it is nondimensional is independent of the size or weight of the aircraft. Present trends in modern fighter aircraft usually results in large negative values of IYMP (i.e., fuselage-heavy aircraft). This is the result of thin wings, jet engine placement and increased weight and fuel cells in the fuselage of the aircraft. It should be noted that the inertia yawing moment parameter can change appreciably in many aircraft as a function of the flight condition being analyzed. An example would be fuel consumption or the addition or release of external stores. Control technique for spin recovery based on IYMP are presented in figure 79 as taken from reference (44).

A brief discussion of the effectiveness of each of the conventional controls will now be presented separately.

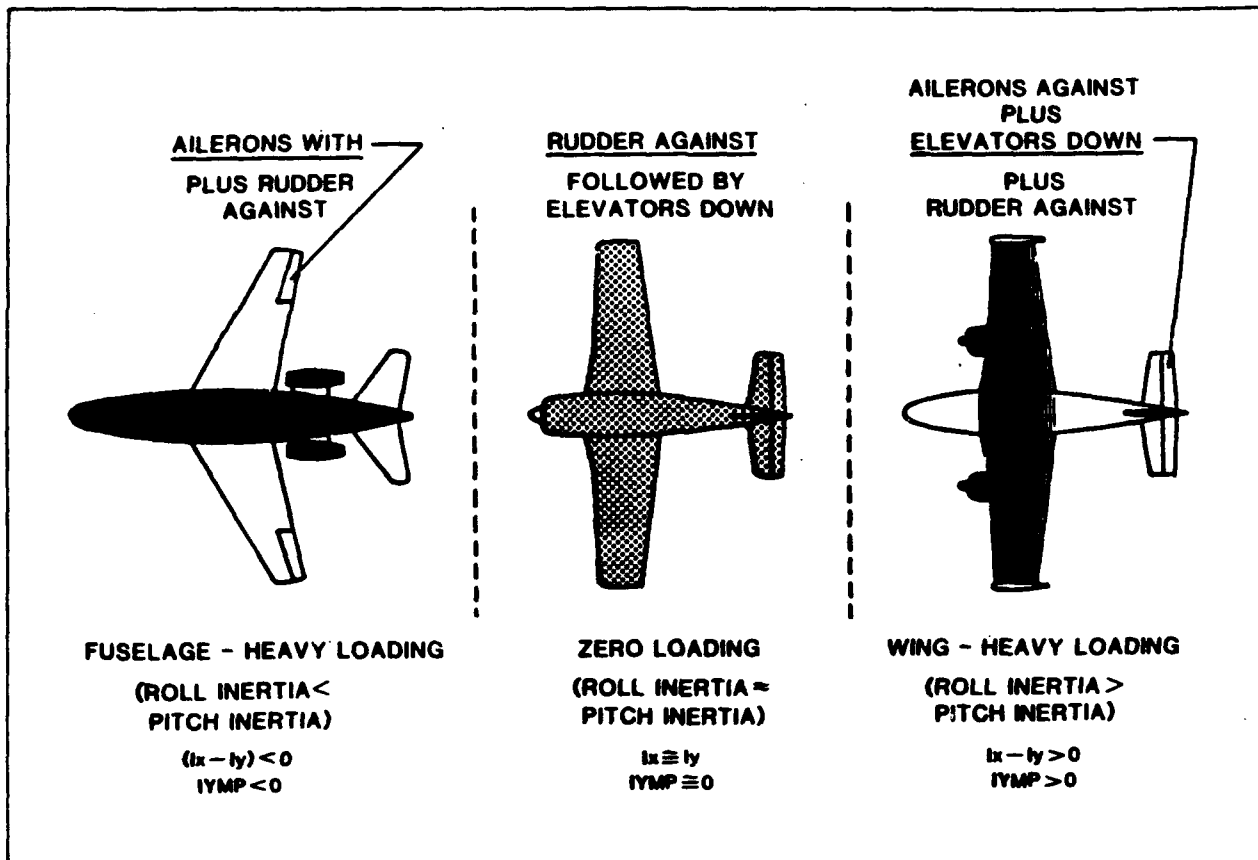


Figure 79. Spin Recovery Control as Determined by Mass Distribution (Reference (45)).

a. Rudder control

Deflection of the rudder to oppose the spinning rotation directly is always recommended to produce an anti-spin aerodynamic yawing moment, but in many cases it is not adequate to provide recovery. If the rudder is not blanked out, opposing rudder input to the direction of the spin reduces the yaw rate. The reduction in yaw rate produces the secondary effect of reducing the inertia-pitch couple and thus the angle-of-attack consequently decreases. The opposing anti-spin rudder input also tends to increase the amount of wing tilt (or helix angle) by tilting the inner wing further below the horizon (reference (33)). When  $I_{YMP}$  is negative (fuselage-heavy loading) this effect tends to increase the anti-spin inertial yawing moment. In this case then, the secondary effect of the rudder input also produces an anti-spin moment contribution.

b. Elevator Control

The longitudinal control surface can only be effective as an anti-spin controller if it can drive the angle-of-attack below  $\alpha_s$  by producing a nose-down anti-spin aerodynamic pitching moment for an erect spin (Reference (46)).

Reference (46) points out that rarely is the elevator capable of producing this much change in pitching moment in a fully developed spin, but its timely use during a PSG or the incipient phase of a spin may reduce the angle-of-attack sufficiently. Recall that the rudder control will also aid in reducing the aircraft's angle-of-attack due to the inertial-pitch coupling effect.

Similar to the rudder, there are important secondary effects due to elevator control that must be considered. Down elevator movement (forward stick) during a fully developed upright spin will cause many spin modes to progress to a higher rotation rate ( $\Omega$ ). This increased rate-of-rotation is achieved by an increase in the pro-spin rolling moment (see equation (19)) (Reference (33)).

$$L_i = (I_z - I_y) r q \quad \text{EQ (19)}$$

This results in an increase in the amount of sideslip and thus, in this case, the outward wing tilt ( $\sigma$ ) is reduced. If IYMP is negative (fuselage-heavy loading) the consequence is a reduction in the anti-spin inertial yawing moment and hence a reduction in the overall effectiveness of the elevator control. When IYMP is positive the elevator will be a much more effective control (See Figure 79).

Note that down elevator tends to increase the shielded area of the fin and rudder thus reducing the rudder's ability to produce anti-spin aerodynamic yawing moments. It is for this reason that there is normally a small time delay in the recovering sequence between the pilot applying opposite rudder control and moving the stick forward typical of many spin recovery techniques.

## c. Aileron Control

For the case of the elevator and rudder controls, their overall effectiveness is a function of the aircraft mass distribution, yet they are always used in the same sense (i.e. opposite rudder and down elevator). For correct anti-spin aileron control this is not true. The correct sense of anti-spin aileron input is a function of IYMP. That is to say, in some cases the application of "pro-spin" aileron (i.e., stick to the right in a spin to the right) will prevent recovery from a spin, in other cases it will be a valuable recovery control. This change in the correct sense of aileron control is due to the various secondary effects of the aileron control input, which have a more powerful influence on the dynamics of the spin recovery than the direct rolling moment effects of the aileron. The reason this is true is because in stalled flight the ailerons are generally not very effective (if at all) in producing rolling moments of any significance.

Instead, the ailerons can still be the primary anti-spin control by causing a small change in bank angle and thereby reorient the aircraft attitude about the spin axis. By using ailerons to reorient the aircraft attitude about the spin axis, a component of  $r$  can be generated on the y-body axis creating pitch rate,  $q$ . The pitch rate can then cause aircraft inertial moments to affect roll and yaw accelerations and as a result disturb the spin equilibrium.

Reference (33) explains the anti-spin inertial yawing moment effect of aileron control using the following example. Consider a fuselage loaded aircraft ( $IYMP < 0$ ) in a right, erect spin (i.e.,  $r, p > 0$ ). In this case the term  $(I_y - I_z) / I_x$  is negative while  $r$  is positive (see equation (7)). The correct aileron deflection for recovery is explained by considering the roll and yaw acceleration equations (equations (20) and (21)) listed below.

$$\dot{p} = \dots + \frac{I_y - I_z}{I_x} qr + \dots \quad \text{EQ (20)}$$

$$\dot{r} = \dots + \frac{I_x - I_y}{I_z} pq + \dots \quad \text{EQ (21)}$$

In order to generate anti-spin roll acceleration ( $p < 0$ ), pitch rate ( $q$ ) must be positive (See equation (20)). Similarly the pitch rate ( $q$ ) must be positive to generate anti-spin yaw acceleration ( $r < 0$ ) (see equation (21)). As illustrated in figure 79 to generate positive pitch rate ( $q > 0$ ) requires that aileron control be applied in the direction of the spin.

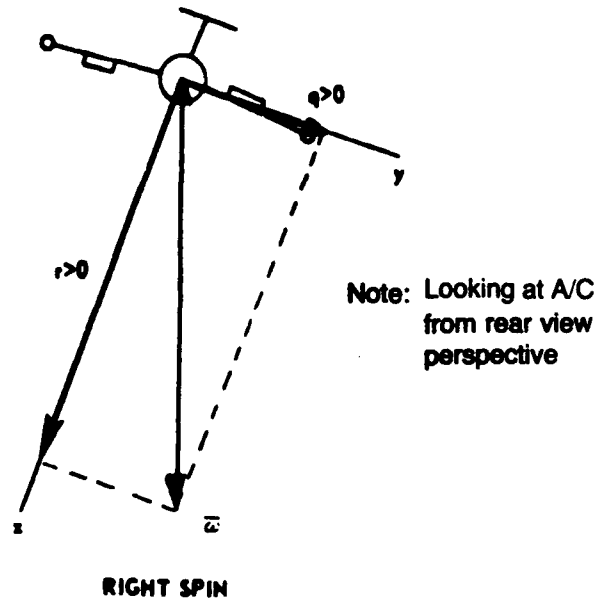


Figure 80 Aircraft Angular Rates in a Right Spin (Reference (46))

If a wing-loaded aircraft ( $I_x > I_y$ ) is considered instead of the fuselage-loaded aircraft, equations (20) and (21) show that aileron against an erect spin will produce an anti-spin yaw acceleration ( $r < 0$ ) but a pro-spin roll acceleration ( $p > 0$ ). In this case aileron against the spin would be recommended. Figure 81 taken from reference (33), summarizes the effectiveness the conventional controls (i.e., rudder, elevator and aileron) have on spin recovery as a function of the relative magnitudes of the pitch and roll aircraft moments of inertia.

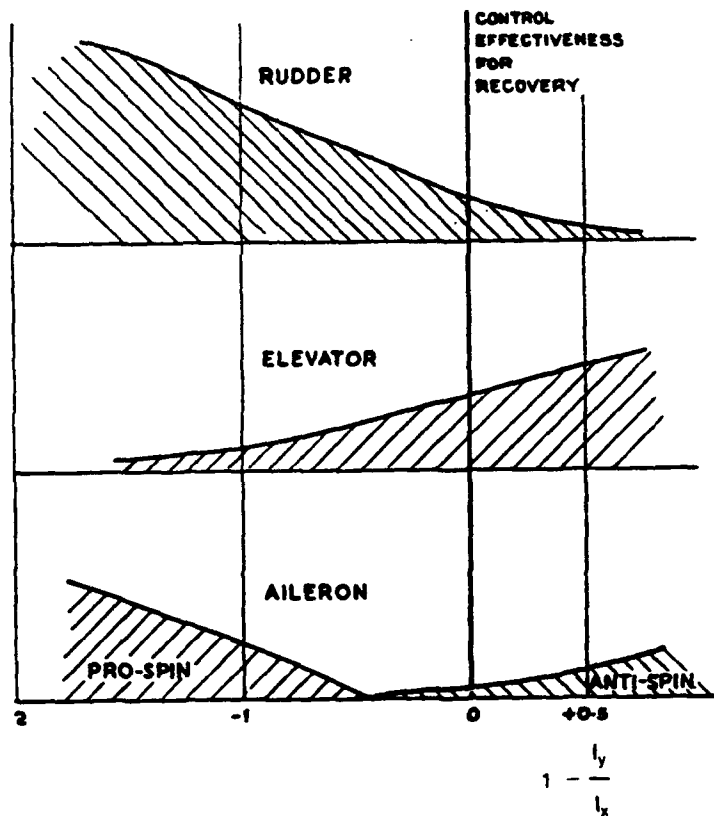


Figure 81. Pictorial Representation of Control Effectiveness for Spin Recovery of a Conventional Aircraft (Reference (33)).

In addition to IYMP, another parameter used often in the literature that has an appreciable influence on the spin recovery is the relative-density factor,  $\mu$  defined by equation (22).

$$\mu = \frac{m}{\rho S b} \quad \text{EQ (22)}$$

The relative density factor is fixed by design requirements and varies according to changes in the aircraft mass and altitude. Aircraft with high relative-density factors normally require more rudder and elevator effectiveness for spin recovery than aircraft with low relative-density factors (other factors being equal) (Reference (45)).

#### 2.3.5.2 Other Means of Spin Recovery

Aircraft configuration changes that could effect the spin dynamics include wing trailing-edge flaps and landing gear deflection (See 1b. of figure 78). On the basis of research conducted in reference (51) and (52) on general aviation type aircraft, the use of flap extension would be expected to have an adverse effect on spin recovery (Reference (45)). The extension of flaps usually causes the spin to be flatter and the spin rate to be slower. In addition the results of reference (52) show that the effectiveness of the rudder for spin recovery decreases when flaps are down due to an additional wake behind the wing.

Extension of the landing gear usually has little effect on the spin and recovery techniques as described in reference 52 for general aviation type aircraft. However slight adverse effects have been documented for lowering the landing gear on some aircraft.

The application of thrust (See 1c. of figure 78) has no effect on spin recovery unless the thrust axis is displaced from the center-of-gravity and thereby produces a moment. Whether the moment produced is favorable for spin recovery depends on the type of moment produced and the aircraft loading.

The capability of today's fighter aircraft flight control systems (FCS) has advanced to such a state that many aircraft now have a spin recovery mode, either manually selected or automatic, to aid the pilot. As the flight control system senses the state of the aircraft, gains in the control system may change and feedback paths may open or close to provide advantageous control surface deflections. Pro-spin control surface settings will not be allowed even if the pilot deflects the stick or pedals such that they are in a pro-spin condition. With any spin recovery procedure, once the nose is down and rotation ceases, dive recovery ensues.

Stores release to alter the balance in inertia and aerodynamic moments is strictly prohibited in most operational flight manuals. Released stores may hit the aircraft during a spin. There is also a possibility for

tactical and ground attack aircraft to inflict damage and casualties on friendly targets while performing ground support or interdiction missions.

The spin chute (4. of figure 78) is a method of spin recovery used during flight test stages of an untried aircraft configuration when inadvertant as well as intentional spins are likely to occur. Addition of the spin chute requires structural and aerodynamic modifications, so they are rarely seen on production aircraft. Performance decreases mainly due to the added weight of the reinforced aft structure. Deployment of a spin parachute creates drag to stop rotation and to point the aircraft in a nose-down attitude. Item 4. of Figure 78 would also include other means of altering the balance in aircraft aerodynamic and inertial moments that would include release of stores and the use of spin rockets.

### 3.0 METHODS OF DEPARTURE RESEARCH AND ANALYSIS

In general, there are five methods/techniques used to study and predict aircraft departure. They are (1) analytical studies (2) wind-tunnel tests (3) dynamic model flight tests (4) piloted simulations and (5) aircraft flight test. Each of these methods has an associated level of confidence with which they can aid in predicting departure characteristics. In addition, utilization of each of these methods is usually integrated in a logical manner within the design process of an aircraft. Each of these methods will now be briefly described in terms of their application to predicting aircraft departure characteristics.

#### 3.1 Wind Tunnel/Analytical Departure Prediction Techniques

##### 3.1.1 Use of Wind Tunnel Data

Conventional low-speed wind tunnel testing provides the means for obtaining static stability derivative data ( $C_{L_\alpha}$ ,  $C_{m_\alpha}$ ,  $C_{m_\beta}$ ,  $C_{n_\alpha}$ ,  $C_{n_\beta}$ ,  $C_{l_\beta}$ ,  $C_{l_\alpha}$ , etc.) of the aircraft. The static coefficients are nonlinear functions of aircraft nonrotating motion parameters as given by equation (23).

$$(C_i)_{\text{STATIC}} = f(\alpha, \beta, M, h, \delta), \text{ where } i = l, m, n, x, y, z \quad \text{EQ (23)}$$

In the early stages of design, analysis of this data can be used to investigate stability and control characteristics of the various candidate configurations. In this respect, application of the documented directional departure criteria (i.e., Weissman, Bihrie Departure Susceptibility Criteria. See Section 4.2.) can be utilized to determine the necessity for fundamental design changes.

Due to the strong nonlinearities and rapid variations encountered in certain angles-of-attack and sideslip ranges, the static wind tunnel tests must be performed with small increments of  $\alpha$  and  $\beta$ ; or preferably with continuous recording. The most important design consideration (for fighter aircraft) to be achieved at this point of testing is to maximize the angle-of-attack where departure (roll reversal, nose slice, etc.) is predicted to occur.

In cases where adverse departure characteristics are found to occur, flow visualization techniques will often be used to help determine the flow phenomena responsible for the problem and thereby suggest fixes. Some of the common flow visualization techniques include surface oil, tuft techniques, smoke, or helium bubble generators. More recently water tunnels have become a popular experimental tool because it provides a convenient, vivid and easily-controlled flow visualization of vortex interactions at high angle-of-attack (Reference (53)). Figure 82 shows a water tunnel flow-visualization photograph of an F-18 model at 40 degrees angle-of-attack.

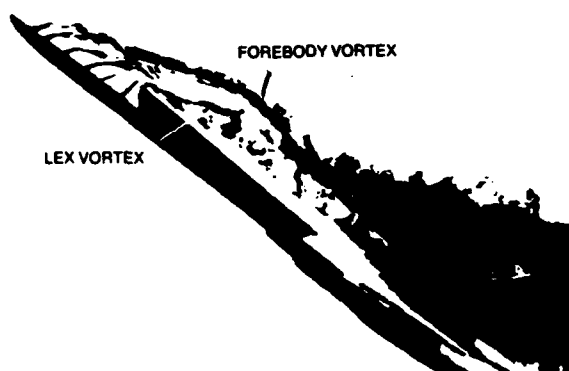


Figure 82. Water-Tunnel Flow-Visualization Photograph of F-18 Model at  $\alpha = 40^\circ$ . (Reference (54) )

In addition to static-force tests, wind tunnel data obtained from forced-oscillation tests and rotary balance tests are necessary to define a high angle-of-attack data package. The forced oscillations test method is most commonly used to determine the dynamic derivatives<sup>1</sup> (i.e.,  $C_{m_q}$ ,  $C_{l_p}$ ,  $C_{l_r}$ , etc.) and the rotary data is used to account for the effects due to a rotating flow field as encountered during a steady spin. Early in the design phase, calculation of stability and control parameters that require the knowledge of the dynamic derivatives typically rely on estimates determined from either analytical techniques or from known derivatives for aircraft with similar configurations. The success of developing a working high angle-of-attack math model relies on properly combining the different types of data to be consistent with the means used to measure the data.

<sup>1</sup> More rigorously, oscillatory derivatives, measured by force oscillation techniques represent a combination of the specific damping derivatives with certain linear-acceleration derivatives, i.e., damping in yaw parameter is given by,  $C_{n_r} = C_{n_{\dot{\beta}}} \cos \alpha_0$ .

Kalviste, (Reference (55)), suggests the following aerodynamic coefficient buildup be used to properly blend the aerodynamic coefficients due to dynamic (i.e., oscillatory and rotational) motion:

$$C_i = \overbrace{C_i \left( \frac{\omega b}{2V_T} \right)}^{(1)} + \overbrace{C_{iP}^F \frac{b}{2V_T} \cdot P_{MOD} + C_{iQ}^F \frac{\bar{c}}{2V_T} Q_{MOD} + C_{iR}^F \frac{b}{2V_T} \cdot R_{MOD}}^{(2)} + \overbrace{C_{i\dot{\alpha}} \frac{\bar{c}}{2V_T} \dot{\alpha}_T + C_{i\dot{\beta}} \frac{b}{2V_T} \dot{\beta}_T}^{(3)}$$

Where:

i = L, Y, D,  $\mathcal{L}$ , M, N

(1) = term obtained from Rotary balance wind tunnel test

(2) = terms measured in the forced oscillation wind tunnel test (designated with superscript F)

(3) = acceleration derivatives measured in a translational acceleration tunnel test or are computed derivatives

$P_{MOD}, Q_{MOD}, R_{MOD}$  = components of total rotation vector along x, y, z-axes and the velocity vector, with  $\Omega$  resolved into three of the four components (for further details see Reference (54))

With,

$\dot{\alpha}_T, \dot{\beta}_T$  = time rate of change of angle-of-attack and sideslip angles due to aircraft translation (equals total values ( $\dot{\alpha}, \dot{\beta}$ ) less the rotational component).

$P_{MOD} = P - \omega \cos \alpha \cos \beta$

$Q_{MOD} = Q - \omega \sin \alpha$

$R_{MOD} = R - \omega \sin \alpha \cos \beta$

With,

$$\dot{\alpha}_T = \dot{\alpha} - Q + (P \cos \alpha + R \sin \alpha) \tan \beta$$

$$\dot{\beta}_T = \dot{\beta} - P \sin \alpha + R \cos \alpha$$

Note that other researchers such as Bihle (Reference (49)) advocate blending the aerodynamic coefficient build-up equations due to dynamics differently than suggested by Kalviste. There currently seems to be no agreed upon "best" approach to this modelling problem other than to say that it is highly dependent upon the intended model application and that one obeys the rule to utilize the data in a means consistent with how it was measured.

### 3.1.2 Rotary Balance Data

It has been shown that the aerodynamic moments generated in the spin due to rotational flow, as measured by a rotary balance are indeed significant (Reference (56)). The use of rotary balance data has helped increase the accuracy of spin prediction analyses as well as raise the level of spin simulation fidelity. A technique cited as far back as 1935 in Reference 55 has gained wide acceptance as a method for collecting rotary data increments. References (49) and (56) describe a NACA 5 ft vertical wind tunnel test section which was utilized for rotary data acquisition in the 1930's. A rotary balance (in use today at the NASA Langley Research Center, L'Institut de Mechanique de Fluides de Lille in France, and elsewhere in the world) measures the forces and moments acting on a model while it is subjected to rotational flow conditions. The force and moment increments are typically determined as functions of nondimensionalized rotation rate,  $\Omega b/2V$ , angles-of-attack and sideslip angle.

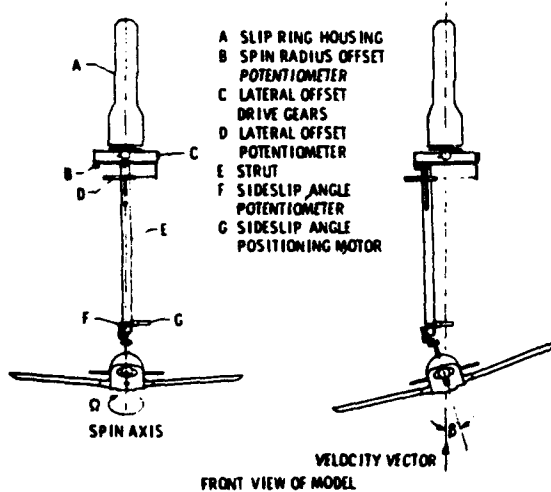
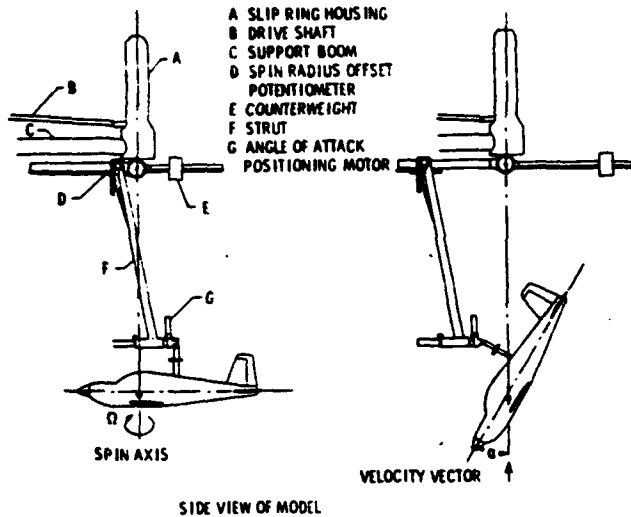
Some of the details of the rotary balance test rig installed in the Langley Spin Tunnel are shown in figure 83. The system's rotary arm rotates about a vertical axis at the tunnel center and is supported by the horizontal boom. The horizontal boom is driven by a motor capable of rotating the system up to 90 rpm in either direction. The forces and moments acting about the model body axis are measured using a six-component strain gauge balance which is attached to the bottom of the rotary balance rig and mounted inside the model (The model is both contour and mass scaled).

The angle-of-attack range of the Langley rig is  $0^\circ$  to  $90^\circ$  and the sideslip angle range is  $\pm 15^\circ$ . Spin radius and lateral displacement motors are used to position the moment center of the balance on, or at a specific distance from the spin axis. A range of  $\frac{\Omega b}{2V}$  values is obtained by adjusting rotational speed and/or tunnel air flow velocity.

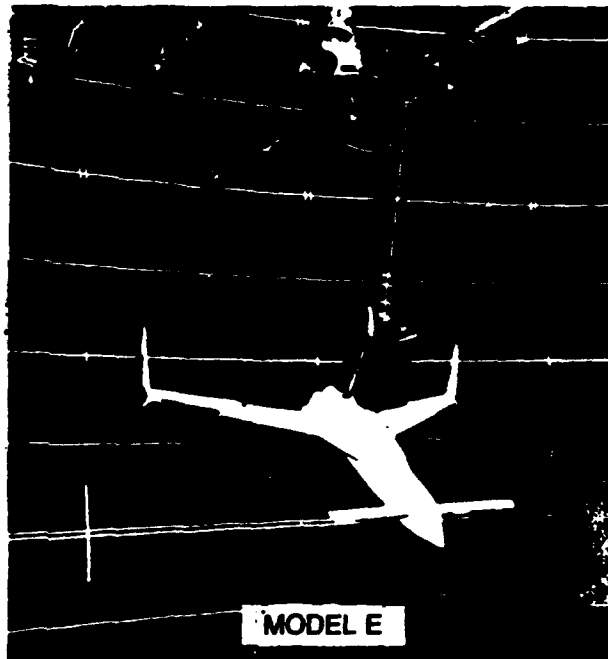
As reported in reference (57), rotary aerodynamic data are obtained using a two step test procedure. This procedure is explained in the following manner by Bihle Applied Research (BAR),

"First the inertial forces and moments (tares) acting on the model at different attitudes and rotational speeds must be determined. Ideally, these inertial terms would be obtained by rotating the model in a vacuum, thus eliminating all aerodynamic forces and moments. As a practical approach, this is approximated closely by enclosing the model in a sealed spherical structure, which rotates with the model without touching it, such that the air immediately surrounding the model is rotated with it. As the rig is rotated at the desired attitude and rate, the inertial forces and moments generated by the model are measured and stored on magnetic tape for later use (Reference (57)).

The second step is to remove the enclosure and record force and moment data with the air on. The tares, measured in step one, are then subtracted from these data, leaving only the aerodynamic forces and moments, which are converted to coefficient form."



a)



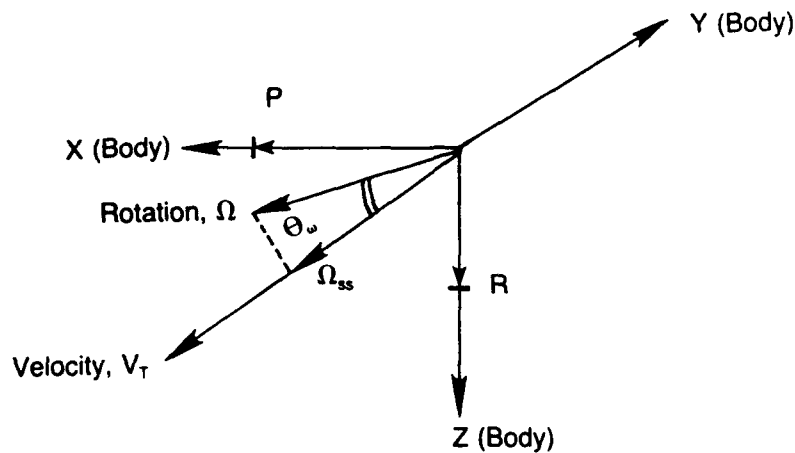
b)

Figure 83. (a) Sketch of Rotary Balance Apparatus

(b) Model Installed on Rotary Balance  
(Reference (49)).

Rotary balance data are obtained while a model/balance is rotating in the wind tunnel with its rotational vector ( $\Omega$ ) aligned with the velocity vector of the wind tunnel (i.e., the model is performing a steady rotation about the free-stream velocity vector.)

As reference (58) points out, in the general case (see figure 84) the rotational ( $\Omega$ ) and velocity ( $V_T$ ) vectors that describe spinning motions are not normally aligned in spinning flight. Therefore, implementation of the rotary balance data as a function of the total rotational rate vector ( $\Omega$ ) would be incorrect. The method suggested by references (49) and (58) involves resolving the steady state component ( $\Omega_{ss}$ ) of the total rotational vector ( $\Omega$ ) along the aircraft velocity vector. One method of determining the magnitude of the steady-state rotational vector ( $\Omega_{ss}$ ) is outlined in figure 84 below as taken from reference (49).



Total Velocity Vector:

$$\bar{v}_T = v\bar{i} + v\bar{j} + w\bar{k}$$

Total Rotational Vector:

$$\bar{\Omega} = p\bar{i} + q\bar{j} + r\bar{k}$$

Steady-State Rotational Vector along Velocity Vector  $\bar{v}$ :

$$\Omega_{ss} = p_{ss}\bar{i} + q_{ss}\bar{j} + r_{ss}\bar{k}$$

$$|\omega_{ss}| = |\Omega| \cos \delta$$

$$\bar{\Omega} \cdot \bar{v} = |\Omega| |\bar{v}| \cos \theta_w$$

$$up + vq + wr = |\Omega| |\bar{v}| \cos \theta_w$$

Substituting:

$$|\Omega_{ss}| = \frac{up + vq + wr}{|\bar{v}|}$$

Figure 84. Analytical Determination of the Magnitude of the Steady State Rotational Vector (Reference (58)).

A more practical method used by BAR to obtain  $\Omega_{ss}$ , is to remove the unsteady effects, e.g., high frequency oscillations, by utilizing a first order transfer function as shown in equations (24) and (25). (Reference (57)).

$$\Omega_{ss} = \frac{1}{\tau_s + 1} * P_w \quad \text{EQ (24)}$$

$$\text{where } P_w = P \cos \alpha \cos \beta + Q \sin \beta + R \sin \alpha \cos \beta \quad \text{EQ (25)}$$

BAR goes on to model the "blend" between the aerodynamic moments due to motion oscillations versus rotational motion in the following manner.

1. The dynamic (damping) derivatives are measured or calculated for small oscillations about each of the model body axes, x, y, and z. These derivatives are consequently multiplied by the oscillatory components of the body rates<sup>1</sup>, not the total rates. As shown in equations (26) through (28), these oscillatory components are calculated as the total body rates less the steady rotational components about each axis.

$$P_{osc} = P_{tot} - P_{ss} \quad \text{EQ (26)}$$

$$Q_{osc} = Q_{tot} - Q_{ss} \quad \text{EQ (27)}$$

$$R_{osc} = R_{tot} - R_{ss} \quad \text{EQ (28)}$$

where:

$$P_{ss} = \Omega_{ss} \cos \beta \cos \alpha$$

$$Q_{ss} = \Omega_{ss} \sin \beta$$

$$R_{ss} = \Omega_{ss} \cos \beta \sin \alpha$$

<sup>1</sup> More rigorously, oscillatory derivatives, measured by forced oscillation techniques represent a combination of the specific damping derivative with certain linear-acceleration derivatives, i.e., damping-in-yaw parameter is:  $C_{n_r} - C_{n_\beta} \cos \alpha_o - C_{n_\alpha} \sin \alpha_o \tan \beta_o$ . Reference (47) notes however that it is more accurate to use the forced oscillation test data with the aircraft angular rate (in this instance, r) than to remove the  $\beta$  term before multiplying it by the angular rate, r (assumption here is that  $\beta_o = 0^\circ$ ).

Note that the relationship between the time derivatives of the Euler angles  $\psi$ ,  $\theta$  and  $\phi$  and the rotational velocity components  $P$ ,  $Q$ , and  $R$  is given by equations (28) - (30),

$$P = -\dot{\psi} \sin \theta + \dot{\phi} \quad \text{EQ (29)}$$

$$Q = \dot{\psi} \cos \theta \sin \phi + \dot{\theta} \cos \phi \quad \text{EQ (30)}$$

$$R = \dot{\psi} \cos \theta \cos \phi + \dot{\theta} \sin \phi \quad \text{EQ (31)}$$

As defined in reference (49) the steady state and oscillatory components of the angular rates are given by,

$$\begin{aligned} P_{ss} &= -\dot{\psi} \sin \theta & P_{osc} &= \dot{\phi} \\ Q_{ss} &= \dot{\psi} \cos \theta \sin \phi & Q_{osc} &= \dot{\theta} \cos \phi \\ R_{ss} &= \dot{\psi} \cos \theta \cos \phi & R_{osc} &= -\dot{\theta} \sin \phi \end{aligned}$$

From the rotational velocity equations given above, it is apparent that the underlying assumptions allowing the rotational velocity components to be resolved into steady state and an oscillatory component, is the fact that the Euler angle rate  $\dot{\psi}$  is assumed to have no unsteady component and the Euler angle rates  $\dot{\theta}$ , and  $\dot{\phi}$  have no steady components. This can be shown by substituting equations (32) - (34) into equations (29) - (31).

$$\dot{\psi} = \dot{\psi}_{ss} + \dot{\psi}_{osc} \quad \text{EQ (32)}$$

$$\dot{\theta} = \dot{\theta}_{ss} + \dot{\theta}_{osc} \quad \text{EQ (33)}$$

$$\dot{\phi} = \dot{\phi}_{ss} + \dot{\phi}_{osc} \quad \text{EQ (34)}$$

Utilizing the rotational and dynamic derivatives in the manner just discussed accounts for both the steady state rotational motion effects and the oscillations that normally occur while an aircraft is in a steady state spinning condition ( $\dot{\psi} = \dot{\psi}_{ss} = \text{constant}$ ).

The authors of reference (49) point out that high angle-of-attack simulations (manned or unmanned) using this modeling technique may still not completely match full-scale dynamics for several reasons. Two major reasons they cite why all phases of a spin time history may not be completely reproduced are (1) Reynolds number effects and (2) dynamic derivative testing techniques. Because of the low tunnel speeds, capable spin tunnel tests are run at a value of Reynolds number which is much lower than that for the full-scale model. Maximum speed of the Langley Spin tunnel is approximately 80 ft/sec resulting in an approximate maximum Reynold's number of  $.5 \times 10^6$  per foot. Note, that the most significant Reynold's number effects occur on the wing for general aviation type aircraft (influence on lift) and on the sharp forebodies of the military fighter type aircraft (primary influence on aircraft yawing moment).

A second reason high angle-of-attack aerodynamic math models of the spin may not correlate well with flight test data concerns the technique used to measure dynamic derivatives. The dynamic derivatives of an aircraft are conventionally measured<sup>1</sup> while forcing a model to oscillate about a non-rotating reference. A more proper representation for spin analysis suggested by reference (56) would be to obtain the dynamic derivatives by superimposing the forced oscillations onto a steady rotating motion. To date, there is no apparatus in this country that is capable of measuring dynamic derivatives in this manner (Reference (49)).

Rotary balance test data is often used to examine the propelling/restoring effects of individual aircraft components on the total aircraft configuration. Figure 85 shows a plot of incremental yawing moment coefficient versus  $\Omega b/2V$  for an aircraft component buildup.

<sup>1</sup> See references (59) and (60) for a detailed discussion of methods used to measure dynamic derivatives in wind tunnels.

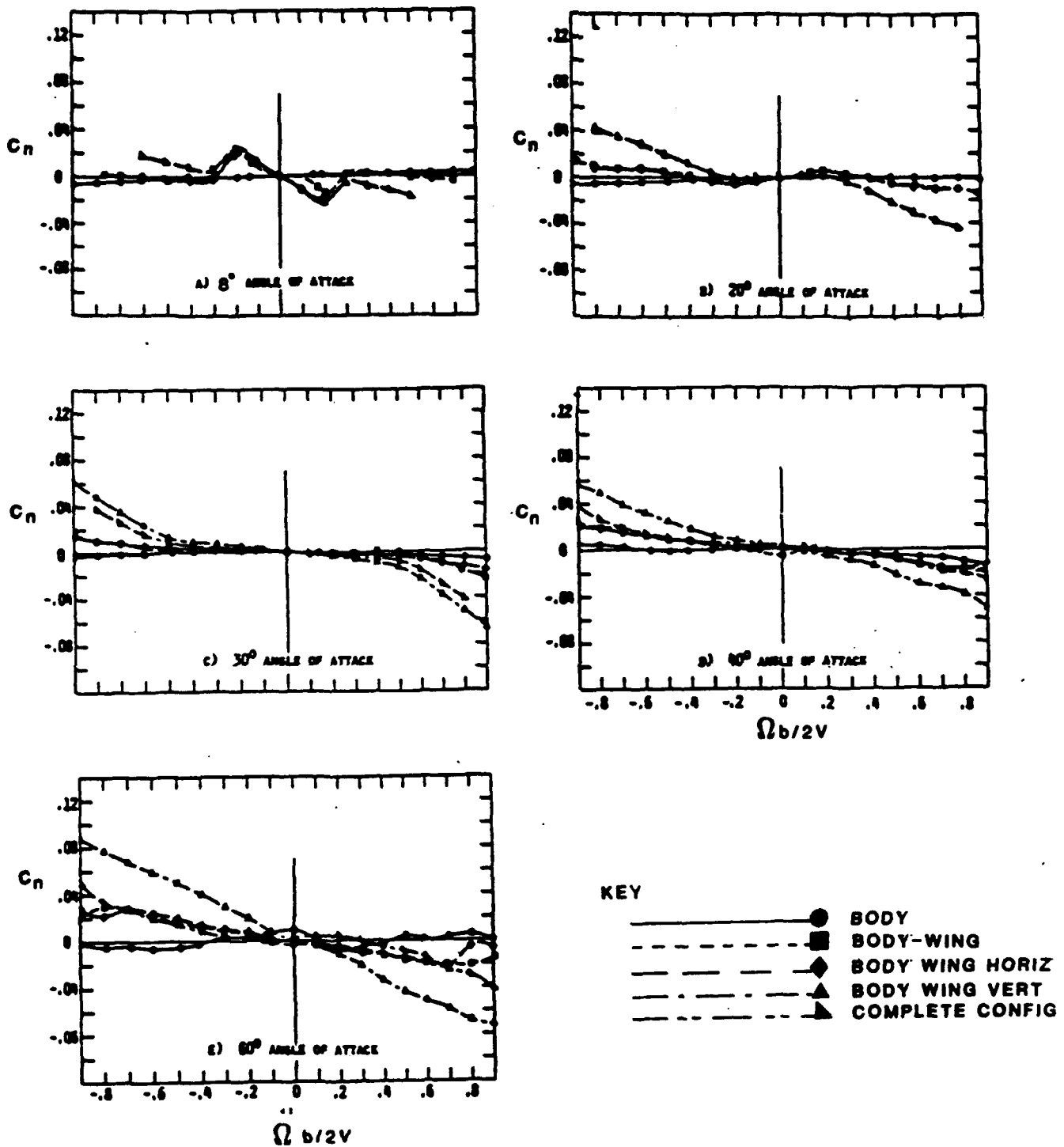


Figure 85. Effect of Aircraft Component Buildup on Aircraft Yawing Moment Coefficient (Reference (61))

From this plot, it is clearly evident that the tail provides the major portion of the inherent aircraft restoring yawing moment. Similar component plots for all forces and moments reveal which aircraft components are the major contributors to forces and moments for an aircraft configuration. Additions or modifications to an aircraft can be put on the rotary balance model to determine their relative effects. References (61) and (62) discuss this subject in detail.

### 3.1.3. Some Observations Concerning High Angle-of-Attack Aerodynamics

One of the most important results of static force tests with regard to high angle-of-attack aerodynamic data is the fact that large out-of-trim values of  $C_n$ ,  $C_y$ , and  $C_l$  often exist. Figure 86 shows the variation of static yawing moment coefficient  $C_n$  as a function of angle-of-attack at zero sideslip and neutral controls as measured for four separate models of an identical configuration (Reference (63)). The configuration tested is shown in figure 87.

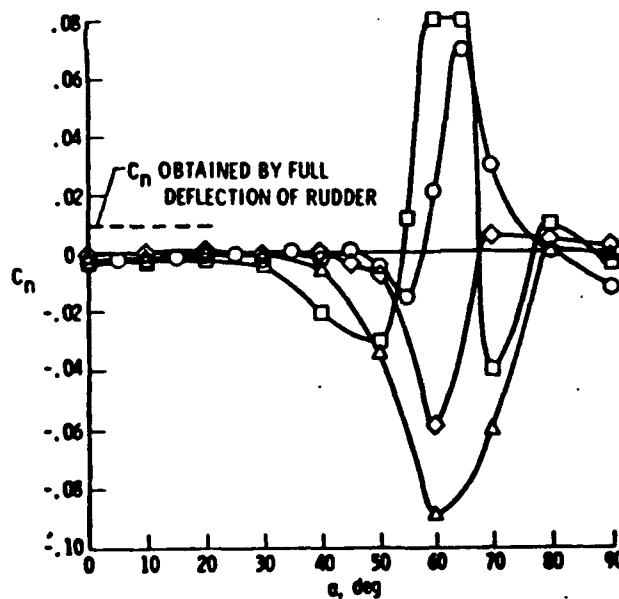


Figure 86. Variation of Yawing-Moment Coefficient With Angle-of-attack for Several Models of the Same Configuration. ( $\beta = 0^\circ$ ; Controls Neutral.) (Reference (63))

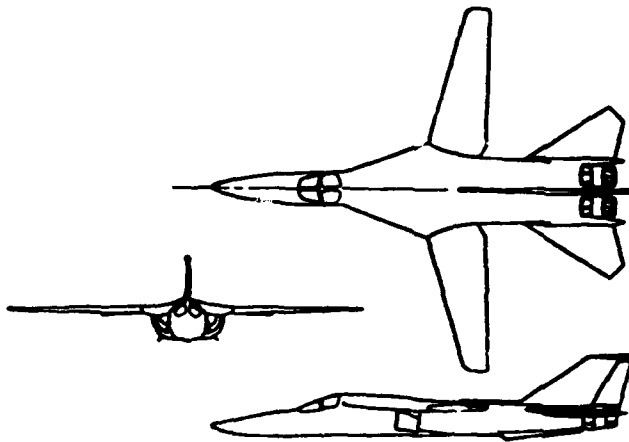


Figure 87. Contemporary Fighter Configuration With Long Pointed Nose (Reference (63))

As pointed out by the authors of reference (63), the value of  $C_n$  remains zero at low angles of attack, but for angles greater than about  $30^\circ$ , large excursions of  $C_n$  occur. Note that the out-of-trim moments at  $\alpha = 60^\circ$  are several times as large as the moments produced by full-rudder deflection at low angles of attack, and would be much larger than moments obtained by rudder deflections at  $\alpha = 60^\circ$  because of the marked reduction in rudder effectiveness at high angles-of-attack due to shielding by the fuselage and wing (see figure (88)) (Reference (63)). The implication of non-zero trim coefficients at increased angles-of-attack means the aircraft may unexpectedly roll or yaw for zero sideslip and neutral lateral/directional control surface deflections.

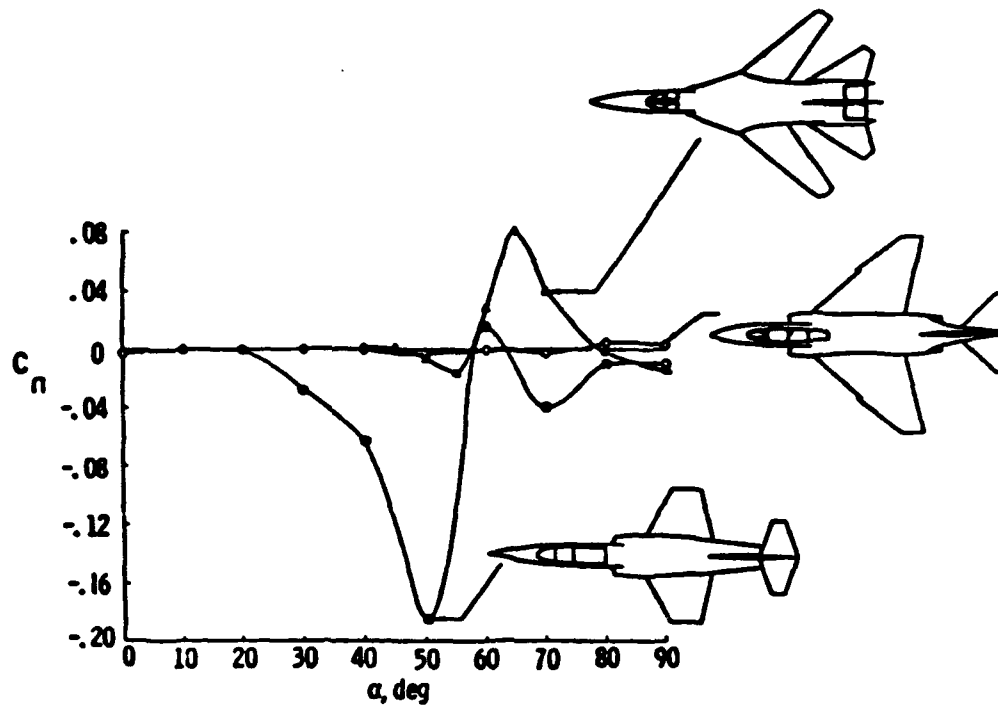


Figure 88. Asymmetric Yawing Moment With Angle-of-attack for Three Airplane Configurations (Reference (63))

The phenomena of non-zero lateral-directional trim values is similarly illustrated by the rotary balance yawing moment data of figure 89. In this figure,  $\Omega b/2V$  is defined as positive for a clockwise rotation of the model (i.e., nose moving to pilot's right).

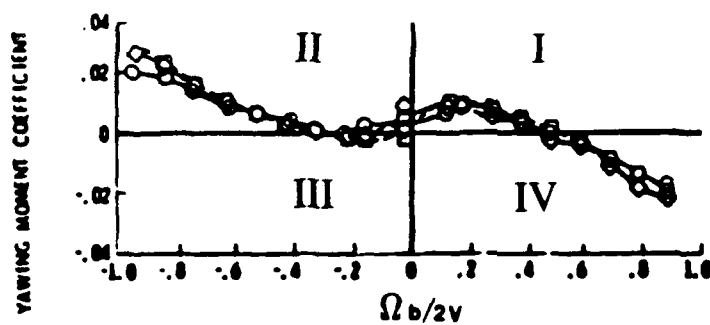


Figure 89. Rotary Yawing Moment Coefficient at 60 Degrees Angle-of Attack and Zero Degrees Sideslip for Three Different Nose Shapes (Reference (64)).

An equally important phenomenon, illustrated in figure 90, is the observation that these large asymmetric yawing moments appear to be random and nonrepeatable even for the same model under identical test conditions (Reference (63)). Figure 90 presents the variations of  $C_n$  with angle-of-attack for zero sideslip and neutral control inputs for several repeated tests. Though this test was conducted at low Reynolds number, other wind tunnel tests investigating the effect of Reynolds number still support the "randomness" of  $C_n$  values, though the magnitude of disparity was less.

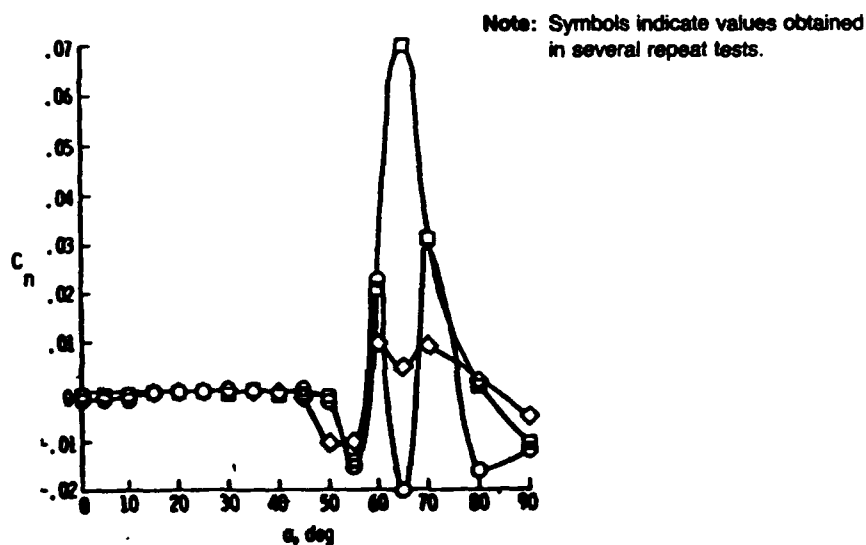


Figure 90. Variation of Yawing Moment Coefficient With Angle-of-attack for the Same Model and Configuration ( $\beta = 0^\circ$ ; Control Neutral). (Reference (63)).

The aerodynamic phenomenon producing the large yawing moments is chiefly attributed to asymmetrical shedding of vortex sheets off the long, sharply pointed forebodies characteristic of many of today's fighter configurations. (see figure 91).

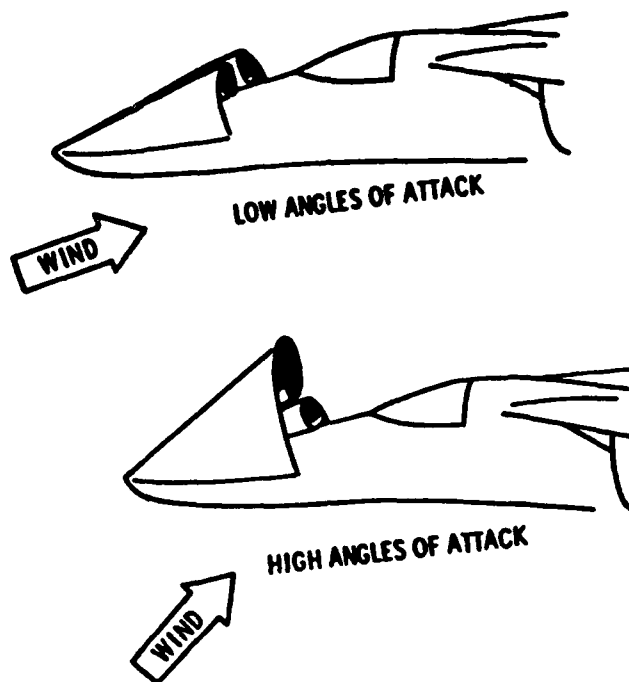


Figure 91. Sketches of Separated Vortex Sheets on Fuselage Forebody. (Reference (63))

The authors of reference (63) explain the flow patterns of such vortices on the fuselage forebody as follows,

"Separation of flow from the fuselage forebody at low angles-of-attack is characterized by two shed vortex sheets. At "low" angles-of-attack these vortex sheets remain nearly symmetrical above the nose (see upper illustration of figure 91). Because of the symmetry of the vortex sheets they do not induce asymmetric forces on the forebody. For higher angles of attack however, the vortex sheet becomes asymmetrical (see lower illustration of figure 91) with one vortex core moving above and away from the forebody while the remaining vortex sheet moves closer to the nose. The asymmetric vortex pattern creates a large negative pressure area on one side of the nose thereby creating a side force on the nose which, in turn, produces a large yawing moment due to the relatively long distance between the nose and the center-of-gravity of the airplane."

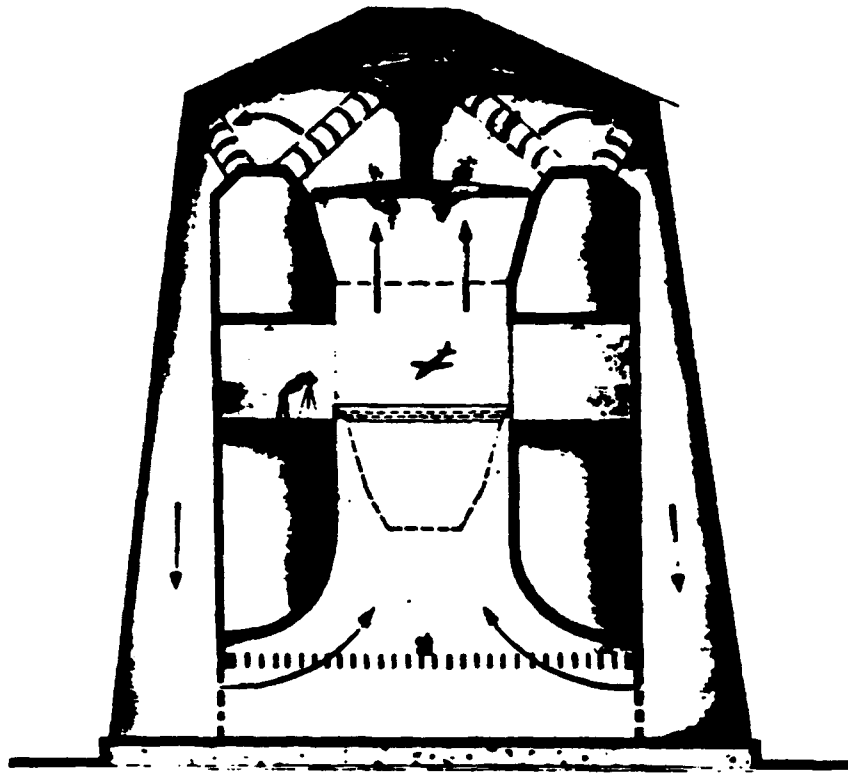
The authors of reference (63) go on to point out that the random out-of-trim moments result from the fact that some slight geometric or aerodynamic asymmetry establishes the sense of the asymmetric moment. In the high angle-of-attack flight regime of concern, the highly turbulent and nonlinear flow present is very conducive to creating the random out-of-trim moments as shown in figures 86, 90, and 92. These results indicate that theoretical studies of the spin and departure characteristics of contemporary fighters should be used with extreme caution (Reference (63)). The high angle-of-attack aerodynamic characteristics of configurations having long pointed noses are especially hard to define.

The reader is referred to references (62) and (65) for a complete discussion of aircraft forebody shapes and their design impact on aircraft stability.

### **3.2. Dynamic Model Flight Testing**

In addition to the use of wind tunnels to acquire static, dynamic, and rotary aerodynamic data for use in analytical studies as just described, dynamic models are also used in free flight wind tunnel tests to determine aircraft spin characteristics as well as stall characteristics. These wind tunnel methods include the spin-tunnel test technique and the wind-tunnel free-flight technique.

The spin-tunnel test technique is used in the vertical wind tunnels in operation at NASA Langley and Lille France (see figure 92a).



a) SCHEMATIC DIAGRAM



b) TEST SECTION AT NASA LANGLEY

Figure 92. Cross-section View of Vertical Spin Tunnel (Reference (27) )

(a) Schematic Diagram

(b) Test Section at NASA Langley

This method studies the spin and spin recovery by hand-launching radio-controlled free-flight aircraft models into the vertically rising airstream. The models are launched at various pitch attitudes with prerotation to initiate the conditions necessary for the model to develop and attain discrete spin modes to be studied.

Test results from using the spin-tunnel test technique are used to determine: (1) aircraft spin modes and recovery characteristics, (2) effects of center-of-gravity position and mass distribution (3) configuration modifications (i.e., external stores) and (4) the size (diameter, riser length) and type of parachute required for emergency spin recovery. (Reference (53)). To investigate/determine the best recovery control procedure, the model operator deflects the aerodynamic controls on the model to predetermined control positions by remote control. At the same time motion-pictures record the spin and resulting recovery (see figure 93b). Using this procedure, many repeat runs, at various control combinations can be investigated to help determine the best recovery technique.

Due to the test procedures employed, the data produced by these tests is restricted to the developed spin and spin recovery. The data can not be used to determine the characteristics of the incipient phase portion of the spin, that would include determining aircraft departure susceptibility. That is, a model may exhibit a spin mode during testing which can not be entered from conventional flight.

Another useful way dynamically scaled models are employed in wind tunnels takes place in the 30 × 60 foot open throat test section of NASA Langley's full-scale tunnel. In this tunnel, a free-flight test technique is used to specifically provide information on flight characteristics up to angles-of-attack that include stall/departure. In this respect, this testing technique helps fill the void of aircraft departure/susceptibility data unobtainable in the vertical tunnel.

The experimental layout of this technique is presented in figure 93.

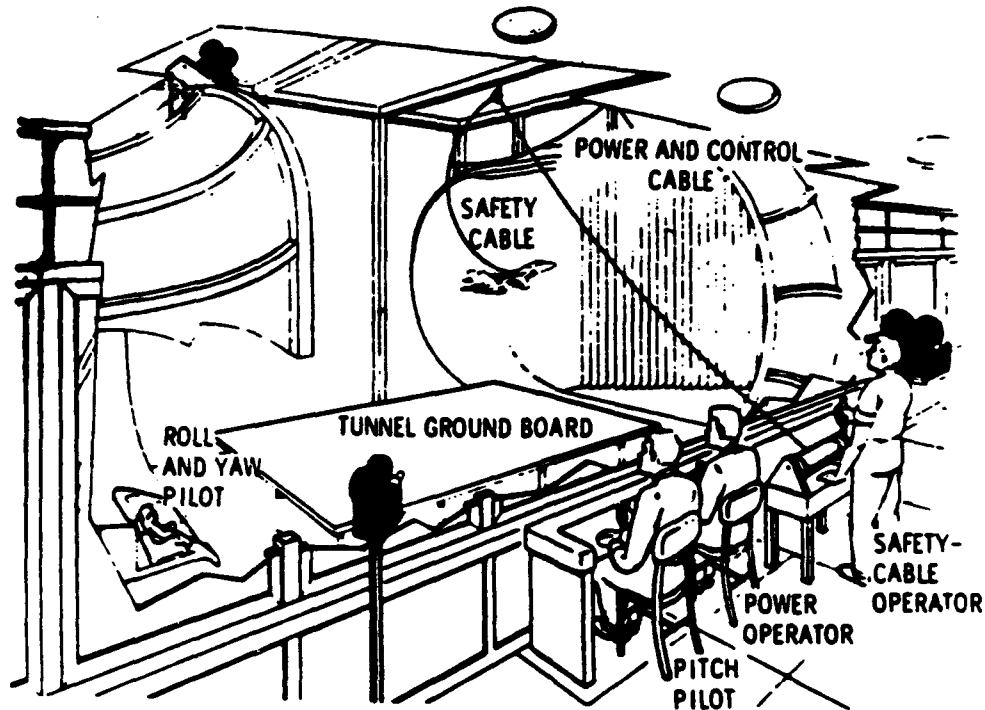


Figure 93. Aircraft Tethered Model Wind Tunnel Testing (Reference (27))

The remote-controlled dynamic model is flown without restraint by two pilots able to view the model's flight. To make control of the model less difficult, one pilot controls only the longitudinal axis motions of the model, while the other pilot controls the lateral-directional axis model motions. In addition to the two pilots, other required test personnel include: (1) a power operator to control the level of thrust and (2) a safety-cable operator.

The cables attached to the model supplies the model with compressed air for thrust control, electric power for actuator control and data sensors, and control signals through a flexible trailing cable (Reference (27)). A portion of the cable is a steel cable used to catch the model when a test is completed or when an uncontrolled motion occurs. It is the job of the cable-operator to keep the cable slack during the entire flight.

The wind tunnel free-flight test technique is most commonly used to investigate the following: (1) evaluation of stability characteristics near stall/departure (2) evaluate pilot control techniques at high angles-of-attack and (3) evaluate the effects of stability augmentation systems and airframe modifications. This third use is particularly suited to evaluation of high- $\alpha$  elements of the flight control system.

One of the primary advantages of this technique is the relatively large models used (at least 1/10-scale for most fighter configurations). Because of their size they can also be used in force tests to obtain static and dynamic aerodynamic characteristics for the analysis of the model motions.

Though this technique can provide the data to predict aircraft departure susceptibility at high angles-of-attack, the severity or duration of a departure, or the expected recovery characteristics can not be evaluated using this method. Also, the progression of a departure to a developed spin likewise cannot be investigated using this method (Reference (27)). For the most part, maneuvers of the model are restricted to 1-g, though mild maneuvering such as bank-to-bank rolls or steady sideslips can be accomplished.

To provide a link between wind-tunnel testing and the full-scale flight testing, researchers have capitalized on the use of outdoor flight tests of dynamically-scaled radio-controlled (R/C) models. The R/C models permit a more precise representation of departure and recovery tendencies before full-scale flight testing. The models are normally launched from a helicopter as shown in figure 94 or from a similar aerial platform.

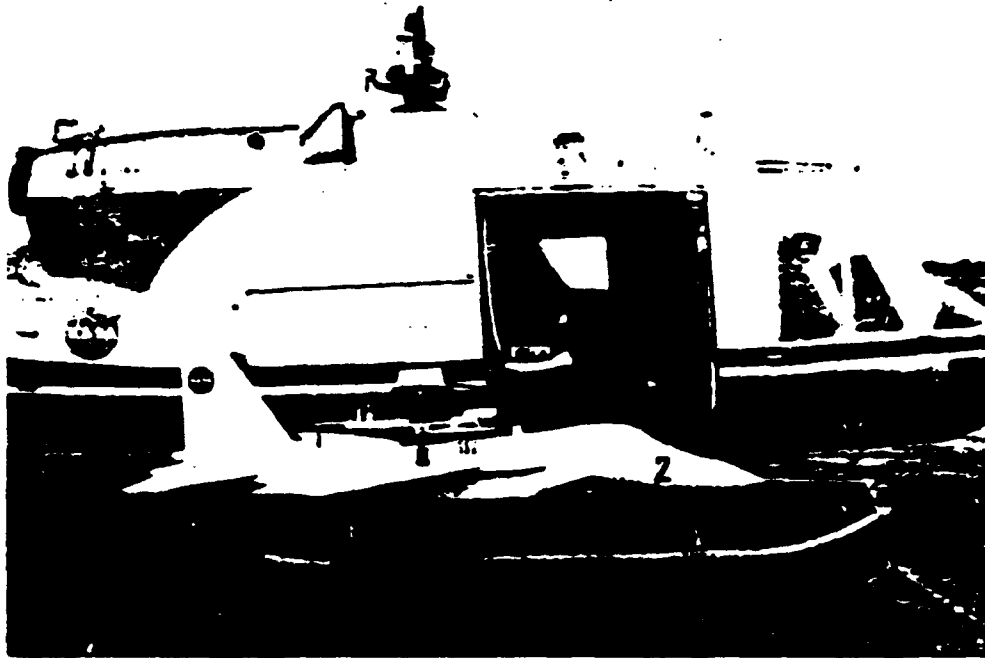


Figure 94. Radio Controlled Model Mounted on Helicopter Launch Platform (Reference (27))

The models carry spin chutes in the event successful recovery is not achieved. Parachutes are always used to recover these unpowered models. Remote ground-based computers are used for the simulation of the flight control system. Signals from the computers as well as commands from one or more controllers are sent to the R/C model's actuation systems. The model sends telemetry signals to computer storage devices and plotters at the ground station. Use of this data helps predict: (1) the spin susceptibility of a configuration (2) control techniques that tend to produce developed spins and (3) the effectiveness of various manual and automatic control techniques for recovery from out-of-control conditions (Reference (27)).

As an example of how R/C models are specifically used, recovery during the incipient phase of a spin may be evaluated by applying recovery controls at various stages of the post-stall motion. The controls may also be neutralized at varying numbers (or fractions) of turns after the stall (Reference (27)).

The outdoor-R/C technique has an advantage over the free-flight vertical spin tunnel method in determining departure susceptibility because the models start from level flight as opposed to being prerotated at approximately 90 degrees angle-of-attack.

The R/C method also has a maneuvering advantage over the free-flight wind tunnel test method because it may be stalled at flight conditions other than just 1G flight. Drawbacks to this method of testing are its expense, the slowness with which tests can be restarted, and the fact that the tests are at the mercy of local weather.

Figure 95 summarizes the particular high angle-of-attack flight regime for which each of the scaled dynamic model test techniques are considered valid.

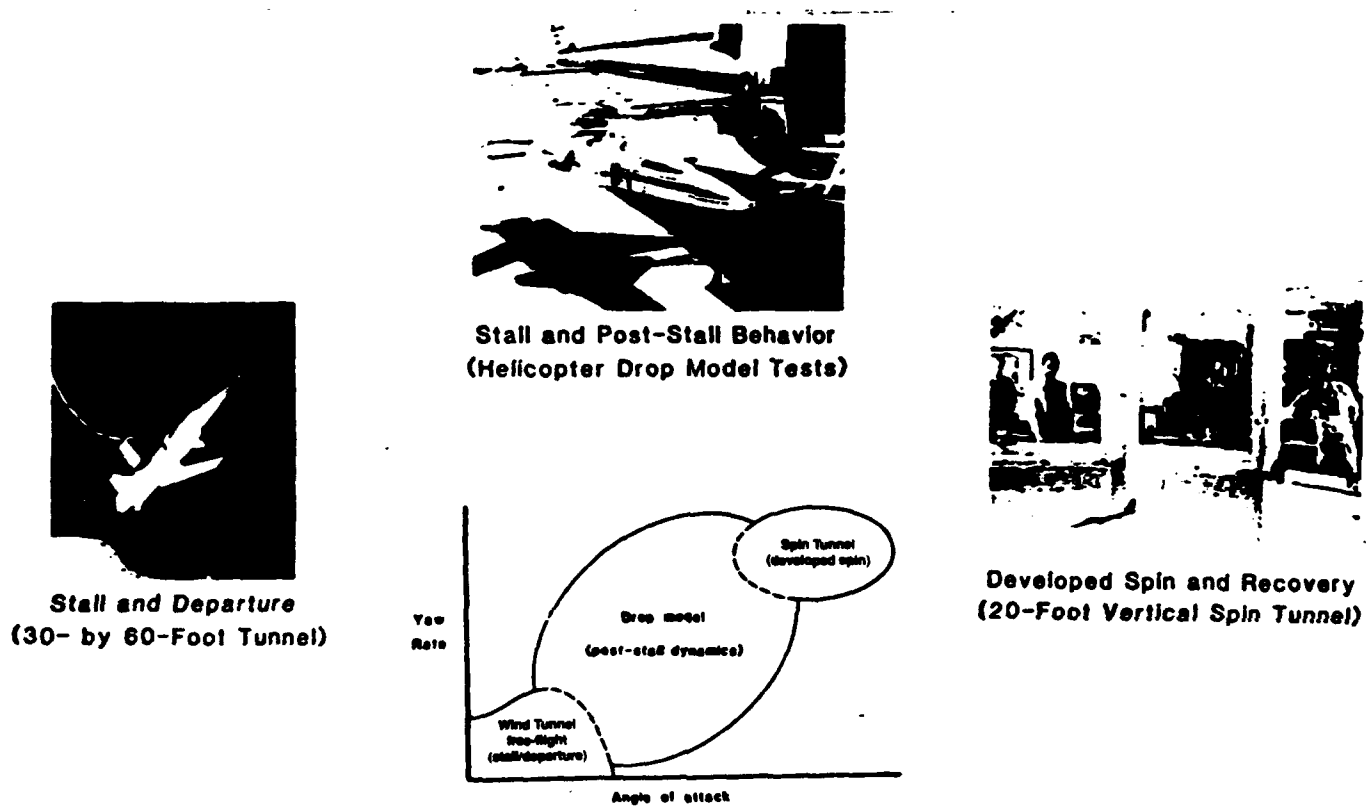


Figure 95. Summary of High- $\alpha$  Scaled-dynamic Testing (Reference (66))

### **3.3. Piloted Simulation**

Analytical studies, wind-tunnel testing and R/C model testing provide significant data as far as predicting how an aircraft will perform during stall/spin/post-stall maneuvering flight. However these test methods fall short of providing data concerning how well the pilot can fly the aircraft and maintain adequate control throughout the entire envelope for all required tasks. This becomes especially true of aircraft with higher order flight control systems. For instance a shortcoming of both the free-flight wind tunnel test (30 × 60 ft NASA Langley tunnel) and the R/C tests, is that the pilot is located a considerable distance from the model. As a result the pilot's perspective is unrealistic because of the remote location of the pilot and the faster angular velocities caused by dynamic scaling relations (Reference (63)). Because of these limitations, the results of these methods are mainly qualitative in providing controllability data (Reference (63)). Manned simulation resolves this problem and avoids the need to math model the nonlinear, time varying characteristics of the pilot as many analytical studies require. Of course, providing realistic environmental flight perceptual cues becomes the substituting limitation of simulators. Withstanding this limitation for the moment (in-flight simulators do not have this limitation in all cases), the primary benefit derived from the use of the manned research simulator is that it can better aid the design of an aircraft and its subsystems around the capabilities of the pilot.

In contrast to full-scale flight test, simulators are safer and less costly, and can provide a means to investigate areas of the flight envelope not capable of today's current operational aircraft. In addition control system changes are normally easily programmed, and in a short time a wide variety of data can be obtained for a test matrix with numerous variants.

The types of aircraft simulators in use today include, training simulators, engineering simulators and research simulators. Each of these types of simulators have varying degrees of complexity tailored to their intended use. In either case, the basic ingredients of a simulator will usually include the following three elements:

1. an aerodynamic data base sufficient to model the desired aircraft flight envelope.
2. an accurate mathematical model of the equations of motion and control system (or physical hardware of components of the control system).
3. realistic display of the cockpit (to include, instruments and force feel system) and flight environment as required (to include motion and visual cue systems).

To study stall/spin/post-stall flight utilizing the manned simulator as a research tool challenges the capabilities of each of today's current technology simulators in some way. Items one through three listed above, are specific areas of concern when investigating high angle-of-attack flying qualities utilizing a manned simulation. More specially these three ingredients address specific fidelity requirements of a flight simulator. Items one and two respectively address aerodynamic math model and dynamic vehicle fidelity, while the third item addresses information fidelity. Fidelity in a simulator means that "something" occurring in a real flight situation is accurately recreated. Lack of fidelity in any of the above ingredients arises when (1) "something" that is present in "real" flight is omitted or (2) something that is not present in flight is introduced.

High angle-of-attack aerodynamic fidelity requires that a comprehensive aerodynamic data base be modelled that includes an adequate  $\alpha$ ,  $\beta$  and Mach number (additionally the data may also be required to be a function of  $\Omega b/2V$ ) range that includes all significant nonlinearities. In this respect, the aerodynamic fidelity of the simulation is confined to the data base modelling limitations. As an example, the credibility of a simulation experiment designed to investigate spinning flight would be seriously questioned if the data base did not include rotary balance data.

Dynamic vehicle fidelity depends on the mathematical models (atmospheric, gust, propulsion, control system, etc.) the computers (analog/digital or hybrid, speed) and the control loaders used in the simulation. The degree of dynamic fidelity not only determines how well the vehicle dynamics are reproduced (off-line studies) but it also influences the quality of feedback information available to a pilot concerning the results of his control inputs.

Information fidelity refers to the ability of the simulator to store and display information accurately to a subject pilot in order to recreate a desired "real" flight situation (Reference (67)). This applies to visual as well as non-visual sources of information. The authors of reference (67) point out that information fidelity can exist and the simulation still be deficient due to lack of perceptual fidelity. (Perception refers to the pilot's ability to perceive the available information). That is, because the simulation may provide the required information, does not necessarily imply that the pilot will perceive it. Lack of perceptual fidelity may be due to a number of factors. The information may be below the pilot's threshold or the information may not be perceived because other intrusive or irrelevant information is present that distracts from the pilot's task (Reference (67)). Another possibility for the lack of perceptual fidelity is that too much relevant information may be received. For instance, in "real" flight "something" may not be perceived due to a high workload whereas it is perceived in the less stressful atmosphere of the simulator (Reference (67)).

In addition to these categories of simulation fidelity just described, often the lack of fidelity may be traced to the simulator architecture. This would include artifacts such as computer time delays.

The result in any lack of equivalence between "real" flight and simulated flight will subsequently effect performance differences in the development of high angle-of-attack flying qualities criteria, or in the simulators use as an aircraft design tool. To minimize the differences between predicted simulation results and actual flight requires that careful thought be given to determine which factors are critical by considering the desired end results of the simulation experiment. Simulation programs designed to study aircraft departure and high angle-of-attack flying qualities must be very attentive to the capabilities of the simulator used. Depending on the specific test objectives, the simulation experiment may require the capability to provide a sustained force environment simulation. For other programs, the objectives might require the use of dual-domed simulators which contain a wide field-of-view useful for air combat maneuvering studies. Still other high angle-of-attack test objectives may be satisfied by utilizing a six degree-of-freedom (DOF) motion base simulator that does not provide either a sustain force environment or a wide visual field-of-view. Table III taken from reference (68) presents a survey of the

simulators most suitable for high- $\alpha$  simulation experiments. The capabilities of each of the simulators surveyed is highlighted and references (69) through (87) can be referred to for more specific information concerning a particular facility.

In summary, flight simulation is the best accepted means for investigating the characteristics of new technologies and aircraft design, but the results must be weighted in light of the capabilities of the simulator used. As the author of reference (87) confides,

"Until confirmed by flight test of the actual vehicle, simulation results should be considered as predictions, at best. Although many studies have been performed over the years to compare simulation results to those of actual flight test, to date there is still no absolute correlation."

On a more optimistic note, the authors of references (53) and (88) report that,

"studies utilizing piloted simulation have indicated that it is an extremely valuable tool for stall spin research. Correlation of results predicted by the simulator with those obtained from subsequent full-scale flight tests for several current fighters have indicated good agreement, particularly with regard to the overall spin resistance of the configuration. In addition, simulations have provided valuable insight into the effects of various automatic spin prevention concepts, and simulation has proved to be of great value in the identification of critical maneuvers."

### **3.4. Full Scale Aircraft Flight Testing**

The most exact measure of an aircraft's high angle-of-attack and departure flying qualities is possible only through a flight test program. Because of the limitations of accurately predicting flight characteristics at high angles-of-attack, flight test programs are heavily relied upon to extract pilot opinions and collect data that is eventually used to define aircraft characteristics that include, defining maneuvering boundaries, the acceptability of stall warning, and the evaluation of stall and post-stall

characteristics. The dangers of flight testing preclude its use in the initial phases of the development of an aircraft, and testing a broad range of specific theoretical criteria is seldom done because of cost and the expediency of using other means.

One of the primary challenges of high angle-of-attack flight testing is the task of configuring the flight test aircraft such that it is equipped with the required testing instrumentation and emergency recovery system (safety of the pilot and aircraft is a constant concern) without altering the aerodynamic and inertial characteristics of the aircraft. If the effects of the test aircraft's "add-ons" are not determined to be negligible, then their effect must be accounted for in any analysis of the flight test data. An example that highlights this concern is the installation of large flight-test nose booms used to mount an angle-of-attack, sideslip vane and pilot static system. As pointed out by the authors of references (65), (90), and (91), this modification of a test aircraft can significantly affect the lateral-directional stability of a test configuration at high angles-of-attack, and could potentially alter the departure susceptibility and recovery characteristics of the airplane (Reference (78)). References (89) and (92) provide more detailed description of the Naval stall/post-stall/spin program and are recommended for further reading on the subject of high angle-of-attack flight testing.

# NADC 88020-60

TABLE III SIMULATOR COMPARISON SUMMARY (Reference (60))

| SIMULATOR  | TYPE  | PRIMARY USE  | MAXIMUM Gs<br>(MOMENTARY)      | CONTINUOUS<br>SUSTAIN Gs     | DEGREES<br>OF<br>FREEDOM | MAXIMUM<br>TOTAL<br>DISPLACEMENT |
|--|---|--|--------------------------------|------------------------------|--------------------------|----------------------------------|
| DFS<br>Dynamic Flight<br>Simulator<br>(NADC)   | Centrifuged<br>Based 50 ft.<br>Arm                                    | High<br>Performance<br>Research and<br>Development<br><br>Training,<br>Testing and<br>Evaluation,<br>Human<br>Factors. | 40Gs<br>(15Gs<br>man-rated)    | 40Gs<br>(15Gs<br>man-rated)  | 3                        | Unlimited<br>(Longitudinal)      |
| VMS<br>Vertical Motion<br>Simulator<br>(AMES)  | Hydraulically<br>Driven<br>Synergistic on<br>Large Motion<br>Platform | Research and<br>Development of<br>V/STOL and<br>Rotorcraft   | 1G<br>(Vertical)               | 1                            | 6                        | 60 ft.<br>(Vertical)             |
| DES<br>Dynamic Environment<br>Simulator<br>(WP AFB)  | Centrifuged<br>Based 20 ft.<br>Arm                                    | Research and<br>Development,<br>Human Factors<br>Studies   | 20Gs<br>(9.5Gs<br>man-rated)   | 20Gs<br>(9.5Gs<br>man-rated) | 3                        | Unlimited                        |
| LAMARS<br>Large Amplitude<br>Multi-mode Aerospace<br>Research Simulator<br>(WP AFB)        | 30 ft. Cantilever<br>Beam   | Research and<br>Development  | 3Gs<br>(Vertical)              | 1                            | 5                        | 20 ft.<br>(Vertical,<br>Lateral) |
| SIX-DEGREES-<br>OF-FREEDOM<br>Large Motion<br>Commercial Simulator<br>(Passenger Aircraft) | Hydraulically<br>Driven<br>Synergistic Six<br>Post Platform           | Training,<br>Pilot<br>Performance<br>Studies   | 2Gs<br>(Vertical)              | 1                            | 6                        | 12.14 ft.<br>(Longitudinal)      |
| FSA<br>Flight Simulator for<br>Advanced Aircraft<br>(AMES)                                 | Moving Cab on<br>Large Motion<br>Platform                             | Research and<br>Development<br>Lateral<br>Dynamics<br>Evaluations  | .31G<br>(Lateral,<br>Vertical) | 1                            | 6                        | 80 ft.<br>(Lateral)              |

TABLE III (Cont'd) SIMULATOR COMPARISON SUMMARY (Reference (60))

| FLEXIBILITY  | VISUAL SYSTEM  | FIELD-OF-VIEW                       | COCKPIT FIDELITY | REMARKS   |
|--|--|-------------------------------------|------------------|---|
| Interchangeable Cab, Displays Variable Control and Aero Model Programmable Visual System | Redifussion SP-2 CRT Computer Graphics   | 48°H × 32°V                         | High             | Can simulate force environment of high performance aircraft available as an R&D and Training tool<br><br>References: 68, 69, 70   |
| Interchangeable Cabs, Variable Control System  | Singer-Link Computer Graphics  | 160°                                | Medium           | - Limited Displacement<br>- Simulates only V/STOL, rotorcraft limited to 1G vertical (Z) .75G horizontal (Y) and .5G longitudinal (X)<br>- Relatively Low Roll, Pitch and Yaw Rates<br><br>References: 71, 72 |
| Interchangeable Cockpit Systems  | Evans and Sutherland Multi-Picture System  | 50°H × 40°V (estimated)             | Low              | - Very low Pitch Angular Acceleration<br>- Low G change capability<br>- Unsited for high performance A/C simulation<br><br>References: 73, 74, 75   |
| Variable Control Systems   | Rigid Model Visual System (terrain board and camera) 24 ft. Diameter Spherical Projection Screen | 266°H × 108°V                       | Medium           | No sustained G capability<br><br>References: 73, 74   |
| Generally Designed for One Aircraft Type Only  | Generally these Systems are Computer Graphics Systems  | Generally Approximately 48°H × 36°V | High             | No sustained G capability Suited for steady-state flight training<br><br>References: 76, 80   |
| Interchangeable Cabs   | Virtual Image TV Display (Terrain Board generated)   | 48°H × 36°V                         | Medium           | No sustained G capability Limited Fidelity<br><br>References: 81, 82  |

TABLE III (Cont'd) SIMULATOR COMPARISON SUMMARY (Reference (60))

| SIMULATOR  | TYPE  | PRIMARY USE   | MAXIMUM Gs<br>(MOMENTARY)   | CONTINUOUS<br>SUSTAIN Gs | DEGREES<br>OF<br>FREEDOM | MAXIMUM<br>TOTAL<br>DISPLACEMENT |
|--|---|---|---|--------------------------|--------------------------|----------------------------------|
| ASUPT<br>Advanced Simulator for<br>Undergraduate Pilot<br>Training<br>(Williams AFB) | Hydraulically<br>Driven<br>Synergistic Six<br>Post Platform | T-37 Simulator<br>Undergraduate<br>Pilot<br>Training<br>Program<br>Operations                                     | .8G<br>(Vertical)   | 1                        | 6                        | 5.75 ft.<br>(Vertical)           |
| Device (2F95)<br>Operational Flight<br>Trainer<br>(NAS-OCEANA)                       | Cascade   | F-14 Pilot<br>Training  | Unknown   | 1                        | 4                        | 3 ft.<br>(Vertical)              |
| McDonnell Douglas<br>Manned Air Battle<br>Simulators<br>(McDonnell Douglas<br>Labs)  | Fixed Base<br>Dome  | Research on<br>Fighter<br>Requirements<br><br>Real Time<br>Battle<br>Simulations<br><br>Interactive<br>Simulation | N/A   | 1                        | 0                        | 0                                |
| In-Flight Simulators   | Experimental<br>Variable<br>Control System<br>Aircraft      | Training,<br>Research<br>on Aircraft<br>Control<br>Systems  | Maximum<br>Gs<br>in which<br>In-Flight<br>Simulator<br>Aircraft<br>can<br>withstand | 1                        | 6                        | 5.5Gs for<br>T-33                |

TABLE III (Concluded) SIMULATOR COMPARISON SUMMARY (Reference (60))

| FLEXIBILITY  | VISUAL SYSTEM   | FIELD-OF-VIEW                         | COCKPIT FIDELITY | REMARKS   |
|--|---|---------------------------------------|------------------|---|
| Designed to Simulate T-37 and T-38 Trainer Only                                      | 7 CRT Computer Graphics System                                  | 300°H × 140°V                         | High             | <ul style="list-style-type: none"> <li>- Training pilot does not feel maximum that he feels in actual T-37 or T-38</li> <li>- Limited flexibility T-37 and T-38 only</li> <li>- Uses G-cueing and not actual sustained Gs</li> </ul> References: 83 |
| Designed to Simulate F-14 Only   | Calligraphic Day/Night Computer Graphics                        | 46°H × 32°V                           | High             | No sustained G capability<br>No cockpit flexibility<br>Training applications on / (F-14)<br><br>References: 84  |
| Simulates Various Fighter Type Aircraft F-15, F/A-17, AV-88 Various Battle Scenarios | Up to Seven Images Projected onto Inner Dome Wall               | Full Field-of-View                    | High             | No aerodynamic motion<br>Strictly a visual simulation<br><br>References: 85   |
| Variable Control System  | Pilot Sees Outside Environment which may not Correspond to Test | Limited to that of In-Flight Aircraft | Medium           | Dynamics limited to simulator A/C<br>Limited cockpit fidelity and flexibility<br><br>References: 86, 87   |

#### **4.0. HIGH ANGLE-OF-ATTACK MILITARY SPECIFICATIONS AND FLYING QUALITIES CRITERIA**

##### **4.1. Military Specifications**

Four military specifications (MIL-SPECS) are important to high angle-of-attack departure flying qualities: MIL-F-8785C, MIL-D-8708B (AS), MIL-S-83691A (USAF) and the proposed revision to MIL-F-8785C, MIL-STD-1797 (USAF). Exact counterparts for civilian aircraft do not exist, although elements of these Mil-Specs are related to sections of the Federal Aviation Regulations.

##### **4.1.1. MIL-F-8785C, Flying Qualities of Piloted Airplanes (Reference (93)).**

Flying qualities criteria for high angle-of-attack flight are treated in section 3.4 of MIL-F-8785C titled, "Miscellaneous Flying Qualities."

The subsections of Section 3.4 that are specifically intended to address high angle-of-attack flying qualities are given below.

- **3.4.1. Dangerous Flight Conditions**
  - .1. Warning and Indication
  - .2. Devices for indication, warning, prevention, recovery.
- **3.4.2. Flight at high angle-of-attack**
  - .1. Stalls
    - .1. Stall Approach
      - .1. Warning speed for stalls at 1g normal to the flight path.
      - .2. Warning range for accelerated stalls
    - .2. Stall Characteristics
    - .3. Stall Prevention and Recovery
      - .1. One-engine-out stalls

.2. Post-Stall Gyration and Spins

.1. Departure from controlled flight

.2. Recovery from post-stall gyration and spins

- 3.4.3. Cross-axis coupling in roll maneuvers

- 3.4.4. Control harmony

.1. Control force coordination

- 3.4.8. Transients following failures

- 3.4.9. Failures

- 3.4.10. Control Margin

- 3.4.11. Direct Force Controls

MIL-F-8785C (Reference (93)) states that stall warning shall be clear but shall not be so excessive as to interfere with the aircraft mission. The specification further states that there shall be no rolling, yawing, or pitching at stall which can not be controlled within 30 degrees for class IV aircraft and 20 degrees for all other aircraft. Stall recovery should be simple with no accompanying excessive altitude loss. MIL-F-8785C goes on to state that aircraft should be *extremely resistant*<sup>1</sup> to departure. Spin recoveries must be smooth and within a maximum of two turns after the initiation of recovery control application.

MIL-F-8785C also addresses warning indications and special devices for preventing all dangerous flight conditions. The specification states that the preferred method of eliminating dangerous flight conditions is through aerodynamic design and mass distribution rather than through the aid of special devices.

---

<sup>1</sup> MIL-S-83691A's definitions of departure susceptibility and resistance are given in Appendix A.

The requirements addressing high angle-of-attack flying qualities, as outlined above, are set in broad, general terms in MIL-F-8785C. The principles are, of course, valid, and it is desirable to build aircraft that match the criteria of no departures and simple control inputs to effect recovery while continuing to advance maneuver capabilities and aircraft mission performance requirements. However, MIL-F-8785's high angle-of-attack descriptions are open to interpretation, and no definite, quantitative guidelines are set as they are in other sections of the specification. Reference (94), MIL-F-9490D clarifies the meaning of MIL-F-8785's high angle-of-attack requirements somewhat, but a gap still exists in defining more quantitative boundaries for safe flight at high angles-of-attack in terms of defined flying qualities parameters. As stated in the Background Information and User's Guide for MIL-F-8785C (Reference (95)):

These requirements remain largely qualitative, thereby furnishing little direct design guidance.

This approach reflects both the complexity of this essentially nonlinear problem and the continuing status of high angle-of-attack design as perhaps more artful than scientific.

#### 4.1.2. High Angle-of-Attack Flight Test Demonstration Requirements and Procedures

MIL-D-8708B (Reference (96)) and MIL-S-83691A (Reference (2)) are the military specifications of the Navy and Air Force respectively that govern aircraft stall, post-stall, and spin flight test demonstration requirements. More specifically, MIL-D-8708B contains the general requirements of the Naval Air Systems Command (NAVAIR) for the contractor demonstration of all phases of aircraft flight that include stall, post-stall and spin flight phases (see section 3.13.2, "Flying Qualities" and section 3.13.3, "Spins"). In contrast to MIL-D-8708B, MIL-S-83691A, written by the Air Force, is specially directed at addressing only high angle-of-attack flight test and evaluation procedures.

The demonstration requirements contained in both these specifications, in addition to the appropriate addendum for the aircraft in question, provide guidelines for test procedures, flight test instrumentation, data gathering devices, test matrices and flight test documentation. The primary

purpose of the contractor's demonstrations are to determine that the airplane can be safely operated by military pilots during trials and to obtain quantitative data necessary to determine safe limits for operation by fleet pilots (Reference (90)). Though MIL-D-8708B and MIL-F-83691A were written to regulate high angle-of-attack flight demonstrations of operational aircraft prototypes, the procedures outlined are often used for theoretical research purposes.

MIL-STD-1797, *Flying Qualities of Piloted Vehicles* (Reference (1)).

Air Force Wright Aeronautical Laboratories (AFWAL) has proposed a document to supersede MIL-F-8785C. Drafts of the proposed document, "*Flying Qualities of Piloted Vehicles*", MIL-STD-1797, are being reviewed by government and industry at the time of this writing. MIL-STD-1797 is an attempt at updating flying qualities specifications to reflect advances in complex, higher order aircraft dynamic response modes, advanced control schemes, high angle of attack flight, and other areas.

MIL-STD-1797 delineates specific guidelines for all conditions of post-stall gyration and spin entry attempts. This is shown below in figure 96 as excerpted from the draft version of the proposed specification.

**4.8.4.3. Post-stall gyrations and spins.** The post-stall gyration and spin requirements apply to all modes of motion that can be entered from upsets, decelerations, and extreme maneuvers appropriate to the Class and Flight Phase Category. Entries from inverted flight and tactical entries \_\_\_\_\_ be included. Entry angles of attack and sideslip up to maximum control capability and under dynamic flight conditions are to be included, except as limited by structural considerations. Thrust settings up to and including MAT shall be included, with and without one critical engine inoperative at entry. The requirements hold for all Aircraft Normal States and for all states of stability and control augmentation systems except approved Special Failure States. Store release shall not be allowed during loss of control, spin or gyration, recovery, or subsequent dive pullout. Automatic disengagement or mode-switching of augmentation systems, however, is permissible if it is necessary and does not prevent meeting any other requirements; re-engagement in the normal mode shall be possible in flight following recovery. Specific flight conditions to be evaluated are: \_\_\_\_\_

#### REQUIREMENT RATIONALE

The conditions for consideration of departure and recovery from post-stall gyrations and spin are delineated.

#### REQUIREMENT GUIDANCE

The related MIL-F-8785C requirement is paragraph 3.4.2.2.

Similar to the introductory requirement for stalls (4.8.4.2), the conditions to be considered are specified for departures and spins. The stated conditions are to be interpreted according to the intended missions, as reflected in the aircraft Class and Flight Phase Categories. For Class II and III aircraft the words "need not" should be inserted in the first blank. For Classes I and IV, insert "shall."

Figure 96. MIL-STD-1797 Requirement: Post-Stall Gyrations and Spins (Reference (1))

## NADC 88020-60

In contrast to MIL-F-8785C, MIL-STD-1797 recommends aircraft be "resistant" rather than "extremely resistant" to departure to ease airframe design constraints and control system complexity as well as to account for a fighter pilot's infrequent desire to depart as a "last ditch" escape maneuver. "Resistant" signifies that the aircraft will only depart with "large and reasonably *sustained misapplication* of pitch, roll and yaw controls."

MIL-STD-1797's requirement for recovery calls for a single technique for all post-stall gyrations and spins. The wording of this requirement is given in figure 97 as excerpted from the draft version of the proposed specification.

**4.8.4.3.2 Recovery from Post-stall Gyration and Spins.** The post-stall characteristics shall be determined. For aircraft that, according to their structural design specification, must be structurally designed for spinning:

a. The proper recovery technique(s) must be readily ascertainable by the pilot, and simple and easy to apply under the motions encountered.

b. A single technique shall provide prompt recovery from all post-stall gyrations and incipient spins, without requiring the pilot to determine the direction of motion and without tendency to develop a spin. The same technique used to recover from post-stall gyrations and incipient spins, or at least a compatible one, is also desired for spin recovery. For all modes of spin that can occur, these recoveries shall be attainable within \_\_\_\_\_. Avoidance of a spin reversal or an adverse mode change shall not depend upon precise pilot control timing or deflection.

c. It is desired that all aircraft be readily recoverable from all attainable attitudes and motions.

d. Safe and consistent recovery and pullouts shall be accomplished without exceeding the following forces: \_\_\_\_\_, and without exceeding structural limitations.

Figure 97. MIL-STD-1797 Requirement: Recovery from Post-Stall Gyration and Spins (Reference (1))

For highly maneuverable aircraft with varied missions and store loadings, the requirements of paragraph "b." may have to be relaxed. However, the recovery technique should remain a single set of unique, simple instructions which do not require excessive pilot skill, timing or workload. As was shown in figures 96 and 97, the format of the proposed MIL-STD-1797 requirements contains blanks for placement of specific words or values. The values to fill these blanks are intended to be supplied by the activity procuring the particular aircraft.

The Background Information and User's Guide for MIL-F-8785C is informative but not binding. It is not an actual part of the specification document. The proposed MIL-STD-1797 specification, on the other hand, has the specification background and rationale as an appendix and is referred to as the Handbook. This is an improvement in that it not only treats high angle-of-attack and departure in greater detail, but because the Handbook comprises a major portion of the actual specification it connotes a more binding tone. Reasons are provided for supplying specific values and criteria to the Standard, but final wording of the Standard for a particular aircraft purchase remains at the discretion of the procuring activity.

By revising MIL-F-8785C in this manner, MIL-STD-1797 is expandable and adaptable for the inclusion of more quantitative high angle-of-attack flying qualities criteria in the future. This is an important feature of this proposed document because as the draft currently exists, there have been few advances to extend the high angle-of-attack flying qualities requirements presented in MIL-F-8785C. The fact remains that the requirements in the proposed specification are still largely qualitative.

#### **4.2 Departure Susceptibility Prediction Criteria**

One of the primary goals of designing a modern Class IV aircraft to have "good" flying qualities involves preventing departures or delaying the possibility of a departure to as high an angle-of-attack in the stall post-stall region as possible. The importance of predicting the departure tendencies of an aircraft as early as possible in the design phase are apparent. As discussed in earlier sections the accurate prediction of aircraft high angle-of-attack characteristics (i.e., prediction of full-scale aerodynamic coefficients and derivatives) is complex. In addition to increased aerodynamic nonlinearities occurring at high angles-of-attack, inertial and kinematic coupling effects become more pronounced, and conventional control inputs may no longer produce the expected dynamic response. Figure 98 (developed from reference (97)) highlights the primary factors which influence an aircraft's tendency to depart from controlled flight.

# **I AIRCRAFT BARE AIRFRAME HIGH-AOA AERODYNAMIC FLIGHT CHARACTERISTICS**

- Nonlinear with respect to angle-of-attack and sideslip
- Flow breakdown and Adverse Vortex Shedding Effects Common

## **Associated Causes of Departure**

1. Aircraft Unstable Directionally with Stable Dihedral Effect (or Vice Versa); Aircraft may Depart but it is not likely to be divergent
2. Aircraft is unstable directionally and has Unstable dihedral effect; Divergent Departure likely

# **II USE OF AERODYNAMIC FLIGHT CONTROLS**

- Aileron and Rudder effectiveness greatly reduced

## **Associated Causes of Departure**

1. Use of aileron may aggravate situation due to adverse yaw generated at high angle-of-attack becoming the dominant control effect.
2. Use of prolonged or misapplication (cross-controlling) of control inputs at High angle-of-attack could induce departure.

# **III INERTIAL COUPLING**

- Moments generated due to Inertial Coupling become more pronounced at large Angles-of-attack

## **Associated Cause of Departure**

1. Increase in inertial coupling effect at large angle-of-attack likely to place the aircraft in a flight condition more susceptible to departure

# **IV KINEMATIC COUPLING**

- Sideslip angle (angle-of-attack) generated due to Kinematic Coupling can become more pronounced with increasing angle-of-attack (sideslip).

## **Associated Cause of Departure**

- From a departure susceptibility viewpoint any generation of large amounts of sideslip (or angle-of-attack) is undesirable because it has the potential to place the aircraft in a flight condition that is more susceptible to departure.

Figure 98. Primary Causes of Aircraft Departure From Controlled Flight

Various means of quantitatively predicting departure susceptibility have been developed. All of the criteria to be presented in this section have been used effectively to some degree (Reference (98)) and (102)). Some are considered "first cut" rules of thumb while others serve as strict design guides and may be suitable for specification incorporation with refinement.

#### 4.2.1. Bihrie Applied Research Departure and Roll Reversal Boundaries

Bihrie Applied Research (BAR) developed a set of departure susceptibility design charts and boundaries (reference (100) and (101) - See figure 99) based on the results of large angle, six degree-of-freedom computer simulations which accounted for both high angle-of-attack aerodynamic and dynamic nonlinearities. Experience led BAR to believe three characteristics were primarily responsible for departure susceptibility: lateral control, dihedral effect ( $C_{l_p}$ ), and static directional stability ( $C_{n_\beta}$ ). Reference (103) describes the matrix of aerodynamic and inertial parameters which were varied in developing the departure boundaries. The maneuver programmed for evaluation was:

1. Aircraft trimmed in a 60 degree bank at 15,000 ft.,  $M = 0.46$ ,  $\alpha = 12$  degrees,  $G_z = 2g$ 's.
2. At  $t = 0^+$ , full trailing edge up horizontal stabilizer applied at a rate of 30 degrees/second.
3. At  $t = 1.5$  sec, full lateral stick at a lateral control surface rate of 30 degrees/second to oppose the turn ("top stick", "aileron against").
4. At  $t = 8.0$  seconds, both controls returned to trim at a rate of 30 degrees/second.
5. Rudders remained at trim throughout the maneuver.

The parameters selected in defining departure and roll reversal boundaries were: (1) peak yaw rate (magnitude and sign), (2) last angle of attack peak value prior to lateral control removal, (3) approximate second order damping ratio of the angle of attack trace, and (4) incremental peak bank angle attained before lateral control was removed. Of these four parameters, the peak angle of attack value of 50

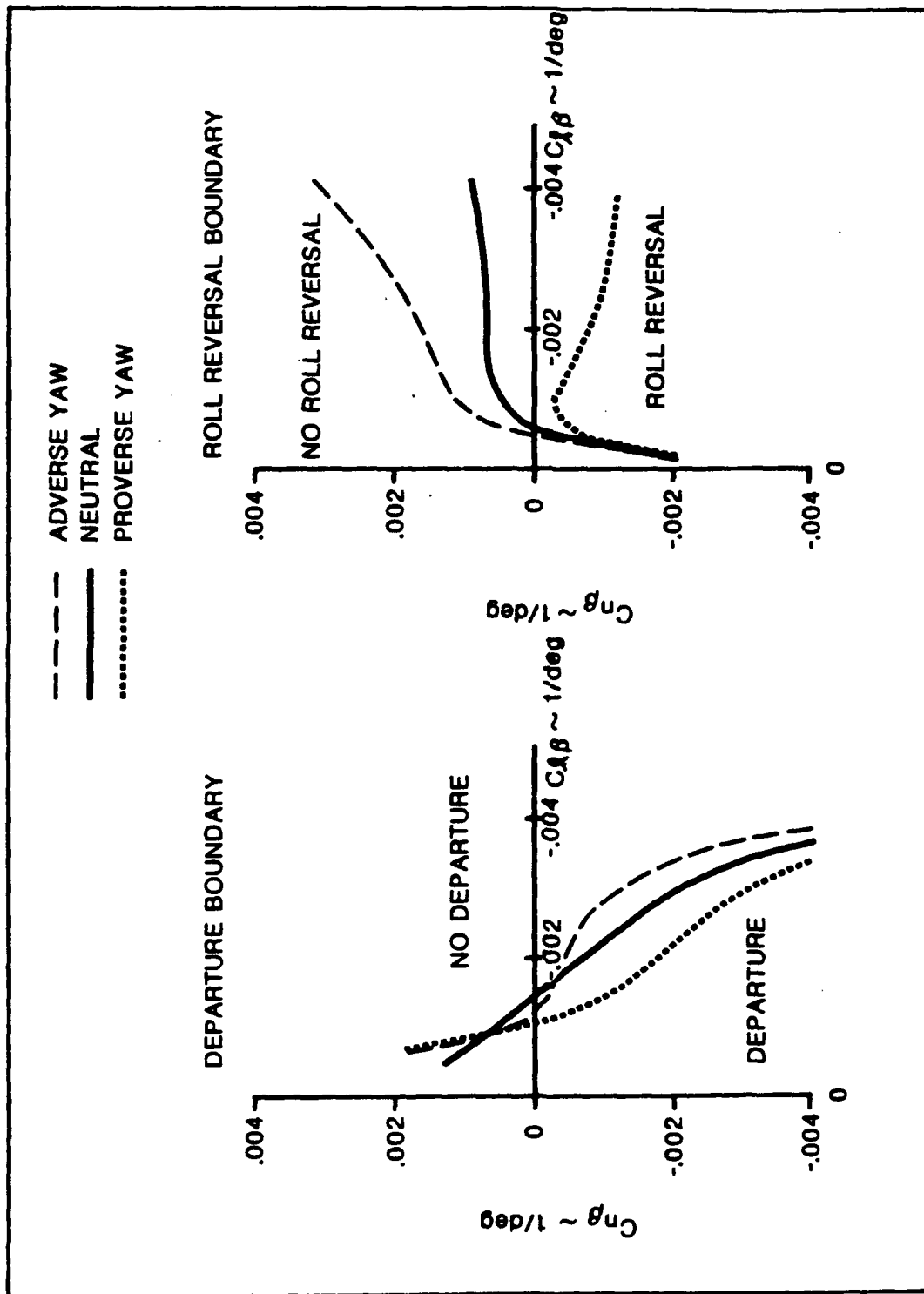


Figure 99. Bihrie Applied Research Departure Susceptibility Design Guidelines (Reference (102))

degrees before lateral control was removed and the zero angle of attack damping were found to be "the best" indicators of departure susceptibility. Based on this, departure and roll reversal boundaries, shown in Figure 99, were drawn.

Note the boundaries are given for three distinct values of  $C_{n_{\dot{\alpha}}}$ . The ratio of  $I_z/I_x$  was always 6.2, and  $I_{xz}$  was always 0. Interpretation of Bihrie Departure design boundaries indicate that a directionally stable aircraft configuration at high angle-of-attack for the most part will be departure resistant. For a directionally unstable configuration a high dihedral effect will tend to prevent departures. Bihrie's evaluation of lateral control yaw characteristics effect (adverse, neutral and proverse yaw) on departure indicate that proverse yaw characteristics reduce the values of directional ( $C_{n_{\dot{\alpha}}}$ ) and lateral stability ( $C_{l_{\dot{\beta}}}$ ) required to avoid departure or uncoordinated roll reversal. Conversely adverse yaw characteristics require increased values of directional and lateral stability to prevent departure and roll reversal from occurring.

Reference (100) also notes the following assumptions used in the development of the criteria boundaries,

- (1) the longitudinal cross-coupling derivative  $C_{m_{\dot{\alpha}}}$  was not modelled.
- (2) the boundaries were developed for longitudinally stable aircraft only throughout the angle-of-attack range (0 to 90 degrees)
- (3) there was no limitation placed on the longitudinal control authority.

#### 4.2.3 Weissman-STI Departure Susceptibility Criteria

Two parameters that are used extensively to predict departure susceptibility are  $C_{n_{\text{PDYN}}}$  and LCDP. Stated simply,  $C_{n_{\text{PDYN}}}$  is an approximation to the undamped natural frequency of the Dutch roll mode and the Lateral Control Departure Parameter (LCDP) defines the necessary condition for the roll angle to lateral control deflection transfer function to be nonminimum phase (all zeros in the left-half complex

plane). Negative values of LCDP usually correspond to roll reversal conditions (roll in the opposite direction of that commanded) and divergence or spin susceptibility is correspondingly predicted (Reference (99)). LCDP approximates the  $\omega_n^2$  term of the  $\phi/\delta_a$  transfer function as given by equation (34),

$$\begin{aligned}\omega_\phi^2 &= \left[ C_{n_\beta}' - C_{l_\beta}' \left( \frac{C_{n_{\delta_a}}}{C_{l_{\delta_a}}} \right) \right] \frac{q S b}{I_z} \\ &= \left( \frac{1}{T_{\phi_1}} \right) \left( \frac{1}{T_{\phi_2}} \right)\end{aligned}\quad \text{EQ (34)}$$

According to reference (98), a value of  $1/T_{\phi_1}$  of  $-0.5$  corresponds to an LCDP value of  $-0.001$ . Figure 100 shows the relationship between  $1/T_{\phi_1}$  and departure susceptibility for the departure simulation experiment described in reference (98). The first mention of these departure parameters was made by Moul and Paulson in 1958. Moul and Paulson were interested in explaining the observed stability of free flight wind tunnel test aircraft models that were statically unstable directionally ( $C_{n_\beta} < 0$ ). Their research (see reference (103)) led to the development of the  $C_{n_{\beta DYN}}$  and LCDP parameters as defined in equations (35) and (36). Positive values for either parameter ( $C_{n_{\beta DYN}} > 0$  or  $LCDP > 0$ ) was determined to be an indicator of departure resistance.

$$C_{n_{\beta DYN}} = C_{n_\beta} \cos \alpha - \left( \frac{I_z}{I_x} \right)_B \sin \alpha \quad \text{EQ (35)}$$

$$\begin{aligned}LCDP &= C_{n_\beta} - C_{l_\beta} \left( \frac{C_{n_{\delta_a}}}{C_{l_{\delta_a}}} \right) \text{ for aileron alone} \\ &= C_{n_\beta} - C_{l_\beta} \left( \frac{C_{n_{\delta_a}}}{C_{l_{\delta_a}}} \right) \times K_1 \left( \frac{C_{n_{\delta_a}}}{C_{l_{\delta_a}}} C_{l_{\delta_r}} - C_{n_{\delta_r}} \right)\end{aligned}\quad \text{EQ (36)}$$

where:

1. For aileron plus rudder proportional to sideslip:

$$K_1 = -\delta_r/\beta$$

2. For aileron plus rudder to aileron:

$$K_1 = \delta_r/\delta_a$$

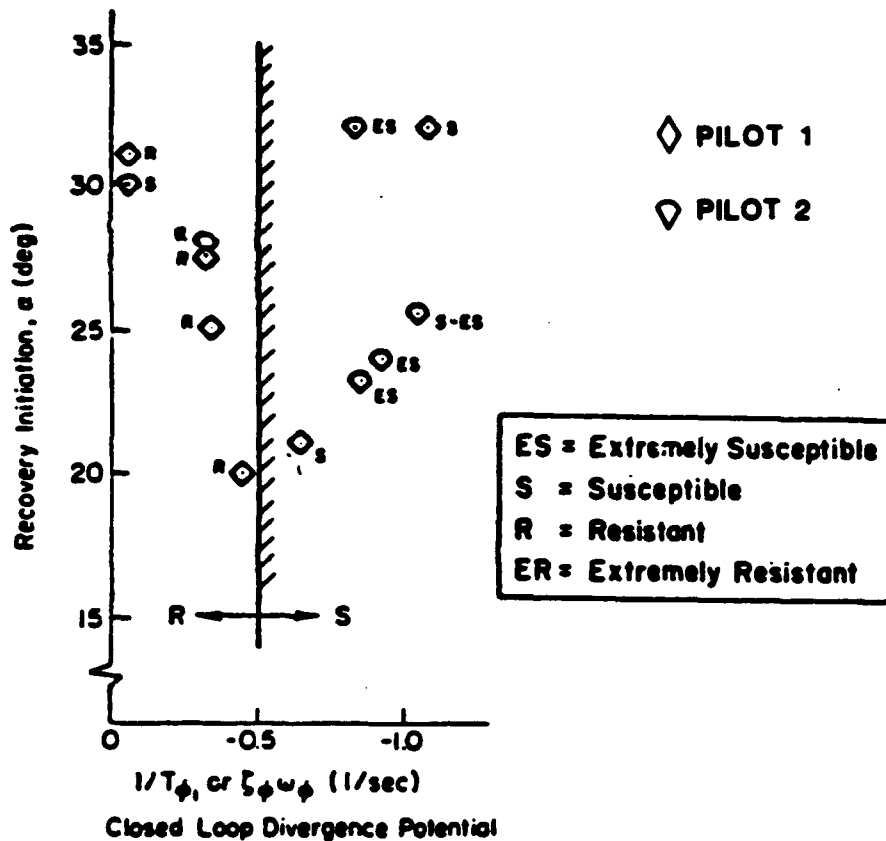


Figure 100. Departure Susceptibility Rating vs. Lateral Closed-loop Divergence Parameter (Reference (98))

Since the work of Moul and Paulson in 1958, various other minimum limits have been proposed for  $C_{n_{\beta DYN}}$  to predict departure as alternatives to  $C_{n_{\beta DYN}} > 0$ . As reference (98) points out, the main reason for these other criteria is that other researchers have recognized that  $C_{n_{\beta DYN}} > 0$  is inadequate in the presence of possible aircraft asymmetries, destabilizing external loads (centerline tanks, etc.) and nonlinear inertial coupling moments present during maneuvering flight. Two of these alternative departure criteria are documented in reference (104). The first one, (original reference (105)) assigned label descriptors to various ranges of  $C_{n_{\beta DYN}}$  based on flight test results which investigated stall behavior as a function of longitudinal control inputs only (See Figure 101).

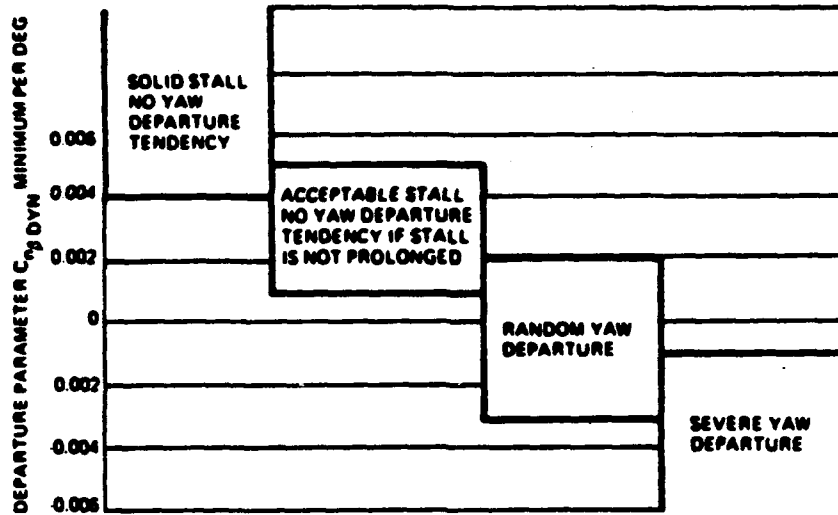


Figure 101. Expected Behavior as a Function of  $C_{n\beta_{DYN}}$  (Reference (104))

A second alternative, developed by Northrop is shown in figure 103. The boundaries shown in figure 102 provide aid in the initial design phases, but regions overlap and are not well defined.

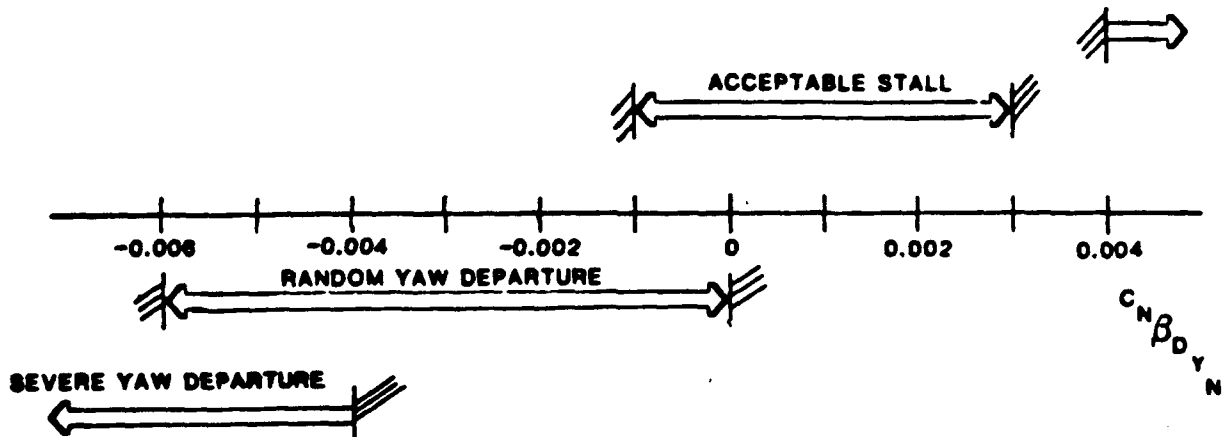


Figure 102. Northrop Departure Criteria (Reference (104))

Finally a third minimum design guide value for  $C_{n\beta_{DYN}}$  is suggested by reference (107) to be 0.004 (1/deg) (Reference (99)).

Probably still the most widely known departure criteria to date is the empirically derived  $C_{n_{pDYN}}$  vs LCDP Departure Criteria Plane developed by Weissman (References (107) and (108)). The departure criteria plane is shown in figure 103. This figure illustrates the first cut at defining departure susceptibility as a function of both the open-loop stability parameter,  $C_{n_{pDYN}}$ , and the closed-loop roll control divergence parameter, LCDP.

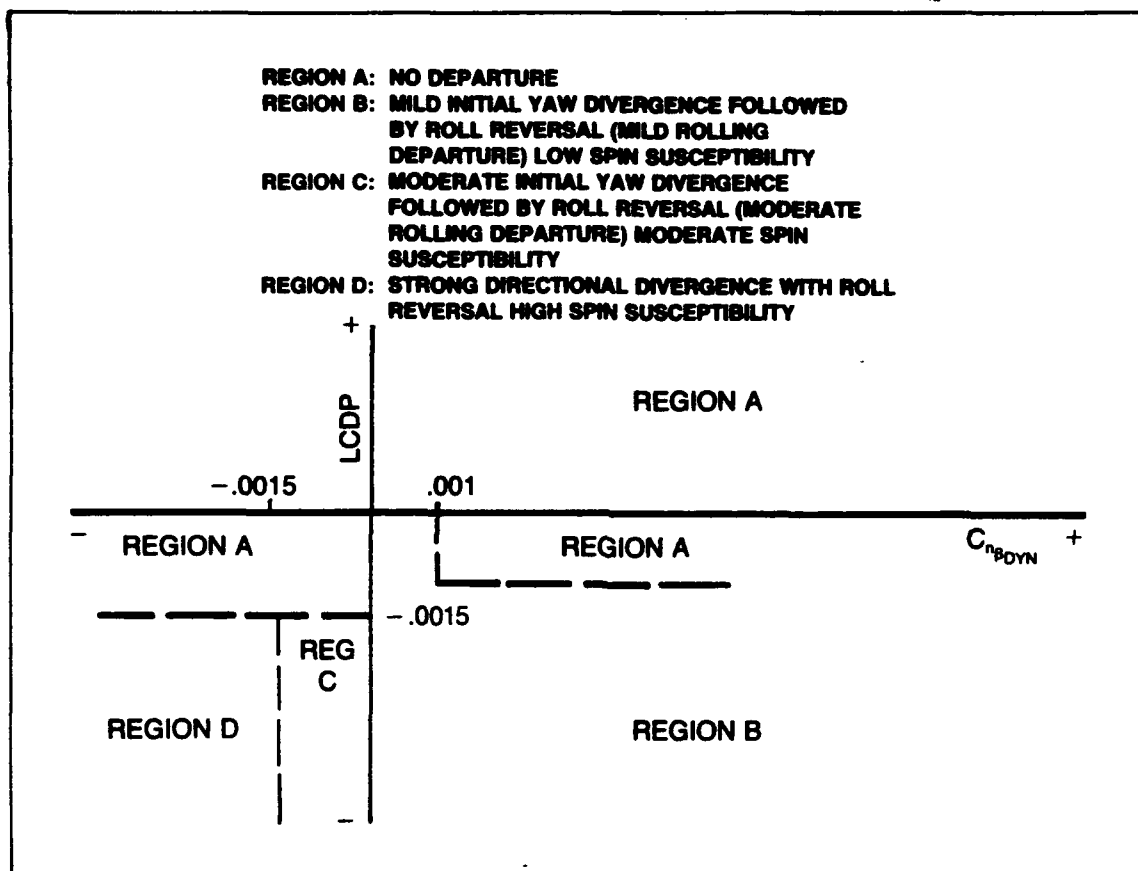


Figure 103. Weissman Departure and Spin Susceptibility Criterion (Reference (107))

Weissman developed this criteria from analyzing time history sensitivity studies to lateral/directional static stability derivatives in a digital six degree-of-freedom off-line simulation. Based on these time history traces Weissman empirically identified regions of increasing roll departure severity and spin susceptibility (see reference (107)). In reference (108) Weissman later correlated flight test data results with his previously defined boundaries (reference (110)) and found good agreement.

The criteria plane of figure 104 has since been modified by Systems Technology Incorporated (STI) based on results of digital and limited fixed base piloted simulations described in reference (98) and past work accomplished at Northrop (Reference (109)). The work done by Skow and Titiriga modified Weissman's original criterion plane by adding boundaries for regions E and F. These two regions identify susceptibility to yaw instead of roll departure (see figure 104). STI's suggested modification to figure 102 involved shifting the E/F boundary to coincide with the C/D boundary. This change was supported by the reference (98) piloted simulation which showed the D/E boundary to be independent of  $C_{n\dot{\rho}_{DYN}}$ . This modification along with other further simplification (i.e., raise the boundary between the E/F and C/D regions; extend the A/B boundary to the LCDP axis) is illustrated in figure 105.

#### 4.2.2.1. STI Departure Rating Scale

In formulating this departure criteria plane, STI first developed a departure rating scale to quantify the pilot evaluations concerning aircraft stall, departure and recovery characteristics. The Cooper-Harper Handling Qualities Rating (HQR) scale was not utilized in the STI simulation, and in general is inadequate for departure research, since any loss of control precipitates a Cooper-Harper HQR of 10. Furthermore, because the simulation objectives were aimed at evaluating aircraft characteristics rather than task tailored performance, the pilots felt use of the Cooper-Harper rating scale was inappropriate (Reference (98)).

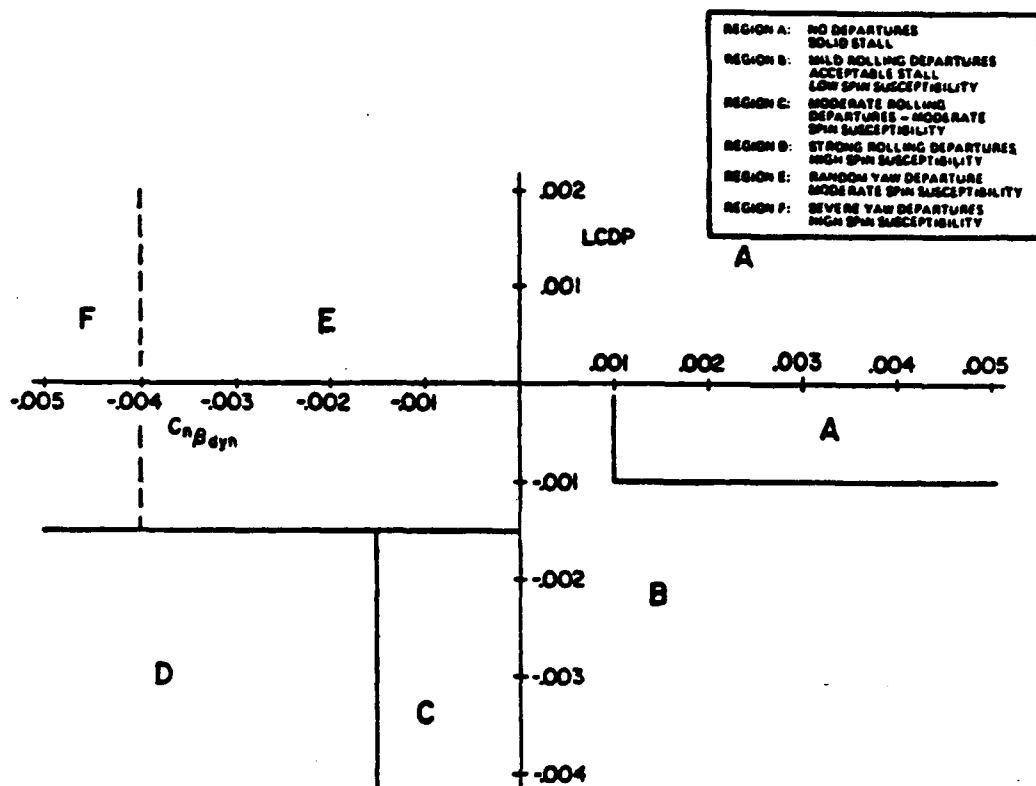


Figure 104. Northrop Modified Weissman Departure and Spin Susceptibility Criterion (Reference (99))

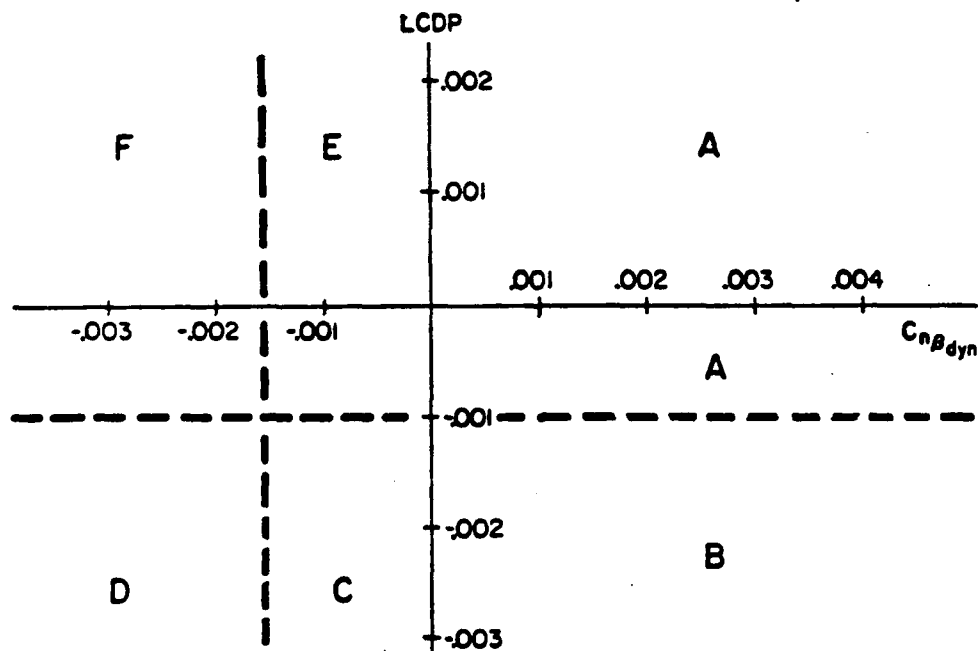


Figure 105. STI Modified Weissman Departure and Spin Susceptibility Criterion (Reference (99))

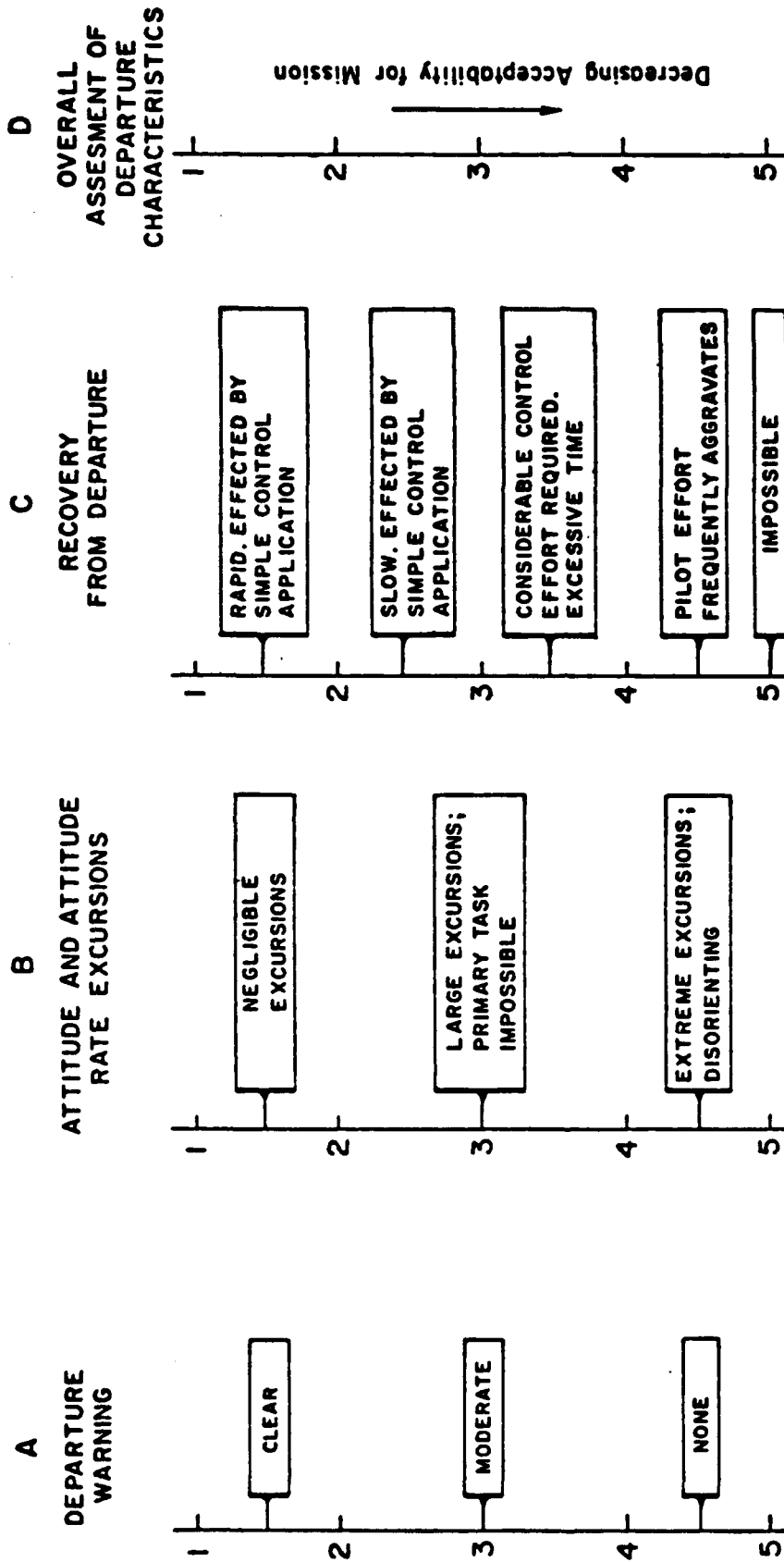
## NADC 88020-60

The STI departure rating scale developed is shown in figure 106. The rating scale is used to solicit quantitative pilot ratings on a scale of 1 to 5 for five individual aircraft departure/recovery attributes and one overall rating based upon the acceptability of the aircraft flying qualities at high angles-of-attack. The scale is designed such that the first two scales address rating the aircraft's departure attributes while the remaining three address rating recovery characteristics. Ratings for the departure attributes are separated into evaluating the departure warning onset (in terms of clarity or lack of warning) and then the severity of the departure/post departure attitude and altitude rate excursions.

The three scales that are designed to evaluate aircraft recovery characteristics separately address, (1) the complexity of recovery control application necessary to effect successful recovery, (2) the importance of control application timing (to include initial control inputs as well as control release), and (3) the amount of time required for recovery.

In summarizing their experience with the use of the departure rating scale, STI found that the pilots accepted and supported its use. In addition, based upon the small statistical sample, they found the numerical ratings given by the pilots were reflective of characteristics "designed into" the vehicle configurations evaluated (Reference (98)). STI notes that aspects of the simulation pertaining to recovery are not necessarily significant because the simulation was not considered valid for simulating spins and spin recovery.

The authors of reference (98) stress that since vehicle attributes were rated, rather than a task performance level, that use of the rating scales must be accompanied by a qualitative assessment/description by the pilot. The qualitative information given in figure 107 is recommended by STI as a minimum framework for soliciting pilot narrative comments to qualify their ratings.



- Describe warning
- Did warning interfere with primary task? If so, to what extent?
- Describe departure sequence
  1. Nose slice
  2. Wing rock
  3. Rolling departure
  4. Pitch up
- What was primary departure variable? ( $\theta, \dot{\theta}, \psi, \dot{\psi}, \phi, \dot{\phi}$ )
- Was altitude loss primarily due to a path divergence or to attitude excursions?
- Fighter
- Trainer

Figure 106. STI Departure Rating Scale (Reference (98))

- **Warning**
  - Type
  - Clarity
  - Margin
- **Departure**
  - Resistance (susceptibility)
  - Type
  - Severity
  - Ability of pilot to delay or prevent
    - Control action taken
    - Demands on the pilot
- **Post-Departure Motion**
  - Type of aircraft motion
  - Severity
- **Recovery**
  - Rapidity
  - Recovery controls
  - Demands
    - Ability to recognize
    - Ability to perform necessary control action

Figure 107. Qualitative Information Required to Qualify Pilot Departure Ratings (Reference (98))

For their simulation experiment (Reference (98)), STI prepared the "Loss-of-Control/Departure/Recovery" debriefing guide (as given in figure 108) to augment the rating chart. This debriefing guide is used to direct the pilot's attention to the key aspects of the simulated maneuvers. The debriefing guide addresses: (1) loss-of-control warning, (2) departure, (3) post-departure maneuver dynamics and (4) departure recovery and controllability. The debriefing guide is written in a questionnaire format and was designed to encourage simple yes/no, multiple choice, or short written answers. Though most of the questions pertain to characteristics of the aircraft motion, Cooper-Harper Handling Quality Ratings (HQR's) are also requested for the two tasks which involve pilot effort to effect control of the aircraft (i.e., prevent departure and accomplish recovery) (Reference (98)).

After the authors had acquired some experience with the use of the debriefing guide, they concluded that its use was highly desirable for the stall/departure/recovery investigation.<sup>1</sup> The authors did however suggest two changes for revision. They are, (1) provision for more space to accommodate lengthy answers and (2) the pilots preferred to provide an overall assessment (STI rating) based upon the *acceptability* of the flying characteristics at high angle-of-attack instead of an assessment of "hazard" (question V of debriefing guide) which changes with situations (i.e., low vs. high altitude). The final Departure Rating Scale settled upon is shown in figure 109.

---

<sup>1</sup> Since the debriefing guide was developed for inflight as well as simulation, some questions are not appropriate for fixed-based or even some moving-base simulations.

| Loss of Control/Departure/Recovery Debriefing Guide   |  | Date _____    |
|---|--|---------------|
| (answer those questions that are appropriate for the maneuver flown) Circle answers wherever possible.  |  | Pilot _____   |
|   |  | Run No. _____ |
| <p><b>I Loss-of-Control Warning</b></p> <p>a) Is warning clear/unclear/nonexistent? _____ STI: _____</p> <p>b) What is the nature of the warning? (Aircraft motions, vibrations, instrument indications, visual cues, motion cues, control system feel cues) _____</p> <p>c) Is warning masked by some other aircraft characteristic? _____ Y N</p> <p>d) Is the warning such that it allows the aircraft to be flown closer to the limit of the envelope? _____ Y N</p> <p>e) Does the warning interfere with the primary task or reduce mission effectiveness? _____ Y N</p> <p>f) Do the aircraft motions/vibrations constitute a mission hazard worthy of a flight restriction? _____ Y N</p> <p>g) Is the warning so inadequate that a flight restriction would be necessary to prevent loss of control? _____ Y N</p> <p><b>II Departure (See MIL-S-83691 definition and discussion)</b></p> <p>a) Did departure occur? _____ Y N</p> <p>b) What were the aircraft motions? (Wing rock, nose slice, pitch up, rolling departure, divergent oscillations) _____</p> <p>c) What was the severity of the aircraft motion? _____ STI: _____</p> <p style="margin-left: 20px;">Mild - Mild Acceleration cues<br/>Intermediate - Rapid motion or acceleration in one or more axis.<br/>Severe - Very rapid motion or acceleration in one or more axis.</p> <p>1) How large were the changes in aircraft attitude? _____</p> <p>2) How fast were the rates? _____</p> <p>3) How large were the accelerations? _____</p> <p>d) Were the aircraft motions and attitudes recognizable? _____ Y N</p> <p>e) Were the aircraft motions disorienting and/or debilitating? _____ Y N</p> <p>f) According to MIL-S-83691 definitions, how would the resistance/susceptibility to departure be described for this maneuver? _____</p> <p>g) Should pilot action prevent or delay departure? (If no pilot action taken so state) _____ Y N</p> <p>1) What pilot actions were taken? _____</p> <p>2) What were/would be the demands on the pilot to prevent departure? (Refer to Cooper-Harper Scale) _____ CH: _____</p> <p>3) Did pilot actions aggravate departure? _____ Y N</p> <p><b>III Post Departure/Maneuver Dynamics</b></p> <p>a) What were the aircraft motions? _____</p> <p>b) What was the severity of the aircraft motion? _____ STI: _____</p> <p style="margin-left: 20px;">Mild - Mild accelerations and rates<br/>Intermediate - Rapid motion or acceleration in one or more axis.<br/>Severe - Very rapid motion or acceleration in one or more axis.</p> <p>1) Were the changes in aircraft attitude large? _____ Y N</p> <p>2) Were the rates fast? _____ Y N</p> <p>3) Were the accelerations large? _____ Y N</p> <p>c) Were the aircraft motions disorienting and/or debilitating? _____ Y N</p> <p><b>IV Recovery</b></p> <p>a) How rapid was the recovery? _____</p> <p style="margin-left: 20px;">Immediate<br/>Slow - After a period of time, short enough to prevent doubt concerning eventual recovery?<br/>Excessive - After a period of time, short enough to produce serious doubts concerning eventual recovery?</p> <p>b) What recovery controls were used? _____</p> <p>c) Were the recovery control applications: _____</p> <p style="margin-left: 20px;">Simple - One, two, or three actions that do not require pilot practice to be effective.<br/>Natural - Control applications that would be considered normal pilot procedure.<br/>Complicated - More than three actions and/or actions require considerable pilot practice to be effective.<br/>Unnatural - Control applications that are unique to this out-of-control recovery and/or would not be considered normal pilot procedure.<br/>Aggravating - to the out-of-control condition.</p> <p>d) What were the demands on the pilot to accomplish recovery? (Refer to Cooper-Harper Scale where appropriate for words describing demands on pilot. Modify words as necessary considering that this task began with an out-of-control aircraft.) _____ CH: _____</p> <p style="text-align: right;">STI: _____</p> <p style="text-align: right;">_____</p> <p><b>V Overall Hazard</b>      Fighter _____      Trainer _____</p> |  |               |

Figure 108. STI Loss of Control/Departure/Recovery Debriefing Guide (Reference (98))

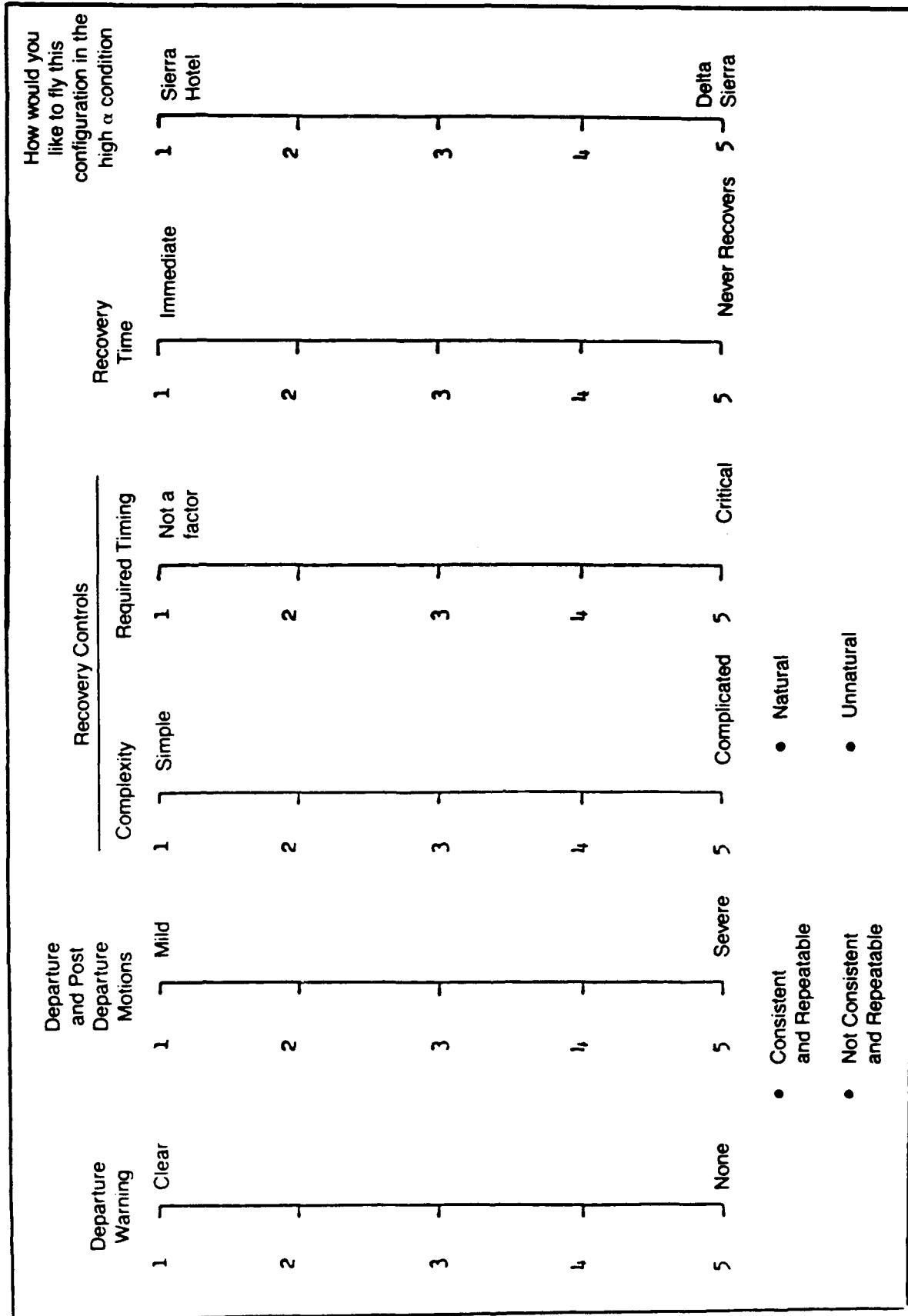


Figure 109. Revised STI Departure Rating Scale (Reference (98))

#### 4.2.2.2. Investigation of the Bihle and Weissman/STI Criteria using a Total-G Simulator

The Naval Air Development Center (NADC) evaluated both the Bihle and Weissman/STI Departure Susceptibility Criteria (References (100), (109), (110)) using a moving base, total G-environment simulator. To confirm the boundaries defined by the two criterion, references 105 and 112 proposed integrating the Bihle departure/roll reversal boundaries ( $C_{l_{\beta}}$  vs.  $C_{n_{\beta}}$ ) into the departure criterion plane developed by Weissman and STI ( $C_{n_{\beta DYN}}$  vs. LCDP). As described earlier, the Bihle Criteria was developed using generic variations of directional stability ( $C_{n_{\beta}}$ ) and dihedral effect ( $C_{l_{\beta}}$ ) for three specific values of the lateral control derivative ratio given by,  $C_{n_{\delta_a}}/C_{l_{\delta_a}}$  (note, lateral control effectiveness  $C_{l_{\delta_a}}$  was held constant at a value approximating typical fighter aircraft while  $C_{n_{\delta_a}}$  was varied to obtain  $C_{n_{\delta_a}}/C_{l_{\delta_a}}$  ratios of 1, 0, and -1.0). Utilizing a six degree-of-freedom computer simulation, a large deflection lateral control input at high angle-of-attack was used to analytically determine both roll reversal and departure characteristics (see figure 99).

Similar to the Bihle Departure Criterion, the Weissman/STI Departure Criterion also attempts to measure aircraft departure susceptibility. The Weissman/STI Criterion is based on the "dynamic" directional stability parameter  $C_{n_{\beta DYN}}$  and the lateral directional stability parameter, LCDP, which are derived from the linearization of the simplified (no dynamic derivatives modelled) lateral/directional equations of motion.

The equations relating  $C_{n_{\beta DYN}}$  and LCDP to the three primary static aerodynamic stability and control derivatives ( $C_{n_{\beta}}$ ,  $C_{l_{\beta}}$ ,  $C_{l_{\delta_a}}$ ) varied by Bihle are given below in equations (37) through (40).

$$C_{n_{\beta DYN}} = C_{n_{\beta}} \cos \alpha - \left( \frac{l_z}{l_x} \right) C_{l_{\beta}} \sin \alpha \quad \text{EQ (37)}$$

$$\text{LCDP} = C_{n_{\beta}} - C_{l_{\beta}} \frac{C_{n_{\delta_a}}}{C_{l_{\delta_a}}} \quad (l_{xz} = 0) \quad \text{EQ (38)}$$

where:

$$C'_{n\beta} = \frac{C_{n\beta} + I_{xz}^2 / I_x C_{l\beta}}{\left[ 1 - I_{xz} / I_x I_z \right]} \quad \text{EQ (39)}$$

$$C'_{l\beta} = \frac{C_{l\beta} + I_{xz} / I_x C_{n\beta}}{\left[ 1 - I_{xz}^2 / I_x I_z \right]} \quad \text{EQ (40)}$$

From the above equations, it is apparent that the Bihle data ( $C_{l\beta}$  VS.  $C_{n\beta}$ ) can be transformed into the Weissman parameters under the assumption that the boundaries defined using Bihle's highly nonlinear maneuver can be interpreted consistently within the contents of the Weissman parameters ( $C_{n_{BDYN}}$  and LCDP) derived from the linearized symmetric flight equations of motion.

Utilizing equation (41) and (42) the Bihle departure boundaries were transformed onto the Weissman/STI Criterion Plane for an F-14A aircraft ( $I_z/I_x = 4.3$ ;  $I_{xz} = 0$ ;  $\alpha_{C_{LMAX}} = 35$  degrees).

$$C_{n_{BDYN}} = C_{n\beta} \cos(35^\circ) - 4.3 C_{l\beta} \sin(35^\circ) \quad \text{EQ (41)}$$

$$\text{LCDP} = C_{n\beta} - C_{l\beta} C_{n_{h_a}} / C_{l_{h_a}} \quad \text{EQ (42)}$$

When this transformation is completed, the integrated criterion plane of figure 110 results. (Most conservative case shown only — Neutral  $C_{n_{h_a}}$ ).

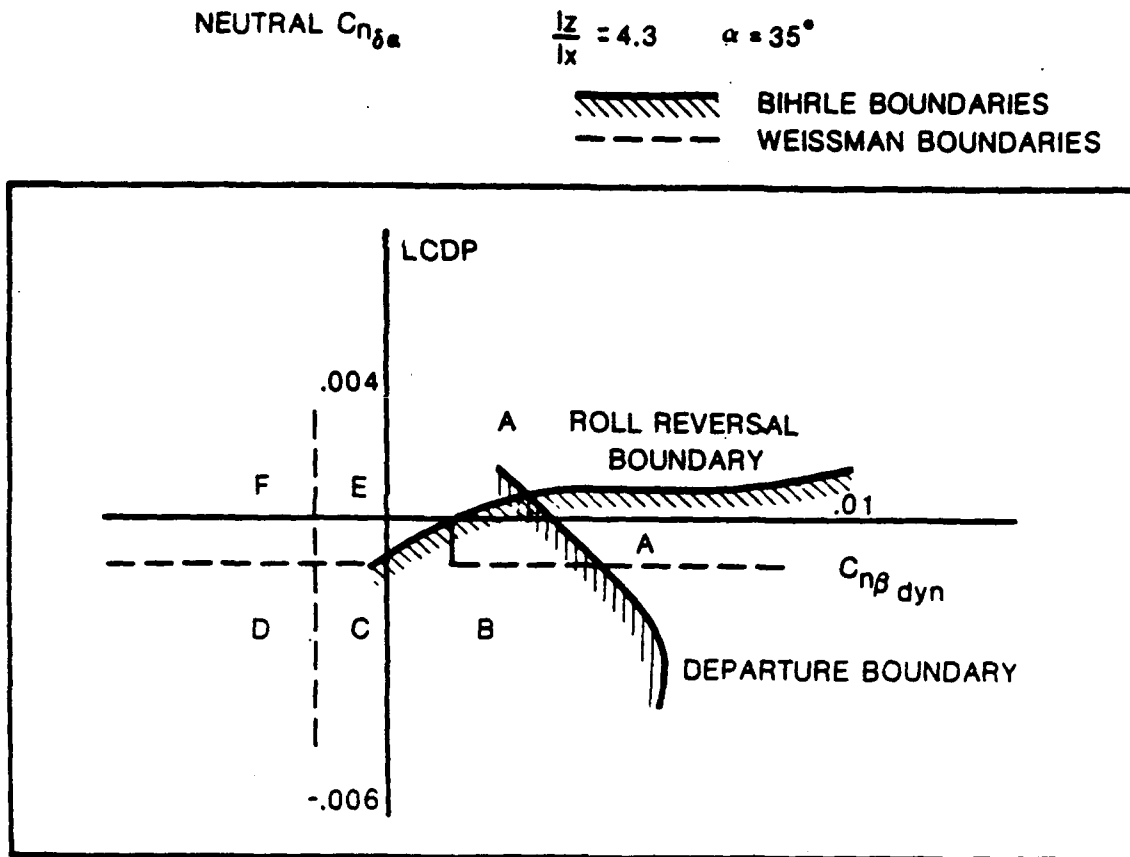


Figure 110. Integrated Bihrlé/Weissman-STI F-14A Departure Susceptibility Criterion Plane (Reference (102))

As reference 106 points out, it can now be seen that Bihrlé's roll reversal boundaries approximately correspond to the  $LCDP = 0$  axis ( $LCDP < 0$  is often used as a boundary to define lateral-directional departures) and Bihrlé's departure boundaries roughly approximate Weissman's region A/B boundary for  $C_{n\beta_{DYN}}$  values between 0.004 and 0.008<sup>1</sup>. On this basis the evaluation/validation of the two departure criteria combined was pursued utilizing the NADC Dynamic Flight Simulator (DFS) facility. (References (102) and (109) may be consulted for detailed descriptions of the simulation facility, experimental design, and the general operations of the piloted simulation conducted.)

<sup>1</sup> Note that the transformation of the Bihrlé departure boundaries to the Weissman/STI plane to define the new A/B boundary is a function of the inertia ratio  $I_z/I_x$ , and the maximum trim angle-of-attack. These parameters would have to be normalized to make the criterion applicable to all aircraft.

Two types of experimental configurations were developed to investigate the "NADC Departure Criteria" plane boundaries. The first set of configurations involved varying values of  $C_{n_{\text{POYN}}}$  and LCDP at angles-of-attack greater than 20 degrees. The second set provided varying values of  $C_{n_{\text{POYN}}}$  and LCDP with angle-of-attack, but attempted to stay within a particular region of the criterion plane (Reference (102)).

The pilots were asked to rate various aspects of the aircraft's response via the departure rating chart and questionnaire developed by STI (see figures 108 and 109). The analysis of the departure pilot ratings (STI Departure Rating Chart) assigned during the evaluations, cross checked with the qualitative comments of the pilots, led to the following results (excerpted from reference (109)):

1. Comparison of Static and Dynamic Simulations

- a. Pilot comments indicate they liked the moving-base portion of the experiment. They felt there were better motion cues and hence a better warning for departure dynamically than statically. Motions seemed more violent dynamically, and recoveries were more realistic. Recovery ratings were down-rated accordingly during dynamic operations.
- b. While it was possible to compare pilot opinion of dynamic versus static runs qualitatively, it was difficult to correlate numerical ratings. Numerical ratings were inconsistent from run-to-run and from pilot-to-pilot, even though comments were consistent.

2. Boundary and Region Correlation

- a. Figure 111 shows the average ratings for selected configurations. The averages are of the overall ratings from the STI scale (the last column only). Pilots experienced no real departures and solid stalls in Region A. While flying in Region B, they suffered only roll reversals and no spins. As soon as a pilot crossed into Region C, however, departures and some spins were unavoidable. Flight into Region D meant violent departures and spins. Lastly, configurations whose stability derivatives mapped into Regions E and F were downgraded because of directional divergences.

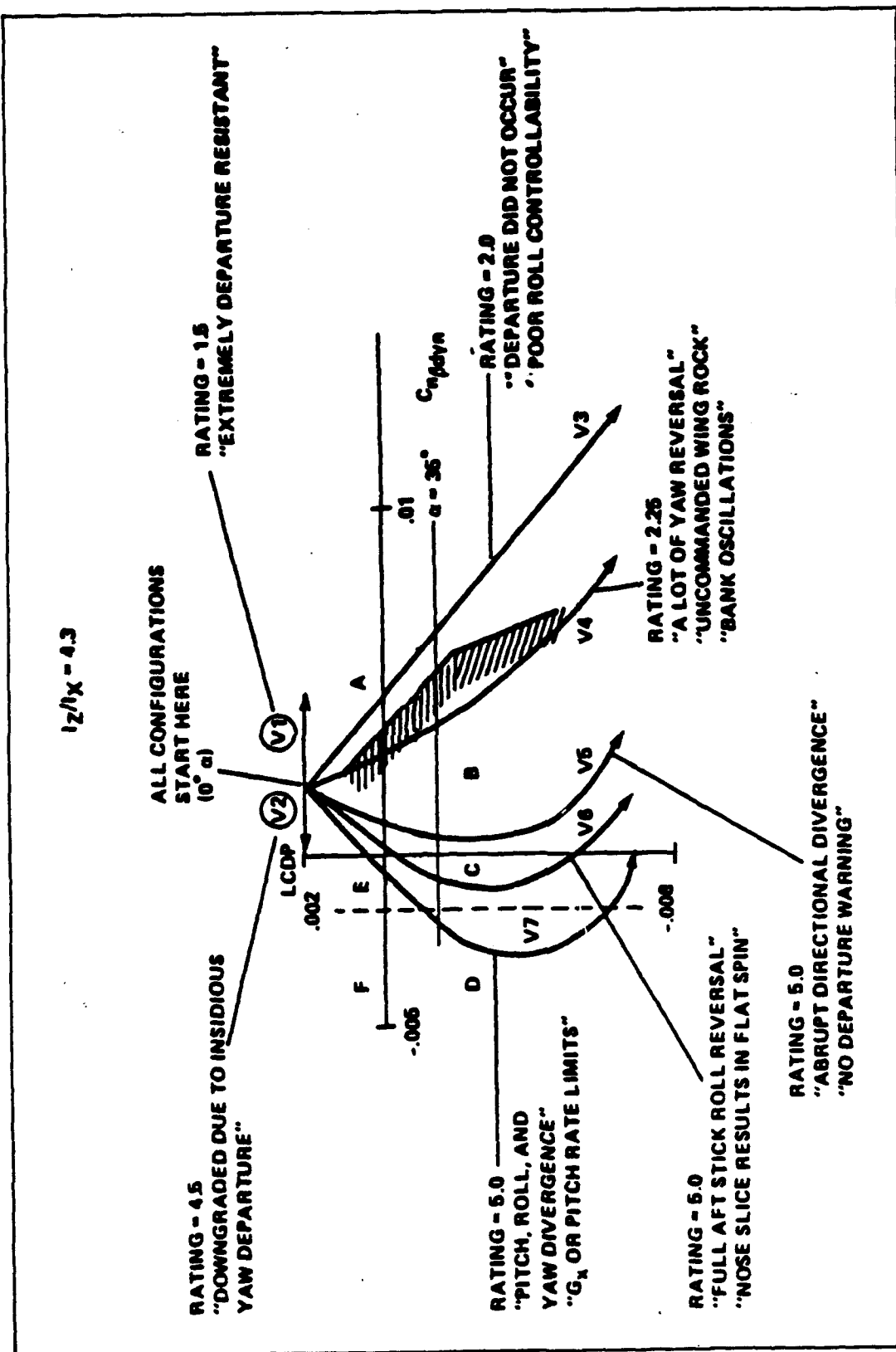


Figure 111. Departure Susceptibility Integration Criterion Boundary Correlation (Avg. Ratings) (Reference (109))

- b. In general, pilot technique and aircraft mission (fighter or trainer) had a lot to do with ratings in Region B. The closer to Region C and the more aggravated the maneuvering required, the worse the rating. Also, strong adverse yaw overrode other characteristics. On the other hand, proverse yaw gave a configuration more favorable ratings. A future experiment could study an adverse yaw in Region A and a proverse yaw in a critical region, C for example, to predict with greater confidence the effect of  $C_{n\delta_a}$ .
- c. As predicted, variation of the inertia parameters, inertia ratio  $I_x$  and  $I_{xz}$ , alone had little effect on the characteristics of a configuration. The negligible effect of  $I_{xz}$ , was evidenced by pilot EE's V10' - V13' runs. This agrees with offline algebraic calculations of  $C_{n\delta_{DOWN}}$  which suggest that even unusually large values of  $I_{xz}$  will not have a significant effect.

### 3. Application of STI Departure Rating Scale

- a. The STI scale had numerous problems which affected rating. Comments were consistent and repeatable, but numerical ratings differed from run to run and from pilot to pilot. In some cases with no departure, pilots rated the warning a 5. The pilot reasoned that warning was nonexistent if there was no departure, hence a 5. However, for similar circumstances, other pilots would rate the warning characteristic a 1 or a "N/A" for "not applicable." Performance, mainly in the form of responsiveness, interfered with departure acceptability. Overall ratings were masked by sluggish conventional handling qualities for safe departure configurations.
- b. Figure 113a shows a recommended departure rating scale. One of the major revisions in the proposed scale is the departure/no departure cutoff. The pilot is immediately asked if he experienced a departure. If he did not, "warning", "motions", "recovery controls", and "time to recover" are all rated "0". However, if the aircraft departed, a rating between 1 and 5 is given.

In either case, the last two new columns are answered.



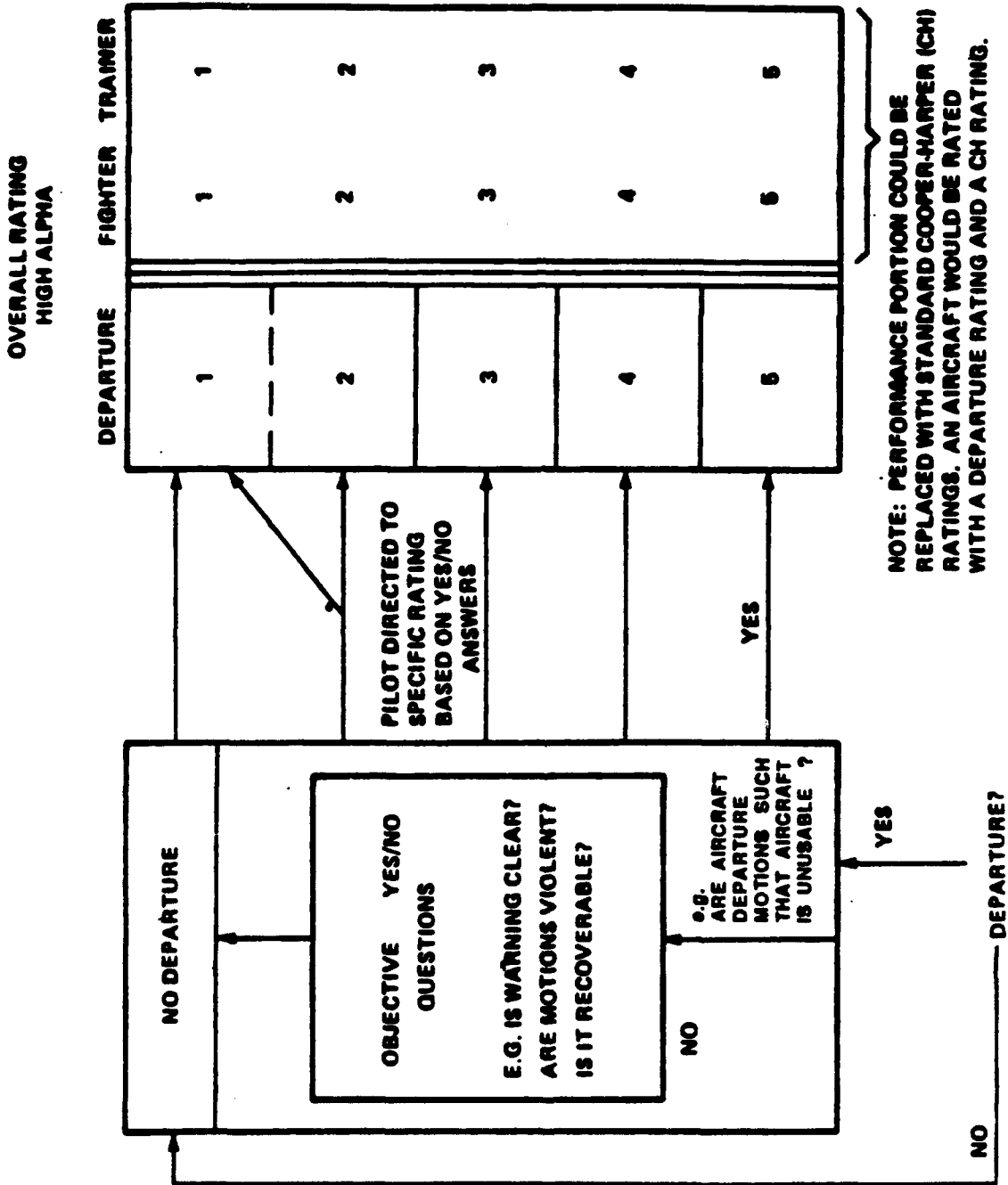


Figure 112(b). NADC Proposed "Cooper-Harper Like" Departure Rating Scale (Reference (109))

- c. Another major revision in the proposed scale is that aircraft departure and performance characteristics are rated by the pilot separately; a sluggish, departure resistant aircraft can be rated a 1 for departure overall and a 3 or 4 as a fighter for slow response time, for example. Also, an attempt has been made at putting more objectives into the scale to help a pilot pinpoint a specific rating.
- d. The natural outgrowth of these modifications was to formulate what can become a Cooper/Harper-like scale (see figure 112(b)). Only objective questions would be asked of the pilot. Using a decision tree, he would be locked into a departure rating. More research is needed to refine such a scale.

#### 4.2.3 Kalviste Departure Susceptibility Criterion.

The Kalviste Departure Criteria extends the static stability analysis approach used to derive  $C_{n_{\text{PDYN}}}$  to include the coupling between the longitudinal and lateral-directional modes of motion and the use of nonlinear aerodynamics. Kalviste's model of an aircraft's high angle-of-attack aerodynamics does not assume (or is limited to) linear variations of the aerodynamic data with sideslip angle,  $\beta$ . Using this approach the stability parameters become a function of both angle-of-attack and sideslip angle. This approach to predicting aircraft departure addresses asymmetric flight (i.e., non-zero sideslip angle) and the often severe aerodynamic nonlinearities that are known to be dominant in the high angle-of-attack flight regime. This is a very important extension of the theory.

Similar to the development of the  $C_{n_{\text{PDYN}}}$  criterion, Kalviste's approach is based on the fact that for an aircraft to be stable in any attitude, it must possess rotational stability. Kalviste has defined three stability parameters, ( $C_{n_{\beta_{\text{cop}}}}$ ,  $C_{m_{\alpha_{\text{cop}}}}$  and  $K$  — where the "cop" subscript indicates that these parameters are derived from the coupled equations of motion) which are used to predict aircraft departure tendencies based on the static rotational characteristics of the aircraft.

A full discussion on the development of Kalviste's Coupled Parameter Departure Criteria has not been included in this work. Instead an abbreviated discussion of Kalviste's development of the criteria is presented in figure 113 in outline format. This synopsis is based on Kalviste's work given by references (111)-(113).

# I. KALVISTE DEPARTURE CRITERIA: MOTIVATION

- A. Stability characteristics of an aircraft are determined by solving the nine nonlinear six degree-of-freedom equations of motion that describe the motion of an aircraft. These equations are given below as they are conventionally written using a body axes coordinate system (see reference (48)).

Aircraft 6 DOF Equations of Motion (Reference (114))

## 1. Force and Moment Equations

$$\dot{u} = \frac{X}{m} + rv - qw - g \sin \theta$$

$$\dot{v} = \frac{Y}{m} + pw - ru + g \cos \theta \sin \phi$$

$$\dot{w} = \frac{Z}{m} + qu - pv + g \cos \theta \cos \phi$$

$$\dot{p} = \frac{I_z}{I_x I_z - I_{xz}} \left[ L + \frac{I_{xz}}{I_z} (N - qr I_{xz}) - qr (I_z - I_y) + pq I_{xz} \left( 1 - \frac{I_y - I_x}{I_z} \right) \right]$$

$$\dot{q} = \frac{I}{I_y} \left[ M - I_{xz} (p^2 - r^2) - rp (I_x - I_z) \right]$$

$$\dot{r} = \frac{I_x}{I_x I_z - I_{xz}} \left[ N + \frac{I_{xz}}{I_x} (L - pq I_{xz}) - pq (I_y - I_x) - qr I_{xz} \left( 1 - \frac{I_z - I_y}{I_x} \right) \right]$$

## 2. Kinematic Equations

$$\dot{\psi} = (q \sin \phi + r \cos \phi) \sec \theta$$

$$\dot{\theta} = q \cos \phi - r \sin \phi$$

$$\dot{\phi} = p + q \sin \phi \tan \theta + r \cos \phi \tan \theta$$

Because of the nonlinearity of the equations of motion their solution is possible only through numerical or analog integration.

Figure 113. Development of the Kalviste Coupled Parameters/Criterion

- B. As reference (115) points out, the solution of these nine equations of motion can be accomplished by perturbation analysis techniques or time history solutions, but with either method it is difficult to isolate the parameters which cause instability. To circumvent this problem conventional stability analysis techniques typically assume a nominal steady state flight condition (i.e., symmetric flight ( $V_o = 0$ ;  $\phi_o = 0$ ) with no angular velocity ( $p_o = q_o = r_o = 0$ ), such that the equations can be simplified and separated into longitudinal ( $u, w, q, \theta$ ) and lateral directional ( $v, p, r, \phi$ ) modes of motion. This analysis technique applies for most airplane motions of practical interest at low-to-moderate angles-of-attack where the assumption that there are no coupling terms ( $L_a, M_p$ , etc.) in the aerodynamic force and moment terms is well documented.
- C. In contrast to the low-to-moderate angle-of-attack flight regime, at high angles-of-attack the coupling between the longitudinal and lateral directional aerodynamic force and moment terms has been documented to be significant (references (33) and (64)). For this reason Kalviste's approach *does not* make use of decoupling the aircraft equations of motion into longitudinal and lateral/directional subsets before analyzing the stability of the aircraft.
- D. Instead of simplifying the analysis of the 6 DOF equations of motion by decoupling the aircraft longitudinal and lateral-directional modes, Kalviste approaches the problem by analyzing the aircraft rotational motion relative to the flight path.

## II. EQUATIONS OF MOTION

- A. Define a new axis system referred to as, "Dynamic Stability Axis" system defined by a system of three angles given by,

- $\alpha$  = Angle-of-attack  
 $\beta$  = Sideslip angle  
 $\mu$  = Aircraft roll angle about the velocity vector

The sequence of rotation from the velocity vector to the aircraft coordinates is  $\mu - \beta - \alpha$ . See the figure below.

### Dynamic Stability Axes System

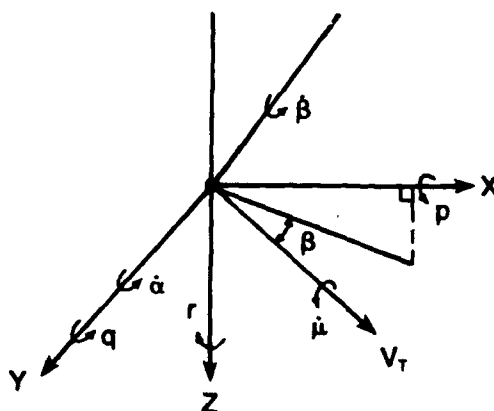


Figure 113 (Cont'd). Development of the Kalviste Coupled Parameters/Criterion

1. This spherical axis system is chosen such that the translational equations of motion that describe the accelerations ( $\dot{u}$ ,  $\dot{v}$ ,  $\dot{w}$ ) along the aircraft body axes,  $x$ ,  $y$ ,  $z$  can be expressed in terms of  $\alpha$ ,  $\beta$  and  $V_T$ . This is done because aerodynamic forces and moments are typically determined in terms of angle-of-attack,  $\alpha$ , sideslip angles,  $\beta$ , and Mach number rather than the velocity components along the body axes,  $v$ ,  $v$ ,  $w$ .
2. Using spherical coordinates, the nine equation-of-motion used to determine aircraft stability are given by the equations given below (Reference (112)).

Aircraft Six-Degree-of-Freedom Equations of Motion For Stability Analysis

$$\dot{P} = \frac{1}{I_{xx}} \left[ (\dot{Q} - PR) I_{xy} + (\dot{R} + PQ) I_{xz} + QR (I_{yy} - I_{zz}) + (Q^2 - R^2) I_{yz} \right] + \mathcal{L}$$

$$\dot{Q} = \frac{1}{I_{yy}} \left[ (\dot{R} - PQ) I_{yz} + (\dot{P} + QR) I_{xy} + PR (I_{zz} - I_{xx}) + (R^2 - P^2) I_{xz} \right] + \mathcal{M}$$

$$\dot{R} = \frac{1}{I_{zz}} \left[ (\dot{P} - QR) I_{xz} + (\dot{Q} + PR) I_{yz} + PQ (I_{xx} - I_{yy}) + (P^2 - Q^2) I_{xy} \right] + \mathcal{N}$$

$$\dot{\phi} = P + (Q \sin \phi + R \cos \phi) \tan \theta$$

$$\dot{\theta} = Q \cos \phi - R \sin \phi$$

$$\dot{\alpha} = Q - (P \cos \alpha + R \sin \alpha) \tan \beta - \frac{L}{V_T \cos \beta}$$

$$+ \frac{g}{V_T \cos \beta} (\cos \alpha \cos \theta \cos \phi + \sin \alpha \sin \theta)$$

$$\dot{\beta} = P \sin \alpha - R \cos \alpha + \frac{1}{V_T} (Y \cos \beta + D \sin \beta)$$

$$+ \frac{g}{V_T} [\sin \beta (\cos \alpha \sin \theta - \sin \alpha \cos \theta \cos \phi) + \cos \beta \cos \theta \sin \phi]$$

Figure 113 (Cont'd). Development of the Kalviste Coupled Parameters/Criterion

$$\dot{V}_T = (Y \sin \beta - D \cos \beta) + g [\sin \beta \cos \theta \sin \phi + \cos \beta (\sin \alpha \cos \theta \cos \phi - \cos \alpha \sin \theta)]$$

$$\dot{h} = V_T [\cos \beta (\cos \alpha \sin \theta - \sin \alpha \cos \theta \cos \phi) - \sin \beta \cos \theta \sin \phi]$$

### 3. Equation of Motion Assumptions (Reference (112))

- a. The airframe is assumed rigid
- b. The earth is assumed to be flat and non-rotating in inertial space, in the region of interest, applying a constant vertical acceleration on the aircraft.
- c. The velocity vector is assumed to be inertially fixed (direction assumed to be constant).
- d. The mass and mass distribution of the aircraft is constant.

## III. BASIS OF THE THEORETICAL DEVELOPMENT

- A. The departure characteristics of the aircraft can be *approximated* by the aircraft *rotational motion* relative to the flight path.

(Note: Kalviste supports this approximation from flight test data which indicates that departure is characterized by the aircraft rotation relative to the direction of flight.)

### B. Rotational Stability

1. *Definition:* The aircraft is defined as rotational stable if small disturbances in  $\alpha$  or  $\beta$  about a trimmed condition cause a moment in a direction to reduce the disturbance and the moment due to the rates (P, Q, R) is in the direction to reduce the rates.
2. Necessary but not sufficient condition for rotational stability is that the aircraft possess position (or static) stability (Moments due to attitude).
3. Because a positionally unstable aircraft can not be stabilized (to the initial trim point) with stabilizing moments due to aircraft rates (they can only decrease the rate of instability if they are stable or increase the rate of instability if they are unstable), Kalviste claims that the *important parameters for aircraft rotational stability* are the aerodynamic moments due to the attitude of the aircraft relative to the velocity vector.

Figure 113 (Cont'd). Development of the Kalviste Coupled Parameters/Criterion

IV. ROTATIONAL MOTION OF THE AIRCRAFT

- A. Is defined relative to the velocity vector solely due to the *static* aerodynamic moment terms of equations (II.2) to yield,

$$\left. \begin{aligned} \dot{P} &= \mathcal{L}(\alpha, \beta, \delta) \\ \dot{Q} &= M(\alpha, \beta, \delta) \\ \dot{R} &= N(\alpha, \beta, \delta) \end{aligned} \right\} \begin{array}{l} \text{zero rotational rate} \\ \text{condition about the} \\ \text{principal axis system} \end{array}$$

- B. Relationship of the angular rates in the dynamic axis system to the aircraft body axis system are given from II.A. as,

$$\begin{aligned} \dot{\mu} &= (P \cos \alpha + R \sin \alpha) \sec \beta \\ \dot{\alpha} &= Q - (P \cos \alpha + R \sin \alpha) \tan \beta \\ \dot{\beta} &= P \sin \alpha - R \cos \alpha \end{aligned}$$

Note, these equations are functions of aircraft rotational rates only since it was assumed that the direction of the velocity vector is constant.

- C. Rotational Stability is determined from the  $\alpha$  and  $\beta$  equations. Differentiating the  $\alpha$  and  $\beta$  equations above yields,

$$\begin{aligned} \ddot{\alpha} &= \dot{Q} - (\dot{P} \cos \alpha + \dot{R} \sin \alpha) \tan \beta \\ &\quad - \left[ (-P \sin \alpha + R \cos \alpha) \tan \beta \right] \dot{\alpha} \\ &\quad - \left[ P \cos \alpha + R \sin \alpha \right] \sec^2 \beta \dot{\beta} \\ \ddot{\beta} &= \dot{P} \sin \alpha - \dot{R} \cos \alpha + (P \cos \alpha + R \sin \alpha) \dot{\alpha} \end{aligned}$$

- D. Similar to IV.A., dynamic coupling terms are assumed equal to zero. The equations of IV.C. thus reduce to,

$$\begin{aligned} \ddot{\alpha} &= \dot{Q} - (\dot{P} \cos \alpha + \dot{R} \sin \alpha) \tan \beta \\ \ddot{\beta} &= \dot{P} \sin \alpha - \dot{R} \cos \alpha \end{aligned}$$

- E. Substituting the P, Q, R equations (IV.A.) into the  $\ddot{\alpha}$ ,  $\ddot{\beta}$  equations (IV.D.) yields the new stability parameters defined by  $\mathcal{L}_{\text{DYN}}$ ,  $M_{\text{DYN}}$  and  $N_{\text{DYN}}$  as given below.

$$\begin{aligned} \mathcal{L}_{\text{DYN}} &\equiv \dot{\mu} = (\mathcal{L} \cos \alpha + N \sin \alpha) \sec \beta \\ M_{\text{DYN}} &\equiv \ddot{\alpha} = M - (\mathcal{L} \cos \alpha + N \sin \alpha) \tan \beta \\ -N_{\text{DYN}} &\equiv \ddot{\beta} = - (N \cos \alpha - \mathcal{L} \sin \alpha) \end{aligned}$$

Figure 113 (Cont'd). Development of the Kalviste Coupled Parameters/Criterion

where:

$\mathcal{L}_{DYN}$  — is the rolling acceleration about the velocity vector

$M_{DYN}$  — is the pitching acceleration which causes a change in angle-of-attack,  $\alpha$ .

$-N_{DYN}$  — is the yawing acceleration which causes a change in sideslip angle,  $\beta$ .

**Note**, Kalviste's use of the subscript (DYN) denotes that the motion is about the "dynamic stability axes, as previously defined. It is also consistent with the previously discussed departure parameter  $C_{n\beta_{DYN}}$ .

## V. Determination of System Stability

A. The stability criteria is developed in terms of the four dynamic stability derivatives,  $M_{a_{DYN}}$ ,  $M_{\beta_{DYN}}$ ,  $N_{a_{DYN}}$ ,  $N_{\beta_{DYN}}$ , by analyzing the stability characteristics of the rotational motion.

(**Note**, the stability derivatives in the dynamic stability axes are calculated by taking the partial derivatives of  $\mathcal{L}_{DYN}$ ,  $M_{DYN}$ ,  $N_{DYN}$  (at trimmed condition) with respect to  $\alpha$ ,  $\beta$ ,  $\mu$ ,  $\alpha$ ,  $\beta$ ).

B. The stability analysis is based on the linearization of the aircraft rotational equations of motion, relative to the velocity vector, due only to static aerodynamic moments. (Eqs IV.B. & IV.C.).

1. The linearized perturbation equations consider a trimmed flight condition of:

- $\alpha_o$
- $\beta_o$  ( $\beta_o$  may be nozero)
- $\delta_o$
- $P_o = Q_o = R_o = 0$

2. Linearized Rotational Equations of Motion

$$\tilde{P} = \mathcal{L}'_{\alpha} \cdot \tilde{\alpha} + \mathcal{L}'_{\beta} \cdot \tilde{\beta} + \mathcal{L}'_{\delta} \cdot \tilde{\delta}$$

$$\tilde{Q} = M_{\alpha} \cdot \tilde{\alpha} + M_{\beta} \cdot \tilde{\beta} + M_{\delta} \cdot \tilde{\delta}$$

$$\tilde{R} = N_{\alpha} \cdot \tilde{\alpha} + N_{\beta} \cdot \tilde{\beta} + N_{\delta} \cdot \tilde{\delta}$$

$$\tilde{\alpha} = \tilde{Q} - (\cos \alpha_o \tan \beta_o) \cdot \tilde{P} - (\sin \alpha_o \tan \beta_o) \cdot \tilde{R}$$

$$\tilde{\beta} = (\sin \alpha_o) \cdot \tilde{P} - (\cos \alpha_o) \cdot \tilde{R}$$

where:  $(\sim)$  denotes perturbation variables about the steady trimmed condition  $\alpha_o$  and  $\beta_o$ .

Figure 113 (Cont'd). Development of the Kalviste Coupled Parameters/Criterion

Observe that this set of equations differs from the set used to derive the stability parameter  $C_{n_{\beta DYN}}$  in two respects,

1. The aerodynamic cross-coupling terms between the two modes are modelled (i.e.,  $\mathcal{L}_\alpha$ ,  $N_\alpha$  and  $M_\beta$ ).
2. The Kinematic cross-coupling terms are modelled by the  $(\cos \alpha_o \tan \beta_o)$  and  $(\sin \alpha_o \tan \beta_o)$  terms. If the cross-coupling terms are zero then the longitudinal and lateral directional motions are uncoupled.
3. System stability is determined from the characteristic equation,

$$S^4 + As^2 + B = 0$$

derived from the matrix form of the laplaced transform of the above equations (V.2.)

where,

$$A = N_\beta \cos \alpha_o - \mathcal{L}_\beta \sin \alpha_o - M_\alpha + N_\alpha \sin \alpha_o \tan \beta_o + \mathcal{L}_\alpha \cos \alpha_o \tan \beta_o$$

$$B = (N_\alpha M_\beta - N_\beta M_\alpha) \cos \alpha_o + (\mathcal{L}_\beta M_\alpha - \mathcal{L}_\alpha M_\beta) \sin \alpha_o + (\mathcal{L}_\alpha N_\beta - \mathcal{L}_\beta N_\alpha) \tan \beta_o$$

4. Conditions For Stability are:

- a.  $A > 0$
- b.  $B > 0$
- c.  $K = A^2 - 4B > 0$

5. If the characteristic polynomial is defined in terms of the coupled modes,

$$s^4 + As^2 + B = s^2 + N_{\beta cop} s^2 - M_{\alpha cop}$$

Then it can be shown that the aircraft is stable if,

- a.  $K > 0$
  - b.  $N_{\beta cop} > 0$
  - c.  $M_{\alpha cop} < 0$

Kalviste Criteria

where,

$$N_{\beta cop} = 1/2 (A + C \sqrt{A^2 - 4B})$$

$$M_{\alpha cop} = 1/2 (-A + C \sqrt{A^2 - 4B})$$

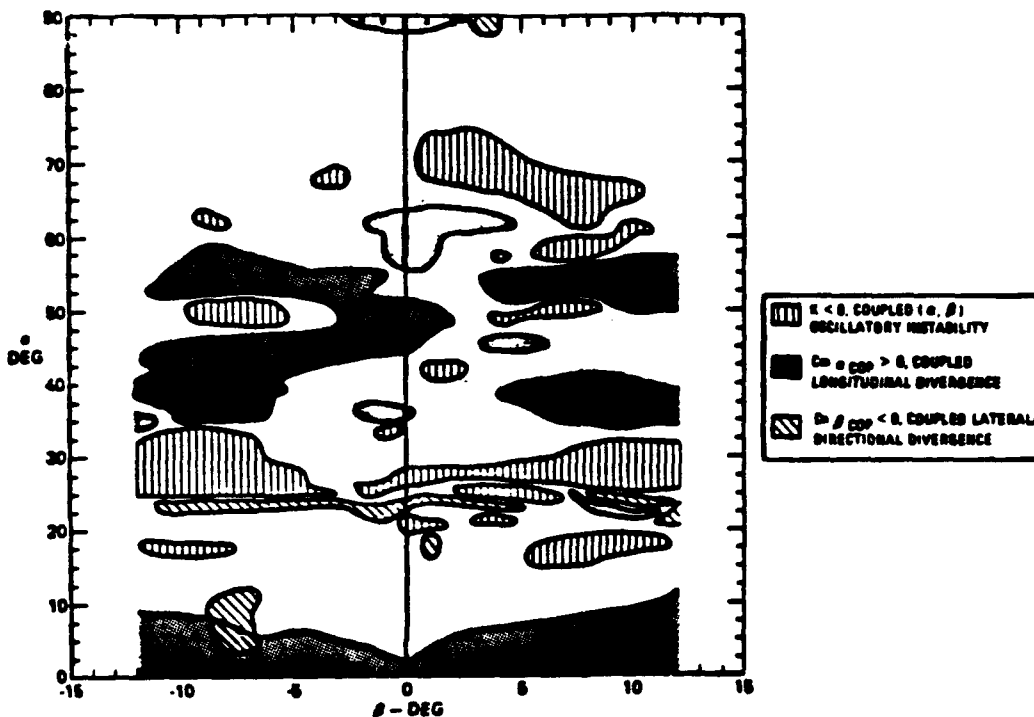
$$C = \begin{cases} 1 & N_{\beta DYN} + M_{\alpha DYN} \geq 0 \\ -1 & N_{\beta DYN} + M_{\alpha DYN} < 0 \end{cases}$$

Figure 113 (Cont'd). Development of the Kalviste Coupled Parameters/Criterion

## VI. Application of The Kalviste Criteria

1. To predict aircraft departure susceptibility, Kalviste makes use of contour mapping techniques (see figure below) to define three regions of aircraft instability as a function of angle-of-attack and sideslip angle. These three regions of instability are,

- a.  $K < 0$  Coupled  $(\alpha, \beta)$  Oscillatory Instability
- b.  $C_{m\alpha_{cop}} > 0$  Coupled longitudinal Divergence
- c.  $C_{n\beta_{cop}} < 0$  Coupled lateral-directional Divergence



Stability Plot for Aircraft Configuration B,  $\delta_H = -18.4^\circ$  (Reference (112))

- 2. If the angle-of-attack and sideslip traces of an aircraft in maneuvering flight pass through regions of instability it indicates that the aircraft will have a *tendency* to depart; it does not necessarily mean the aircraft will depart.
- 3. There are two possible effects of an unstable region on aircraft motion. They are,
  - a. If the unstable region is small it can diverge into a stable region.
  - b. If the unstable region is large, the divergence can cause the aircraft rates to build up into a developed post-stall gyration or spin.

Figure 113 (Cont'd). Development of the Kalviste Coupled Parameters/Criterion

4. By its very nature (inclusion of aerodynamic and Kinematic coupling), it can be seen that the Kalviste Criteria can further improve the departure prediction accuracy over the  $C_{n_{\text{dyn}}}$  parameter in advanced design stages when nonlinear static wind tunnel data is available. As explained in reference (111), this type of analysis is made feasible by the use of digital computer programming and automatic plotting capability. The computer is used to perform nonlinear interpolations of tabular functions of two variables ( $\alpha$ ,  $\beta$ ) that have continuous first derivatives through the  $\alpha$ ,  $\beta$  range. An iteration procedure is then used to compute the contour lines.

Figure 113 (Concluded). Development of the Kalviste Coupled Parameters/Criterion

#### 4.2.4. Other Departure Susceptibility Criterion

Two other departure susceptibility criteria that are proposed in the literature are, (1) the  $\alpha_{-\beta}$  versus  $\alpha_\delta$  criterion originally developed by Jenny of McDonnell Aircraft Company (McAir) (1971) (see Reference (115) and (2)). The more recent McAir effort is reflected in the  $C_{n\beta\text{APPARENT}}$  Departure Criterion (1981) (see reference (116)).

As pointed out in reference (99), the  $\alpha_{-\beta}$  versus  $\alpha_\delta$  departure Criterion is an alternate form of the  $C_{n\beta\text{DYN}}$  and LCDP departure parameters. The  $\alpha_{-\beta}$  versus  $\alpha_\delta$  criteria for departure resistance are,

$$1. \alpha_{-\beta} > 0$$

$$2. \alpha_\delta > \delta_{-\beta}$$

Where the  $\alpha_{-\beta}$  and  $\alpha_\delta$  parameters are defined by equations (43) and (44) respectively.

$$\alpha_{-\beta} = \alpha - \tan^{-1} \left( \frac{C_{n\beta} I_x}{C_{l\beta} I_z} \right) \quad \text{EQ (43)}$$

$$\alpha_\delta = \alpha - \tan^{-1} \left( \frac{C_{n\delta} I_x}{C_{l\delta} I_z} \right) \quad \text{EQ (44)}$$

The first criterion given above,  $\alpha_{-\beta} > 0$  implies that  $C_{n\beta\text{DYN}} > 0$  while the second criterion,  $\alpha_\delta > \alpha_{-\beta}$  implies that  $\text{LCDP} > 0$ . In concurrence with reference (98), a short coming of this criterion is that it does not provide any correlation to the type or degree of instability that might occur. In this respect the  $C_{n\beta\text{DYN}}$  and LCDP parameters as related in the Weissman/STI plot would appear to be more useful.

The  $C_{n\beta\text{APPARENT}}$  Criterion is an attempt to modify the open-loop  $C_{n\beta\text{DYN}}$  departure parameter to include the effects of control deflections and nonlinear aerodynamic data with respect to sideslip angle. The expression that defines  $C_{n\beta\text{APPARENT}}$  is given below in equation (45) as taken from reference (116).

$$C_{n\beta\text{APPARENT}} = \left( \frac{C_n(\beta) + C_n(\delta)}{\beta} \right) \cos \alpha + \frac{I_z}{I_x} \left( \frac{C_l(\beta) + C_l(\delta)}{\beta} \right) \sin \alpha \quad \text{EQ (45)}$$

Where,

$C_n(\beta)$ ,  $C_l(\beta)$  are the moment coefficients as a function of  $\beta$  at a given angle-of-attack for the basic airframe with lateral and directional controls fixed.

$C_n(\delta)$ ,  $C_l(\delta)$  are the moment coefficients produced by one or more control surfaces.

The criterion for departure resistance using the  $C_{n\beta\text{APPARENT}}$  parameter is that  $C_{n\beta\text{APPARENT}}$  be positive. This criterion is similar to each of the previous presented criteria in that it is based purely on statics. Reference (116) contains a detailed description of McAir's success with the utilization of this criterion in the development of the F/A-18 aircraft control laws to assess departure susceptibility.

#### 4.2.5. Summary of Departure Susceptibility Parameters/Criteria

Correlation of the departure susceptibility criteria described in this section (Bihrie Departure and Roll Reversal Boundaries, Jenny's  $\beta$  plus  $\delta$  Axis Stability Indicator, Weissman,  $C_{n\beta\text{DYN}}$  versus LCDP Criterion and Kalviste's Coupling Parameter Criterion) with simulation and in-flight data was addressed by reference (99). The authors of reference 99, Johnston and Heffley, concluded that collectively these various open- and closed-loop parameters present a fairly accurate picture of the high angle-of-attack lateral/longitudinal stability and controllability of the class IV aircraft they examined (i.e., F-4J, A-7, F-14A and F-18A). Johnston and Heffley note that the results (obviously) are highly dependent upon the accuracy of the static aerodynamic coefficients available and how the data is employed.

## NADC 88020-60

Based on assessments for each of the four fighter/attack aircraft examined and comparisons across aircraft, the parameters/criterion of figure 114 were determined to be the more useful in predicting high angle-of-attack stability and controllability characteristics and in directing attention to the important aerodynamic and inertia properties (reference (99)).

| Parameter   | Predicted High-AOA Stability and Controllability Characteristics                 |
|---|--|
| $C_{n_{\text{BDYN}}}$   | Open-loop departure susceptibility   |
| $C_{n_{\text{pcop}}}, C_{m_{\text{acop}}}$  | Open-loop adverse lateral-directional longitudinal coupling in asymmetric flight |
| LCDP  | Closed-loop roll reversal susceptibility   |
| $1/T_{\phi_1}$  | Closed-loop departure susceptibility   |
| <p><i>Criterion:</i> "The empirically derived <math>C_{n_{\text{BDYN}}}</math> vs LCDP Criterion was found to predict the general departure susceptibility of all four aircraft "quite well."</p> |  |

Figure 114. Summary of High-AOA Stability and Controllability Parameters/Criteria (Reference (99)).

## 5.0 CONCLUSIONS

The desire of modern military aircraft to be capable of maneuvering at relatively high angles-of-attack and therefore subjected to conditions where the flow becomes highly asymmetric, has added significant complexity to the understanding of the flight dynamics of the aircraft and the determination of viable criteria for defining "good" flying qualities in this flight regime. In addition to flying at relatively high angles-of-attack and non-zero sideslip angles, military fighter aircraft are characterized by long slender forebodies and sharp leading-edge swept wings particularly conducive to complex flows at higher angles-of-attack. These flight conditions and aircraft configurations induce flow phenomena such as flow separation, vortex shedding, vortex bursts, etc. which are highly nonlinear and strongly affect the static and dynamic aircraft parameters. Thus, the development of high angle-of-attack flying qualities must begin with an understanding of the aerodynamic model that describes the aircraft motion most accurately (within the scope of engineering practicality).

To gain a satisfactory understanding of the flight dynamics of an aircraft exposed to the complex flows just described, a thorough review of high angle-of-attack aerodynamics was presented and included the stall (definition, causes, and methods of control), pitch-up, deep-stall, and the spin (definition, causes, dynamics of the spin, and spin recovery).

A review of the established methods for predicting departure from controlled flight was discussed next. These methods included wind tunnel and analytical techniques in addition to piloted simulations, dynamic flight testing and full-scale flight testing. Each of these testing methods contributes different "ingredients" of knowledge necessary to understand the high angle-of-attack characteristics of a particular aircraft. In some cases a particular test's value lies in its use for application early in the design phase. In other cases the value of a test takes on added significance when addressing specific flight regimes. One example of this is the importance of rotary balance data to more accurately math model the dynamics of a steady spin.

The discussions of high angle-of-attack data revealed by wind tunnel testing has proven the existence of significant static and dynamic cross-coupling effects between the lateral-directional and longitudinal degrees-of-freedom. The implication of this fact is that the equations of motion must be considered simultaneously and not in two separate groups as often done in more linear flight regimes. Further complexity is introduced into establishing an accurate high angle-of-attack math model in cases where aggressive dynamic maneuvering invalidates the application of linear theory and the use of stability derivatives to model the aircraft motion. Also well documented is the existence of non-zero aerodynamic moments ( $C_n$  and  $C_l$ ) at zero sideslip conditions for fighter aircraft at high angles-of-attack. This phenomenon was once thought to be a byproduct of the wind tunnel or model (i.e., would not be realized in actual full-scale flight). Today, however, this phenomenon is attributed to the asymmetrical shedding of vortices from the long forebodies typical of modern fighter aircraft.

A review of the major military specifications concerned with providing requirements and guidelines for high angle-of-attack flight was given with an emphasis on the specifications intended use. The specifications reviewed include, MIL-F-8785C, "Flying Qualities of Piloted Airplanes," MIL-STD-1797, "Military Standard Flying Qualities of piloted vehicles," and MIL-D-8708B and MIL-S-83691A, "High Angle-of Attack Flight Test Demonstration Requirements and Procedures." The status of high angle-of-attack flying qualities criteria and specifications to date is still primarily qualitative in nature. The major shift in the design guidelines provided by MIL-F-8785C's revision, MIL-STD-1797, is that aircraft be "resistant" rather than "extremely resistant" to departure to ease airframe design constraints and control system complexity. Much, if not all, of the high angle-of-attack flying qualities criteria that has been developed over the last decade has focused on predicting regions (chiefly as a function of angle-of-attack) of aircraft departure susceptibility. In general, the research efforts concentrated in this area have produced departure susceptibility criteria that are based on an aircraft's static aerodynamics ( $C_{l_\beta}$ ,  $C_{n_\beta}$  chiefly), control effectiveness ( $C_{l_\delta}$ ,  $C_{n_\delta}$ ) and inertial properties. The Weissman/STI departure susceptibility criterion correlates regions of departure on a parameter plane of  $C_{n_{PDYN}}$  versus LCDP. The departure parameters, LCDP and  $C_{n_{PDYN}}$  are derived from the uncoupled, lateral/directional, linearized

equations of motion. Other forms of this criterion are also found in the literature such as the  $\alpha - \beta$  versus  $\alpha_\delta$  departure criterion (Jenny). The  $C_{n_{\text{APPARENT}}}$  criterion is an attempt to modify the open-loop  $C_{n_{\text{DYN}}}$  departure parameter to include the effects of control deflections and nonlinear aerodynamic data with respect to sideslip angle. Both the  $\alpha - \beta$  versus  $\alpha_\delta$  departure criterion and the  $C_{n_{\text{APPARENT}}}$  departure criterion do not delineate regions (or levels) of departure as the Weissman/STI departure criterion does. Bihrie Applied Research has defined departure and roll reversal boundaries that are functions of the aircraft's static directional stability,  $C_{n_\beta}$ , and dihedral effect,  $C_{l_\beta}$ . In the development of the Bihrie departure boundaries a linear model was not assumed. Finally the Kalviste Departure Susceptibility criterion extends the static stability analysis used to derive  $C_{n_{\text{DYN}}}$  to include the coupling between the longitudinal and lateral-directional modes of motion and the use of nonlinear aerodynamics. This open-loop stability approach to predict aircraft departure susceptibility addresses asymmetric flight and the nonlinear aerodynamics that are known to be dominant in the high angle-of-attack flight regime. Each of these criteria are especially useful early in the design phase when the departure parameters such as  $C_{n_{\text{DYN}}}$ , LCDP, etc can still be impacted.

## 6.0 RECOMMENDATIONS

### 6.1 General

The design of a more departure resistant fighter aircraft has been one of major objectives driving the configuration design of the latest F-series aircraft that include the F-14, F-15, F-16, F-18 and F-20. This capability is being realized through the use of improved high- $\alpha$  aerodynamic design and digital flight control systems. But even beyond this objective, researchers see a strong need for future advanced fighter aircraft to have the capability to maneuver in the post-stall flight regime. Manned simulation studies, as documented in references (117) and (118), indicate its tactical utility and the increased combat effectiveness afforded via high- $\alpha$  maneuvering. To maneuver successfully requires the design intergration of an additional reaction control system. Thrust vectoring has received the most attention in this respect and is one of the major technology drivers in the current DARPA sponsored X-31A Technology Demonstrator Program.

The design of safe, effective fighter aircraft in the combat environment of the foreseeable future is reaching a critical point. Accepted flying qualities design guidelines (necessary to establish stability and control requirements) must be established to address flight operations in the high- $\alpha$  regime. Current military flying qualities specifications concentrate on preventing aircraft departure. Parameters/Criteria to define desired high- $\alpha$  flying qualities in the post-stall region outside the realm of departure are still unanswered. As a consequence, in concurrence with reference (1), the following research technology areas must still be more definitively addressed,

- Definition of the post-stall region
- Control power requirements to provide deep stall recovery capability.
- Control power requirements to prevent departures from controlled flight.
- Engine operating requirements and means to fulfill them.

- Post-stall warning and pilot cues.
- Multiaxis, nonlinear dynamics at high  $\alpha$ , with good representation of the aerodynamics
- Roll, pitch and yaw rate capability (where rolling about the flight path is mostly body-axis yawing)
- Deceleration/acceleration capability (nobody wants to stay long in a state of very low energy)
- Maximum allowable/usable sideslip and yaw rate at high angle of attack
- Aerodynamic means to improve departure/post-stall characteristics, compatible with high performance, low observables, . . .
- Thrust vectoring control power requirements for high- $\alpha$  stabilization and control
- Cockpit display and visibility requirements at high angle of attack

## **6.2. AERODYNAMIC MATH MODELS AT HIGH ANGLES-OF-ATTACK**

### **6.2.1. Determination of Forced Oscillation Data**

The following recommendation reiterates a data acquisition procedure for determining forced oscillation data suggested by Kalviste (Reference (55)). Reference (55) suggests that forced oscillation test data acquisition procedures be modified to measure aerodynamic coefficients to more accurately math model the nonlinear dependence of the dynamic derivatives as a function of angular rate. The motivation for this change is illustrated in figure 115. Figure 115 depicts the rolling moment derivative as a function of three amplitudes that the forced oscillation test was run at. It is clear from the data that at large angles-of-attack the derivative becomes highly dependent on the amplitude of the oscillation. Similar variations in the derivative also occur with variations in the oscillation frequency (Reference (55)). To address the nonlinear variations of the aerodynamic coefficients, the forced oscillation test

data derivatives are an "average" value of the derivative over a full cycle of oscillation (Reference (55)). There are obvious shortcomings in using such a procedure but proposed alternative methods have yet to be proven. Implementation of Kalviste's method would involve taking measurements only at the time when the rate is at the maximum value (both positive and negative maximum values). Reference (55) then recommends averaging these values over many cycles of oscillation. Using this technique, changes in the frequency and amplitude of the test oscillation will change the maximum rate of oscillation and hence yield the dynamic coefficient as a nonlinear function of rate (Reference (55)).

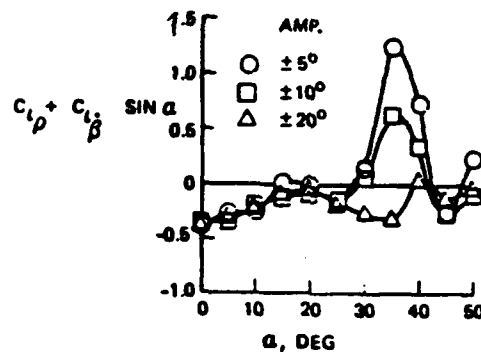


Figure 115. Forced Oscillation Wind Tunnel Test Rolling Moment Derivative Due to Roll Rate Variation With Oscillation Amplitude (Reference (55))

#### 6.2.2. Determination of Aerodynamic Rotary Balance Data

In a rotary balance wind tunnel test, the model is rotated at a constant rate about an axis parallel to the free stream velocity vector of the wind tunnel. As discussed earlier in section 3.1.2., the modelling of rotary balance data becomes extremely important when modelling the dynamics of a spin. Thus far only rotary increments to static stability derivatives can be determined. Reference (47) points out that this represents a shortcoming with respect to how dynamic derivatives (i.e.,  $C_{n_p}$ ,  $C_{l_p}$ ,  $C_{m_q}$ , etc.) are traditionally measured. Traditionally dynamic derivatives are measured while forcing a model to oscillate about a nonrotating reference. However reference (47) contends that a more proper way of representing

the aerodynamic model for spin analysis would be to superimpose the forced oscillations onto a steady rotating motion. For example, a total yawing moment coefficient due to roll rate would be calculated as,

$$C_{n_{\text{Tot}}} = C_{n_p}(M, \alpha) + C_{n_{\text{ROTATIONAL}}}(\text{rb}/2V, \alpha, \beta, \delta)$$

Dynamic derivatives measured using the latter method have indicated differences from those obtained using conventional techniques (Reference (49))

### 6.3 Extension of Current High Angle-of-Attack Flying Qualities Criteria

For the most part, the major focus of high angle-of-attack flying qualities criteria development has been on the prediction of aircraft departure and roll reversal susceptibility. The methods presented in the last section overviewed many of the more widely accepted/applied departure susceptible criteria and pointed out the fact that there is much overlap and redundancy among the parameters and criteria. Almost without exception these criteria are based on aircraft static stability requirements. From a linear model perspective, this approach aims at satisfying the necessary but not sufficient condition that a body must be statically stable (statically stable is used here in the classical sense such that the forces and moments produced by a small disturbance from a condition of equilibrium will initially tend to return toward the equilibrium condition on its own accord once the disturbance is removed) to ensure the linear system is dynamically stable. A shortcoming of this approach is that the linearity of the system is presumed in a highly nonlinear portion of the flight envelope.

In an attempt to correct this shortcoming and more accurately model the high angle-of-attack flight regime, Kalviste (Reference (119)) has proposed to expand his departure criterion to include nonlinear dynamic effects. By taking this approach, Kalviste hopes to define flying qualities parameters that address transient maneuvering flight and are not theoretically limited to only trimmed or steady maneuvering flight conditions. This trend in basic research must continue so that aircraft flying qualities specifications can incorporate boundaries for defining safe maneuvering flight at high angles-of-attack. In doing so, the specifications will better be able to guide the design of future aircraft as they are intended to do.

NADC (Code 6053) is currently working on extending aircraft open-loop aircraft departure susceptibility criteria to address the effects of asymmetric flight (i.e., nonzero sideslip angle,  $\beta$  and or bank angle,  $\phi$ ) and steady aircraft maneuvering (i.e., nonzero angular rates,  $P, Q, R$ ). References (120)-(123) have documented the significance of dynamic coupling between longitudinal and lateral-directional motions at high angles-of-attack on aircraft open-loop stability. As an example, reference (123) made use of a generalized trim routine to calculate steady-state (or trim) operating points for various asymmetric and steady maneuvering flight conditions. At each of these flight conditions, stability (determined from the eigenvalues) of the bare airframe could then be determined and graphically mapped on an appropriate "stability maneuvering plot" (see figures (116) to (118)).

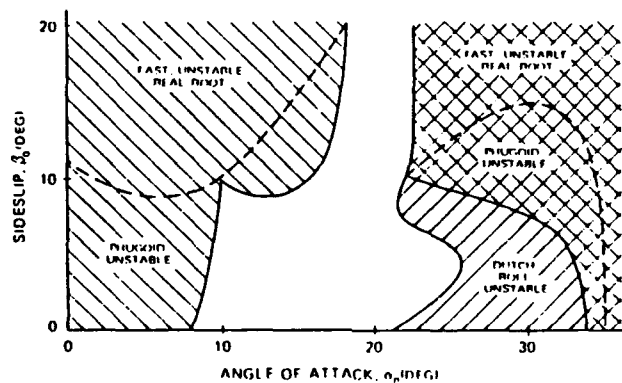


Figure 116. Effects of Angles of Incidence on Aircraft Stability (Reference (123))

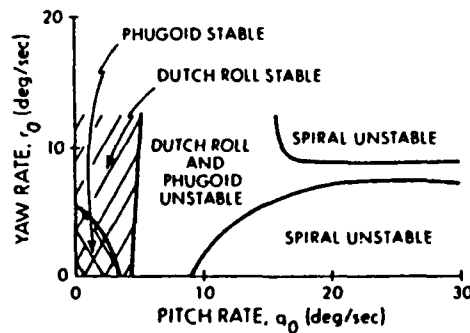


Figure 117. Yaw-rate/Pitch-rate Effects on Aircraft Stability (Reference (123))

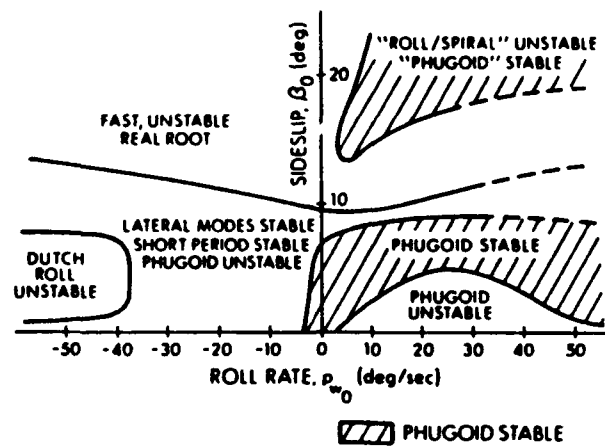


Figure 118. Stability Boundaries for Sideslip/Roll-Rate Variations (Reference (123))

From an open-loop stability perspective, these "stability maneuvering plots" are useful for indicating regions where aircraft maneuvering should be avoided to prevent "unforced" departures.<sup>1</sup>

The goal of our research is to determine if there exist parameters analogous to  $C_{n_{p_{DYN}}}$  such that the maneuvering stability regions typified by figures (116) to (118) can be predicted for an aircraft configuration (for its particular maneuvering flight envelope) without directly calculating the bare airframe eigenvalues. By accomplishing this, this open-loop departure susceptibility criterion could aid the aircraft designer in terms of tailoring aircraft aerodynamics for the maneuvering flight conditions expected of the aircraft.

<sup>1</sup> Reference (123) uses the term "unforced" departure to describe aircraft departures from controlled flight due to instabilities of the basic airframe.

References

1. MIL-STD-1797 (USAF), "Military Standard Flying Qualities of Piloted Vehicles," 31 March 1987.
2. MIL-S-83691A, "Military Specification, Stall/Post-stall/Spin Flight Test Demonstration Requirements for Airplanes," April 15, 1972.
3. Anderson, John D., Jr., *Introduction to Flight*, McGraw-Hill, New York, 1978.
4. Karamcheti, Krishnamurty, *Principles of Ideal-Fluid Aerodynamics*, John Wiley and Sons, Inc., New York, 1966.
5. Bertin, John, J. and Michael L. Smith, *Aerodynamics for Engineers*, Prentice-Hall Inc., Englewood Cliffs, N.J. 1979.
6. White, Frank M., *Fluid Mechanics*, McGraw-Hill, Inc., N.Y., 1979
7. Schlichting, Herman, *Boundary-Layer Theory*, McGraw-Hill Inc., New York, 1979.
8. Lan, Chuan-Tau Edward and Jan Roskam, *Airplane Aerodynamics and Performance*, Roskam Aviation and Engineering, Ottawa, Kansas, 1980.
9. Chang, Paul K. *Control of Flow Separation*, McGraw-Hill, Inc., N.Y., 1976.
10. Lachmann, G.V. (ed.), *Boundary Layer and Flow Control*, 2 Vols, Pergamon, 1961.
11. Pletcher, R.H. and C.L. Dancey, "A Direct Method of Calculating through Separated Regions in Boundary Layer Flow," *Journal of Fluids Engineering*, Sept. 1976 pg. 568-72.
12. Tritton, D.J., *Physical Fluid Dynamics*, Van Nostrand Reinhold (UK) Co. LTD., Berkshire, England, 1982.
13. Chang, Paul K., *Separation of Flow*, Pergamon Press, New York, 1970.
14. Kuethe, Arnold, M. and Chow, Chuen-Yen, *Foundations of Aerodynamics*, John Wiley & Sons Inc., 1986.

*References (Cont'd)*

15. Abbott, Ira, H. and Albert E. Von Doenhoff, *Theory of Wing Sections*, Dover Publications, New York, 1959.
16. McCormick, Barnes, W., *Aerodynamics, Aeronautics, and Flight Mechanics*, John Wiley & Sons, New York, 1979.
17. Conner, F., Willey, C., and Twomey, W., "A Flight and Wind Tunnel Investigation of the Effect of Angle-of-Attack Rate on Maximum Lift Coefficient," NASA CR-321, 1965.
18. Harper, P.W. and Flanigan, R.E., "The Effect of Change of Angle-of-Attack on the Maximum Lift of a Small Model," NACA TN-2061, 1949.
19. Ericsson, Lars E., and J. Peter Reding, "Unsteady Airfoil Stall, Review and Extension," *Journal of Aircraft*, Vol. 8 No. 8 pg. 609-616, August 1971.
20. Halfman, R.L., Johson, H.C., and S.M. Haley, "Evaluation of High Angle-of-Attack Aerodynamic - Derivative Data and Stall-Flutter Prediction Techniques," NACA TN 2533, 1951.
21. Ericsson, L.E. and J.P. Reding, "Unsteady Airfoil Stall" NASA CR 66787, 1969.
22. Lomax, H., Heaslet, M.A., Fuller, F.B. and L. Sluder, "Two and Three Dimensional Unsteady Lift Problems In High Speed Flight," T.R. Rept. 1077, 1952, p. 18.
23. Carta, F.O., "Unsteady Normal Forces on an Airfoil In a Periodically Stalled Inlet Flow," *Journal of Aircraft*, Vol. 4, No. 5, Sept.-Oct. 1967, pp. 416-421.
24. Ericsson, L.E., "Comment on Unsteady Airfoil Stall," *Journal of Aircraft*, Vol. 4, No. 5, Sept-Oct. 1967, pp. 478-480.
25. Carr, Lawrence W., "Dynamic Stall Progress In Analysis and Prediction," AIAA, Atmospheric Flight Mechanics Conference, 12<sup>th</sup>, Snowmass, CO, August 18-21, 1985, AIAA-Paper 85-1769.
26. Ham, N.D., and M.S. Garelick, "Dynamic Stall Considerations in Helicopter Rotors," *Journal of the American Helicopter Society*, Vol. 13, No. 2, Apr. 1968, pp. 49-55.
27. Chambers, Joseph R., and Sue B. Grafton, "Aerodynamic Characteristics of Airplanes at High Angles-of-Attack," NASA TM 74097 December, 1977.

*References (Cont'd)*

28. Perkins, Cortland, D., and Robert E. Hage, *Airplane Performance, Stability and Control*, John Wiley and Sons, 1949.
29. Langdon, S.D., *Fixed Wing Stability and Control Theory and Flight Test Techniques*, USNTPS-FTM-No. 103, August 1, 1969.
30. Jones, Robert T., "Properties of Low-aspect Ratio Pointed Wings at Speeds Below and Above the Speed of Sound," NACA TN No. 1032, 1946.
31. Polhamus, E.C., "A Concept of Vortex Lift of Sharp Edge Delta Wings Based on a Leading Edge-Suction Analogy," NASA TN D-3767, Dec. 1966.
32. Polhamus, E.C., "Application of the Leading-edge-Suction Analogy of Vortex Lift to the Drag Due to Lift of Sharp-Edge Delta Wings," NASA TN D-4739, August 1968.
33. Dickinson, B., *Aircraft Stability and Control For Pilots and Engineers*, Sir Isaac Pitman & Sons LTD, London, 1968.
34. Torenbeck, Egbert, *Synthesis of Subsonic Airplane Design*, Delft University Press, Delft, Holland, 1982.
35. Chambers, J. and Sue Grafton, "Aerodynamic Characteristics of Airplanes at High Angles-of-Attack," NASA TM-74097, Dec. 1977.
36. Strom, Thomas, H., and William J. Alford Jr., "Flight at Supernormal Attitudes," Society of Automotive Engineers Technical Paper Series, Report No. 821469 Oct. 1982.
37. Goldberg, Carl, "Bring Them Down Safely," *Model Airplane News*, September 1943.
38. Blanchard, W.S., Jr., "A Flight Investigation of the Ultra-Deep-Stall Descent and Spin Recovery Characteristics of A 1/6 Scale Radio-Controlled Model of the Piper DA-38 Tomahawk," NASA Contractor Report 156871, March 1981.
39. Alford, William J., Jr., "Potential Trimmed Flight Path Characteristics of a Modified Light-Weight Fighter Airplane at Supernormal Angles-of-Attack," Dynamic Engineering Technical Report TR-059, 29 March 1982.

*References (Cont'd)*

40. Taylor, Robert T., and Ray, Edward J.: "Deep Stall Aerodynamic Characteristics of T-Tail Aircraft." Conference on Aircraft Operating Problems, NASA SP-83, pp. 113-121.
41. White, Maurice, D.; and Cooper George, E., "Simulator Studies of the Deep Stall." Conference on Aircraft Operating Problems, NASA SP-83, 1965, pp. 101-111.
42. Lina, Lindsay J.; and Moul, Martin T. "A Simulator Study of T-Tail Aircraft in Deep Stall Conditions." AIAA Paper No. 65-781, 1965.
43. Kershner, William K., *The Advanced Pilot's Flight Manual*, Iowa State University Press, Ames Iowa, 1985.
44. Kohlman, D.L., *Introduction to V/STOL Airplanes*, Iowa State University Press, Ames Iowa, 1981.
45. Bowman, James S., Jr.: "Summary of Spin Technology as Related to General Aviation Airplanes," NASA TN D-6575, 1971.
46. Anonymous, *Flying Qualities - Volume III*, Flight Dynamics Division, 6520 TH Test Group, Air Force Flight Test Center, Edwards AFB, California, Jan. 1982.
47. Johnston, Donald E. and Robert K. Heffley, "Investigation of High Angle-of-Attack Flying Qualities Criteria and Design Guidelines," AFWAL-TR-81-3108, Dec. 1981.
48. Etkin, Bernard. *Dynamics of Flight Stability and Control*, John Wiley and Sons, New York, 1982.
49. Bihrlle, W. Jr., and B. Barnhart, "Spin Prediction Techniques," *Journal of Aircraft* Vol. 20, No. 2 Feb. 1983.
50. Bamber, M.J. and Zimmerman, C.H., "Spinning Characteristics of Wings I - Rectangular Clark Monoplane Wing," NACA TR-519, 1935.
51. Stone, Ralph W. Jr.; Burk, Sanger M., Jr.; and Bihrlle, William, Jr.: "The aerodynamic Forces and moments on a 1/10-Scale model of a Fighter Airplane in Spinning Altitudes as Measured on a Rotary Balance in the Langley 20-Foot Free Spinning Tunnel," NACA TN 2181, 1950.
52. Gale, Lawrence J., "Effect of Landing Flaps and Landing Gear on the Spin and Recovery Characteristics of Airplanes," NACA TN 1643, 1948.

*References (Cont'd)*

53. Chambers, Joseph R., "Overview of Stall/Spin Technology", AIAA Paper-80-1580, Aug. 1980.
54. Erickson, G.E., "Water Tunnel Flow Visualization and Wind Tunnel Data Analysis of the F/A-18," NASA CR-165859, May 1982.
55. Kalviste, Juri, "Use of Rotary Balance and Forced Oscillation Test Data in a Six Degree-of-Freedom Simulation," AIAA-Paper 82-1364, San Diego, August 9-11, 1982.
56. Bamber, M.J. and C.H. Zimmerman, "Spinning Characteristics of Wings-Rectangular Clark-Y Monoplane Wing," NACA TR-519, 1935.
57. Barnhart, Billy, "F-14 Rotary Balance Tests for an Angle-of-attack Range of 0° to 90°," NADC Rep No. 81293-60, January 1983.
58. Butler, R.W., and T.F. Langham, "Sensitivity of Aircraft Spinning Motion to Dynamic Cross-Coupling and Acceleration Derivatives," AEDC-TR-78-12, Oct. 1978.
59. Orlik-Ruckermann, K.J., "Review of Techniques for Determination of Dynamic Stability Parameters in Wind Tunnels," AGARD Dynamic Stability Parameters, Lecture Series, No. 114, Feb. 1981.
60. Orlik-Ruckmann, K.J., "Techniques for Dynamic Stability Testing in Wind Tunnels," AGARD CR-235; Dynamic Stability Parameters, pp. 1-1 to 1-24, May 1978.
61. Ralston, J.N., "Influence of Airplane Components on Rotational Aerodynamic Data for a Typical Single-engine Airplane," AIAA-83-2135, 1983.
62. Barnhart, B., W. Bihrie and E. Dickes, "A Preliminary Design Guide for Departure/Spin Resistant Forebody Configurations," BAR 85-10, Bihrie Applied Research, Inc., January, 1986.
63. Chambers, Joseph, R., and James S. Bowman, Jr., "Recent Experience with Wind-tunnel and Analytical Techniques for Prediction of Spin Characteristics of Fighter Aircraft," AIAA, Flight Mechanics Conference, Tullahoma, TN, May 13-15, 1970, AIAA Paper-70-565.
64. Bihrie, W., Jr., and J.S. Bowman, "Influence of Wing, fuselage, and Tail Design on Rotational Flow Aerodynamics Beyond Maximum Lift," *Journal of Aircraft*, Vol. 18, No. 11, November 1981, p. 920.

*References (Cont'd)*

65. Headley, J.W., "Analysis of Wind Tunnel Data Pertaining to High Angle-of-Attack Aerodynamics; Volume I - Technical Discussion and Analysis of Results," AFFDL-TR-78-94, July 1978.
66. Fratello, David J., Croom, Mark, A., and Luat T. Nguyen, "Use of the Updated NASA Langley Radio-Controlled Drop-Model Technique for high-alpha studies of the X-29A Configuration," AIAA-Paper 87-2559, Monterey, CA, August 17-19, 1987.
67. Warren, Rik and Gary E. Riccio, "Visual Cue Dominance Hierarchies: Implications for Simulator Design," AIAA Paper 85-1946.
68. Anonymous, "DFS Task Report," VEDA Inc., VEDA Rep. No. 33142-83U/P3019-01, June 1983.
69. R.J. Crosbie, J. Eyth, G.T. Thomas, et al, "NAVAIRDEVCEEN Dynamic Flight Simulator, F-14 Spin Simulation Program, System Description and Specification Report", Report No. NADC-81145-60, April 1981.
70. R.J. Crosbie, "Development of New Centrifuge Control Algorithms", NADC Report NAVMAT 3920-1, November 15, 1982.
71. Elson, B.M., "Advanced Research Simulator slated for 1981 Operation," *Aviation Week and Space Technology*, February 4, 1980, pp. 72-77.
72. "Ames Expands Rotorcraft Capability", *Aviation Week and Space Technology*, January 17, 1983, pp. 65-71.
73. *Flight Control Development Laboratory* (Ohio: Air Force Flight Dynamics Laboratory, Air Force Wright Aeronautical Laboratories Technical Brochure.)
74. *Northrop Flight Simulation Facilities* (California: Northrop Corporation Aircraft Group, October 1977.
75. Stein, K.J., "Corporation Model Cuts USAF Test Costs", *Aviation Week and Space Technology*, January 17, 1983.
76. K.J. Stein, "Near-Term Goal of Total Simulation Training Seen", *Aviation Week and Space Technology*, March 9, 1981, pp. 215-222.

*References (Cont'd)*

77. K.J. Stein, "New Simulator Visual System Designed", *Aviation Week and Space Technology*, February 8, 1982, pp. 75-77.
78. K.J. Stein, " 'Total Simulation' Seen in Training", *Aviation Week and Space Technology*, September 8, 1980, pp. 52-59.
79. K.J. Stein, "Helicopter Simulators Aid in Crew Training," *Aviation Week and Space Technology*, June 8, 1981, pp. 305-310.
80. M. Baret, "Six Degrees of Freedom Large Motion System for Flight Simulators," *AGARD - CP 249*, April 1978.
81. "AMES Research Facilities Summary 1974", *NASA/AMES Research Center Technical Brochure*.
82. D. Key, B. Odeneal, and J. Sinacori, "Mission Environment Simulation for Army Rotocraft Development - Requirements and Capabilities," *AGARD-CP-249*, April 1978.
83. Gum, W. Albery, "Advanced Simulation in Under-graduate Pilot Training: An Overview", Air Force Human Resources Lab - Brooks AFB, Report No. AFHRL-TR-75-59, December 1975.
84. D. Bischoff, and A. Burgess, "Flight Fidelity Evaluation of the Aerodynamic Update of the F-14A Operational Flight Trainer (Device 2F95)", Report No. NATC-SA-C15R-76, December, 1982.
85. "Real-Time Scenarios Aid McDonnell Weapons Work," *Aviation Week and Space Technology*, January 17, 1983, pp. 57-62.
86. Markman, Steven R., "Capabilities of Airborne and Ground Based Flight Simulation," AIAA Paper 85-1944.
87. Knotts, Louis, and Michael Parrag, "In-flight Simulation at the U.S. Air Force and Naval Test Pilots Schools", Avin/Calspan Advanced Technology Center, Buffalo, N.Y.
88. Nguyen, Luat, T., "Control System Techniques for Improving Departure/Spin Resistance for Fighter Aircraft," SAE Paper 79-1083, December 1979.

*References (Cont'd)*

89. W.R. Buris and J.T., Lawrence, "Aerodynamic Design and Flight Test of U.S. Navy Aircraft at High Angles-of-Attack," Presented to AGARD Fluid Dynamics Panel Specialists' Meeting, 26-28 April 1972.
90. Skow, A.M. and A. Titiriga, Jr., "A Survey of Analytical and Experimental Techniques to Predict Aircraft Dynamic Characteristics at High Angles-of-Attack," AGARD CP-235, Dynamic Stability Parameters, pp. 19-1 to 19-37, May 1978.
91. Gilbert, William, P. and Peter C. Carr, "Effects of Fuselage Forebody Geometry on Low-Speed Lateral-Directional Characteristics of Twin-Tail Fighter Model at High Angle-of-Attack," NASA TP-1592, December 1979.
92. Nial, J.A., "Status of U.S. Navy's Stall/Post-Stall/Spin Flight Testing," AIAA Paper No. 72-787, August 1972.
93. Anonymous, "Military Specification, Flying Qualities of Piloted Airplanes," MIL-F-8785C, November 5, 1980.
94. MIL-F-9490D, "Military Specification, Flight Control Systems- Design, Installation, and Test of Piloted Aircraft, General Specification for," June 6, 1975.
95. Moorhouse, David, J., and Robert J. Woodcock, "Background Information and User's Guide for MIL-F-8785C, Military Specification-Flying Qualities of Piloted Airplanes," AFWAL-TR-81-3109, July 1982.
96. MIL-D-8708B, Amendment 1, "Military Specification, Demonstration Requirements for Airplanes," June 3, 1982.
97. Tinger, Herbert L., "Analysis and Application of Aircraft Departure Prediction Criteria to the AV-8B Harrier II," AIAA Paper-87-2561, 1987.
98. Johnston, D.E., Mitchell, D.G., and Thomas T. Meyers, "Investigation of High Angle-of-Attack Maneuver Limiting Factors. Part I: Analysis and Simulation, AFWAL-TR-80-3141, Sept. 1980.
99. Johnston, Donald E., and Robert K. Heffley, "Investigation of High Angle-of-Attack Flying Qualities Criteria and Design Guides," AFWAL-TR-81-3108, December 1981.

*References (Cont'd)*

100. Bihrlé, W., Jr., and B. Barnhart, "Design Charts and Boundaries for Identifying Departure Resistant Fighter Configurations, NADC-76154-30, July 1978.
101. Bihrlé, W., Jr., and B. Barnhart, "Departure Susceptibility and Uncoordinated Roll-Reversal Boundaries for Fighter Configurations," *Journal of Aircraft*, Vol. 19, No. 11, Nov. 1982.
102. Anonymous, *Data Report: High Angle-of-Attack Departure Criteria Experiment*, VEDA Report 33079-85U/P3303-001, 12 March 1985.
103. Moul, M.T., and J.W. Paulson, *Dynamic Lateral Behavior of High Performance Aircraft*, NACA RM L58E16, 1958.
104. Skow, A.M., "A Survey of Analytical and Experimental Techniques to Predict Aircraft Dynamic Characteristics at High Angles of Attack," AGARD-CP-235.
105. Greer H. Douglass, "Summary of Directional Divergence Characteristics of Several High-Performance Aircraft Configurations," NASA TN D-6993, 1972.
106. Mello, John and James Agnew, "McAir Design Philosophy for Fighter Aircraft Departure and Spin Resistance," SAE Paper No. 791081, presented at Aerospace Meeting, Los Angeles, Dec. 3-6, 1979.
107. Weissman, Robert, "Criteria for Predicting Spin Susceptibility of Fighter-Type Aircraft," ASD-TR-72-48, June 1972.
108. Weissman, Robert, "Preliminary Criteria for Predicting Departure Characteristics/ Spin Susceptibility of Fighter-Type Aircraft," *AIAA Journal of Aircraft*, Vol. 10, No. 4, April 1973.
109. Rhodeside, Glenn, R., "Investigation of Departure Susceptibility Criteria Using the Dynamic Flight Simulator," NADC-TR-85091-60, June 1985.
110. Rhodeside, Glenn R., "Investigation of Aircraft Departure Susceptibility Using a Total-G Simulator," AIAA Paper No. 86-0492, Reno Nevada, January 1986.
111. Kalviste, Juri, *Analysis of Aircraft Departure Characteristics*, Northrop Report NOR-77-67, Oct. 1977.

*References (Cont'd)*

112. Kalviste, Juri, "Aircraft Stability Characteristics at High Angles-of-Attack," Dynamic Stability Parameters, AGARD Conference Proceedings No. 235, May 1978.
113. Skow, A.M., "A Survey of Analytical and Experimental Techniques to Predict Aircraft Dynamic Characteristics at High Angles of Attack," Dynamic Stability Parameters, AGARD Conference Proceedings No. 235, May 1978.
114. Henderson, C., Clark, J., and M. Walters, "V/STOL Aerodynamics and Stability and Control Manual," NADC-TR-80017-60, 15 January 1980.
115. Hodgkinson, John, "Prediction of Lateral and Directional Divergence of High Angles-of-Attack," McAir Report Number EH 844, 15 October 1971.
116. Pelikan, R.J., "F/A-18 High Angle-of-Attack Departure, Resistant Criteria for Control Law Development," AIAA Paper-83-2126, Gatlinburg, Tennessee, August 1983.
117. Herbst, W.B., "Supermaneuverability" National Conference of DGLR, Munich, October 1983.
118. Martin, Joseph, "A Case for VATOL Flight Demonstration Report No. DTNSRDC 80 018, 1980.
119. Anonymous, "Aircraft Stability and Control Parameters - Volume I Technical Proposal", NB87-129, August 1987.
120. Phillips, W.H., "Effects of Steady Rolling on Longitudinal and Directional Stability," NACA TN 1627, Washington, June 1948.
121. Abzug, M.J., "Effects of Certain Steady Motions on Small Disturbance Airplane Dynamics," *Journal of the Aeronautical Sciences*, Vol. 21, No. 11, November 1954, pp. 749-762.
122. Johnston, D.E. and Hogge, J.R., "The Effects of Non-symmetric Flight on Aircraft High Angle-of-Attack Handling Qualities and Departure Characteristics," AIAA Paper No. 74-792, New York, August 1974.
123. Stengel, Robert F. and Paul W. Berry, "Stability and Control of Maneuvering High-Performance Aircraft," *Journal of Aircraft*, Vol. 14, No. 8, August 1977, pp. 787-794.

**APPENDIX - A**

**GLOSSARY OF DEFINED TERMS**

Viscosity - property of a fluid that relates the local stresses in a moving fluid to the strain rate of the fluid elements.

Newtonian Fluid - A fluid which obeys the linear law given by:  $\tau = \mu \, du/dy$ . Fluids which do not obey this law are called nonnewtonian.

Mean Camber line - locus of the points midway between the upper surface and the lower surface as measured perpendicular to the chord line.

Taper Ratio ( $\lambda$ ) ratio of the tip chord to the root chord,  $\lambda = C_t/C_r$

Aerodynamic Center (a.c.) - defined as the point about which the moment coefficient is independent of the angle-of-attack.

Center-of-pressure (c.p.) - defined as the point about which the pitching moment vanishes. For a symmetrical airfoil the c.p. position is at the quarter-chord for all values of the lift coefficient. The c.p. position for a cambered airfoil varies as a function of the lift coefficient,  $C_L$  ( $-\infty < X_{cp} < \infty$ ).

Aspect ratio - a fineness ratio of the wing defined as  $b/c$  for a rectangular wing and  $b^2/S$  for a non-rectangular wing.

Supernormal Flight (SNF) - is concerned with flight at extraordinary angles-of-attack ( $\alpha > \alpha_{C_{L_{MAX}}}$ ), the resulting substantial changes in the pitch and flight path angles, and the attainment of flight path and vertical velocities which are not otherwise available to the pilot (Dynamics Engineering Inc. Reference (36)).

Separated flow - defined classifications excerpted from reference (8) as follows:

1. Trailing-edge separation. This type of flow separation is to be expected with turbulent flow. Thick (less than 15 percent) airfoils have a well-rounded suction peak and only a moderate adverse pressure gradient which covers the rear portion of the airfoil. For such airfoils, the flow separation is near the trailing edge, and the separation point moves upstream with increasing angle of attack. The thickness of the turbulent boundary layer may be reduced and some improvement in  $C_{L_{MAX}}$  achieved by increasing the Reynolds number.
2. Thick-section separation bubble. With laminar flow at low Reynolds numbers, the flow separates on the forward portion of a thick airfoil. This type of separation is often followed by reattachment of the turbulent boundary layer downstream; it may reseparate near the trailing edge. If the Reynolds number is increased, the extent of the forward separation is reduced because the separation point shifts downstream until transition occurs upstream of the laminar separation point, thus reverting to the trailing edge type of separation.
3. Short-bubble separation. The size of the short bubble is of the order of 0.5-1 percent of chord length. On the thinner airfoils, where a suction peak of a sharper nature occurs close to the leading edge, a laminar separation starts. With an increase in angle of attack, the separation point moves up to the leading edge. The separated layer becomes turbulent and at medium or high Reynolds numbers, it reattaches to form a short bubble. With increasing Reynolds number, this bubble tends to contract until it suddenly bursts and causes an abrupt stall. At very high Reynolds numbers, a trailing-edge stall may form instead of the short bubble type. The very short bubble then acts merely as a transition-fixing device.
4. Long-bubble separation. Although this kind of bubble is termed "long" it is only approximately 2 percent of chord length. On very thin airfoils whose thickness is less than 6 percent, the laminar flow that separates at the leading edge at low Reynolds numbers reattaches following transition to

turbulent flow and forms a long bubble. With increasing angle of attack, this bubble extends to the trailing edge. Although this long-bubble separation causes a gentle stall in contrast to the abrupt stall of the short bubble, it nevertheless exerts a substantial influence on drag, lift, and pitching moment over a considerable range of angles of attack. Close to stall, a short-bubble type separation may occur when the Reynolds number becomes sufficiently large.

Geometric Similarity - A model and prototype are geometrically similar if all body dimensions in all three coordinates have the same length-scale ratio (reference (6)).

Kinematic Similarity - A model and prototype are kinematically similar if they have the same length-scale ratio and also the same time-scale ratio. The result is that the velocity-scale ratio will be the same for both (reference (6)).

Dynamic Similiarity - A model and prototype are dynamically similiar if they have the same length-scale ratio, time-scale ratio, and force-scale (or mass scale) ratio. It follows that dynamic similiarity exists simultaneously with kinematic similiarity if model and prototype forces are in constant ratio (reference (6)).

Table A-1 Dynamic-Scaling Factors

|                                  | Scale Factor*      |
|----------------------------------|--------------------|
| Linear Dimension                 | $N$                |
| Relative-density, $(m/\rho_1)^3$ | $1$                |
| Froude number, $V/\sqrt{g}$      | $1$                |
| Weight, mass                     | $N^3/\sigma$       |
| Moment of inertia                | $N^5/\sigma$       |
| Linear velocity                  | $N^{0.5}$          |
| Linear acceleration              | $1$                |
| Angular velocity                 | $N^{-0.5}$         |
| Time                             | $N^{0.5}$          |
| Reynolds number $(V_1/\nu)$      | $N^{1.5}\nu/\nu_0$ |

\*Model values are obtained by multiplying full-scale aircraft values by the appropriate scale factor.

MIL-F-8785C Classification of Airplanes

Class I: Small, light airplanes such as,

light utility

Primary trainer

light observation

## **NADC 88020-60**

- Class II** Medium weight, low-to-medium maneuverability airplanes such as
- Heavy utility/search and rescue
  - Light or medium transport/cargo/tanker
  - Early warning/electronic countermeasures/airborne command, control, or communications relay
  - Antisubmarine
  - Assault transport
  - Reconnaissance
  - Tactical bomber
  - Heavy attack
  - Trainer for Class II
- Class III** Large, heavy, low-to-medium maneuverability airplanes such as
- Heavy transport/cargo/tanker
  - Heavy bomber
  - Patrol/early warning/electronic countermeasures/airborne command, control, or communications relay
  - Trainer for Class III
- Class IV** High maneuverability airplanes such as
- Fighter/interceptor
  - Attack
  - Tactical reconnaissance
  - Observation
  - Trainer for Class IV

MIL-S-83691A Definitions of departure susceptibility and Resistance:

Extremely susceptible to departure: departure from controlled flight will generally occur with the normal application of pitch control alone or with small roll and yaw control inputs.

Susceptible to departure: departure from controlled flight will generally occur with the application or brief misapplication of pitch and roll and yaw controls that may be anticipated in operational use.

Resistance to departure: departure from controlled flight will only occur with a large and reasonably sustained misapplication of pitch and roll and yaw controls.

Extremely resistant to departure: departure from controlled flight can only occur after an abrupt and inordinately sustained application of gross, abnormal, pro-departure controls.

# NADC 88020-60

## DISTRIBUTION LIST (CONTINUED)

REPORT NO. NADC-88020-60

*No. of Copies*

|   |   |
|---|---|
| McDonnell Aircraft Co. ....<br>St. Louis, MO 63166<br>(Attn: D. R. Riley)   | 1 |
| Northrup Corp. ....<br>Hawthorne, CA 90250<br>(Attn: Juri Kalviste)   | 1 |
| Lockheed Georgia Co. ....<br>Marietta, GA 30061<br>(Attn: Mr. M. Jenkins)   | 1 |
| Grumman Aerospace Corp. ....<br>Bethpage, NY 11714<br>(Attn: Mr. M. Lapins)<br>(Attn: Mr. H. Beaufriere)                      | 2 |
| The Boeing Co. ....<br>Seattle, WA 98101  | 1 |
| Rockwell International ....<br>Columbus, OH 43216<br>(Attn: Mr. W. Palmer)  | 1 |
| General Dynamics Corp. ....<br>Ft. Worth, TX 76108  | 1 |
| Systems Technology Inc. ....<br>Hawthorne, OH 90250   | 1 |
| Dept. of Aero and Mechanical Sciences ....<br>Princeton University,<br>Princeton, NJ 08540<br>(Attn: Dr. R. Stengel)          | 1 |
| DARPA ....<br>1400 Wilson Blvd.<br>Arlington, VA 22209<br>(Attn: LT Col. J. Retelle)  | 1 |
| Bihrie Applied Research ....<br>400 Jericho Turnpike<br>Jericho, NY 11753<br>(1 for Mr. W. Bihrie)<br>(1 for Mr. B. Barnhart) | 2 |
| Eidectics International ....<br>3669 W. 240th Street<br>Torrance, CA 90505  | 2 |

# NADC 88020-60

## DISTRIBUTION LIST

REPORT NO. NADC-88020-60

*No. of Copies*

|  |    |
|--|----|
| ONT .....                                      | 2  |
| Arlington, VA 22219-5000                       |    |
| (Attn: W. King)                                |    |
| NAVAIR .....                                   | 4  |
| (2 for library)                                |    |
| (2 for AIR-5301)                               |    |
| NAVAIRTESTCEN .....                            | 4  |
| Patuxent River, MD 20670                       |    |
| (2 for SA)                                     |    |
| (2 for AT)                                     |    |
| AFWAL .....                                    | 3  |
| Wright Patterson AFB, OH 45433                 |    |
| (Attn: Mr. T. Chord, Code FIGC)                |    |
| (Attn: Mr. F. George, Code FIGC)               |    |
| (Attn: Mr. T. Gentry, Code FIGC)               |    |
| NASA Langley Research Center .....             | 3  |
| Hampton, VA 20350                              |    |
| (Attn: Mr. W. Gilbert)                         |    |
| (Attn: Mr. L. Nguyen)                          |    |
| (Attn: Mr. J. Boeman)                          |    |
| NASA Dryden Research Center .....              | 2  |
| Edwards, CA 93523                              |    |
| (Attn: Mr. E. Enevoldson)                      |    |
| (Attn: Mr. D. Berry)                           |    |
| Arvin/Calspan Advanced Technology Center ..... | 1  |
| Buffalo, NY 14225                              |    |
| (Attn: Mr. E. Rynaski)                         |    |
| NAVAIRDEVCEEN .....                            | 17 |
| (1 for 60)                                     |    |
| (1 for 605)                                    |    |
| (12 for 6053, Mr. R. Seltzer)                  |    |
| (1 for 60C, Mr. L. Lehman)                     |    |
| (2 for 8131, Library)                          |    |
| Defense Technical Information Center .....     | 2  |
| Cameron Station, Bldg. #5                      |    |
| Alexandria, VA 22314                           |    |
| (2 for retention)                              |    |